Technological University of the Shannon: Midlands Midwest

Ollscoil Teicneolaíochta na Sionainne: Lár Tíre Iarthar Láir

Modification of PEGDMA hydrogels for use in the fabrication of peripheral nerve guidance conduits

A thesis submitted for the degree of
Doctor of Philosophy
to the
Technological University of the Shannon: Midlands Midwest
By
Gavin Nicholas Burke B.Sc.

Based on research carried out under the supervision of

Dr. Ian Major

Dr. Declan Devine

Submitted

October 2021

Declaration

I hereby declare that this thesis submitted to the Technological University of the Shannon: Midlands Midwest for consideration for the degree of Doctor of Philosophy is a result of my work and has not, in the same form or altered form, been presented to this institute or any other institute in support for any degree other than for which I am now a candidate

_____   _____

Gavin Burke   01/10/21

Acknowledgements

I would like to take this opportunity to thank each of my supervisors for helping me reach this point. Valerie started me on the path as a postgraduate and taught me much of the fundamentals and attitude necessary to shape me into the scientist I am today, I'll always be grateful for the opportunity she gave me. Ian stepped in and took over upon Val's departure, providing a steadying hand and offering his expertise to help overcome the many obstacles that occurred throughout this project, I would not have made it this far without him. Declan for his part provided me with much needed levity and his approach to problem solving was eye opening, I would like to thank him for the guidance he offered throughout this thesis.

For their technical assistance with my thesis, I would like to thank the following people: Irina, Tom and Alan for carrying out SEM analysis, Junior and Shane B with DMA testing, Crevan and Martin for HPLC, Ian and Rob for conductivity analysis, Margaret for her knowledge of Raman as well as Alex for so much.

There are many amazing senior staff who had the misfortune of giving advice and explaining basic concepts to me throughout this thesis. In particular, Alan M, James, Mark, Sean (giving me your number was your biggest mistake!) and Therese, you were selfless and deserve all the thanks you get.

Big thanks to those in the office of research (more than once, you guys saved my bacon), and the lab technicians in the main campus (HPLC supplies Whoo!).

I would like to thank all the postgrad students who I came to know over the course of my thesis, we helped each other as much as we hindered each other but all told you enriched the experience of being a postgrad for me and made it one of the most fun experiences of my life.

Special thanks to Conor (such fren, very help), Andrew, Declan C, Emily, Evert, Fashli, Maya, Romina and Shane H, you guys were not only friends but also excellent sounding boards for my (terrible 90% of the time) ideas. Solving the mystery of how you maintained your patience with me throughout would entail its own PhD investigation.

To my extended family, especially Nanny, Granda, Nancy, Cathy, and Seamus, (I got too many aunts, uncles, and cousins to make a comprehensive list, our family is way too Catholic!) thanks for being there for me and helping me get through this thesis.

To my immediate family, for all the words of encouragement you offered, the insightful questions like 'why is it taking you so long to finish' and the understanding you had for my screams of anguish when I couldn't answer such questions, thank you. Mam, John, Dean, Jamie, and Kaydee I love you all. Also, Dean, Jamie and Kaydee I will actively seek out opportunities to lord this over you, be prepared, my smugness is coming.

Finally, and most importantly I want to thank my partner Danielle and our wonderful son Theodore. Theodore you are the greatest source of pride in my life and Danielle you have been there for me from the very beginning and supported me every step of the way, I would have never finished this thesis without your help, I love you both.

Abstract

Peripheral nerve injury is a worldwide issue affecting millions. More than 719,000 people are receiving surgical treatment for peripheral nerve injury each year in the US alone. There is presently a market for the repair of peripheral nerve injury using natural or synthetic nerve grafts with the autograft (current gold standard) having well known drawbacks in the form of donor site morbidity and a low rate of success for injuries greater than 3 cm. Therefore, there is an opportunity in the market of peripheral nerve injuries to repair gaps greater than 3 cm while also preventing secondary sites of morbidity. This thesis describes the development of a polyethylene glycol dimethacrylate (PEGDMA) based product to fill this clinical need.

Initial work in this thesis focused on comparing the material property profiles of four different monomer concentrations of PEGDMA (600MDa) stored in physiological solutions at 37°C over a 28-day period. To achieve this goal, polymer constructs were prepared (25, 50, 75 and 100 wt. % PEGDMA) in water and cross-linked by UV-induced photopolymerisation. Thereafter the material properties were examined after 0, 2, 14 and 28 days for their swelling characteristics, wettability, surface topography, chemical properties, polymer morphology, mechanical properties, and cell response. From this data, it was decided that the 50 and 100 wt. % PEGDMA hydrogels were most suited to replicate the conditions of peripheral nerve tissue.

Electroactive bioglass was selected as an additive to increase the conductivity of PEGDMA to enhance conductivity. The materials properties of the new PEGBio composites were subsequently tested with additional analysis of the conductivity of samples. From these subsequent tests it was determined that the PEGBio 2.5 wt. % samples provided the greatest boost to conductivity. Following on from this the project looked to address PEGDMAs lack of degradability. To improve degradability, PEGDMA was polymerised with ten different thiol monomers, both mercaptopropionates and mercaptoacetates. Following an initial polymerisation check, it was determined that mercaptopropionates were more successfully polymerised than mercaptoacetates. The material properties of the new PEG-thiol composites were subsequently tested as per previous tests with further study determining that dipentaerythritol hexa(3-mercaptopropionate) (DiPETMP) successfully enhanced the biodegradability of PEGDMA.

To increase the bioactivity of PEGDMA based hydrogels the introduction of bioactive factors was analysed. A series of high-throughput tests combining three drugs (N-acetyl cysteine (NAC), Ibuprofen (Ibu) and Progesterone (Prog)) were carried out to pick the most synergistic three-drug combination to boost cellular proliferation in PC-12 and Schwann cells. Ultimately concentrations of 75 µM NAC, 16.25 µM Ibu and 30 µM Prog were selected. Following this, a study to determine the rates of NAC, Ibu and Prog release from PEGDMA-DiPETMP found that drug release was completed after 1, 3 and 21 days respectively. In the final section of this thesis, attempts were made to control the 3D architecture of the final composition, leading to a combination of PEGDMA, DiPETMP, Bioglass and the drugs NAC, Ibu and Prog (PEGCombo) being prepared via UV chamber polymerisation. Its properties were monitored over a 28 day period, ultimately it was determined that further adjustments to PEGCombos composition were needed to enhance its potential use as a nerve guidance conduit.

Abbreviations

μg	Microgram
μM	Micrometre
3D	Three dimensional
Akt	Protein Kinase B
ATR-FTIR	Attenuated total reflectance Fourier transform infrared spectroscopy
C=C	Carbon-Carbon double bond
cAMP	Cyclic adenosine monophosphate
cm	Centimetre
DiPETMP	Dipentaerythritol hexa(3-mercaptopropionate)
DMEM	Dulbecco's modified eagle's medium
DSC	Differential scanning calorimetry
E	Young's modulus
EDX	Energy dispersive X-ray
ERK	Extracellular signal-regulated kinases
ETTMP 1300	Ethoxilated-trimethylolpropan tri(3–mercaptopropionate) 1300
ETTMP 700	Ethoxilated-trimethylolpropan tri(3–mercaptopropionate) 700
FCS	Foetal calf serum
g	Gram
G'	Storage modulus
G''	Loss modulus
GDMA	Glycol dimercaptoacetate
GDMP	Glycol di(3–mercaptopropionate)
HA	Hyaluronic acid
HPLC	High performance liquid chromatography
Ibu	Ibuprofen
IGF	Insulin-like growth factor
Kow	Octanol-water partition coefficient
kPa	Kilopascal
LOD	Limit of detection
LOQ	Limit of quantification
mg	Milligram

ml	Millilitre
mm	Millimetre
MPa	Megapascal
mS	MilliSiemen
mV	Millivolt
Mw	Molecular weight
NAC	N-acetyl cysteine
NaOH	Sodium hydroxide
NSAID	Non-steroidal anti-inflammatory drugs
PAM	Polyacrylamide
PBS	Phosphate buffered saline
PCL	Poly-E caprolactone
PCL4MP	Polycaprolactone tetra(3–mercaptopropionate)
PCLEEP	Polycaprolactone-coethyl ethylene phosphate
PEG	Poly- ε-caprolactone
PEGBio	Polyethylene glycol dimethacrylate-Bioglass composite
PEGDA	Polyethylene glycol diacrylate
PEGDMA	Polyethylene glycol dimethacrylate
PETMA	Pentaerythritol tetramercaptoacetate
PETMP	Pentaerythritol mercaptopropionate
PGA	Polyglycolic acid
PI3K	Phosphatidylinositol 3-kinase
PKA	Protein kinase A
PLA	Polylactic acid
Prog	Progesterone
PVP	Polyvinylpyrrolidone
Ras	Guanosine nucleotide binding protein as part of Ras superfamily
Rho	Guanine nucleotide binding protein as part of Ras superfamily
ROK	Rho associated kinase
RSD	Relative standard deviation
SC	Schwann cells
SDS	Sodium dodecyl sulphate
SEM	Scanning electron microscopy

S-H	Sulphur-Hydrogen bond
SLA	Stereolithography
STAT-3	Signal transducer and activator of transcription 3
TEMPIC	tris[2–(3–mercapto- propionyloxy) ethyl]isocyanurate
Tg	Glass transition temperature
Tm	Melting temperature
TMPMP	Trimethylol-propane Tri (3–mercaptopropionate)
TPO	Diphenyl(2,4,6-trimethylbenzoyl)phosphine oxide
UV	Ultraviolet
Wd	Weight dry
Wredry	Weight redried
Ws	Weight swollen
ZIP	Zero interaction policy
δ	Delta score
Ω	Resistance (Ohms)

Table of contents

Contents

List of Figures

List of Tables

Research Context

Peripheral nerves are complex, multi-component structures, which allow sensory, motor, or autonomic function. These nerves may be damaged by trauma, infection, cancer, metabolic conditions, immune dysfunction, or genetic disorders. Over 1 million surgical procedures are conducted in Europe and the USA every year, and the current global market is estimated to be worth over €6M per annum. The method of surgical intervention employed is classified according to the length of the gap needed to be bridged and is divided into three categories no-gap/short gap (< 1cm), small gaps (1-3 cm) and large gaps (>3 cm). For gaps less than 1 cm, surgical reconnection is possible by suturing whereas allografts and autografts are employed in small gaps. For gaps greater than 3 cm, there is no device that completely restores function. Allografts promote inferior repair to autografts, giving pain and repeat surgeries, thus autografts are the current gold standard. Autografts do not solve the problem of complete functional recovery completely with limitations such as supply of donor nerves, donor site morbidity, scarring at the donor site, nerve mismatch at the injury site, and failure rates of up to 50% reported. Consequently, patients suffer pain, numbness, loss of sensory function, muscle atrophy and problems with movement, fatigue, and depression. Therefore, there is a real clinical need to develop an alternative with improved functional outcome for damaged peripheral nerves.

Research Questions

The initial question at the outset of this project was - *how to develop peripheral nerve guidance conduit capable of replacing the current gold standard for large gap peripheral nerve injuries?* With this question in mind a thorough review of the literature was conducted, upon which, the materials properties of the current state of the art polymeric devices were compared to the materials property requirements required for peripheral nerve repair leading to the identification of 5 main attributes to develop namely mechanical strength, electrical signalling, degradability, biological signalling, and controlled architecture. To date, no existing implants on the market have been capable of fulfilling each of these properties.

Research Aims

The main aims of this study focused on producing a novel nerve guidance conduit capable of improving on autografts for the repair of peripheral nerves with a gap greater than 3 cm. To this end several key properties were identified and assessed based on expert reviews as being necessary for the formation of an ideal nerve guidance conduit, these include:

- Mechanical properties

- Electrical conductivity

- Biodegradability

- Controlled biological signalling

- Complex 3D architecture

Research Objectives

Each Chapter in this thesis has a primary objective which works towards allowing the final nerve guidance conduit to possess one of these properties.

The initial aim of this study was to examine the stability of a range of PEGDMA hydrogels over a 28-day period in simulated physiological conditions. PEGDMA (600 MDa) hydrogels were prepared with four different monomer concentrations (25, 50, 75 and 100 wt. % PEGDMA) in water and cross-linked via photopolymerisation. Upon examination of the swelling characteristics, the materials properties were examined after 2-, 14- and 28-days immersion in physiological solutions at 37°C.

↓

After the identification of the ideal weight percentage of PEGDMA, PEGBio composites were prepared (0.5, 1, 1.5, and 2.5 wt. % PEGBio) using Bioglass45S5 to improve the mechanical strength and electrical conductivity of PEGDMA. Following crosslinking the materials properties were again determined. This led to the selection of the 2.5 wt. % PEGBio as the ideal sample with which biological factors could be added.

↓

Following the selection of the ideal PEGBio wt. % an initial selection of ten thiol based monomers were copolymerised with PEGDMA in 1:1 thiol to ene ratios, and were characterised to determine the ideal copolymer for peripheral nerve repair. Following selection, the rates of degradation were determined for the Dipentaerythritol mercaptopropionate (DiPETMP) based copolymer in comparison to a pure PEGDMA hydrogel used as control.

↓

To assist the natural repair processes of the peripheral nerve repair potential synergies produced by combining NAC, Ibu and Prog were identified by treatments carried out on the cell lines

RT4-D6P2T (Schwann) and PC-12 (Rat adrenal gland). With synergy finding software utilised to identify synergies. With the aim of determining the release rates of these drugs from PEGDMA-DiPETMP hydrogels a novel HPLC process was developed which could separate, identify, and quantify the rates of release for each drug through the adaption of pre-existing USP methods.

A study of the impact SLA had on the properties of PEGDMA was carried out to determine whether SLA would negatively impact the overall properties of the peripheral nerve guidance conduits. Following this the project looked at the preparation of a PEGDMA based hydrogel, which incorporated the different properties determined in the previous sections. To this end, a PEGDMA-DiPETMP based hydrogel containing 2.5 wt. % bioglass and a synergistic combination of NAC, Ibu and Prog was prepared by UV chamber polymerisation. This hydrogels' material properties were then characterised as per previous sections.

Project Output

Papers

- *Burke G., Barron V., Geever T., Devine D., Geever L., Higginbotham C.* (2019) Journal of the mechanical behaviour of biomedical polymers, volume 99, page 1-10, (IF 3.485)* **Evaluation of the Materials Properties, Stability and Cell Response of a Range of PEGDMA Hydrogels for Tissue Engineering Applications**

- *Burke G., Cao Z., Devine D., Major I.* (2019) Polymers special issue "Polymers in Biomedical engineering", volume 11, (IF 3.164)* **Preparation of biodegradable Polyethylene glycol dimethacrylate hydrogels**

- *Burke G., Devine D., Major I.* (2020) Polymers special issue "3D and 4D Printing of (Bio)Materials", volume 12, (3.426)* **Effect of Stereolithography 3D Printing on the Properties of PEGDMA Hydrogels**

- *Burke G., O'Donnell C., Devine D., Major I.* (in preparation)* **Drug release from a degradable PEGDMA based polymer**

Posters and Presentations

- *Burke G., Bennett J,. Barron V., Higginbotham C.* Bioengineering in Ireland (BINI) 2014 (Poster and presentation) **Developing a Deeper Understanding of the Materials Properties of Polyethylene Glycol Dimethacrylate (PEGDMA) Hydrogels for Tissue Engineering Applications**

- *Burke G., Killion J.A., Pilkington L., Geever L.M., Lyons J.G., McCullagh E., Barron V., Higginbotham C.* Bioengineering in Ireland (BINI) 2015 (Poster and presentation) **Controlled Release of Anti-Inflammatory Drugs from Chemically Cross-linked Hydrophilic-Hydrophobic polymers**

- *Burke G., Devine D., Barron V., Major I. 1st annual* AIT research series 2018 (Poster) **Evaluation of the mechanical and thermal properties of thiolated-PEGDMA**

- *Burke G., Devine D., Barron V., Major I. 3rd Annual 3D Printing & Bio-printing in Healthcare Conference 2019 (Poster)* **Comparison of the material properties of conventional and Stereolithography polymerised PEGDMA hydrogels**

- *Burke G., Devine D., Barron V., O'Donnell C., Major I. 2nd annual* AIT research series 2019 (Poster) **Evaluation of drug release rates in thiolated-PEGDMA hydrogels**

Book chapters

- *Crowley E., Dalton M., Burke G.,* Bioresorbable polymers (2017) **Cytotoxicity and Biocompatibility of Bioresorbable Polymers** De Gruyter pp.1-14

- *Burke G., Dalton M., Hocter E., Geever L., Major I., Devine D.* Bioresorbable polymers (2017) **Biodegradation and Biodegradable Polymers** De Gruyter pp.101-117

Chapter 1

Literature Review

1.0 Literature review

This PhD thesis looks to highlight the need for the development of a novel treatment of peripheral nerve injuries. The topics being discussed include the makeup of peripheral nerves, the ease with which they can become damaged and the limitations of self-repair. Subsequently the current surgical treatments, state-of-the-art in the field will be discussed and then the logic behind the different factors which influenced the choice of polymer and additives throughout this study will be highlighted.

1.1 Peripheral nerve

1.1.1 Peripheral nerve damage

The nervous system can be divided into the subsections of the central nervous system and the peripheral nervous system. The central nervous system consists of the brain and the spinal column with the spine being subdivided into five distinct regions, the cervical, thoracic, lumbar, sacral and coccyx regions (Hynes, 2013). From within these groupings, spinal nerve pairs emerge and spread throughout the body. There are eight cervical, twelve thoracic, five lumbar, five sacral and one coccygeal nerve pairings, each spinal nerve is then associated with being either an efferent ventral or afferent dorsal root nerve. Efferent neurons act as the motor neurons which carry impulses from the brain to the peripheral nervous system, the afferent neurons act as the sensory neurons, carrying electrical impulses from the peripheral nervous system into the central nervous system and on towards the brain.

The nerves that make up the central nervous system are well protected through a combination of several factors, these include the skull protecting the brain, the spinal column segments protecting the spinal cord and the meninges, a triple layered membrane which protects both the brain and spinal cord. It is no surprise then that injuries to the spinal column can be quite rare in comparison to peripheral nerve injuries with 275,000 people suffering from spinal cord injuries within the US (Shoichet *et al.*, 2008) 0.09% of their total population, with a further

10,000 cases documented each year (Carlson and Gorden, 2002). This is compared with peripheral nerve injury which is a common global illness, affecting over 300,000 people in Europe and being shown to affect up to 1.5% of the general populace in the US (J *et al.*, 1998; Taylor *et al.*, 2008).

Peripheral nerves are made up of multiple parts, there are the protective layers (working from the outside in) the epineurium, the perineurium and the endoneurium (Griffin *et al.*, 2013; Vijayavenkataraman, 2020). The epineurium is a dense irregular connective tissue which encloses the entire peripheral nerve and protects against outer stresses and is composed mostly of the basal lamina and other connective tissues. Inside the epineurium the perineurium wraps around fascicles (bundles of nerve fibres) separating and insulating them from one another, within these fascicles the endoneurium is surrounded by the endoneurial sheath and a myelin sheath (Grinsell and Keating, 2014). Schwann cells produce the myelin which is wrapped multiple times around a specific length of the nerve separated by the nodes of ranvier into internodes. Sheaths both protect and insulate the axons as they carry electrical signals to and from the brain (Frostick, Yin and Kemp, 1998; Liu *et al.*, 2019). Figure 1.1 shows there is also connective tissue and blood vessels in the peripheral nerve makeup. These nerve cells consist of a cell body, dendrites to carry electrical signals to the cell and axons to carry signals away from the cell.
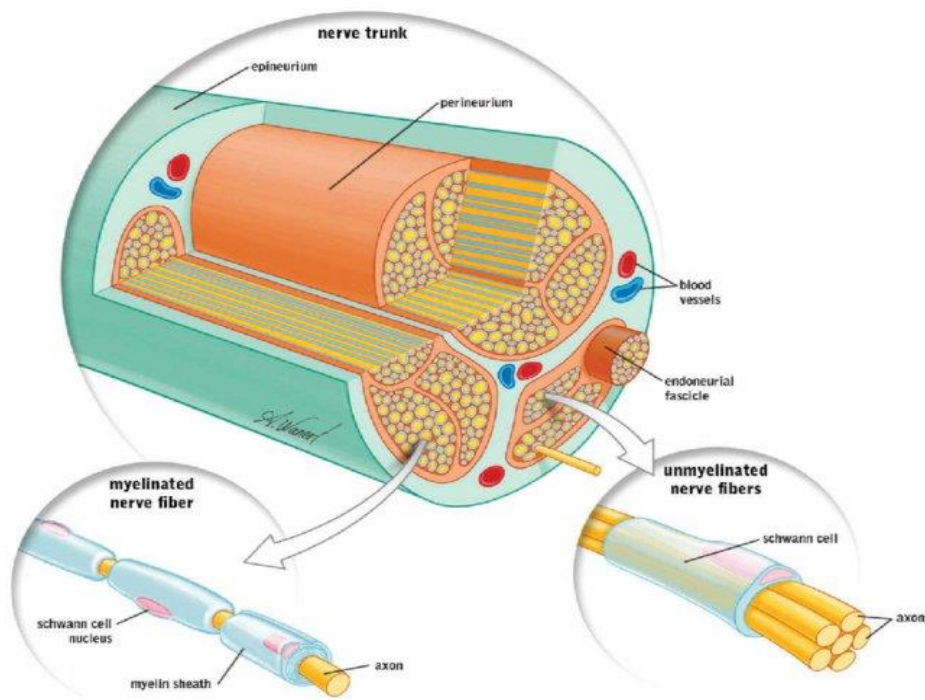
Figure 1-1 A *labelled cross-section of the anatomy of a peripheral nerve printed as illustrated by* (Ilfeld, Preciado and Trescot, 2016) *with permission from Pacira biosciences.*

There are a number of reasons for peripheral nerve injury, the most common being traumatic events such as open fractures, nerve crushing or through accidental severing in surgical procedures (Ryu, Beimesch and Lalli, 2011) but peripheral nerve injury can also be caused by degenerative illnesses such as diabetes (Kiziltan *et al.*, 2007; Mauricio, Alonso and Gratacòs, 2020), maintained vibrations in the construction industry (white finger) and immune disfunction (Willison, Jacobs and van Doorn, 2016). Following injury, the central nervous system and peripheral nervous system have varied repair mechanisms. Repair within the central nervous system is extremely limited, typically resulting in low percentage chance of functional recovery, whereas the peripheral nervous system (especially if the gap between severed nerves is small (<5mm)) possesses the potential to re-extend and re-innervate resulting in at least a partial recovery of function. However complete recovery is highly unusual (Salgado *et al.*, 2013) with peripheral nerve repair often resulting in patients experiencing pain, having an inability to grip objects and ultimately muscle atrophy. An ever-growing percentage of the populace are living with nerve injuries, resulting in upwards of 1 million treatments

internationally each year (Bringing the science of nerve repair to life, 2013). There is an imperative to efficiently treat peripheral nerve injury.

The modern incarnation of peripheral nerve injury classification originated with Seddon in the early forties (Seddon, 1943). This classification focused on differentiating nerve injuries into permanent injuries ((i) neurotmesis) and temporary injuries, (ii) neurapraxia (iii) axonotmesis). This version of classification, although a vast improvement on what went before was found to be lacking by the leaders in the field of the time (Sunderland, 1951). Subsequently, this characterisation was improved upon by dividing the axonotmesis category into three separate degrees of injury based on the degree of damage to the endonuerium and perineum resulting in a version of peripheral nerve injury classification very similar to the one utilised today (Sunderland, 1951).

As outlined by the work of (Ryu, Beimesch and Lalli, 2011), Sunderland first degree injuries result in neurapraxia, a loss of function while maintaining the axons continuity, as the axons basic structure remains undamaged with a good clinical prognosis of complete recovery following treatment in 3 to 4 months. From second degree injuries onwards as a result of axonal damage, Wallerian degradation is present in all cases of peripheral nerve injury (Chhabra *et al.*, 2014). In second degree to fourth degree injuries (known as axonotmesis) neurapraxia is compounded by additional damage to peripheral axons while connective structures remain intact. In second degree injuries the endoneurial sheath and Schwann cells are left intact, leading to a good clinical prognosis for full functional recovery although at a slower pace than that of first degree injury (recovering at a max rate of 1mm/day) (Chhabra *et al.*, 2014).

Third degree injuries occur when the endoneurium is disrupted but the perineurium is left intact, these injuries can cause fibrosis to occur intra-fascicularly. As such third degree injuries typically result in a clinical prognosis of extremely delayed return of both motor and sensory

function, furthermore the return of function never matches pre-injury levels (Sunderland, 1951). In fourth degree Injuries the clinical prognosis is even worse, if there is to be any return of motor or sensory function surgical intervention is required. In fourth degree injuries the perineurium and endoneurium have been severed, with only the epineurium remaining intact. The untreated clinical outcome of these injuries is increased scarring and more advanced degeneration of the proximal stump (Chhabra *et al.*, 2014). The last classification outlined is fifth degree injury, this injury type occurs when there is a complete severance of the epineurium resulting in neurotmesis. This injury type leads to the most advanced scarring in nerves, resulting in a neuroma at the proximal end of the cut and Wallerian degeneration at the distal end (Chhabra *et al.*, 2014). More recently the addition of a sixth category has led to a classification system similar to the one shown in Table 1-1.

Table 1-1 Modern classification system for peripheral nerve injury as taken with permission from (Chhabra *et al.*, 2014)

Degree of nerve injury	Myelin	Axon	Endo-neurium	Peri-neurium	Epi-neurium	Tinel sign	MRN (signal intensity)	Recovery potential	Rate of recovery	Surgery
I Neurapraxia	±					No	Nerve-incr T2 SI Muscle-Normal	Full	Upto 12 weeks	None
II Axonotmesis	Yes	Yes	No	No	No	Yes	Nerve-incr T2SI and diffusely enlarged Fascicles-enlarged or effaced due to edema Muscles-denervation	Full	1mm/day	None
III	Yes	Yes	Yes	No	No	Yes		Usually slow, incomplete	1mm/day	None or Neurolysis
IV NIC-neuroma in continuity	Yes	Yes	Yes	Yes	No	Yes but no advancement	Nerve-focally enlarged with heterogeneous SI. Underlying diffuse abnormality ± Fascicles-disrupted with heterogeneous SI-NIC Muscles-denervation	Poor to none	Poor to none	Nerve repair, graft or transfer
V Neurotmesis	Yes	Yes	Yes	Yes	Yes	Yes but no advancement	Complete nerve discontinuity ± hemorrhage and fibrosis in the nerve gap and end-bulb neuroma proximally. Epineurial thickening Muscles-denervation	None	None	Nerve repair, graft or transfer
VI Mixed injury (I to V)	Variable combination of above across the cross section of the nerve					Some fascicles (II, III)	Variable findings along the circumferential segment of the nerve (I-V) with heterogeneous SI due to fibrosis Muscles-denervation	Variable, can be poor to none	Variable, depends upon the injury (I-V)	Neurolysis, Nerve repair, graft or transfer

MRN: Magnetic resonance neurography, SI: Signal intensity

1.1.2 Peripheral nerve repair

During the first number of days following peripheral nerve injury, myelin and the axon will breakdown both proximal and distal of the nerve injury. Retrograde degeneration can result in degeneration of several millimetres (mm) up to centimetres (cm) following injury. Further, there can be a possible loss of axonal diameter dependent on the time taken for functional connections to be re-established.

Over the subsequent days to weeks these alterations to the proximal nerve fibre are associated with chromatolytic changes to the neuronal cell body (dissolution of nissl bodies of the neuronal cell) and are a sign that the metabolic activity of the neuron has shifted away from a neurotransmission focus to a focus on regenerating axonal sprouts and growth. This focus continues until functional connections have been re-established in the periphery. In the distal segment of the nerve, Schwann cells and infiltrating macrophages begin the process of clearing myelin, tissue and axonal debris in the organised pattern of anterograde changes associated with Wallerian degeneration (Stoll, Jander and Myers, 2002).

In the following weeks to months once the debris has been fully removed, several axonal sprouts will begin to grow, crossing the site of injury. Some of the axonal sprouts will enter the correct endoneurial tubes (Haftek and Thomas, 1968; Nguyen, Sanes and Lichtman, 2002) using the aligned bands of Bungner as a substrate for regeneration and proceed to extend at a rate of between 1-3mm/day (Ide, 1996). During this period of time the target muscle atrophies due to a lack of use, the greater the time taken to re-innervate the more atrophied the muscle becomes.

1.1.3 Properties of the peripheral nerve

As discussed above the stages of peripheral nerve injury are extensive, to prepare a treatment for peripheral nerve damage it becomes necessary to understand the properties that must be replicated by a peripheral nerve device. The peripheral nerve is a complex structure that is made up of nerve fibres, connective tissues, and blood vessels. These three distinct tissues will have different reactions to external factors such as compressive or tensile stresses. Thus, the focus of our work will primarily be on the properties of nerve fibres and the properties of nerve fibres and their replication.

Nerve fibres start to present structural abnormalities in 20% of distal and 30% of proximal nerve fibres at a maintained compressive strength of 6.66 kilopascals (kPa) (Dyck *et al.*, 1990) for a period of just 2 minutes. Based off this, a minimal strength of 6.5 kPa would appear to be desirable for any potential nerve conduits. This work did not however give an indication as to how these rates compared to structural abnormalities in non-stressed nerve fibres. In contrast to the work conducted by (Dyck *et al.*, 1990), it was found by (Kwan *et al.*, 1992) that a rabbit tibial nerve recorded an ultimate mechanical stress of 11,700 kPa (11.7 MPa), indicating that mechanical properties of peripheral nerves can differ from species to species greatly. As such mechanical properties of a nerve guidance conduit should be tailored species to species or even person to person.

Based on this research it can be concluded that for the protection of the recovering nerve an ideal nerve guidance conduit should have a compressive strength falling in the range of 1 MPa to 12 MPa. Research conducted by others however found that increasing gel stiffness had an adverse effect on neurite outgrowth (Balgude *et al.*, 2001; Flanagan *et al.*, 2002) indicating a preference for growth on softer gels. This would lead to gels needing to be on the softer end in terms of the compressive strength unless they are in contact with suitable support cells to help induce axonal growth (Georges *et al.*, 2006) making gels closer to the 1 MPa compressive

strength range more desirable than the 12 MPa range. Focusing on tensile strength Rydevik et al. (Rydevik *et al.*, 1990) found that the tensile strength of peripheral nerves were similar to their compressive strengths, with deformation occurring once tensile stress moves beyond 0.5 MPa and reaching ultimate tensile strengths of 11,700 kPa (11.7 MPa). This was backed up by the work of (Borschel *et al.*, 2003) who found the ultimate tensile stress of fresh whole rat peripheral nerve to be 1,400 kPa (1.4 MPa) whereas that of a repaired nerve was 780 kPa (0.78 MPa) indicating that ideally the tensile strength of samples would fall in the range of 0.5 to 12 MPa range nearly mirroring compressive strength, preferably on the lower end of the strength range.

Mechanical properties are one of the key factors which must be considered for the successful re-innervation of a peripheral nerve, there are numerous other factors including physical guidance, electrical properties, biological cues, and porosity which must be considered when preparing a nerve guidance conduit. In Table 1-2 these properties are shown along with the currently held views as to what property would constitute the ideal nerve guidance conduit can be seen.

Table 1-2 The key materials properties and their requirements for the preparation of an ideal nerve guidance conduit

Materials properties	*Materials property requirement*
Physical guidance	Physical cues are required for modulating axon alignment, diffusion of growth factors secreted by the injured nerve ends, reduction of scar tissue infiltration and functional repair (Schmidt and Leach, 2003; Schlosshauer *et al.*, 2006; W. T. Daly *et al.*, 2012; Gu, Ding and Williams, 2014).
Mechanical properties	Need to match mechanical properties of native peripheral nerves (Nectow, Marra and Kaplan, 2012) (Viscoelastic, with ultimate tensile strength values of 11.7 MPa at 38% elongation previously reported (Topp and Boyd, 2006; Nectow, Marra and Kaplan, 2012)). Strike a balance between rigidity and flexibility (Topp and Boyd, 2006; Nectow, Marra and Kaplan, 2012).
Electrical properties	Transmit electrical signals, enhance neurite extension. Electrical conductivity in the range 5 mS/cm (Collier *et al.*, 2000; Runge *et al.*, 2010; Moroder *et al.*, 2011; Huang *et al.*, 2012; Hardy, Lee and Schmidt, 2013; Gu, Ding and Williams, 2014; Xu, Jeremy M Holzwarth, *et al.*, 2014)
Biological cues	Enhance cell response and promote axon alignment through the use of biological factors(Collier *et al.*, 2000; Baier Leach *et al.*, 2003; Leach *et al.*, 2004; Seidlits *et al.*, 2010; Khaing *et al.*, 2011; Suri *et al.*, 2011; Anandagoda *et al.*, 2012; Khaing and Schmidt, 2012)
Degradation	Nerve regeneration in a 10 mm nerve gap using a physical guidance conduit takes approximately 28 days, with blood, growth factors and proteins filling the tube and forming fibrin cables in the first week, protein migration through the fibrin cables in the second week and guided axon alignment along the fibrin cables in the 3rd and 4th weeks(Schmidt and Leach, 2003). Conduit degradation should ideally not occur during this initial repair period. Biodegradable materials have been shown to be better than non-degradable materials due to long-term concerns about nerve compression (Schmidt and Leach, 2003; de Ruiter *et al.*, 2009). Need to avoid swelling during degradation (Nectow, Marra and Kaplan, 2012).
Biocompatibility	Provide functional mechanical support without provoking an adverse inflammatory response during conduit degradation process (Nectow, Marra and Kaplan, 2012; W. Daly *et al.*, 2012). Reduce neuroma and scar tissue formation (Schlosshauer *et al.*, 2006; de Ruiter *et al.*, 2009; Nectow, Marra and Kaplan, 2012).
Porosity and permeability	Wall thickness of 0.6 mm, porosity of 80% and pore size ranging between 10–40 µm have been shown to improve nutrient diffusion and reduce neuroma formation (Kehoe, X.F. Zhang and Boyd, 2012).
Handling and Suturing	Easy to handle and fit without adverse swelling during degradation. Mechanical properties of the conduit should allow the incorporation of sutures to attach its proximal and distal nerve segments (Schlosshauer *et al.*, 2006)
Sterilization	Readily sterilizable without adversely affecting structure or properties of conduit
Fabrication	Readily scalable for reproducible, reliable manufacturing

1.1.4 Current surgical treatment

The first documented repair of peripheral nerves occurred over 400 years ago, therefore the treatment of peripheral nerve injury is not a new process (Evans, 2001). At present the gold standard for peripheral nerve repair with a gap greater than 5 mm is the autograft, a technique involving the extraction of a nerve from a donor site (typically sural) and insertion into the gap between the nerve ends providing a smaller gap for nerves to re-innervate. The sural nerve has typically been used due to its relative lack of importance and that it can provides up to 40 cm of peripheral nerves if taken from both legs (Palispis and Gupta, 2017). Although it has been the gold standard of peripheral nerve repair for over 50 years, autografts have several drawbacks such as the need for multiple surgeries, the loss of function at donor sites and a success rate of only 50 % (W. Daly *et al.*, 2012). As such there have been ongoing attempts to replace nerve autografts as the principal method of peripheral nerve repair, leading to research into areas such as xenografts (nerve graft from a different species), allografts (nerve graft from a non-identical member of the same species), Isografts (nerve graft between genetically identical members of the same species), nerve wraps and nerve guidance conduits. Each of these techniques have their own drawbacks for example allografts which have the benefit of a single patient surgery site and a success rate comparable to autografts, are more likely to cause neuroma formation than autografts and also requires temporary immunosuppression (Ray and Mackinnon, 2010). Xenografts which have a ready supply of nerve donors run into the issue of increased likelihood of donor rejection as well as the possibility of cross species disease transfer (Arslantunali *et al.*, 2014). Whereas isografts which are almost never rejected and do not require immunosuppression, require the presence of a genetically identical donor i.e.: a monozygotic twin, therefore making isograft application extremely limited.

Due to these known drawbacks associated with the various grafts available current research in peripheral nerve repair has been most active in the development of nerve wraps and nerve

guidance conduits (Pfister *et al.*, 2011). Nerve wraps act as a protective cover for damaged peripheral nerves, providing an interface between the nerve and surrounding tissue. Nerve wraps are advantageous in the sense that they form a semi-permeable membrane around the injury site allowing the passage of small molecules such as metabolites, water molecules and nutrients, while preventing the transfer of larger molecules such as neurotrophic factors (INTEGRA, 2005). However, they have been shown to lack the ability to induce functional recovery in injuries greater than 1 cm, nerve guidance conduits on the other hand provide a sealed environment that facilitates the growth of peripheral nerves. These devices have the benefit of providing a method to deliver different factors which are essential for axonogenesis and myelinogenesis, having been used to deliver multiple neurotrophic factors in the past. Nerve wraps and nerve guidance conduits scope in the market of peripheral nerve treatment is large, at present the number of nerve guidance conduits and wraps developed and tested in human and animal models is large, with 10 having achieved FDA approval (Kehoe, X. F. Zhang and Boyd, 2012; Gaudin *et al.*, 2016). Despite their widespread use they have not been capable of replacing autografts as the gold standard of peripheral nerve repair. This comes down to both the clinical outcome and the limitation in nerve gap length. At present no nerve guidance conduit or nerve wrap possesses a better clinical outcome than that provided by autografts, further there is no FDA approved nerve guidance conduit or nerve wrap for the treatment of a nerve gap greater than 3 cm in length.

1.2 Current state in research for peripheral nerve repair

Section 1.1.4 outlined why there is a demand for a product in the peripheral nerve repair market which is not faced with the limitations currently present in FDA approved products. There is a need for a peripheral nerve conduit/wrap with a greater efficacy than that produced by nerve autograft and provides a viable option for the treatment of peripheral nerve gaps greater than 3 cm in length. The aim of this project is to develop a polymer construct, which meets this currently unmet need in the peripheral nerve repair market.

There is a consensus on the factors which make up an ideal nerve guidance conduit/wrap, it is felt that the limitation in the aforementioned products is due to their inability to meet one or more of these criteria. Due to its inherent need to be placed into the body in contact with both the damaged nerve and its surrounding tissues, the first property a nerve guidance conduit should possess is biocompatibility. Biocompatibility in nerve guidance conduits refers to the ability to act as a scaffold capable of creating an enclosed environment supporting reinnervation of the nerve without causing undesirable effects such as inflammation or haemolysis.

To improve biocompatibility, mechanical strength must match closely with native peripheral nerve tissue (0.05 MPa in situ and 11.7 MPa at break) (Dyck *et al.*, 1990; Kwan *et al.*, 1992) nerve guidance conduits replace lost nerve tissue and as such must be capable of handling mechanical strains nearing the levels associated with typical nerves. Further, there needs to be a certain level of flexibility associated with the nerve guidance conduit which allows for the bending of nerves and to prevent the nerve guidance conduit from dislocating from one end of the peripheral nerve. Nerve guidance conduits must also be electrically conductive (12 kOhm, (5mS/cm)) with much work being done to enhance tissue engineered materials conductivity (Gu, Ding and Williams, 2014; Park *et al.*, 2020). This alleviates a common issue with functional repair following injury is the lack of electrical stimulation posterior of the injury,

causing muscle atrophy, conductivity reduces this risk, allowing transfer of electrical signals for enhanced mobility and sensory capability post injury (Park *et al.*, 2020).

There are several other criteria to be met when achieving biocompatibility. A polymer needs to be controllably degradable, if a polymer is present and non-degradable it may be detrimental to the repair of nerves due to the constriction of the outwardly growing nerve or possibly through the leaching of toxic substances from the polymer. There is a need for controlled release of biological factors throughout the nerve repair process, with the aim of directing the nerve repair process and maximising cellular proliferation. To this end much research has been conducted with Catrina and Madduri et al. among others having made progress with the release of multiple neurotrophic factors namely NGF and GDNF using a combination of slow releasing silk fibroin and faster releasing collagen, whereas other researchers including Manoukian et al. have made further advancements gaining control of the release of voltage gated ion blocked channels blocker 4-Aminopyrridine through the incorporation of aligned microchannel matrixes wherein porosity controls rates of release. Others have looked to use the structure of polymers to control the rates of biodegradation and thereby control factor release, with Hong et al. using the controlled degradation of a multi-layered PLGA scaffold to create controlled release rates (Catrina and Madduri, 2013; Hong *et al.*, 2018; Manoukian, S. *et al.*, 2019).

Also, it is paramount to control the inner diameter of the nerve guidance conduits as well as its wall thickness. Thicknesses greater than 0.81mm significantly reduce axonal growth within the nerve guidance conduit with wall thicknesses falling in the range of 0.07 to 0.4mm being utilised by others to either match native tissues thicknesses or to maintain similarity to native mechanical properties (Belkas, Shoichet and Midha, 2004; Mobasseri *et al.*, 2015; Huang *et al.*, 2018).

Aside from the material that makes the scaffold, the scaffolds structure plays a critical role in determining the success or failure of peripheral nerve repair. The typical nerve guidance conduit is made of a tube with a single hollow lumen and plays no active role in restricting the growth of nerve. This leads to a randomised reinnervation which may not correctly attach the damaged nerve stumps (Brushart *et al.*, 1995); over longer distances this effect is exacerbated. To combat this effect much effort has been placed into developing more complex scaffolds. These more complex scaffolds mimic the design of nerve fascicles would have including multiple lumens to physically guide axonal regeneration reducing the degree of dispersion which is associated with axon regeneration and contain factors encouraging nerves to grow (Yao *et al.*, 2010). The addition of physical objects, such as fibres or filaments, to the inner lumen of a nerve guidance conduit is also considered as a possible factor in assisting nerve growth. When looking at short gaps, nerve stumps will produce fibres connecting each stump and stimulating reinnervation, over longer distances the fibres will not reach each other, the inclusion of artificial fibres/filaments could theoretically replicate this role (Wang *et al.*, 2009).

An additional factor which has been receiving attention in recent times is conduit porosity. If the conduit porosity can be accurately controlled, then there is potential to selectively limit the entrance of fibroblasts which have been shown to inhibit nerve regeneration and induce scar formulation at the nerve injury site (Chamberlain *et al.*, 2000; Atkins *et al.*, 2006). The outcomes of research in the study of porosity was initially mixed, with semi-permeable membranes (capable of preventing cells from entering, while allowing exchange of factors being shown to prevent the entry of fibroblasts, while simultaneously having decreased improvements to functional nerve recovery when compared to fully permeable membranes, indicating that it was possible that fibroblasts may have a beneficial impact on nerve repair (Kim *et al.*, 1993). This was later attributed to fibroblasts playing a role in enhancing the secretion of neuregulin, which in turn increased the migratory activity of schwann cells

(Dreesmann *et al.*, 2009). With this in mind and with further studies showcasing that semi-permeable membranes significantly enhanced nerve conduction velocity repair (an indicator of effective recovery from injury) when compared with fully permeable membranes, it could be seen that physical prevention of fibroblast migration through control of porosity would positively affect peripheral nerve repair (Chang *et al.*, 2009; Lackington, Ryan and O'Brien, 2017).

1.2.1 Hydrogels for peripheral nerve repair

Hydrogels are hydrophilic polymers which can be swollen while maintaining their water insoluble networks (Annabi *et al.*, 2014). Due to their high-water content hydrogels can mimic the properties of soft bodily tissues. This fact along with the ability to fine tune their properties, has led to their use in a number of fields including tissue engineered scaffolds (Islam *et al.*, 2016), drug delivery (Marcelo *et al.*, 2016), implantable devices (Nawrotek *et al.*, 2016), biosensors (Tan *et al.*, 2016) and materials controlling the activity of enzymes. Described as natural, synthetic or hybrid, hydrogels have been around since the 1950s and are extremely varied. They can be physically crosslinked by non-covalent methods, chemically crosslinked by covalent methods or crosslinked by a mix of both. This diversity strongly contributes to their usefulness in a wide variety of fields (Buwalda *et al.*, 2014). As was outlined above, with the realisation that degradable materials were a necessity for peripheral nerve repair the focus for nerve guidance conduits shifted towards degradable polymers such as hyaluronic acid (HA) and polyglycolic acid (PGA) (Peng *et al.*, 2018; Entekhabi *et al.*, 2021). Extensive research has been conducted in this area and at present the biomaterials which have been tested in animal and human models for use as nerve guidance conduits is extensive. These include the natural hydrogels collagen, chitosan, fibronectin, gelatin and Polycaprolactone-coethyl ethylene phosphate (PCLEEP) along with the degradable synthetics including PGA, poly- ε-caprolactone (PCL) and Polylactic acid (PLA) and also the non-degradable hydrogels such as

silicone (Chew *et al.*, 2007; Ding *et al.*, 2011; Gu *et al.*, 2012; Xie *et al.*, 2015; Almansoori *et al.*, 2020; Cheng *et al.*, 2020; Itai *et al.*, 2020; Ye *et al.*, 2020).

1.3 Material selection

In section 1.1.3 the compressive strength best suited to a nerve guidance conduit was highlighted to be in the 1 MPa to 12 MPa range, to achieve this range it was necessary to have a hydrogel which can easily manipulate its material properties while also having a straightforward fabrication process. With these criteria in mind this project looked to develop a nerve guidance conduit using polyethylene glycol dimethacrylate (PEGDMA), capable of repairing nerve gaps greater than 3 cm long.

1.3.1 PEGDMA

PEGDMA is uniquely positioned to treat peripheral nerve injury as its molecular weight and crosslinking density can be manipulated to alter its mechanical properties. Over the past twenty years, PEGDMA has found itself in a position of increasing prominence in biomedical applications, through the controlled variation of monomer molecular weight, water content and monomer concentration; it is possible to fine tune its materials properties for a range of applications including structural scaffolds, biodegradable drug delivery vehicles (enzymatic degradation) and cell carriers (Han and Hubbell, 1997; Cruise *et al.*, 1998; Lin *et al.*, 2005; Van De Wetering *et al.*, 2005). For tissue engineering applications, not only are the mechanical properties of the polymer important, the rate of degradation is also an essential consideration, as rapid degradation can lead to inflammation, inadequate mechanical support and poor tissue repair (Habibovic *et al.*, 2006; Barron *et al.*, 2015).

Over the past 20 years, photopolymerisable hydrogels have generated great interest as cell carriers, support structures and delivery vehicles for biological cargos (Cruise *et al.*, 1999; Hutmacher, 2000; Lee and Mooney, 2001; Khademhosseini and Langer, 2007; Van Tomme, Storm and Hennink, 2008; Bulman *et al.*, 2012; Zustiak *et al.*, 2013; Annabi *et al.*, 2014; Toh and Loh, 2014; Zhu, Ninh and Bettinger, 2014). Of particular interest are polyethylene glycol

(PEG) based hydrogels that can be rapidly crosslinked by free radical polymerisation in the presence of a biocompatible photoinitiator and ultraviolet (UV) light (Nguyen and West, 2002; Vernon *et al.*, 2003; Killion *et al.*, 2011; Bäckström *et al.*, 2012). Interestingly, these photopolymerised PEG hydrogels can be implanted preformed or UV cured *in situ* thereby allowing localised delivery of smaller doses of therapeutic agents with a reduced likelihood of systemic side effects (West and Hubbell, 1995).

Over the years, a range of PEG-based hydrogels have been developed with a range of different chemical linkages including glycolide, lactide, diacrylate, dimethacrylate and ε-caprolactone, these crosslinkages have allowed the degradation time of tissue-engineered scaffolds and the permeability of drug delivery vehicles to be tailored for specific applications (Han and Hubbell, 1997; Cruise, Scharp and Hubbell, 1998; Lin *et al.*, 2005; Van De Wetering *et al.*, 2005). Of special interest is polyethylene glycol diacrylate (PEGDA), which was originally developed by Hubbell *et al.* for the prevention of restenosis and wound repair post-surgery (Hill-West *et al.*, 1994; Sawhney *et al.*, 1994; Chowdhury and Hubbell, 1996). Since then PEGDA has been synthesized using a range of different monomers including acrylic acid, acrylamide and allylamide for drug delivery, cell carrying and tissue engineering applications (Sawhney, Pathak and Hubbell, 1993; Cruise *et al.*, 1998; Scott and Peppas, 1999; Mellott, Searcy and Pishko, 2001; Lee *et al.*, 2014). By varying the monomer concentration, molecular weight, crosslink density and water content, the polymer morphology, and mechanical properties of polyethylene dimethacrylate (PEGDMA) hydrogels can be modulated. Mechanical properties are of particular interest at this stage, having compressive modulus values of 26 MPa and 15 MPa for 100 weight percent (100 wt. %) and 75 wt. % samples which can more than match the limit at break of nerve tissue (Killion *et al.*, 2011).

Water molecules play an important role in the properties of these gels, providing free volume for chain mobility (LaPorte, 1997). Indeed, the polymer morphology and mechanical properties

post hydration are affected by chain configuration and network defects pre-hydration, as internal stress states within the chains can influence the degree of swelling and expansion (LaPorte, 1997; Wu *et al.*, 2010). Moreover, once hydrated, the polymer chains can move to accommodate changes in stress or biological gradients (Wang *et al.*, 2015).

1.4 Electrical conductivity

Although peripheral nerves have a relatively good capacity for recovery (compared to the central nervous system) the functional recovery of a damaged peripheral nerve is often inhibited by a lack of electrical stimulation distal of the site of injury causing muscle atrophy (Stoll and Muller, 1999; Caillaud *et al.*, 2019). This results in the peripheral neurons undergoing progressive decreases in their regenerative abilities as well as the Schwann cells in distal stump of the nerve losing their ability to support the regenerating axon (Elzinga *et al.*, 2015), these factors compound one another resulting in slow regrowth of the regenerating axons (Sulaiman and Gordon, 2013; Willand *et al.*, 2016).

To alleviate the impact a lack of stimulation has on peripheral nerve repair several studies have been carried out with the aim of increasing the electrical stimulation occurring at the site of nerve repair including the synthesis of electrically conductive polypyrrole-Poly(D, L-lactic acid) and preparation of carbon nanotubes interfaced phosphate glass microfibres (Xu, Jeremy M Holzwarth, *et al.*, 2014; Ahn *et al.*, 2015). These components with a conductance in the range of 1-15 mS/cm suffer a glaring limitation in their fabrication however, with both compositions requiring a 3-day preparation time, precluding their use for preparing a bespoke conduit to suit an individual patient post injury. PEGDMA samples are electrically inert, with the aim of maintaining ease of fabrication while enhancing the conductivity of PEGDMA we identified boron-doped electroactive bioglass as a potential source of enhanced electrical conductivity and set out to achieve a conductance in the range of 5 mS/cm.

1.4.1 Use of Bioglass for peripheral nerve repair

The use of electroactive bioglass for the purpose of peripheral nerve regeneration was first highlighted as a proof of concept more than 10 years ago (Bunting *et al.*, 2005). It was demonstrated that fibres of bioglass could provide a biocompatible and bioresorbable scaffold that supports axonal regeneration across 0.5 cm gaps in the sciatic nerves of adult male Wistar rats. Further, the results of this study showed bioglass filled nerve conduits to have regrowth rates comparable to the industry gold standard nerve autograft and much greater than the results found for the empty nerve conduit or the untreated groups. Since then, there have been several examples of polymer/bioglass composites for the purpose of peripheral nerve repair. Nerve guidance conduits were prepared by rolling glass microfibers into compressed collagen, when compared with the controls of cover slips coated in poly-D-lysine and laminin, the collagen/bioglass conduits produced increased neurite outgrowth and axon sprouting when seeded *in vitro* with dorsal root ganglion cells (Kim *et al.*, 2012).

Others utilised nano-bioglass and microbiology grade gelatin to produce a nano bioglass/gelatin conduit which was shown to be biocompatible, having cell viability results comparable to untreated Chinese Hamster Ovary (CHO) cells *in vitro* and after a period of one month were shown to be capable of repairing a 10 mm nerve gap in adult male Wistar rats (Koudehi *et al.*, 2014). As of yet no polymer/bioglass composites has received FDA approval, bioglass itself however is FDA approved, having been used for years in numerous tissue engineering fields, including orthopaedic implants, dental fillings and angiogenesis (Miguez-Pacheco, Hench and Boccaccini, 2015). In this study tailor-made calcium doped boron bioglass particles were prepared by world-leading bioglass experts in Dalhousie University in Canada. The study of the impact this custom made electroactive bioglass has on the electrical conductivity of the base PEGDMA polymer will be discussed further in section 4.0.

1.5 Degradability

As non-degradable materials inhibit nerve repair, research for the nerve guidance conduits switched to the use of degradable materials such as HA (natural) and PGA (synthetic). The degradation process must be controllable as rapid degradation undermines the structural integrity of the nerve guidance conduit leaving regenerated axons unprotected whereas regeneration that is too slow can result in nerve compression or possibly chronic immune response (Schmidt and Leach, 2003; Ciardelli and Chiono, 2006; de Ruiter *et al.*, 2009).

There are many well-known natural polymers which are readily degradable however a common limitation of synthetic polymers is their lack of degradability (Pathak and Navneet, 2017). As degradation of biomaterial scaffolds is a critical factor in successful tissue regeneration, it is imperative for the degradation rate to be a prime consideration. Several issues can arise if the rate of polymer degradation is not correctly controlled; if the degradation rate is too slow, it can impair tissue repair, whereas there is an increased likelihood of inflammation if the degradation rates are too fast (Ifkovits and Burdick, 2007). Many different approaches are currently being employed to improve degradation rates such as copolymerisation with degradable natural polymers and the addition of biodegradable peptide linkages (Patterson and Hubbell, 2010). However, these methods suffer from limitations, including increased immunological responses, as well as poor mechanical performance (Nair and Laurencin, 2007). PEGDMA is well known to suffer the limitations common to many synthetic polymers not breaking down over a biologically relevant timeframe, the present study identified thiol (Sulphur-Hydrogen bond (S-H) containing) monomers as potential components for enhancing the degradability of PEGDMA.

1.5.1 Thiol-ene chemistry

Thiols readily react with the carbon-carbon double bond (C=C) found in PEGDMA and other similar hydrogels to form a thiol-ene. Thiol-ene reactions have been well studied in the past (Morgan, Magnotta and Ketley, 1977; Cramer *et al.*, 2003; Zhou *et al.*, 2013) and function on the premise of a thiol (S–H) group readily reacting with a C=C bond to form a thio-ether (this is shown in Figure 1-2, where a PEGDMA-based hydrogel has been incorporated with dipentaerythritol hexa(3–mercaptopropionate) (DiPETMP)). There are several key advantages to the use of thiol-ene reactions, most importantly thiol-based monomers have been shown to improve the degradation rates of several PEG-based hydrogels synthesised from PEGDA, PEG-PLA and PEG-Norbornene (Rydholm, Bowman and Anseth, 2005; Aimetti, Machen and Anseth, 2009; Manzo and Ioppolo, 2015). The process of thiol-ene degradation having been well-defined, operate as a pseudo-first-order degradation process through the hydrolytic degradation of the ester linkage, meaning under ideal circumstances (where ester hydrolysis is the only factor that affects degradation) then the change in degradation time is directly proportional to the increase in OH ions. i.e.: a 10 fold increase in OH ions would produce a 10 fold increase in the rate of degradation (Shih and Lin, 2012).

Of note when undergoing polymerisation thiol-ene hydrogels experience a decreased shrinkage when compared with regular PEG based hydrogels. A common feature of acrylate polymerisations being the shrinkage which occurs during photopolymerisation. To explain this phenomena (Ligon *et al.*, 2017) state that pure methacrylate resins will gel with resin conversions as low as 20%, with the final conversion of approximately 70% every new bond formed increases the degree of shrinkage stress. Because thiol-ene systems polymerise by step growth, the kinetic chains can be found to be significantly shorter eg: thiol-methacrylate systems or even non-existent thiol-nonhomopolymerisable ene. Thus, causing the shift of the polymer gel point well beyond 30% double bond conversion. The benefits of this decreased

shrinkage are mostly seen when looking to maintain reliable production processes for peripheral nerve guidance conduits. Other benefits associated with the use of a thiol-ene based polymer for nerve guidance conduits includes their enhanced flexibility of fabrication. Thiol-ene based reactions can be initiated by radical-mediated additions or by Michael type addition reactions and do not suffer from oxygen inhibition, which is a common limitation of acrylate polymerisations (Lu, Stansbury and Bowman, 2005; Rydholm, Bowman and Anseth, 2005; Shih and Lin, 2012).
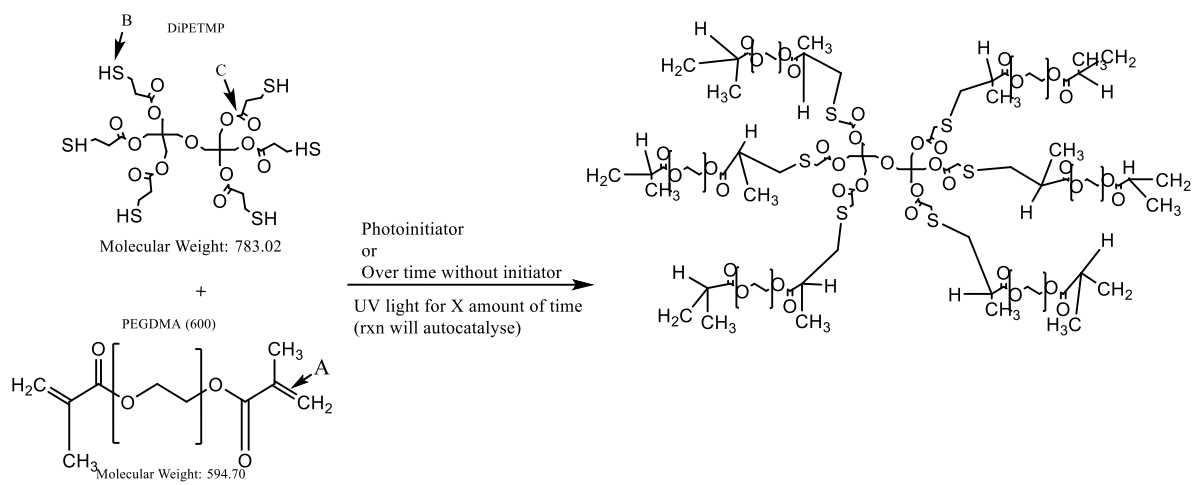
Figure 1-2 Photopolymerisation of PEGDMA and DiPETMP; Arrows A and B respectively point to the reactive points for PEGDMA and DiPETMP; Arrow C points to one of the ester bonds that is broken during the hydrolytic degradation.

Also beneficial to their use in nerve guidance conduits, the thiol-ene reaction fits the criteria of being considered a click reaction. Namely, they maintain a very high rate of C=C double bond conversion during polymerisation (Lowe, 2014). This decreases the likelihood of potentially harmful unreacted monomers being present in the final fabricated composite which could negatively impact peripheral nerve repair.

1.6 Biological factors

A key challenge to be tackled when preparing a nerve guidance conduit is the controlled release of factors capable of positively impacting the molecular mechanisms and signalling cascades which impact the nerve repair process. To this end an understanding of the molecular pathways through which peripheral nerve repair takes place is required.

Following injury for axon regeneration to take place it is essential for myelin and myelin associated glycoproteins to be removed. Within two days of axons being separated from their sensory or motor neurons, Schwann cells in the isolated nerve stump de-differentiate from their myelinating form (signalling focus) to their differentiating form (focus on starting the process of reconnecting the severed ends) in response to Schwann cell derived mitogens (Allodi, Udina and Navarro, 2012; Gordon, 2014). Through the release of cytokines, Schwann cells recruit macrophages into the distal nerve stump which then phagocytose the myelin and myelin associated proteins (Gaudet, Popovich and Ramer, 2011). Simultaneously Schwann cells upregulate the genes at the regenerating nerve front needed to increase production of tubulin, actin, and growth-associated protein 43. Schwann cells also initiate the increased production of neurotrophic factors including nerve growth factor (NGF), brain derived neurotrophic factor (BDNF), neurotrophin (NT) 4/5, glial cell-line derive neurotrophic factors (GDNF) and leukaemia inhibitory factor (LIF) which in turn influence the major molecular pathways and signalling cascades of the peripheral nerve repair process (Pellegrino *et al.*, 1986; Liu, Yang and Yang, 1995; Welin *et al.*, 2009; Gaudet, Popovich and Ramer, 2011; Jessen, R and Lloyd, 2015).

There are four major pathways which have a large influence on peripheral nerve repair. These are the phosphatidylinositol-3 kinase-Akt (Pl3K/Akt) pathway, the Ras-ERK pathway, the Rho-ROK pathway and the cyclic AMP (cAMP) pathway (Chan *et al.*, 2014). The Pl3K/Akt signalling cascade is a key survival pathway that balances trophic factor support of neurons

and blocks apoptosis. It also plays a role in growth, differentiation, and directional signalling. The use of neurotrophic factors such as insulin like growth factor (IGF) 1 and 2 has been shown to activate this pathway leading to enhanced neurite outgrowth and improved muscular function post injury (Kimpinski and Mearow, 2001; Emel *et al.*, 2011). The PI3K-Akt pathway is activated through the adaptor proteins Gab-1 and Ras both of which lead to increased neuronal survival (Chan *et al.*, 2014; Li *et al.*, 2020).

Separately to the PI3K-Akt pathway, Ras also upregulates the expression of the mitogen associated protein kinase ERK-1/2 resulting in an increase to neurite outgrowth(Christie and Zochodne, 2013). The Ras-ERK pathway plays an important role in growth cone formation as well as axon protein synthesis and cytoskeletal formations with increased ERK activation resulting in increased neuronal survival (Kimpinski and Mearow, 2001; Chierzi *et al.*, 2005; Li *et al.*, 2020).

Fitting the theme of boosting repair post injury, the cyclic AMP pathway is involved in several neuronal mechanisms including guidance, neurite growth, dedifferentiation of Schwann cells from signalling to regeneration focus and neurite survival (Shin *et al.*, 2013; Gordon, 2014; Boerboom *et al.*, 2017). Increased production of cAMP results in the upregulation of STAT-3 and PKA expression (Chan *et al.*, 2014), STAT-3 boosts the transcription of several proteins including growth associated protein (GAP) 43, CD 44 and integrin α7β1 which in turn contribute to neurite outgrowth whereas increased expression of PKA plays a role cytoskeletal formations and axon protein synthesis similarly to ERK (Chierzi *et al.*, 2005; Christie and Zochodne, 2013; Chan *et al.*, 2014; Lin *et al.*, 2016).

The Rho-ROK pathway contrasts with the other major pathways in that it can negatively impact peripheral nerve repair, with excess Rho expression inhibiting cytoskeletal assembly, decreasing the expression of PKA (which upregulates both RI3K and ERK expression) and

inhibiting the outgrowth of axons post injury (Cheng *et al.*, 2008; Zochodne, 2012; Li *et al.*, 2020). Typically the Rho-ROK pathway is responsible for breakdown of neurite growth cones however the unregulated expression of this pathway can result in decreased nerve repair, with inactivation of Rho signalling being shown to enhance axon regeneration *in vivo* (Lehmann *et al.*, 1999).

Through these molecular processes Schwann cells allow for the regeneration typically seen post-trauma in peripheral nerves. The limitation of this process however is that following an initial spike in growth factor expression, there is a subsequent drop in expression which directly impacts the extent of recovery seen in peripheral nerves (Reynolds and Woolf, 1993; Sensenbrenner, Lucas and Deloulme, 1997; D. C. Lee *et al.*, 2017). Due to these limitations, a common goal for peripheral nerve guidance conduits is the controlled administration of external factors to the site of injury. These external factors should ideally impact the molecular pathways outlined above over an extended period.

With the goal of impacting these molecular pathways three FDA approved drugs were selected, namely N-acetyl cysteine (NAC), Ibuprofen (Ibu) and Progesterone (Prog) (*FDA Briefing Document NDA 021945 Hydroxyprogesterone Caproate Injection (trade name Makena) Bone, Reproductive, and Urologic Drugs Advisory Committee (BRUDAC) Meeting*, 2019; *Drug Approval Package: Acetadote (Acetylcysteine) NDA #021539*, no date; *Ibuprofen Drug Facts Label | FDA*, no date). Figure 1-3 illustrates the ways in which these pathways are activated and indeed interact with one another as well as where each drug interacts with the signalling pathways to boost peripheral nerve repair. With the goal of obtaining controlled biological signalling in the final nerve guidance conduit two key aims were identified. One is to determine which drug concentrations will synergise best to cause prolonged increases in peripheral nerve repair, the other is to determine the rates at which NAC, Ibu and Prog are released from the degradable PEGDMA-DiPETMP hydrogel.
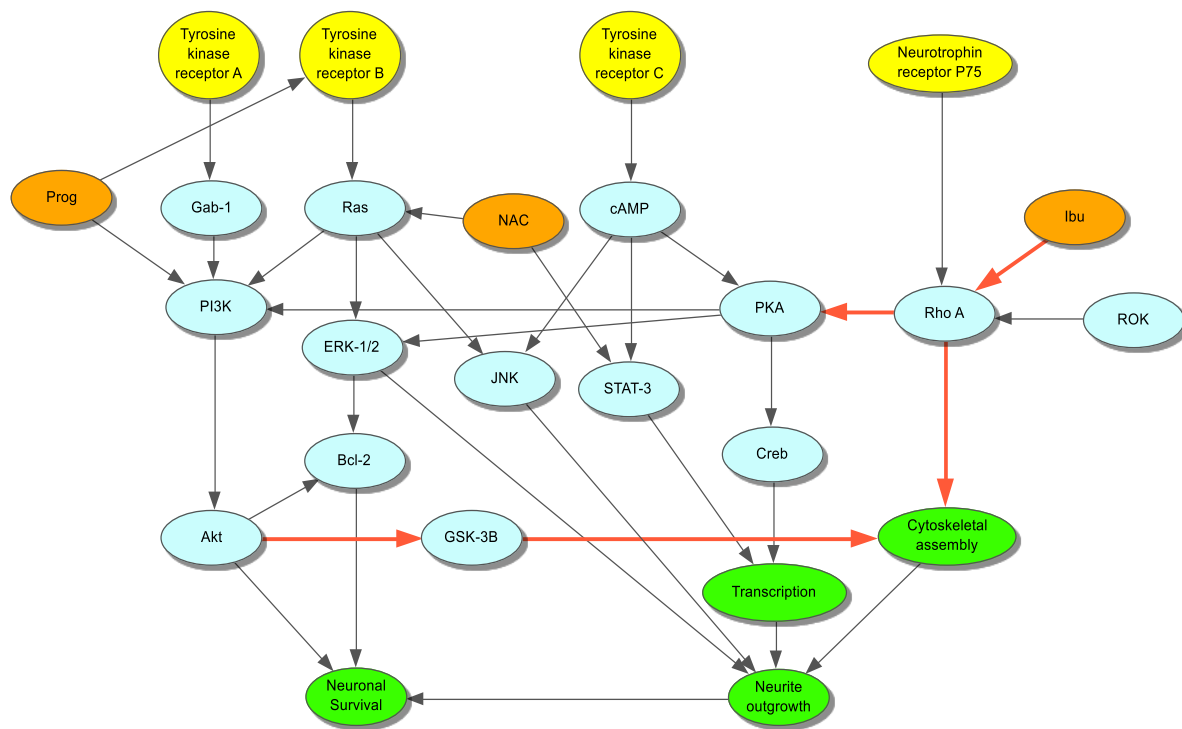
Figure 1-3 Simplified diagram of the major molecular pathways of peripheral nerve repair, highlighting target sites for NAC, Ibu and Prog. Adapted from the works of (Good and George, 2001; Allodi, Udina and Navarro, 2012; Chan et al., 2014; Knott, Assi and Pearse, 2014; Houlton et al., 2019; Li et al., 2020). Yellow=membrane spanning receptors, Blue=signalling cascades, Green=endpoints, Orange=Drugs of interest. Grey arrows represent increased activation of targets, red arrows represent inhibition of targets.

1.6.1 Drug synergy

The use of three different drugs to impact the signalling cascades of peripheral nerve repair provides several benefits, chief among them being the ability to directly target and boost each of the major pathways. Another advantage of this approach is the potential for synergy between NAC, Ibu and Prog. Whereas separately each drug has strong interactions with the peripheral nerve repair signalling cascades, due to their ability to either directly or indirectly affect multiple pathways, there is potential for synergistic effects to occur. An example of this can be seen in the use of NAC to produce a therapeutic effect with much of the available literature utilising concentrations as high as 4500 µM to produce therapeutic outcomes (Zhang *et al.*, 2005; Reid *et al.*, 2009; Catapano *et al.*, 2017), whereas when used in a synergistic fashion

with Allopurinol, concentrations as low as 9 µM have been shown to activate PI3K and ERK pathways (Wang *et al.*, 2013). The potential use of drugs to synergistically produce a therapeutic outcome is not new, with it being common practice in the fields of cancer treatment and antimicrobial research over the last 40 years to use two or more drugs at lower doses to produce desirable effects while minimising the risk of unwanted side effects (Hoffner, Svenson and Källenius, 1987; Kingston *et al.*, 1989). More recently there has been an attempt to identify ratios of drugs which produce the idealised result rather than focus only on lowering the concentration of drug while maintaining therapeutic outcomes, to this end software based synergy calculators have come to the fore, employing high throughput screening to determine these idealised drug ratios (Dicko, Mayer and Tardi, 2010; Yadav *et al.*, 2015; Ianevski *et al.*, 2017). This study will look to identify potential synergies between NAC, Ibu and Prog, through a high-throughput screening focus utilising the synergy finder software developed by Ianevski (Ianevski *et al.*, 2017). This software employs a zero interaction policy (ZIP), an approach to synergy prediction created by Yadav et al.(Yadav *et al.*, 2015) that assumes two non-interacting drugs have minimal effects on one another's dose response curves. Using their independent dose response curves the software determines the relative shift in expected cell viability when the drugs are combined. This deviation from the expected dose response curves gives two delta (δ) scores (one for each dose response curve) which when averaged gives a summary of the interaction between drugs which in turn allows for the determining of the most efficient drug concentrations to improve cellular proliferation.

1.6.2 N-acetyl cysteine

N-acetyl cysteine (NAC) is a drug well known for its use in the treatment of Paracetamol overdose and as an antimucosal agent, NAC is also well known for its antioxidant properties. In the molecular pathways of peripheral nerve repair NAC has multiple modes of action, being capable of upregulating expression of two of the pathways associated with increased neuronal survival. NAC directly increases the expression of both Ras in the Ras-ERK pathway and STAT-3 one of the downstream molecules of the cAMP pathway which in turn boosts neurite outgrowth (Van Irene and Greene, 1998; Wang *et al.*, 2013). NAC also indirectly boosts the PI3K pathway due to Ras playing a role in upregulating PI3K (Chan *et al.*, 2014; Li *et al.*, 2020). *In vivo* and *in vitro* testing of the neuroprotective properties of NAC have been carried out with concentrations as low as 1.5 mg/kg boosting PI3K and STAT3 expression when used synergistically with Allopurinol (Wang *et al.*, 2013).

1.6.3 Ibuprofen

Ibuprofen (Ibu) is a non-steroidal anti-inflammatory drug (NSAID) commonly used in the treatment of pain, inflammation and fever (Davies, 1998). With regard to peripheral nerve repair Ibu has been of interest due to the discovery that NSAIDs can inhibit Rho A expression making the use of an NSAID highly desirable for interrupting the Rho-ROK pathway and enhancing axonal regeneration post injury (Zhou *et al.*, 2003; Hiraga *et al.*, 2006). To this end the use of Ibu, an NSAID which features on the World Health Organisations list of essential medicines and has already been shown to boost functional outcomes post nerve injury, became a prime candidate for incorporation into a nerve guidance conduit (*WHO | Essential Medicines List and WHO Model Formulary*, 2017). Several *in vivo* studies have been carried out investigating the therapeutic effects of Ibu for peripheral nerve repair with concentrations ranging from 60 mg/kg (290 µM) up to 124 mg/kg (600 µM) (Zhou *et al.*, 2003; Fu, Hue and Li, 2007; Madura, Tomita and Terenghi, 2011).

1.6.4 Progesterone

Progesterone (Prog) is a steroid typically thought of as a female sex hormone, however it has also been found to have potential benefits when repairing damaged tissues, upregulating macrophage activation during wound healing, providing neuroprotective properties and also being found to positively affect the clinical outcomes of nerve injuries (Koenig, Gong and Pelissier, 2000; Routley and Ashcroft, 2009; Coronel *et al.*, 2011). Similarly, to NAC, Prog interacts directly with the molecular pathways which positively influence the outcomes of peripheral nerve repair namely the Ras-ERK pathway and PI3K-Akt pathways. Prog does this by increasing the expression of PI3K and also boosting the responses of tyrosine kinase receptor B through the $GABA_A$ receptors which subsequently boosts Ras expression (Koenig, Gong and Pelissier, 2000; Porcher *et al.*, 2011; Sagare-patil *et al.*, 2013). As Ras then boosts JNK expression, progesterone can also indirectly impact the cAMP pathway.

Being a hormone very small concentrations of Progesterone are present in the body (with concentrations of 0.2 ng/ml being the normal range for women (which increases up to 20 ng/ml mid ovulation cycle) and lower concentrations being found in men (Francisco, 2019; Seladi-Schulman and Kay, 2020), *interestingly vitro* and *in vivo* testing have highlighted the potential of elevated Prog concentrations for boosting nerve repair with treatments in the concentration range of 10 to 50 µM (3.3 to 16 mg/kg) Prog boosting clinical outcomes post injury (Leonelli *et al.*, 2007; Routley and Ashcroft, 2009; Yu *et al.*, 2010; Coronel *et al.*, 2011).

1.6.5 Controlled drug release

The rate at which drugs are being delivered from a nerve conduit to the site of damage is an important consideration for a nerve guidance conduit. As delays in treatment of peripheral nerve injuries can result in incomplete or improper repair of the nerve there is a necessity for the timely release of factors capable of boosting nerve repair. Although it has been noted that delays of up to one week in treatment may not negatively impact nerve repair (Zhang *et al.*, 2005; Fu, Hue and Li, 2007), corresponding with the predicted decreases in native expression of growth factors (Reynolds and Woolf, 1993; Sensenbrenner, Lucas and Deloulme, 1997; D. C. Lee *et al.*, 2017). In the previous phases of this thesis the degradable PEGDMA-DiPETMP composite has been highlighted for its physical properties and degradability comparing well with desirable range of properties needed for nerve guidance conduits (Gu *et al.*, 2011), their release rates have yet to be studied. Combining this knowledge with the differences already seen when comparing the chemical and structural properties of NAC, Ibu and Prog (as shown in Table 1-3 and Figure 1-4), which likely play a role in determining their release rates, this study looked to establish the rates of release for NAC, Ibu and Prog from PEGDMA-DiPETMP based hydrogels both as singular drugs and in combination with one another as part of the thiol-ene based hydrogel.

Originally the three drugs were to be distinguished in solution by UV-vis absorbance, as there was a degree of overlap in the max absorbances of NAC, Ibu and Prog (<230nm, 224nm and 240nm respectively), the use of high performance liquid chromatography (HPLC) to separate and quantify the drugs following dissolution was necessitated (Suzuki, Kadowaki and Tamaoki, 1980; Kang *et al.*, 2003; Narendra *et al.*, 2012). At present there are several validated HPLC methods for NAC, Progesterone and Ibuprofen (Monterroza and León, no date; Phenomenex Inc, 1395; USP, 2008, no date b, no date a; Sana *et al.*, 2012), while these methods are valid for each drug singularly they do not provide an adequate method to separate and

quantify NAC, Ibu and Prog when they are simultaneously being released into solution from a singular source. A novel HPLC method capable of eluting and quantifying NAC, Ibu and Prog was developed by adapting the previously validated methods for each drug. With the aim of utilizing this method for routine future analysis the resolution, asymmetry, precision, and Linearity of NAC, Ibu and Prog as singular drugs, in dual drug combinations and with all three drugs within PEGDMA-DiPETMP hydrogels was determined.

Table 1-3 Chemical properties of N-acetylcysteine, Ibuprofen and Progesterone

Drug	Mw (g/mol)	Hydrophilicity (log kow)	Water solubility (mg/ml)	Crystallinity
N-acetyl Cysteine	163.19	-0.66 (0.21878)	100	Crystalline powder (Tm 109.5 C)
Ibuprofen	206.28	3.97 (9332.54301)	21	Crystalline solid (Tm 157 C)
Progesterone	314.46	3.87 (7413.10241)	0.00881	Crystalline powder (Tm 121-132 C)

Figure 1-4 Structures of (A) N-acetyl cysteine (B) Ibuprofen and (C) Progesterone

1.7 Controlled architecture

Throughout the early sections of this thesis the polymerisation of hydrogels was carried out using traditional UV curing. UV curing is a chemical reaction by which a polymerizable monomer or macromolecular monomer is exposed to UV radiation in the presence of a photoinitiator to form crosslinks. Being used since the 1940s and 50s this technique has been well studied, with several advantages including control over the spatial and temporal parameters of curing but also several disadvantages such as oxygen inhibition and the potential for unreacted monomer to be present post-cure (Stoddard *et al.*, 1945, 1962, 1969; Martin, 1959; O'Brien and Bowman, 2006; Bowman and Kloxin, 2008). Also, UV curing limits polymer geometries to shapes which can be prepared as a mould, with light being evenly spread across the monomer surface a necessity for successful polymerisation, limiting the degree of structural complexity which these techniques can achieve.

To successfully prepare a nerve guidance the control of its structural shape and design is an important consideration. With the ability to flexibly create nerve guidance conduits of varying sizes providing potential avenues for enhancing peripheral nerve repair, this can be seen when comparing the inner lumen diameter of commercially available conduits, with diameters ranging from 1.5 to 10mm (Agnew and Dumanian, 2010; Chiriac *et al.*, 2011). Additionally it is important to adjust the thickness of conduits, as seen in the work of Pateman et al. (Pateman *et al.*, 2015) where PEGDA based conduit wall thicknesses below 250 µm were too fragile for handling. With the goal of controlling the 3D architecture of PEGDMA-based hydrogels the 3D printing technique stereolithography (SLA) was identified.

1.7.1 SLA for peripheral nerve repair

Having been around for more than 30 years now, SLA has found itself as an emerging technology in the field of tissue engineering, with applications in bone and liver scaffolding as well as personalised drug delivery processes (Hull, 1984; Kim *et al.*, 2010; Skoog, Goering and Narayan, 2014; Awad *et al.*, 2018). In more recent times SLA has found itself receiving great interest for their potential use in nerve guidance conduit preparations. With Lee et al. demonstrating the potential to utilise SLA to print PEGDA scaffolds on top of electrospun combinations of PCL/gelatin fibres with a Printrbot® rapid prototyping platform. Demonstrating SLAs ability to enhance PEGDAs mechanical properties while also allowing for PCL/gelatin fibres to be highly aligned within the scaffold, improving neurite outgrowth (S. J. Lee *et al.*, 2017). In the work conducted by Evangelista et al. PEGDA based scaffolds were prepared using a 3D Systems model 250/50 printer, showing the potential of SLA to create multi-lumen channels for peripheral nerve repair applications, although they also demonstrated that single lumen SLA prepared conduits demonstrated significantly superior axon regeneration, highlighting the need for further studies to be conducted (Evangelista *et al.*, 2015).

SLA has proven to be advantageous over traditional polymerisation techniques by allowing for curing at extremely low resolutions (as low as 0.43 µm in the xy axis and 1 µm in the z-axis), allowing for greater control over hydrogel porosity, a factor which can play a significant role in determining the differentiation and function of cells (*PICO2 HD - Products - Asiga*, no date; Maruo and Ikuta, 2002; Peppas *et al.*, 2006; Annabi *et al.*, 2010). Unlike conventional UV chamber curing which utilises a mould to spatially control the final shape of the polymer, the SLA process takes place with a resin bath (with transparent base) placed over a movable laser with a platform lowered from above (as detailed in Figure 1-5). Polymerisation occurs when the laser causes a localised solidification of photo-crosslinkable monomers creating a solid

layer. Following this solidification of the first layer the platform moves allowing a new layer to be cured on top in a similar manner to the additive manufacturing techniques of (Arcaute, Mann and Wicker, 2006; Wang *et al.*, 2016).
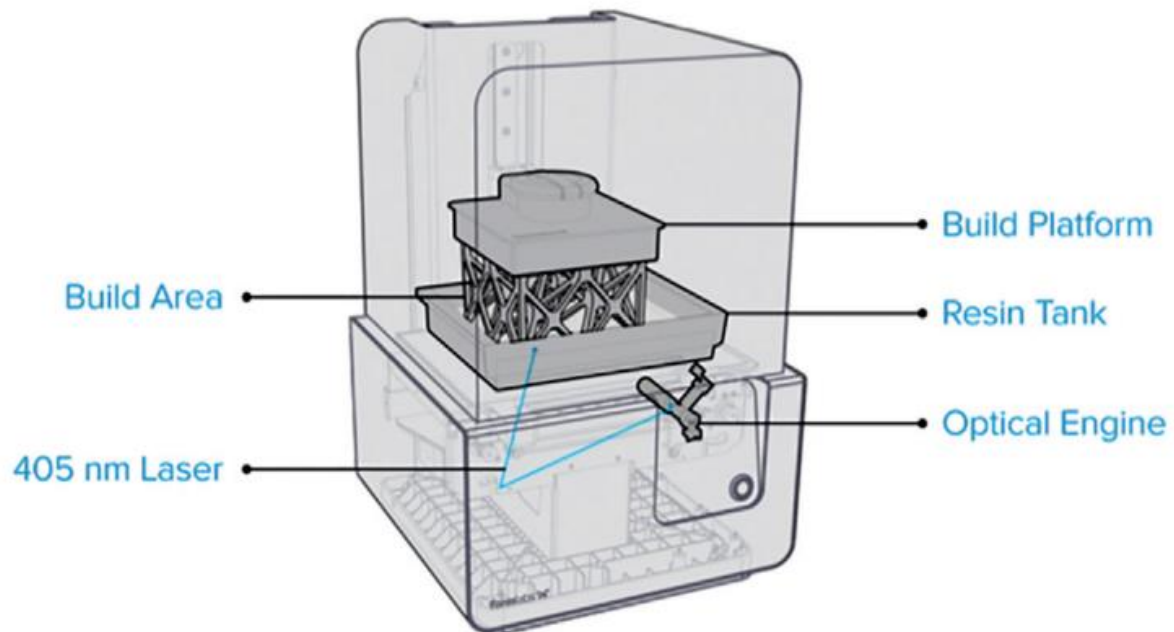
Figure 1-5 Schematic of Form 2 Stereolithography printer reproduced with permission (Whitley et al.*, 2017)*

SLA also holds the advantage of being viewed as a readily accessible technology to the general public with low-end printers being purchased for as little as €500 whereas models with specialised features such as quick material change systems (DWS Lab Xfab), extremely high resolutions (Asiga Pico 2) or large build size plus remote print control (Sharebot Antares) can cost anywhere from €6000 to €80,000. Several of the more notable commercially available SLA are shown in Table 1-4.

Table 1-4 Common SLA printers and their notable features

Model name/maker	Notable features	Resolution (um)	Price (€)	Information source
Photon 3D Printer ANYCUBIC	Very affordable UV Lamp-masking screen print	XY: 47 Z: 25-100	500	Anycubic3d.com(*LCD Photon|3D printer|ANYCUBIC 3D Printer- Think Big, Make Bigger*, no date)
Moai PEOPOLY	Relatively affordable Relatively good resolution (condition dependent) Full access to laser exposure settings	XY: 70 Z: 5	1,100	Peopoly.net(*Moai - Affordable Laser SLA Printer – Peopoly*, no date)
Form2 FORMLABS	Wide assortment of resins (with more on the way) Automated resin system Easy to use software for uploading/altering files	XY: 140 Z: 25-100	3,800	Formlabs.com(*Form 2: Desktop Stereolithography (SLA) 3D Printer	Formlabs*, no date)
Fabpro 1000 3D SYSTEMS	Brand recognition Very fast print speed (4 times faster than comparable SLA printer) Optimised to reduce printing costs	XY: 65 Z: 30-50	4,300	3dsystems.com(*FabPro 1000 | 3D Systems*, no date)
XFAB DWSLAB	Design allowing easy refill/change between resins	XY: 250 Z: 10-100	6000	dwslab.com(*DWS LAB - XFAB*, no date) aniwaa.com(*DWS XFAB review - plug-and-play resin 3D printer (SLA)*, no date)
PICO2^{HD} ASIGA	Extreme print resolution Patented print process allowing 200nm resolution Automatic pausing when resin levels are low	XY: 27 Z: 1	10,400	asiga.com(*PICO2 HD - Products - Asiga*, no date)
Antares SHAREBOT	Very large print size (250mm x 250mm x 250mm) Remote operation of machine through a network	XY: 100 Z: 50	43,200-86,400	Sharebot.it(*Sharebot Antares - Sharebot*, no date) aniwaa.com(*Sharebot Antares review - professional SLA 3D printer (stereolithography)*, no date)

In this project the formlabs Form 2 SLA was chosen to 3D print PEGDMA based hydrogels due to its relatively low cost, flexibility in the use of resins which are not in-house and in the ease with which files can be uploaded to its software. Although PEGDMA and similar

hydrogels have numerous advantages and have seen a great deal of interest to date its use as a base for the 3D printing technique SLA has been focused more to the viability of the 3D printing technique (Dhariwala *et al.*, 2004; Arcaute, Mann and Wicker, 2006; Martinez *et al.*, 2017; Healy *et al.*, 2019). A common limitation of SLAs layer by layer approach to photocuring is the potential to leave areas of the forming polymer under or over-polymerised, thus affecting properties of samples prepared by this method. As the impact SLA has on PEGDMAs material properties are yet to be fully explored this will need to be investigated prior to continued utilisation.

Chapter 2

Materials and Methods

2.0 Materials and Methods

Throughout this thesis several materials and experimental methods are employed with the aim of preparing a PEGDMA based polymer to fit the requirements for peripheral nerve repair. In this section the materials and techniques used throughout this thesis will be outlined.

2.1 Materials

The macromolecular monomer polyethylene glycol dimethacrylate (MW 600) was purchased from Polysciences (Polysciences Gmbh, Hirschberg an der Bergstrasse, Germany). The photoinitiator Irgacure 2959 (4-(2-hydroxyethoxy) phenyl-(2-hydroxy-2-propyl)ketone) was obtained from Ciba Specialty Chemicals (Basel, Switzerland). The RPMI 1640 cell media, MC3T3 cells and PC-12 (CRL-1721) cells were purchased from ATCC (Middlesex, UK). Alamar blue was ordered from Invitrogen-Biosciences (Dun Laoghaire, Ireland). Nerve growth factor 7S (murine) L-cysteine and Phosphate buffered saline (PBS) tablets were obtained from Sigma Aldrich (Vale Rd, Ballyraine Lower, Arklow, Co. Wicklow, Ireland).

Electrically conductive Boron-doped Bioglass45S5 was used as received from the Daniel Boyd group (UK).

Pentaerythritol mercaptopropionate (PETMP), Di-Pentaerythritol mercaptopropionate (DiPETMP), pentaerythritol tetramercaptoacetate (PETMA), ethoxilated-trimethylolpropan tri(3–mercaptopropionate) 700 (ETTMP 700), ethoxilated-trimethylolpropan tri(3–mercaptopropionate) 1300 (ETTMP 1300), trimethylol-propane Tri (3–mercaptopropionate) (TMPMP), tris[2–(3–mercapto- propionyloxy) ethyl]isocyanurate (TEMPIC), glycol dimercaptoacetate (GDMA) glycol di(3–mercaptopropionate) (GDMP) and polycaprolactone tetra(3–mercaptopropionate) (PCL4MP 1350), were supplied by Bruno Bock (Marschacht, Germany). Sodium hydroxide (NaOH) solutions were prepared from solid NaOH tablets

purchased from Thermo Fisher Scientific (Dublin, Ireland). RT4-D6P2T cells and Dulbeccos modified Eagles medium (DMEM) were obtained from ATCC. Poly-L lysine was purchased from Sigma Aldrich.

N-acetyl cysteine and Ibuprofen were purchased from the Tokyo Chemical Industry UK Ltd (Oxford, UK). and Progesterone was purchased from Fluorochem Ltd (Derbyshire, UK).

Sodium Dodecylsulfate (SDS) was purchased from AppliChem (AppliChem GmbH, Ottoweg Darmstadt, Germany). The solvent Acetonitrile 200 was purchased from Lennox (Dublin, Ireland). Phosphoric acid was purchased as an 85 wt. % solution from Thermo Fisher scientific.

The Formlabs Form2 3D printer as well as resin tanks and print platform were purchased from Formlabs (Berlin, Germany) and the photoinitiator Diphenyl(2,4,6-trimethylbenzoyl) phosphine oxide (TPO) was purchased from Tokyo Chemical Industry UK ltd (Oxford, UK).

2.2 Characterisation of the base PEGDMA hydrogel

2.2.1 PEGDMA photopolymerisation

Prepolymerised PEGDMA mixtures were prepared by combining desired amounts of macromolecular monomers, distilled H_2O and 0.1 wt. % Irgacure 2959 photoinitiator as shown in Table 2-1. The batches were placed in a 50 mL beaker, mixed in the dark using a magnetic stirrer for 2 hours until a homogenous mixture was achieved. The solutions were pipetted into cylindrical silicon moulds and photopolymerisation was carried out for 10 minutes in a UV curing system (Dr. Grubel UV-Electronik GmbH) with a spectral range of between 315–400 nm at an average intensity of 10–13.5 mW/cm^2. After which time, gelation had occurred. The chemical structure of PEGDMA can be seen in Figure 2-2. Following photopolymerisation samples were stored in 50ml universals containing PBS @ 37°C until testing.
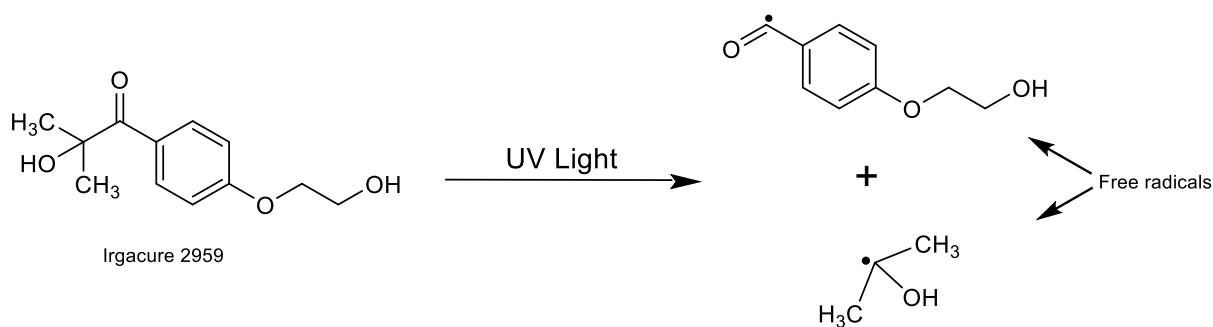
Figure 2-1 Mechanism by which Irgacure 2959 breaks into free radicals to cleave the bonds of PEGDMA 600
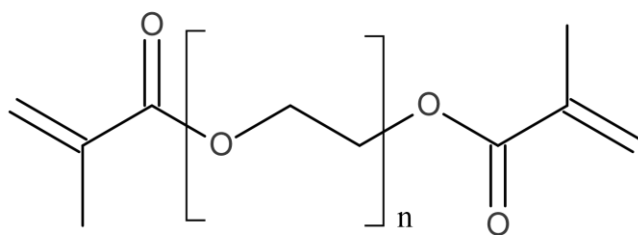
Figure 2-2 Chemical structure of PEGDMA (Mw 600)

Table 2-1 Weight percentages of PEGDMA hydrogels

PEGDMA hydrogel	PEGDMA (600) wt. %	dH$_2$O wt. %	Irgacure 2959 wt. %
100 wt. %	100	-	0.1
75 wt. %	75	25	0.1
50 wt. %	50	50	0.1
25 wt. %	25	75	0.1

2.3 PEGDMA materials properties

2.3.1 Phosphate buffered saline preparation

Phosphate buffered saline (PBS) was made up by adding 5 PBS tablets to a Durant beaker holding one litre of deionised water and allowing for the tablets to dissolve and mix thoroughly. PBS was used throughout this project to simulate the effect of submergence in physiological solution in a similar fashion to other in-house works (Killion *et al.*, 2013; Grehan *et al.*, 2014). The pH of PBS should be 7.4 matching the values provided in previous literature for simulated physiological solution (Marques, Loebenberg and Almukainzi, 2011). To ensure this, a

71

calibrated Jenway 3520 pH meter was used to check the pH of any PBS once made up. The pH was altered by the dropwise addition of 1M sodium hydroxide or 1M Hydrochloric acid depending on whether the solution is too acidic or alkaline respectively until the correct pH is achieved.

2.3.2 Chemical property evaluation

Attenuated total reflectance Fourier transform infrared spectroscopy (ATR-FTIR) was carried out on thinly cut samples of hydrogel. Prior to the analysis, all the samples were dried overnight in a vacuum oven. This allowed for the determination of bonds present in the material outlining whether polymerisation had occurred post-UV curing. A Perkin Elmer Spectrum One (Perkin Elmer, Waltham, MA, USA) fitted with a universal ATR sampling accessory was used to showcase whether residual monomer was left over (n=3). All data was recorded at room temperature in the spectral range of 4000-650 cm^{-1}, utilising 4 scans per sample cycle and a fixed universal compression force of 80 N. Subsequent analysis was carried out using Spectrum software.

2.3.3 Swelling studies

Swelling experiments were performed on samples in phosphate buffer solution (PBS) (pH 7.4). After photopolymerisation, samples with an average weight of 0.225±0.75 g were placed in a 50ml universal and immersed in 15ml of PBS solution at 37°C until reaching equilibrium weight and weighed. Further immersion was not required as the swelling ratio of PEG hydrogels were shown to remain the same over a 28 day period in previous work (Park *et al.*, 2009). The swollen hydrogels (W_s) were weighed by removing from the PBS, rinsing with deionized water, and drying with a tissue. After allowing the pieces to dry at room temperature for 5 minutes the mass was determined on a microbalance (Sartorius MC 210P, Germany). For calculating dry weights, the samples were placed in a vacuum oven for 24 h at 80°C, 50mBar

of pressure, and their weights measured. The mean swelling ratio of the samples was calculated using the formula given by (Park *et al.*, 2009):

$$Mean\ swelling\ ratio\ (Q) = \left(\frac{W_s - W_d}{W_s}\right) \times \frac{100}{1} \qquad \text{Equation 1}$$

Following this, the equilibrium water content of the sample is calculated using the formula stated by (Killion *et al.*, 2012):

$$EWC = \left(\frac{W_s - W_d}{W_d}\right) \times \frac{100}{1} \qquad \text{Equation 2}$$

where W_s and W_d are the weights of the hydrogels in the swollen state and the dried state, respectively. phosphate buffer solution (PBS) (pH 7.4). Testing was carried out in quadruplicate (n=4).

2.3.4 Thermal properties

To determine if the glass transition temperature of the PEGDMA hydrogels changed over the 28-day period in PBS at 37°C, the thermal properties of the materials were examined using differential scanning calorimetry (DSC) (TA Instruments, UK). Samples were taken out of the PBS solution, rinsed in deionized water, and dried at 80°C in a vacuum incubator with pressure 50mBar overnight. Between 8 and 12mg of each sample was weighed using the Sartorious microbalance, heated at a rate of 20°C/minute from room temperature to 200°C, cooled to -70°C using the cooling compartment of a modulated DSC machine and reheated to 200°C at a rate of 5°C/minute. From the subsequent thermographs it was possible to determine the glass transition temperature (T_g), for each sample on day 0, 2, 14 and 28 (n=2). Volatiles were removed from the purging head with nitrogen gas at a rate of 30 ml/min. Calibration of the instrument was performed using indium as standard.

2.3.5 Mechanical properties

On days 0, 2, 14 and 28, the PEGDMA samples were taken out of PBS solution, allowed to dry on a sheet of tissue paper for 5 minutes and cooled down to room temperature. Unconfined

compression testing was performed on a Lloyd screw-driven mechanical testing machine (Lloyd Lr10K, Bognor Regis, UK) using a load cell of 2.5 kN and a crosshead speed of 0.5 mm/minute (n=5). A pre-load of 5 N was employed and samples were compressed to 60% strain. Stress strain curves were generated from which it was possible to calculate Youngs modulus (E) from the turning point of the toe region section of the graph using the following formula:

$E = \sigma/\varepsilon$ *Equation 3*

Where σ represents stress and ε represents strain, subsequently this test also determined the stress at limit for each hydrogel samples.

2.3.6 Wettability

The wettability of the PEGDMA hydrogels was evaluated via water contact angle (Goniometry) analysis. Upon removal from the PBS solutions, samples were rinsed in deionised water and blotted dry with filter paper. 10μl of deionised water was placed on the surface of the polymers, an image of the droplet was recorded and the change in angle of the droplet was measured over a 25 second period. Measurements were conducted on days 0, 2, 14, and 28 of immersion in PBS at 37°C. Contact angles were recorded in quintuplicate on each sample, with 3 of each hydrogel being tested for wettability.

2.3.7 Surface properties

Scanning electron microscopy (SEM) was performed on a Mira SEM (TESCAN, Oxford Instruments, Abingdon, UK) using a range of magnifications in high vacuum mode by scanning a beam of high energy electrons across the surface of the samples with resolution of 20 μm at 15 kV. Samples 5mm in diameter and 1mm in height were sectioned into two pieces. Thereafter the surface of the samples and the cross-section were examined. As a first step the samples were placed on an aluminium stub and were gold coated using Bal-tec SCD 005 sputter coater

for 110 sec at 0.1 mBar vacuum before testing. Energy dispersive X-ray (EDX) analysis was carried out to determine the chemical make-up of samples using the EDX system.

2.4 PEGDMA cell culture

Initial cell work was conducted using the osteoblast precursor cell line MC3T3 obtained from a mouse skull to act as a model cell line until nerve-like cell lines were available, MC3T3 cells were advantageous as they had been used in house previously for other studies and could be sourced in-house minimising delays to the project (Chikarakara *et al.*, 2015). Further work was carried out utilising PC-12 cells, a cell line derived from a pheochromocytoma in a rat adrenal medulla which has the potential to differentiate into nerve-like cells, this cell line was then used as a predictive model for potential impacts on nerve cells. Both cell lines were thawed from frozen and routinely subcultured using media as outlined in Table 2-2 with foetal horse serum being added to PC-12 cells as is recommended by their supplier for modulation of cellular attachment (Greene and Tischler, 1976; Meth and Schoenfeld, 2019). Further while being incubated cells were placed in a sterile CO_2 incubator @ 37°C.

Table 2-2 Constituents, Storage temperatures and volumes used to make up cell media

Medium component	Storage temperature [°C]	MC3T3 constituents Volume [ml]	PC-12 constituents Volume [ml]
Foetal Calf serum (FCS)	- 20	10	25
Foetal Horse serum	- 20	-	25
Penicillin/Streptomycin	- 20	0.5	5
MEM alpha	+ 4	50	-
DMEM (Hepes modification + L-Glutamine)	+ 4	-	445

All cell culture techniques were carried out aseptically in a class II laminar flow hood. To achieve a satisfactory level of sterility, sterility checks of cells and cell media were regularly conducted.

2.4.1 Cell culture sterility check

To confirm the sterility of any materials which had been made up, a small aliquot of sample would be removed and placed into a solution of media. This solution was then incubated at 37°C in an incubator for 7 days, any contamination of sample would result in the formation of a cloudiness in the media indicating the material would need to be re-made. This process was carried out throughout the length of the project.

2.4.2 MC3T3 cell splitting

Medium was removed from the flasks and cells rinsed gently with 2ml of 37°C PBS. Attached cells were detached by adding 2ml of 37°C trypsin and placed in a CO_2 incubator for 5 minutes. The trypsin was inactivated by adding 2ml of complete medium and cells were removed to be centrifuged at 400rpm for 5 minutes. The supernatant was removed, and pellet re-suspended in complete medium to be re-seeded in new T75 flasks.

2.4.3 Preparation of polymer samples for cytotoxicity assessment

PEGDMA samples were photopolymerised as outlined in section 2.2.1. Subsequently for the direct contact assay cylindrical samples of each PEGDMA weight percentage (5mm in diameter and 1mm in height) were cut into 8ths. These pieces were then placed into a 6 well plate and sterilised using the protocol set out in Table 2-3.

For the elution assay 3 cylindrical samples (5mm in diameter and 1mm in height) were placed into a 6 well plate and sterilised using the protocol set out in Table 2-4. These samples came from the same polymerised batch of PEGDMA as used in the direct contact assay.

Table 2-3 Outlining the order of polymer treatment prior to cytotoxicity assessment for direct contact assay.

Stage	Volume used (ml)	IPA (Mins)	PBS (Mins)	Cell media (Mins)
1	4.5	30	-	-
2	4.5	30	-	-
3	4.5	-	30	-
4	4.5	-	30	-
5	4.5	-	-	30
6	4.5	-	-	30

Table 2-4 Outlining the order of polymer treatment prior to cytotoxicity assessment for elution assay.

Stage	Volume used (ml)	IPA (Mins)	PBS (Mins)	Cell media (Mins)
1	4.5	30	-	-
2	4.5	30	-	-
3	4.5	-	30	-
4	4.5	-	30	-
5	4.5	-	-	30
6	4.5	-	-	Overnight

2.4.4 Direct contact assay

Cells were seeded on a 24-well plate to a density of $4*10^4$ cells/well and incubated overnight falling in a similar range to the densities utilised by others (Mackle *et al.*, 2011). Following incubation one 8th of hydrogel samples were aseptically added to the 24-well plate in triplicate as per Table 2-5. Three wells received no cells acting as a negative control, three others were not treated with hydrogels acting as a positive control. This 24-well plate was subsequently incubated overnight prior to cytotoxicity assessment using the Alamar blue assay.

Table 2-5 Layout of 24-well plate identifying treatment applied to each well for direct contact assay

Media + no cells	100% Hydrogel	75% Hydrogel	50% Hydrogel	25% Hydrogel	Media + cells
Media + no cells	100% Hydrogel	75% Hydrogel	50% Hydrogel	25% Hydrogel	Media + cells
Media + no cells	100% Hydrogel	75% Hydrogel	50% Hydrogel	25% Hydrogel	Media + cells
-	-	-	Polymer + no cells	Polymer + no cells	Polymer + no cells

2.4.5 Elution assay

Elution assays are beneficial for a number of reasons, in polymer engineering applications they can be utilised to indicate the presence of potentially cytotoxic unreacted monomers and in a more general sense they serve an important function in cytotoxicity measurements, allowing for the simulation or exaggeration of clinical use conditions so as to determine the potential toxicological hazard without causing significant changes in the test sample (ISO/EN10993-5, 2009). In this work Elution assays were carried out throughout with the aim of monitoring any potential effects on cells which may be caused by elute from polymerised samples.

MC3T3 cells were seeded on a 24-well plate to a density of $4*10^4$ cells/well and incubated overnight in a fashion like the direct contact assay. Following incubation, the media was aspirated off and replaced in each of the sample wells with 1ml of media taken from the elution assay 6-well plate prepared 24 hours previously as outlined in section 2.4.3. The layout of this well plate is outlined in Table 2-6. This 24-well plate was subsequently incubated overnight prior to cytotoxicity assessment using the Alamar blue assay.

Table 2-6 Layout of 24-well plate identifying treatment applied to each well for elution assay

Media + no cells	Media + cells	100% Hydrogel	75% Hydrogel	50% Hydrogel	25% Hydrogel
Media + no cells	Media + cells	100% Hydrogel	75% Hydrogel	50% Hydrogel	25% Hydrogel
Media + no cells	Media + cells	100% Hydrogel	75% Hydrogel	50% Hydrogel	25% Hydrogel
-	-	-	-	-	-

2.4.6 Alamar blue assay

The Alamar blue assay was selected for use in this project due to a combination of its high accuracy and its ability to determine metabolic activity of cells via non-cytotoxic means, allowing for multiple cellular metabolic activity measurements as opposed to the singular measurements seen in MTT and neutral red assays (O'Brien *et al.*, 2000). Following the addition of 100µl of Alamar blue to each test well, the 24-well plate was incubated in the dark at 37°C for 4 hours. Following incubation 100µl was taken from each well and added in triplicate to a 96-well plate. Absorbance was measured at both 570nm and 600nm, exported to excel and analysed via Graphpad PRISM statistical analysis. Providing results which could compare mean absorbance between samples as well as percentage metabolic activity compared to a control well. Metabolic activity was calculated using the equation 3.

% cell metabolic activity = (% PEGDMA absorbance/Control absorbance)*100　　　*Equation 4*

2.5 Modification of PEGDMA hydrogels to increase electroactivity: addition of electroactive bioglass 45S5

2.5.1 PEGDMA/Bioglass composite photopolymerisation

Upon characterisation of the polymers outlined in Table 2-1 it was determined that the 50 wt. % and 100 wt. % samples held the most desirable characteristics for use in the treatment of peripheral nerve repair. As such, varying concentrations of electroactive bioglass were added to the 50 wt. % samples as outlined in Table 2-7. The PEGDMA/bioglass (PEGBio) samples were mixed for 2 hours without bioglass as per the procedure above. The bioglass 45S5 was then added and samples were homogenised using an IKA t18 ultra turrax manual homogenizer at an average speed of 10000 rpm. The solutions were pipetted into silicone moulds and photopolymerisation was carried out for 10 min in a UV curing system as described in section 2.2.1 with the addition of a new tensile mould matching the ASTM standards for tensile testing

(ASTM-D638-14, 2014) to be used for conductance measurements. Following photopolymerisation samples were stored in 50ml universals containing PBS @ 37°C until testing.

Table 2-7 Weight percentages of PEGDMA/Bioglass (PEGBio) composite hydrogels

PEGBio composite	PEGDMA (600) wt. %	dH$_2$O wt. %	Bioglass 45S5 wt. %	Irgacure 2959 wt. %
5 wt. %	47.5	47.5	5	0.1
2.5 wt. %	48.75	48.75	2.5	0.1
1.5 wt. %	49.25	49.25	1.5	0.1
1 wt. %	49.75	49.75	1	0.1
0 wt. %	50	50	-	0.1

2.6 PEGBio materials properties

The materials properties of the PEGBio compositions were determined using the same methods as those described for the determination of PEGDMAs materials properties in section 2.3 with the addition of a new test. This test was for the purpose of conductance measurement (using HR2 high resistance/low conductance meter).

2.6.1 Conductance meter calibration

The HR2 high resistance/low conductance meter being used for the first time, was standardised prior to conductivity testing. HR2 meter was zeroed by attaching the sensitive and non-sensitive terminals, flipping the centre switch to ohms (Ω), and shorting the positive and negative clips together. Following this zeroing 100 Ω, 1000 Ω and 1,000,000 Ω resistors were tested using both the HR2 meter and a Rapid 328 digital multimeter. The results recorded with both instruments were recorded in Table 2-8.

Table 2-8 Resistance recording comparisons between HR2 high resistance/low conductance meter and Rapid 328 dmm

Resistor used (Ω)	HR2 reading (mV)	Rapid 328 reading (mV)
100	95	95
1,000	991	988
1,000,000	999,000	1,050,000

2.6.2 Bioglass conductance measurement

Bioglass 45S5 has been added to the polymer composition to both improve the compressive strength of the material and induce an electrical current along the length of the material. To confirm the bioglass carries an electrical current the sensitive clips were placed into a container filled with bioglass and any current which ran though the sample was recorded.

2.6.3 Conductance testing

Following an initial re-immersion in PBS for 60 minutes to simulate conditions within the body, the negative and positive HR2 sensitive clips were attached to the PEGBio samples 3 cm apart from each other, results were then compared to the properties of standard nerve tissue.

2.7 PEGBio cell culture

2.7.1 PC-12 Cell splitting

Cell suspension was removed aseptically from the T75 flask and placed into a 15ml universal. The cells were removed to be centrifuged at @ 400rpm for 5 minutes. The supernatant was removed, and pellet re-suspended in complete medium to be re-seeded in new T75 flasks.

2.7.2 Cytotoxicity

Cytotoxicity assessment of PEGBio samples was carried out in a similar manner to that used for analysing the PEGDMA samples, with the addition of coll IV coated plates being used to adhere PC-12 cells to the well-plate surface.

2.7.3 Neurite extension

Neurite extension assays were conducted to determine if PC-12 cells could be differentiated into nerve like cells when attached to PEGDMA surface and cultured in medium containing nerve growth factor 7s (murine). NGF was resuspended in 10ml of PC-12 media to give a concentration of 10µg/ml. 500µl of this solution was added to 48.5ml of Alpha DMEM, 0.5ml of foetal horse serum and 0.5ml of pen/strep solution to give a final concentration of 1000ng/ml conforming to John Hopkins protocol standards. Solution was then stored for use in a fridge at 4°C prior to use. Following this, PC-12 cells were seeded in a collagen IV coated 6-well plate. Seeding concentrations of 30,000, 60,000 and 100,000 cells/well were used to determine if seeding density impacted PC-12 differentiation. Results were recorded visually using an Olympus CKx41 microscope with IS (300) capture software and neurite extension data was prepared using ImageJ software with NeuronJ plugin.

2.7.4 PEGBio cell attachment

Conducted to test the viability of PEGBio composites for the use of peripheral nerve repair this assay involved initially coating the different weight percentages of PEGBio in collagen IV solution, allowing samples to dry, placing samples into a 24-well plate, and seeding the wells to a concentration of 50,000 cells/well. Following attachment to PEGBio hydrogel composites, cells were to be treated with differentiation medium causing PC-12 cells to become nerve-like cells. Results were recorded using an Olympus CKx41 microscope with IS (300) capture software.

2.8 Modification of PEGDMA hydrogels to increase biodegradability: addition of thiol monomers via click chemistry

2.8.1 Hydrogel Fabrication

The pre-cured mixtures were prepared by combining the desired amounts of macromolecular monomers and Irgacure 2959 photoinitiator, as shown in Table 2-9. The batches were placed in 50 mL beakers and mixed using a magnetic stirrer at 200 rpm for 20 min at room temperature. Due to a lack of miscibility between thiol monomers and water, future testing was carried out using 100 wt. % PEGDMA instead of 50 wt. % PEGDMA. The solutions were pipetted into cylindrical and tensile silicone moulds, and photopolymerisation was carried out for 10 minutes as described in section 2.2.1, after which time polymerisation of samples was verified.

Table 2-9 Combination of monomers in 1:1 molar ratios

Monomer	PEGDMA (g)	Thiol (g)	Photoinitiator (mg)
PEGDMA	13.00	0.00	13.00
PETMP	7.00	5.70	12.70
DiPETMP	5.20	7.88	13.08
PETMA	5.00	8.60	13.60
ETTMP 700	4.00	9.33	13.33
ETTMP 1300	2.50	10.83	13.33
TMPMP	5.50	7.31	12.81
TEMPIC	5.00	8.76	13.76
GDMA	10.00	3.50	13.50
GDMP	9.00	3.77	12.77
PCL4MP	4.00	9.00	13.00

2.8.2 Polymerisation Verification

Post-UV exposure samples were viewed as having polymerised if they had formed a hydrogel; the polymerised samples were removed from the polymer moulds, washed to remove excess water, and stored. The un-polymerised samples were exposed to UV again to ensure that delayed polymerisation was not occurring, and after 30 min of further exposure any unreacted monomers were considered as having unsuccessfully polymerised.

2.9 Thiol-ene materials properties

The materials properties of the different thiol-ene compositions were determined using the same methods as those described for the determination of PEGBios materials properties in sections 2.3 and 2.6 with several alterations as outlined in sections 2.9.1 and 2.9.2. Several new tests were carried out for the purpose of chemically characterising the thiol-ene bond, determining degradation rates of thiol-ene hydrogels as well as secondary thermal measurement and a tensile strength measurement (utilising a TA Q-800 analyser fitted with a Peltier temperature control) as detailed in sections 2.9.3 to 2.9.5.

2.9.1 Swelling Studies

Gel fraction was calculated using the formula outlined by others previously (Killion *et al.*, 2013), where Wredry refers to the weight after the sample has been swollen and subsequently dried:

$$Gel\ fraction = \left(\frac{W_d}{W_{redry}} \right) \times \frac{100}{1} \qquad\qquad Equation\ 5$$

2.9.2 Compression Testing

Testing was carried out using a screw-driven mechanical testing machine (Lloyd Lr10K) fitted with a 2.5 kN load cell (n = 4). The samples were equilibrated in phosphate buffer (pH 7.4) at room temperature for 48 h before testing, and an unconfined compression was carried out at a speed of 1 mm/min using samples that were 28 mm in diameter and 2.5 mm in height. A pre-load of 5 N was employed, and the samples were compressed to a 70% strain. Stress-strain curves were generated, from which Youngs modulus was calculated based on the linear section of the graph, with the toe region (if any was present) being ignored. For each hydrogel sample, the stress at limit was calculated based on the load at the compressive limit.

2.9.3 Raman Characterisation

Raman spectra were obtained similarly to (Hurley *et al.*, 2019) using a Renishaw inVia Raman confocal microscope (Renishaw Instruments, Gloucestershire, UK), with a 785 nm laser excitation operating at 300 mW. Spectra were collected between 100 and 3200 cm^{-1} over the course of 8 spectral scans (run time of 10 s each). A 20x lens with a 50 μm laser spot size and a path grating of 1200 lines/mm (633/780) were used throughout. Similar to the work carried out by others (Bäckström *et al.*, 2012), the differences in peak heights at 1640 cm^{-1} were used as an indicator of the degree of crosslinking, and peaks were normalised to the 1470 cm^{-1} peak representative of CH$_2$ bending.

2.9.4 Dynamic Mechanical Analysis

Dynamic mechanical analysis was performed using a TA Q-800 analyser (TA Instruments, New Castle, DE, USA) fitted with a Peltier temperature control. Samples were tested using a tensile mode tester, samples were in the swollen equilibrium state. Prior to testing, all samples were blotted free of water using filter paper to minimise slippage and fixed at a compression load of 5.0 ± 0.2 N during testing. For tensile analysis samples were equilibrated at 37 °C and underwent ramp displacement at a rate 100.00 μm/min, from which stress-strain curves were prepared and tensile strength at limit determined. For thermal analysis, storage/elasticity (G′) and loss (G″) moduli were obtained under dynamic conditions over a temperature range of -80 °C to 20 °C. With an oscillatory ramp of 15.0 and static force of 0.0100N being applied throughout.

2.9.5 Accelerated Degradation Study

To assess whether the addition of thiols improve the degradation rates of PEGDMA, a comparative accelerated degradation study was carried out. Cylindrical samples of PEGMA and PEGDMA-thiol composites with an average weight of 200 mg were stored in either 5 mM

or 5M NaOH, and their change in weight was monitored following the procedures outlined by Browning and Cosgriff-Hernandez et al., 2014 and Lam and Hutmacher et al., 2008, respectively (Lam *et al.*, 2008; Browning *et al.*, 2014). To highlight the degree of breakdown, pictures were taken weekly after the first month of degradation, and the experiment continued until it was no longer possible to retrieve samples from their NaOH solutions.

2.10 Thiol-ene cell culture

Cytotoxicity testing of PEGDMA-DiPETMP hydrogel samples was carried out utilising the previously described PC-12 cells as well as RT4-D6P2T cells. RT4-D6P2T cells (referred to hereafter as Schwann cells or SCs) are derived from a schwannoma in a rat peripheral nervous system. Direct contact and elution assays were carried out as described in sections 2.4.4 and 2.4.5 utilising the Alamar blue assay with alterations to methods outlined in sections 2.10.1 to 2.10.4.

2.10.1 Schwann cell splitting

Splitting of Schwann cells was carried out similarly to that of the MC3T3 cell line detailed in section 2.4.2 with the difference occurring in the make-up of Schwann cell culture media which is detailed in Table 2-10.

Table 2-10 Constituents and volumes used to make up cell media

Medium component	Schwann cell constituents Volume [ml]
Foetal Calf serum (FCS)	50
Penicillin/Streptomycin	5
DMEM **(Hepes modification + L-Glutamine)**	445

2.10.2 Direct contact and elution assay

Schwann cells and PC-12 cells were seeded on a 24-well plate to a density of $4*10^4$ cells/well and incubated overnight in keeping with sections 2.4.4 and 2.4.5. Following incubation one 8th of hydrogel samples were aseptically added to the 24-well plate in triplicate as per Table 2-5. Three wells received no cells acting as a negative control, three others were not treated with hydrogels acting as a positive control. This 24-well plate was subsequently incubated overnight prior to cytotoxicity assessment using the Alamar blue assay.

Table 2-11 Layout of 96-well plate highlighting layout for thiol-ene direct contact and elution assays

Media + cells	Media + cells	Media + cells	PEGDMA Elution	PEGDMA Elution	PEGDMA Elution
PEGDMA Direct contact	PEGDMA Direct contact	PEGDMA Direct contact	-	-	-
-	-	-	Media + no cells	Media + no cells	Media + no cells
PEG-DiPETMP Elution	PEG-DiPETMP Elution	PEG-DiPETMP Elution	PEG-DiPETMP Direct contact	PEG-DiPETMP Direct contact	PEG-DiPETMP Direct contact

2.10.3 Poly-L lysine coating

For PC-12 tissue culture, plates were coated with Poly-l lysine instead of collagen IV, a commonly utilised plate coating for PC-12 cell adhesion (Magalingam, Radhakrishnan and Haleagrahara, 2016; Wang *et al.*, 2018).

2.10.4 Alamar blue assay

Alamar blue cytotoxicity was determined based on fluorescence quantification as opposed to absorption measurements due to fluorescence measurements increased sensitivity and accuracy as stated by the manufacturer (Invitrogen, no date), excitation was carried out at 530nm with emission read at 590nm.

2.11 Modification of PEGDMA hydrogels to increase bioactivity: addition of active pharmaceutical ingredients

2.12 Drug synergy analysis

2.12.1 Drug synergy plate seeding

To establish drug synergy via high throughput screening, 96 well-plates were seeded with either Schwann cells or PC-12 cells at concentrations of $2*10^4$ cells/ml in adherence with the work of Wei et al., (Wei *et al.*, 2003) and incubated overnight prior to treatment with NAC, Ibu and Prog. Well plates were prepared for each drug combination in quadruplicate (n=4).

2.12.2 Drug synergy treatment

To carry out drug synergy analysis of three drugs rather than two as is commonplace (Sulkowski *et al.*, 2017; Lallo *et al.*, 2018; Pollyea *et al.*, 2018) a battery of screenings were carried out. In the first set of screenings initial concentrations of NAC, Ibu and Prog were selected as 44.13 µM, 600 µM and 38.16 µM respectively based on the works of Wang *et a*l., Fu, Hue and Li., and Routley *et al*. (Fu, Hue and Li, 2007; Routley and Ashcroft, 2009; Wang *et al.*, 2013), with two further drug treatments of a higher concentration and four of lower concentration (determined by doubling or halving the original concentration respectively) as outlined in Table 2-12. Well plates were then treated with two drugs (NAC-Ibu, Ibu-Prog or Prog-NAC). At 24, 48 and 72 hours post exposure the impact of drugs on cellular activity was determined via Alamar Blue fluorescence measurement and compared as a percentage of control wells untreated by drug.

Table 2-12 Initial Drug synergy concentrations

	N-acetyl cysteine (µM)	Ibuprofen (µM)	Progesterone (µM)
Concentration 1	0	0	0
Concentration 2	2.758	32.5	2.385
Concentration 3	5.516	75	4.77
Concentration 4	11.032	150	9.54
Concentration 5	22.065	300	19.08
Concentration 6	44.13	600	38.16
Concentration 7	88.26	1200	76.32
Concentration 8	176.52	2400	152.64

Following analysis of impact of the initial drug combinations on Schwann cells and PC-12 metabolic activity, the second concentration range of drugs was selected as shown in Tables 2-13 to 2-15. For the second range of drugs, the concentration ranges of Ibuprofen were lowered to the range of 16.25 µM to 450 µM as concentrations above this range were found to inhibit the metabolic activity measurements of PC12 and Schwann cells. For NAC and Prog concentration ranges, changes were made based off the outcomes seen when in combination with individual drugs as opposed to generalised trends, leading to the second set of drug synergy concentration ranges being dependent on the co-treated drug. Ultimately this meant NAC and Prog had different drug concentrations when being used to treat Schwann cells in combination with Ibu or with each other.

Table 2-13 NAC and Ibu concentrations for second set of drug synergy tests

	N-acetyl cysteine (µM)	Ibuprofen (µM)
Concentration 1	0	0
Concentration 2	2.758	16.25
Concentration 3	5.516	32.5
Concentration 4	11.032	75
Concentration 5	22.065	100
Concentration 6	44.13	150
Concentration 7	88.26	300
Concentration 8	176.52	450

Table 2-14 Ibu and Prog concentrations for second set of drug synergy tests

	Ibuprofen (µM)	Progesterone (µM)
Concentration 1	0	0
Concentration 2	16.25	25
Concentration 3	32.5	50
Concentration 4	75	75
Concentration 5	100	100
Concentration 6	150	150
Concentration 7	300	200
Concentration 8	450	300

Table 2-15 NAC and Prog concentrations for second set of drug synergy tests

	N-acetyl cysteine (µM)	Progesterone (µM)
Concentration 1	0	0
Concentration 2	25	2.385
Concentration 3	50	4.77
Concentration 4	75	9.54
Concentration 5	100	19.08
Concentration 6	150	38.16
Concentration 7	200	76.32
Concentration 8	300	152.64

Upon analysis of secondary drug combinations it was determined that combinations which caused the highest proliferative effect following 24 hours exposure resulted in decreased proliferation thereafter due to a combination of contact inhibition and nutrient depletion as outlined by Abercrombie, (Abercrombie, 1979). As such the decision was taken to switch to the use of synergy analysis of the initial 24 hour responses using SynergyFinder software developed by Ianevski *et al*. (Ianevski *et al.*, 2017) in order to determine final drug treatment combinations.

In the final drug combination, Ibu was added as a fixed 16.25 µM concentration to all test wells based off its synergistic performances with both NAC and Prog in the second phase of drug screening. With the fixed Ibu concentration, NAC and Prog concentrations were prepared based on their synergies 24 hours post treatment with the goal of having the drug concentrations in the centre of the plate match the maximum synergy in section 3.14.2.4 as shown in Table 2-

16. PC-12 cells and Schwann cells were treated as per the first two drug screenings with the well plate layout shown in Table 2-17. Drug Synergy was determined as per the secondary drug combinations section and images of cells pre- and post-treatment were prepared using an Olympus CKx41 microscope with IS (300) capture software.

Table 2-16 NAC, Ibu and Prog concentrations for final drug synergy tests

	N-acetyl cysteine (µM)	Ibuprofen (µM)	Progesterone (µM)
Concentration 1	0	0	0
Concentration 2	25	16.25	10
Concentration 3	50	16.25	20
Concentration 4	75	16.25	30
Concentration 5	100	16.25	40
Concentration 6	150	16.25	80
Concentration 7	200	16.25	125
Concentration 8	300	16.25	200

Table 2-17 96 well plate layout for final drug concentrations (NAC on the X-axis and Prog on the Y-axis)

Control (0,0)	25	50	75	100	150	200	300				
10								No cells	Blank	-	-
20								No cells	Blank	-	-
30								No cells	Blank	-	-
40								No cells	Blank	-	-
80								No cells	Blank	-	-
125								No cells	Blank	Blank	-
200								No cells	Blank	Blank	-

2.13 Drug release characterisation

2.13.1 PEG-Drug photopolymerisation

To determine both the release rates of N-acetyl Cysteine, Ibuprofen and Progesterone from PEGDMA-DiPETMP copolymers as well as potential interactions between the therapeutic drugs, 7 combinations of drug were prepared with fixed concentrations of 1 mg/ml in PEGDMA-DiPETMP mixtures as outlined in Table 2-18 and photopolymerised as described in section 2.8.1. Concentrations of 1 mg/ml were utilised to ensure released drugs fell within the limits of quantification identified in section 2.13.4.1.

Table 2-18 Drug combinations prepared in PEGDMA-DiPETMP hydrogels

Name	N-acetyl Cysteine	Ibuprofen	Progesterone
NAC	1mg/ml		
Ibu		1mg/ml	
Prog			1mg/ml
NACIbu	1mg/ml	1mg/ml	
NACProg	1mg/ml		1mg/ml
IbuProg		1mg/ml	1mg/ml
NACIbuProg	1mg/ml	1mg/ml	1mg/ml

2.13.2 Drug dissolution

Cylindrical samples with approximate weight of 220mg were placed in quadruplicate into 50ml McCartney bottles containing 20ml of PBS solution (pH 7.4±0.1) with 0.5% Sodium dodecyl sulphate (SDS) to enhance the solubility of Progesterone (all drugs were maintained at sink conditions). McCartneys were then placed into an INFORS HT ecotron shaking incubator at 37°C and 70rpm, PBS-SDS solution was removed and completely replaced at regular intervals until complete release of drugs was similar to the work of Malcolm et al. (Malcolm *et al.*, 2005).

2.13.3 Drug quantification

The concentration of drug present in each removed PBS aliquot was determined using a Waters 2695 HPLC system with a Luna C(18) column attached. Adapting the US pharmacopeia methods for N-acetylcysteine, Ibuprofen and Progesterone a mobile phase was prepared consisting of 72:28 Acetonitrile:H_2O with pH adjusted to pH3.3 using phosphoric acid. Detection of peaks was carried out using a Dual UV spectrophotometer measuring absorption at 214nm and 253nm (covering the lambda max peaks for NAC (214nm), Ibu (214nm) and Progesterone (253nm)) with a 10µl injection and flowrate of 1ml/min.

2.13.4 System of suitability

To determine the suitability of the above HPLC method several validation studies were carried out as outlined in sections 2.13.4.1 and 2.13.4.2.

2.13.4.1 LOD and LOQ

Following ICH guidelines, the limit of detection (LOD) and limit of quantification (LOQ) for NAC, Ibuprofen and Progesterone was determined. Each drugs LOD was determined individually to be the point at which a response was found to be 3 times greater than baseline noise, the results of which are shown in Table 6-2. The LOQ was determined to be the lowest concentration at which there was a deviation in peak area of less than 2% (n=6) for each drug.

2.13.4.2 Validation of methods

Following the United States Pharmacopeia guidelines on HPLC, tests were carried out to determine the resolution, asymmetry, precision, and Linearity of N-acetylcysteine, Ibuprofen and Progesterone as singular drugs, dual drug combinations and as a combination of all three drugs.

2.13.5 In vitro release kinetics

To determine the *in vitro* release kinetics of the fabricated hydrogels, the kinetic models for zero order, first order, Higuchi, Hixson-Crowell and Korsmeyer-Peppas type release were utilized. Subsequently once the type of drug release was determined, the drug transport mechanisms were determined for Ibuprofen and Progesterone as outlined by others. In short drug release results were run through a release type specific equation (eg: Korsmeyer-Peppas specific formula is $Mt / M_\infty = Kt_n$) then based on n-value drug transport mechanisms can be determined as shown in Table 2-19 (Dash *et al.*, 2010; Guerra-Ponce *et al.*, 2016).

Table 2-19 n-values relation to drug transport mechanism

n-value	Drug transport mechanism
0.5	Fickian diffusion
0.45 < n = 0.89	Non -Fickian transport
0.89	Case II transport
Higher than 0.89	Super case II transport

2.14 Final performance of modified PEGDMA hydrogels

2.15 3D printed PEGDMA characterisation

2.15.1 Hydrogel fabrication

Two mixtures, UV polymerised PEGDMA and SLA polymerised PEGDMA were prepared by mixing PEGDMA with 0.1 wt. % Irgacure 2959 photoinitiator or 1 wt. % TPO respectively. UV chamber PEGDMA was photopolymerised as described in section 2.2.1. The SLA batches of PEGDMA were prepared in a 500ml beaker and stirred as previously described. Following mixing SLA monomer mix was added to a form 2 resin tank and printed on a Form 2 SLA 3D printer (Formlabs Inc. USA). Samples were printed with a layer thickness of 50um then postcured using a Procure 350 UV chamber (3D systems) for 10 minutes. Following photopolymerisation samples were stored in 50ml universals containing PBS @ 37°C until testing.

2.15.2 3D printed PEGDMA materials properties

PEGDMA samples prepared via SLA and UV chamber polymerisation were characterised by methods explained previously (sections 2.3.2 (Chemical characterisation), 2.3.6 (Wettability measurement), 2.3.4 (Thermal properties), 2.9.1 (Swelling studies) 2.9.2 (Compressive) and 2.9.4 (Tensile and Thermal properties)) and compared to one another to determine if polymerisation via SLA impacted the properties of PEGDMA based hydrogels.

2.16 PEGCombo polymerisation and characterisation

2.16.1 PEGCombo fabrication

For the final section a combination of PEGDMA, Bioglass, DiPETMP, NAC, Ibu and Prog (referred to as PEGCombo) was prepared as shown in Table 2-21 and printed via UV chamber polymerisation as described in section 2.8.1. Samples were not printed via SLA as initial print attempts with SLA resulted in a loss of control over print resolution and rate of polymerisation, leading to premature polymerisation of the entire polymer resin with outcomes shown in Figure 7-8.

Table 2-20 Final compositions of PEGDMA, DiPETMP, Bioglass, NAC, Ibu, Prog and Irgacure 2959 in PEGCombo

Component	Amount	Notable feature
PEGDMA	42.89g	1:1 molar ratio
DiPETMP	64.99g	1:1 molar ratio
Bioglass 45S5	2.8g	2.5 wt. %
N-acetyl cysteine	1.371mg	75 µM
Ibuprofen	0.381mg	16.5 µM
Progesterone	1.056mg	30 µM
Irgacure 2959	112mg	0.1 wt. %

2.16.2 PEGCombo materials properties

Following photopolymerisation of PEGCombo samples, a study was carried out to compare the changes in materials properties of samples stored in PBS solution with those stored in 5mM NaOH @ 37°C. This study was conducted with testing of properties after 0, 2, 14 and 28 days. Samples were chemically characterised utilising ATR-FTIR, and RAMAN spectroscopy as described in sections 2.3.2 and 2.9.3 and thermally characterised via DMA and DSC as described in 2.3.4 and 2.9.4. Samples were also compared for their wettability as described in section 2.3.6, compressive and tensile strengths as in sections 2.3.5 and 2.9.4 and surface properties as in section 2.3.7. Conductivity determination and accelerated degradation testing were also carried out, with testing described in sections 2.6.3 and 2.9.5.

2.17 Statistical analysis

Data are expressed as means ± standard error of the mean. Differences within groups were analysed using one-way ANOVA methods with 95% confidence intervals. Tukey's post hoc multi-comparison tests were performed to determine where differences occurred between groups. A *p value* of less than 0.05 was considered statistically significant (*$p < 0.05$, **$p < 0.01$ and ***$p < 0.001$). Linear regression analysis was conducted, and slopes were calculated to compare cumulative release profiles. All data from phase 1 and phase 2 testing were analysed using GraphPad Prism version 5. Data analysis of later sections was carried out using Graphpad Prism 7.

Chapter 3

Characterisation of the base PEGDMA hydrogel

3.0 Characterisation of the base PEGDMA hydrogel

The initial focus was to characterise the material properties of different combinations of PEGDMA and distilled H_2O, with the goal of identifying the best PEGDMA wt. % to replicate the properties of native peripheral nerve tissues most accurately. Furthermore, if PEGDMA was to be used for peripheral nerve repair it was necessary to predict its impact on nerve like cells.

To achieve these aims 25, 50, 75 and 100 wt. % PEGDMA combinations were prepared and stored in 50ml universals containing PBS @ 37°C until testing. Testing of samples was carried out following polymerisation (day 0) and subsequently after 2, 14 and 28 days in PBS solution. Testing consisted of analysis of PEGDMAs chemical, thermal, and mechanical properties as well as determination of polymer swellability, wettability and surface properties. Following material characterisation, the in-vitro effects of the different PEGDMA samples on MC3T3 and PC-12 cells was analysed to determine the impact of PEGDMA hydrogels on cellular activity.

3.1 PEGDMA material characterisation
3.1.1 Chemical properties

Fourier transform infrared spectroscopy (FTIR) was conducted to confirm the successful photopolymerisation of the PEGDMA monomer. Successful polymerisation can be confirmed by the disappearance of the peaks associated with acrylate groups, in particular, the C-H bending of the $H_2C=CH-C=O$ group at 815 cm^{-1} (Decker and Moussa, 1987; Wu *et al.*, 2010), the C-O-C stretching at 1167 cm^{-1} (Wu *et al.*, 2010; Dobić, Filipović and Tomić, 2012) and the C=C bending of the $CH_2=CH$ groups at 1637 cm^{-1} (Silverstein and Webster, 1998). When viewing the results shown in Figures 3-1 and 3-2 the two peaks at 815 cm^{-1} and 1167 cm^{-1} disappeared when comparing the PEGDMA monomer with the photopolymerised PEGDMA. However, the peak at 1637 cm^{-1} attributed to bending of the $CH_2=CH$ group was present albeit

a much less sharp peak. This can be attributed to the possibility of residual unreacted monomer still being present in the samples, however this is unlikely as there is a wash step following curing to remove unreacted monomer. Therefore, the most likely cause of the peak is the unreacted peaks which would make up the outer layer of the PEGDMA network. This can be seen in Figure 3-4, in which the outer layer of the polymer network will be unable to polymerise with adjacent PEGDMA monomers. This is in agreement with what can be seen in the literature relating to PEGDMA hydrogels (Killion *et al.*, 2011).
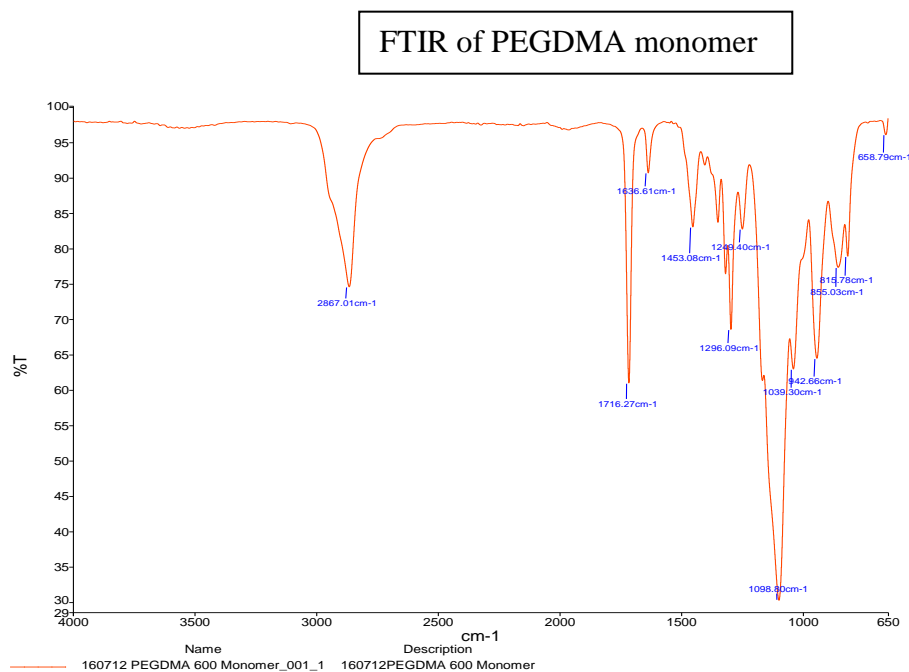
Figure 3-1 Labelled FTIR spectra of PEGDMA 600 monomer including peaks associated with monomer at 1637, 1167 and 815 cm^{-1}

FTIR of different wt. % Unhydrated PEGDMA polymers

%T

2866.66 1723.33 1453.33 1246.66 1093.33 860.00 946.66 1033.33

4000.0   3000   2000   1500   1000   650.0

cm-1
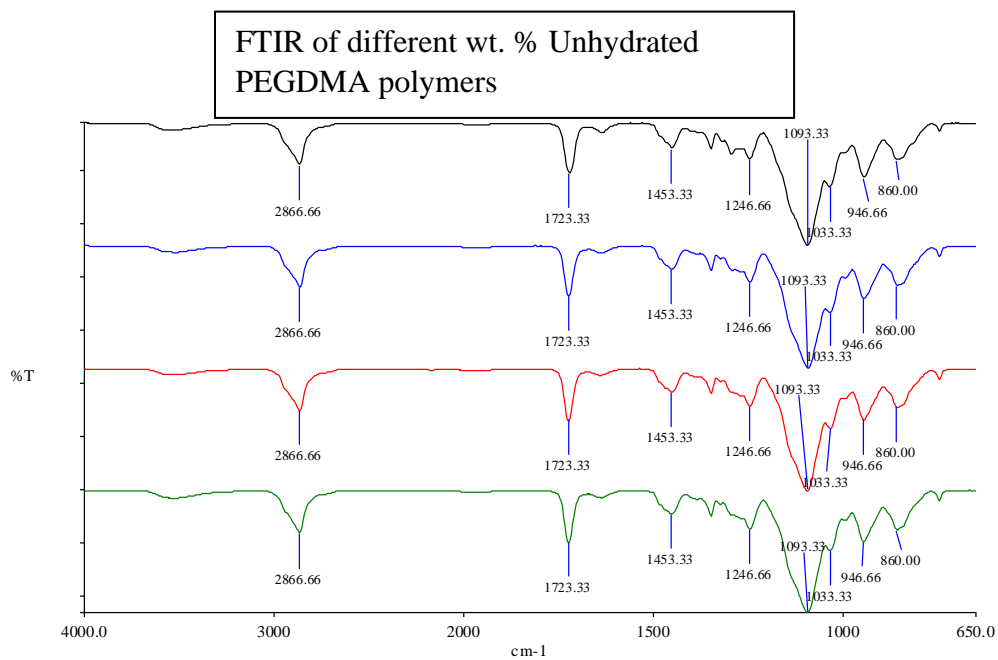
Figure 3-2 Unhydrated labelled FTIR of the 25 (Black), 50 (Blue), 75 (Red) and 100 wt. % (Green) PEGDMA compositions highlighting the different peaks associated with PEGDMA spectra.

FTIR overlay of different wt. % Unhydrated PEGDMA polymers

99.9
95
90
85
80
%T   75
70
65
60
54.0

4000.0   3000   2000   1500   1000   650.0

cm-1
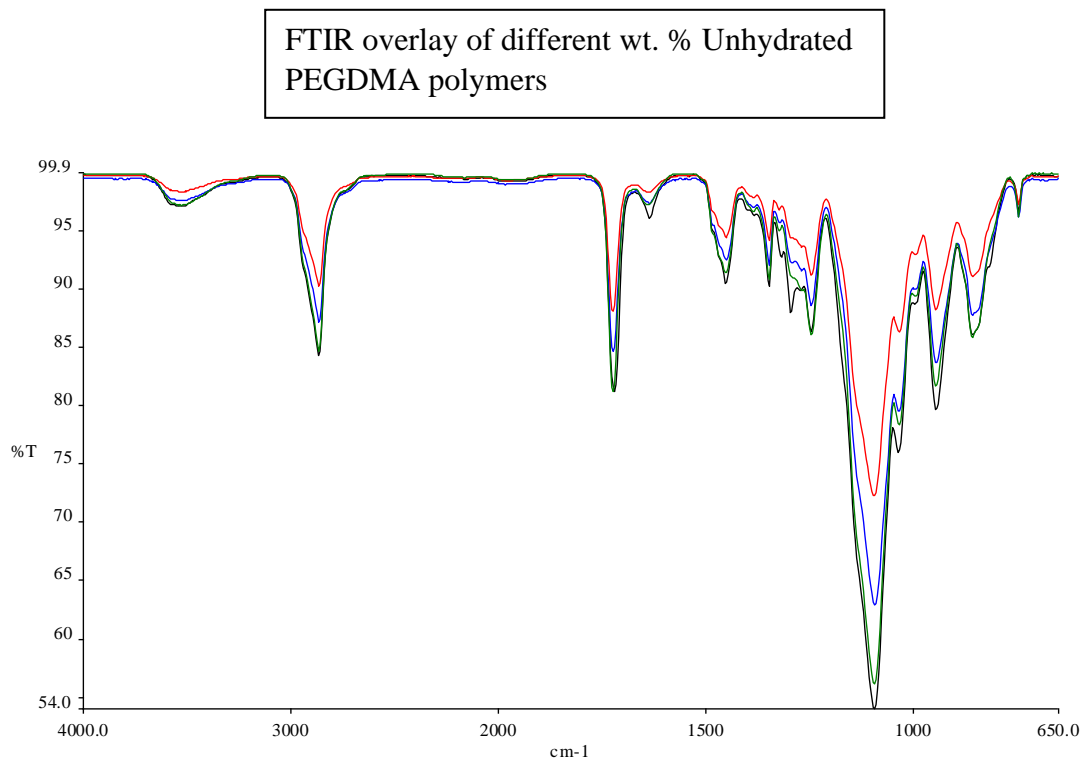
Figure 3-3 Combined FTIR overlay of the photopolymerised 25 (Black), 50 (Blue), 75 (Red) and 100 wt. % (Green) PEGDMA monomer concentrations immediately after UV curing

100
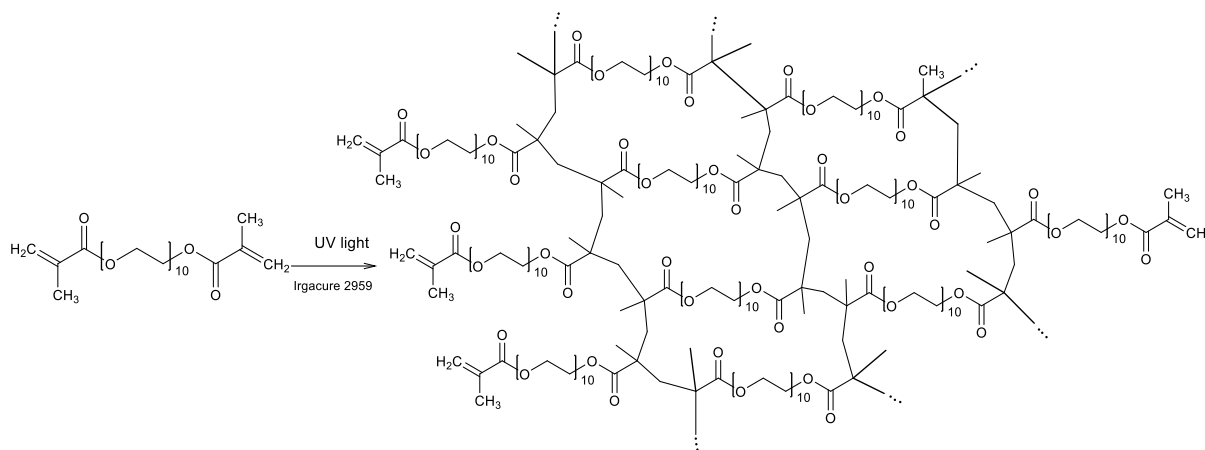
Figure 3-4 Mechanism of PEGDMA 600 Mw UV photopolymerisation (chains are connected by cleaved CH2 bonds at opposite ends of the molecule and continuations of molecules represented by continuous decimals)

3.1.2 Swelling studies

The swelling ratio of a polymer provides an indication of crosslinking density, molecular weight between crosslinks and mesh size (Lee *et al.*, 2006; Zustiak *et al.*, 2013) and the equilibrium water content can be used to distinguish between different hydrogels based on the amount of water they can uptake (LaPorte, 1997). In this study, both swelling ratios and equilibrium water content were established across the four concentrations of PEGDMA.

After 24 hours in PBS, each of the four different PEGDMA weight percentages had reached their equilibrium weight with the 25 wt. % hydrogel having the highest water content and 100 wt. % PEGDMA having the lowest as shown in Figure 3-5, indicating that increasing monomer concentration results in increased crosslink density agreeing with the established literature (Brandl, Sommer and Goepferich, 2007). The swelling ratio is given as the increase in hydrogel weight following water absorbance, expressed as a fraction of initial weight. Of note was the fact there was statistically significant differences observed in the equilibrium water content between the 100 wt. % and both 50 wt. % and 25 wt. %, the 75 wt. % and the 25 wt. % and the 50 wt. % and the 25 wt. % samples.

A similar trend was observed for the swelling ratio, with 25 wt. % PEGDMA having the highest swelling ratio of 72 in PBS, while the 100 wt. % hydrogels had the lowest mean values of 38 in PBS as seen in Figure 3-6. As in the case of the equilibrium water content, statistically significant differences were observed within the water and PBS test groups, with the additional significant difference observed between the 25 wt. % samples stored in water compared to PBS.

From these results it can be observed that with decreasing monomer percentage there is an increase in swellability suggesting a decrease in crosslink density. Research has shown in the past that increasing crosslink density results in decreasing cell attachment for PEG-based hydrogels (Bryant and Anseth, 2002) due to a decrease in surface area for cells to interact. Although whether crosslink density is truly indicative of polymer surface area has been debated (Peyton *et al.*, 2006). Based on these results the samples with the greatest surface area and therefore greater conductivity to cell adhesion would be those with lower monomer concentration.

Equilibrium Water content of 25, 50, 75 and 100 wt. % PEGDMA samples
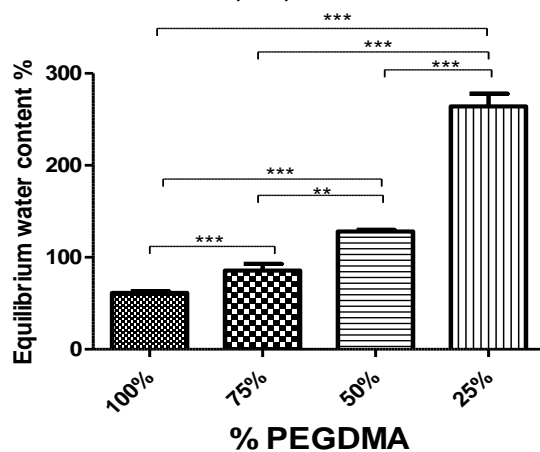
Figure 3-5 Equilibrium water content of 25, 50, 75 and 100 wt. % PEGDMA samples, statistical analysis was carried out using Graphpad Prism 5 (n=5) with p-values of less than 0.05 being considered statistically significant (*p < 0.05, **p < 0.01 and ***p < 0.001)

Mean swelling ratio of differing weight percentages of PEGDMA after 24 hours
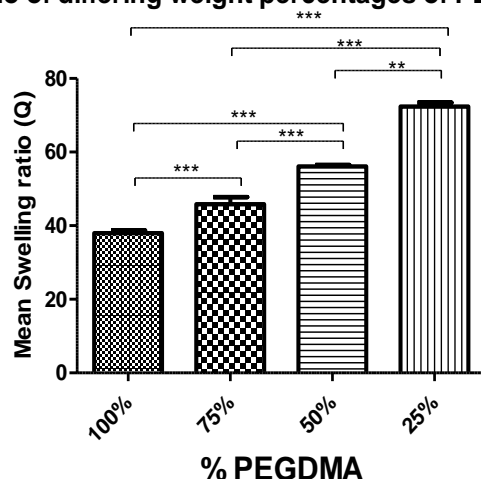
Figure 3-6 Mean swelling ratio of differing weight percentages of PEGDMA after 24 hours, statistical analysis was carried out using Graphpad Prism 5 (n=5) with p-values of less than 0.05 being considered statistically significant (*p < 0.05, **p < 0.01 and ***p < 0.001)

3.1.3 Thermal properties

In this section the thermal properties of the PEGDMA wt. %s were examined across four time points and at four weight percentages. As can be seen in Figure 3-7, the 100 wt. % PEGDMA sample recording the highest mean value of -34.5°C and the 25 wt. % recording the lowest value of -41°C, suggesting that despite having a lower crosslink density, the internal stress states are higher at lower monomer concentrations of PEGDMA allowing for lower Tgs to occur. On immersion in PBS at 37°C, an increase in Tg was observed for all PEGDMA compositions.

After two days in PBS at 37°C, no statistical differences were observed between the groups, with values of -38.9°C, -37.4°C, -39.8°C and -40°C recorded for the 100 wt. %, 75 wt. %, 50 wt. % and 25 wt. % samples respectively. The thermal properties established for PEGDMA match well with the work conducted on PEGDMA (Killion *et al.*, 2011) and also compares well with the similar work carried out on PEGDA (Lin *et al.*, 2006). Results show similar decreases in glass transition temperature resulting from a decrease in PEGDMA weight

percent, highlighting the influence crosslink density and water content have on polymer stiffness.

After 14 days, another slight increase in Tg was observed compared to days 0 and 2, but as before was not significant across the groups. After 28 days in PBS, there was an increase in Tg across all groups except the 75 wt. % samples when compared to 14 days in PBS, with the greatest change observed between the unhydrated and conditioned samples for the 100 wt. % sample, where an increase of 13°C was recorded.

Of note though, after 28 days statistically significant differences were observed between the 100 wt. % sample and both the 50 wt. % and 25 wt. % samples with values of -32.5°C, -37°C and -37.5°C recorded respectively. This suggests that after 28 days, hydration is modulated by the percentage crosslinking, with the 25 wt. % samples having the lowest crosslink density, thereby allowing greater chain mobility and a lower Tg which is in agreement with the predictions made in literature (Loshaek, 1955; Stejny, 1996).

Glass transition temperatures were consistent with compressive data seen in section 3.2.4 whereby the higher concentration PEGDMA samples had higher values. Further there appeared to be an increase in Tg over the 28 day period, indicative of chain stiffening over time in PBS solution. When comparing all samples, it could be seen that the 50 wt. % samples had consistently lower Tg values than either the 100 or 75 wt. % results. Indicating a greater chain mobility in the 50 wt. % samples compared to either the 100 or 75 wt. % samples.

Tg values for different PEGDMA monomer wt. %s after 2 days in physiological conditions
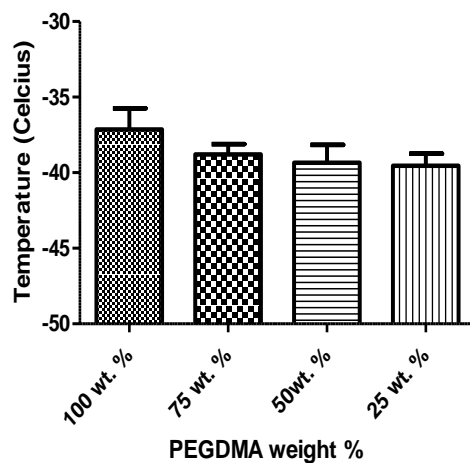
Figure 3-7 Measure of Tg results for 4 weight %s of PEGDMA after two days in physiological solution, statistical analysis was carried out using Graphpad Prism 5 (n=2) with p-values of less than 0.05 being considered statistically significant (*p < 0.05, **p < 0.01 and ***p < 0.001)
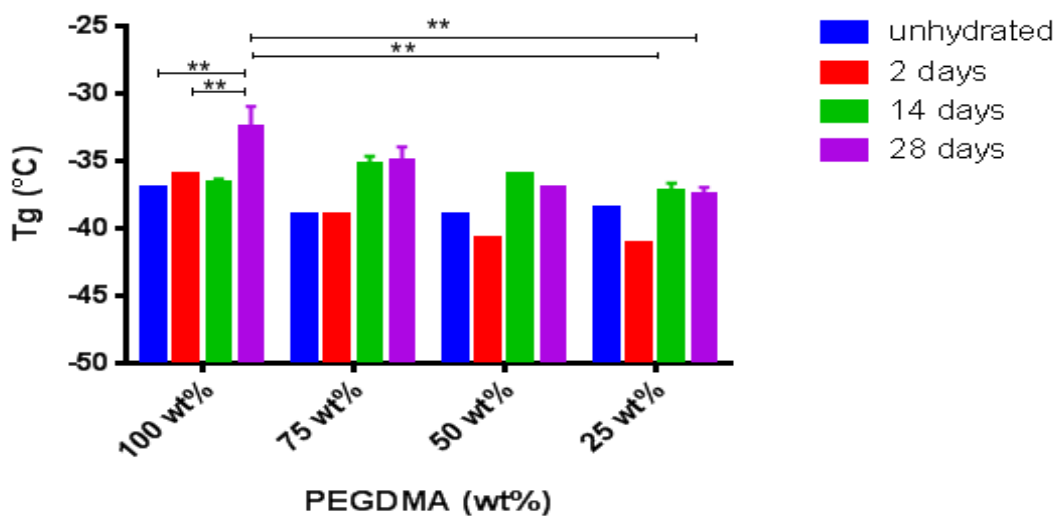
Figure 3-8 Data showing the changes in Tg for each wt. % of PEGDMA over a 28 day period, statistical analysis was carried out using Graphpad Prism 5 (n=2) with p-values of less than 0.05 being considered statistically significant (*p < 0.05, **p < 0.01 and ***p < 0.001)

3.1.4 Mechanical strength

The compressive strength at 60% strain and the compressive modulus were established from the stress strain curves as described in section 2.3.5, with the 25 wt. % PEGDMA samples showing the lowest compressive strength with mean values of 1.32 MPa recorded for the unhydrated samples and the 100 wt. % hydrogels showing the largest values of 3.85 MPa (Figure 3-9). Although there was no statistically significant difference in the compressive strength of the 100 wt. % and 75 wt. % samples, statistically significant differences were recorded between both the 100 wt. %, the 75 wt. % and both the 50 wt. % and 25 wt. % PEGDMA compositions. Regarding, compressive modulus (Figure 3-9), the 100 wt. % PEGDMA hydrogels had the highest modulus, with mean values of 9.3 MPa recorded compared to 2.3 MPa for the 25 wt. % samples, with statistically significant differences recorded between groups, suggesting that compressive modulus is affected by increasing polymer content. This indicates the compression strength and moduli values increased with increasing PEGDMA content, further over time spent in solution, however, no statistically significant differences were observed. This was a possible indication that as gels swelled there was a decrease in the mechanical strength of hydrogels, shown particularly in the compressive moduli where there were drops in compressive moduli of between 2 and 4 MPa across the 100, 75 and 50 wt. %s. The difference between the 100 and 50 wt. % results was not very large when considering the difference in monomer content.
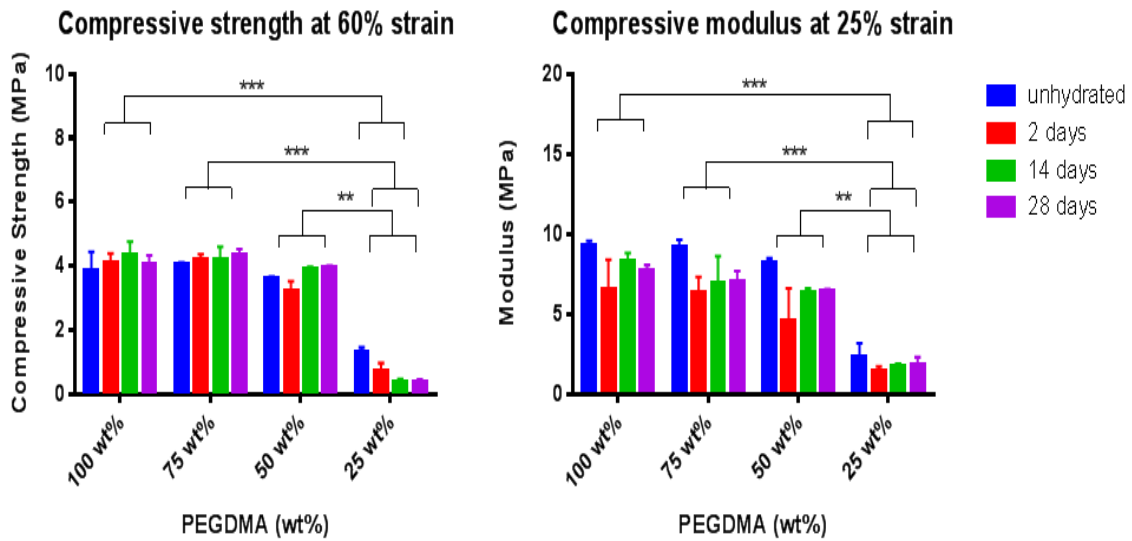
Figure 3-9 Changes to compressive strength and Youngs modulus over a 28 day period across four PEGDMA concentrations, statistical analysis was carried out using Graphpad Prism 5 (n=5) with p-values of less than 0.05 being considered statistically significant (*p < 0.05, **p < 0.01 and ***p < 0.001)
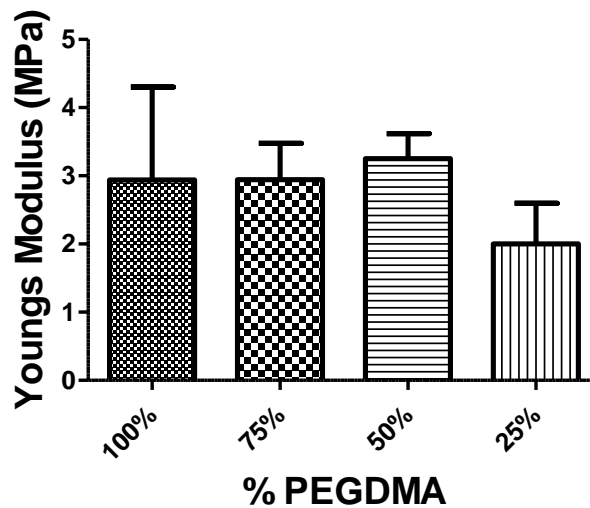
Figure 3-10 Data showing the impact of PEGDMA weight percentage on its compressive properties after two days in physiological solution, statistical analysis was carried out using Graphpad Prism 5 (n=5) with p-values of less than 0.05 being considered statistically significant (*p < 0.05, **p < 0.01 and ***p < 0.001)

3.1.5 Wettability measurement

It has been noted by others that a polymer must possess a contact angle of lower than 90° to be considered hydrophilic with hydrophilicity increasing the closer a samples wettability gets to 0° (Bracco and Holst, 2013), and in cell work it has been found that moderately hydrophilic materials in the range of 40-60° lend themselves better to cell adherence than hydrophobic materials (Arima and Iwata, 2007). Viewing the data shown in Figures 3-11, 3-12 and 3-13 it could be seen that there was a wide variance in changes to wettability going from day 0 to day 21 for each of the PEGDMA weight percentages.

The 25 wt. % sample saw an initial decrease in wettability from approximately 70° to approximately 50°. The 75 wt. % samples saw an initial increase from 60° to 80° which then decreased back to 60° with a similar fluctuation occurring for the 100 wt. % samples, going from 50° to 65° and back again to 45°. The 50 wt. % PEGDMA sample was shown over these time points to have a contact angle most consistent with the range of 40° to 60° with a result hovering around 60° across all time points. It is also worth noting that the 50 wt. % had wettability measurements most closely matching what has been reported in the literature (Suh and Jon, 2005). Based on this data the 50 wt. %s contact angles for the 14- and 28-day time points were also carried out with results shown in Figure 3-14.

In this data the 50 wt. % samples maintained a wettability in the approximate 40° to 60° range. The 50 wt. % PEGDMA sample provided the best wettability measurements, with a maximum angle recorded at day 2 of 64° and a minimum angle recorded at day 14 of 42°. The wettability levelled off, reaching angles of approximately 60° for days 21 and 28. The 50 wt. % PEGDMA sample was highlighted as having the wettability measurements which fitted most closely with the wettability set out as ideal by (Arima and Iwata, 2007) for cell adhesion. It should also be noted that 100 wt. % PEGDMA samples also possessed wettability in the 40 to 60° range at

day 0, had a comparable day 2 wettability of 66° and at day 21 all PEGDMA wt. %s demonstrated wettability in the 40 to 60° range.

Contact angle at time 0 across different PEGDMA %s
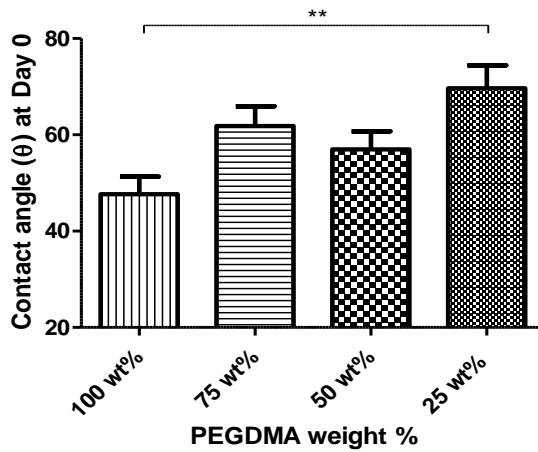
Figure 3-11 Mean contact angle results across the different unhydrated PEGDMA weight percentages, statistical analysis was carried out using Graphpad Prism 5 (n=9) with p-values of less than 0.05 being considered statistically significant (*p < 0.05, **p < 0.01 and ***p < 0.001)

Contact angle after 2 days in physiological conditions across PEGDMA %s
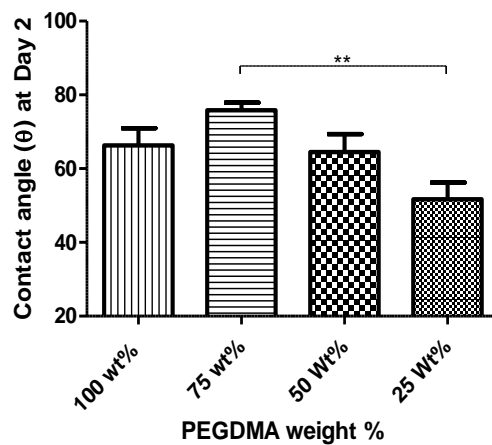
Figure 3-12 Mean contact angle results across the different PEGDMA weight percentages after 2 days in physiological solution, statistical analysis was carried out using Graphpad Prism 5 (n=9) with p-values of less than 0.05 being considered statistically significant (*p < 0.05, **p < 0.01 and ***p < 0.001)

Contact angle after 21 days in physiological conditions across PEGDMA %s
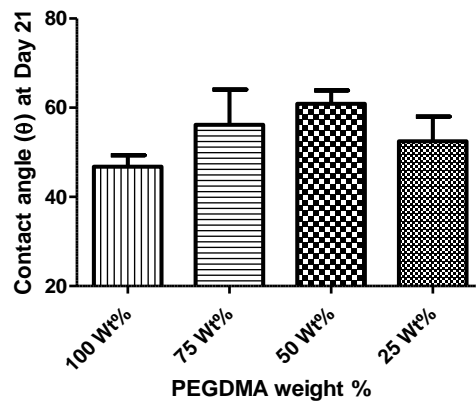
Figure 3-13 Mean contact angle results across the different PEGDMA weight percentages following submersion in physiological solution for 21 days, statistical analysis was carried out using Graphpad Prism 5 (n=9) with p-values of less than 0.05 being considered statistically significant (*p < 0.05, **p < 0.01 and ***p < 0.001)
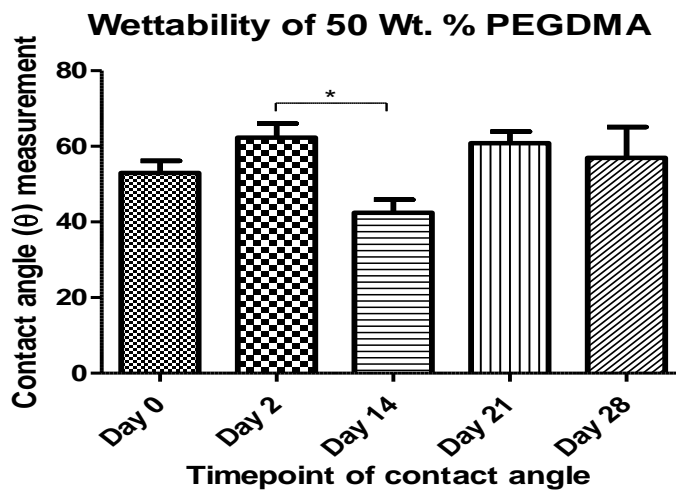
Figure 3-14 Mean contact angle results across days 0 to 28 for the 50 wt. % PEGDMA samples, statistical analysis was carried out using Graphpad Prism 5 (n=9) with p-values of less than 0.05 being considered statistically significant (*p < 0.05, **p < 0.01 and ***p < 0.001)

3.1.6 Surface properties

Figure 3-15 shows SEM images comparing the four different PEGDMA wt. %s across four different timepoints. When unhydrated the four PEGDMA surfaces maintained a rough appearance when compared with hydrated results. Following hydration all PEGDMA samples proved to be much smoother and when comparing the earliest hydrated results (day 2) with the latest (day 28) there were no discernible differences for any PEGDMA wt. %. This would suggest there are no major changes caused to the surface topography from immersion in PBS. Further there were no signs of erosion when looking at the surface of the polymer following 28 days of immersion in PBS. Across days 2 to 28 white crystals could be seen on the surface of the PEGDMA samples. Using EDX, the white particles on the surface were determined to be salt particles from the PBS solution. Surface roughness for each image has been quantified and added to Appendix F, variation in surface roughness was noted and may be attributed to cryofracture process.
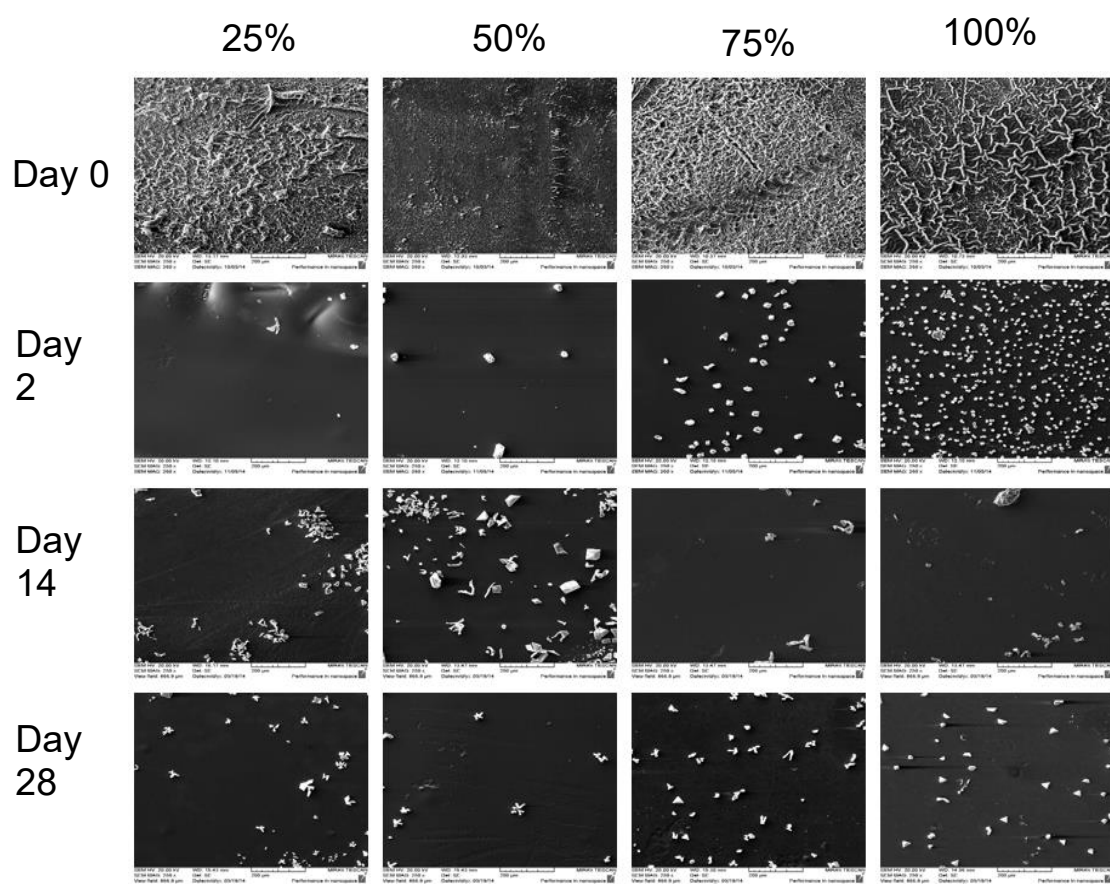
Figure 3-15 SEM (magnification 250x) of PEGDMA surface taken for different weight percentages across days 0,2,14 and 28

3.2 PEGDMA Cell Culture Studies

3.2.1 Direct contact

As mentioned in section 3.2.2, decreases in the weight remaining of each hydrogel and the pH of the PBS storage solutions were observed. To determine whether these changes would lead to a cytotoxic response, the cell metabolic activity of MC3T3 cells was examined and subsequently PC-12 cells were analysed. As shown in Figures 3-16 to 3-19 there was no observed adverse effect to the metabolic activity of the cells grown in direct contact with the hydrogels or using media conditioned with hydrogel elute. In Figures 3-16 and 3-18 (MC3T3 cells) the 100 wt. % PEGDMA samples were shown to have the smallest impact on MC3T3 metabolic activity, having values closest to the control and being significantly higher than the 25 and 50 wt. % in direct contact and elution analysis. In the elution assay, all test conditions were shown to have significantly higher metabolic activity values than the 25 wt. % PEGDMA sample, with metabolic activity values falling to 55 % of control wells. While this result is concerning, as the MC3T3 was not representative of a nerve like cell line, more weight was placed on the PC-12 metabolic activity outcomes. When viewing Figures 3-17 and 3-19 not only was there no cytotoxic effect, PEGDMA appeared to have a proliferative effect on PC-12 cells. Taken together, these results suggest that all four PEGDMA hydrogels were non-cytotoxic and that there was no leakage of unreacted monomers from the polymer into the medium after washing.

MC3T3 Direct Contact Assay for PEGDMAwt. %s
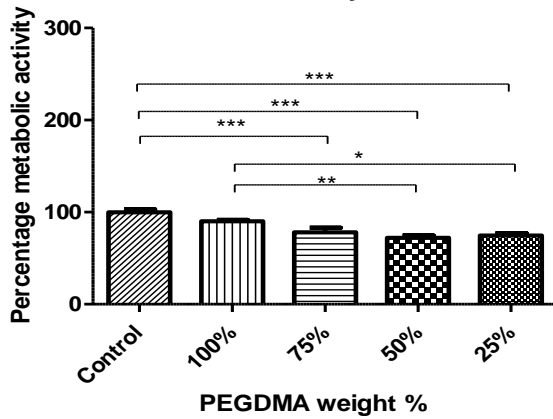
Figure 3-16 Comparison of metabolic activity of MC3T3 cells 24 hrs direct contact assay using multiple percentages of PEGDMA as a percentage of control cells, statistical analysis was carried out using Graphpad Prism 5 (n=9) with p-values of less than 0.05 being considered statistically significant (*p < 0.05, **p < 0.01 and ***p < 0.001)

PC-12 Direct contact assay for PEGDMA wt. %s
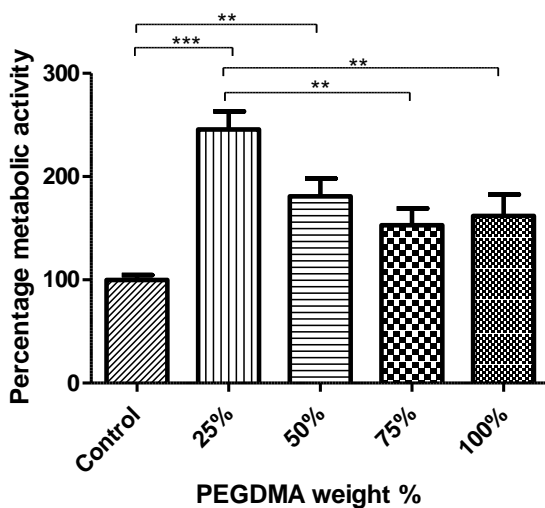
Figure 3-17 Direct contact assay using Alamar blue showing PC-12 cell metabolic activity as percentage of control 24 hrs after direct contact assay with PEGDMA samples, statistical analysis was carried out using Graphpad Prism 5 (n=9) with p-values of less than 0.05 being considered statistically significant (*p < 0.05, **p < 0.01 and ***p < 0.001)

114

3.2.2 Elution assay

Elution assay of MC3T3 cells for PEGDMA wt. %s
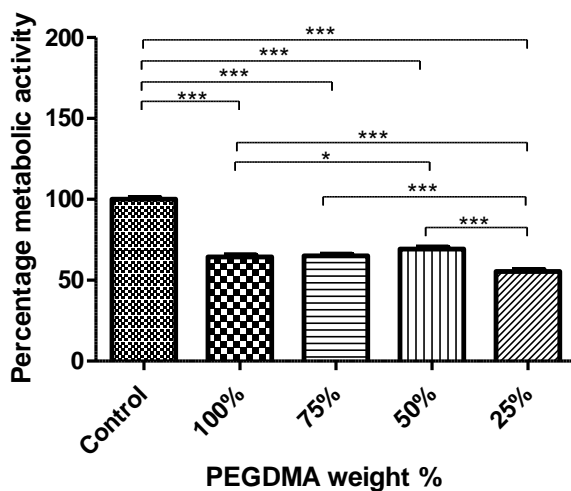
*Figure 3-18 Elution assay results showing metabolic activity of MC3T3 cells after 24 hrs exposure to PEGDMA elute as a percentage of control, statistical analysis was carried out using Graphpad Prism 5 (n=9) with p-values of less than 0.05 being considered statistically significant (*p < 0.05, **p < 0.01 and ***p < 0.001)*

Elution assay of PC-12 cells for PEGDMA wt. %s
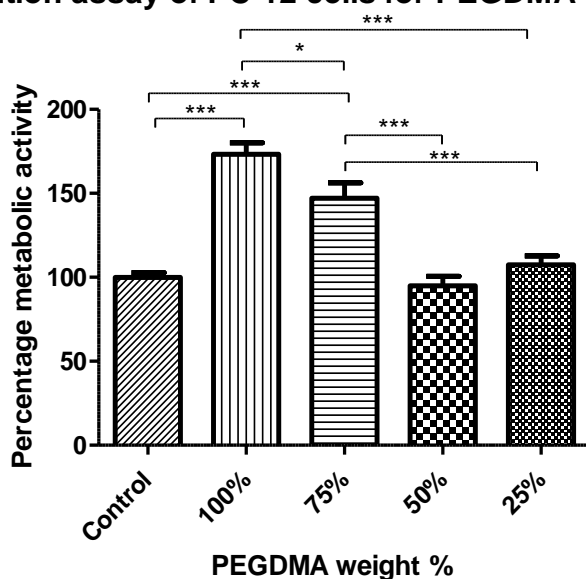
*Figure 3-19 Elution assay results showing metabolic activity of PC-12 cells after 24 hrs exposure to PEGDMA elute as a percentage of control, statistical analysis was carried out using Graphpad Prism 5 (n=9) with p-values of less than 0.05 being considered statistically significant (*p < 0.05, **p < 0.01 and ***p < 0.001)*

3.2.3 PEGDMA cell attachment

Cell adhesion plays an integral role in the repair and maintenance of tissues as it pertains to a cells ability to stick to an extracellular matrix or to another cell (Khalili and Ahmad, 2015). In this test, samples were prepared as per section 2.7.4 and then microscopically imaged to highlight cell adhesion. PEGDMA cell attachment provides a visual cue as to the impact PEGDMA had on PC-12 cell attachment. Shown in Figures 3-20 and 3-21, over the first 48 hours PEGDMA has no negative impact on the proliferation or attachment of PC-12 cells, with cells being shown to both attach and proliferate over the two days shown. Furthermore, it could be seen that PC-12 cells were in fact proliferating under the polymer and therefore in direct contact with the different PEGDMA wt. %s, this was particularly evident in the 25, 75 and 100 wt. % samples.
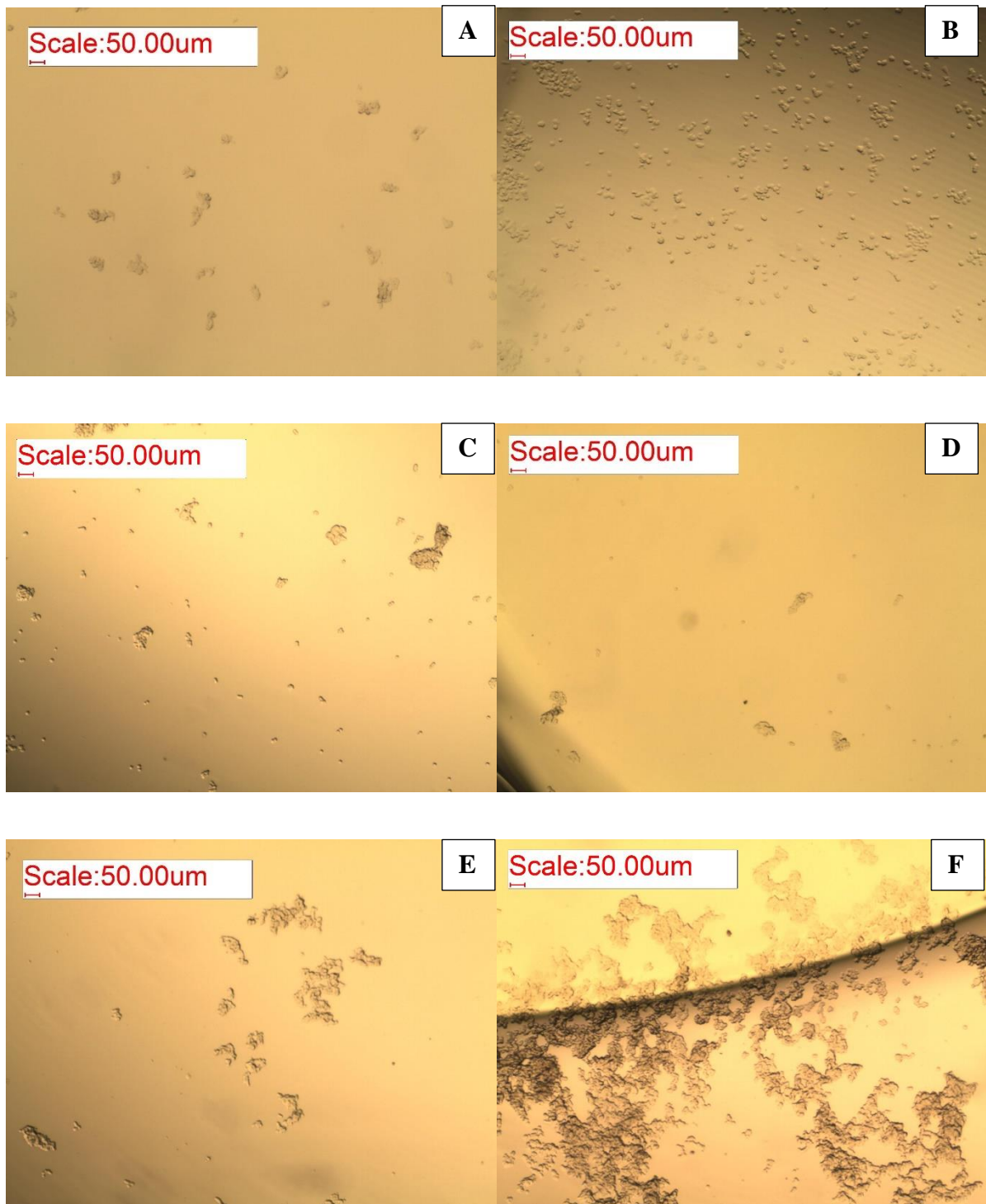
Figure 3-20 PEGDMA samples coated with Collagen type IV [25 µg/ml] using PC-12 cells seeding density (7 x 10⁴ cells/ ml) after 24 hr, magnification x40. A = Negative Control (No ColI IV), B = Positive Control (ColI IV), C = 25% PEGDMA/ ColI IV, D = 50% PEGDMA/ ColI IV, E = 75% PEGDMA/ ColI IV, F = 100% PEGDMA/ ColI IV. um in scale bar corresponds to µm
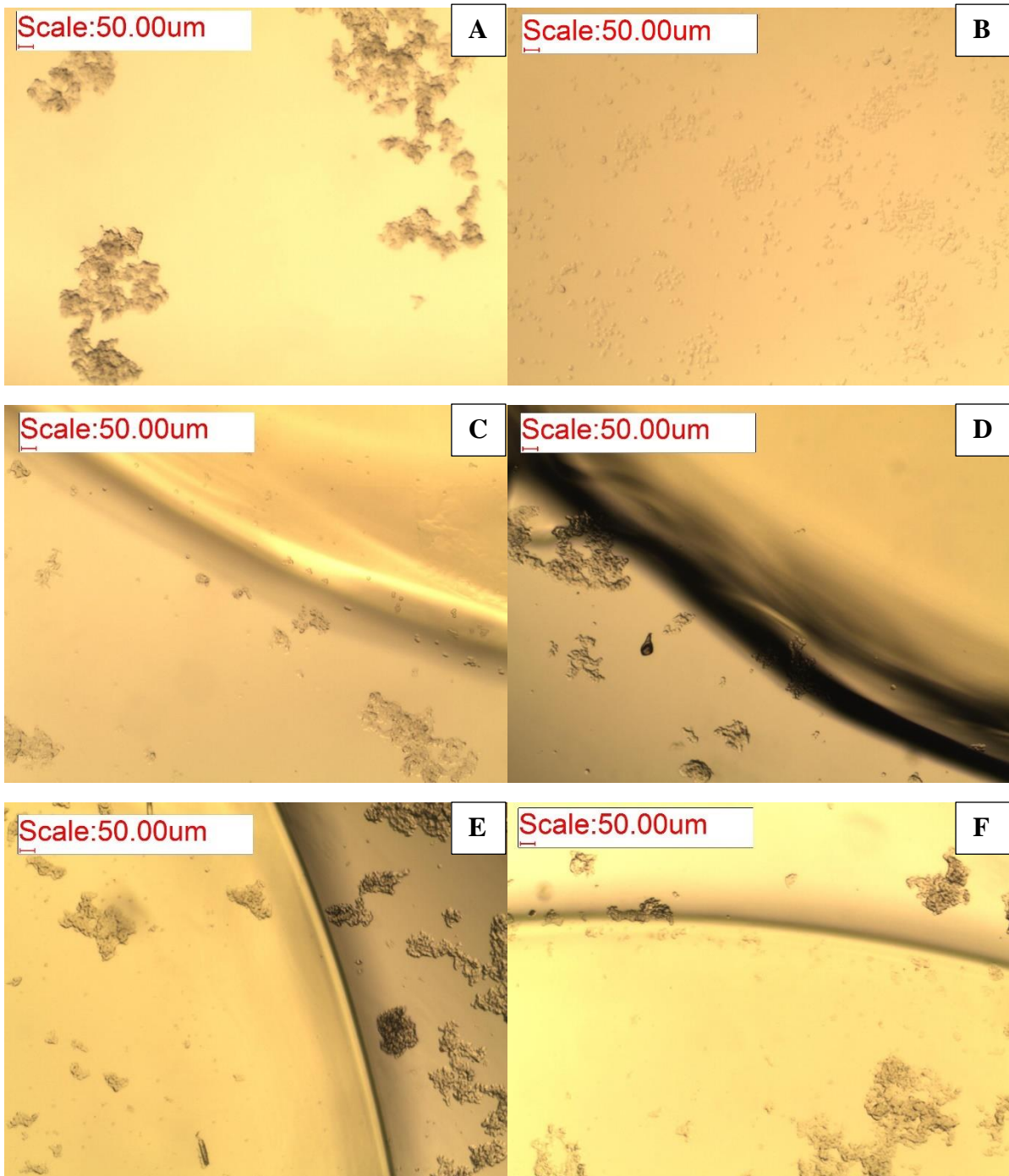
Figure 3-21 PEGDMA samples coated with Collagen type IV [25 µg/ml] using PC-12 cells seeding density (7 x 10⁴ cells/ ml) after 48 hr, magnification x40. A = Negative Control (No ColI IV), B = Positive Control (ColI IV), C = 25% PEGDMA/ ColI IV, D = 50% PEGDMA/ ColI IV, E = 75% PEGDMA/ ColI IV, F = 100% PEGDMA/ ColI IV. um in scale bar corresponds to µm

3.3 Summary

When looking at the chemical properties of the different wt. % PEGDMA polymers shown in Figures 3-3 and 3-4 it could be seen that all composites underwent successful photopolymerisation due to the disappearance of the peaks at 815 cm^{-1} and 1167 cm^{-1} (Coates, Ed and Coates, 2000). In section 3.2.3 it was determined that the lower the monomer concentration was, the greater the chance the polymer would assist in the process of cell adhesion, highlighting that the lower monomer concentrations would be more likely to induce the desired effect for a nerve guidance conduit. When viewing the thermal properties of the polymers, it was determined that the 50 wt. % and 25 wt. % samples had a greater chain mobility when compared with the higher monomer concentrations. Up to this point the 25 wt. % and 50 wt. %s were comparable, however the results for the 25 wt. % samples were disappointing when looking at mechanical properties, then when comparing the mechanical properties of the other samples it was shown that the 50 wt. % had properties comparable with the 100 wt. % samples. Further in Section 3.2.5 it could be seen that the 50 wt. % samples maintained a wettability measurement close to the ideal range of 40° and 60° throughout the 28 days of measurement a feat only mirrored by 100 wt. % samples (Arima and Iwata, 2007). These tests highlighted the 50 wt. % and 100 wt. % PEGDMA samples as the best percentages with which to prepare a nerve guidance conduit for peripheral nerve repair. In the cell culture sections 3.3.1-3.3.3 it could be seen all PEGDMA samples produced a positive impact on PC-12 cell metabolic activity both in direct contact and elution assays, while demonstrating a non-cytotoxic effect in the MC3T3 cell line for the direct contact assay, this taken together with the disappearance of FTIR peaks at 815 cm^{-1} and 1167 cm^{-1} mentioned above provide strong evidence for the successful polymerisation of PEGDMA. As methacrylate monomers are known to be cytotoxic (ISO/EN10993-5, 2009; Pradeep and Sreekumar, 2012). As the 50 wt. % was cheaper to prepare than 100 wt. % samples, it was initially selected for further testing.

Chapter 4

Modification of PEGDMA hydrogels to increase electroactivity: addition of bioglass

4.0 Modification of PEGDMA hydrogels to increase electroactivity: addition of bioglass

In the previous chapter, the 50 wt. % PEGDMA samples were selected as the most suitable polymer concentration with which to modify to further enhance its properties for Peripheral nerve repair. The second phase of this thesis focused the enhancement of PEGDMAs electrical conductivity. To achieve this, varying amounts of the electroactive bioglass 45S5 were added the 50 wt. % (referred to as 0 wt. % PEGBio samples in this section) PEGDMA, producing 0.5, 1, 1.5 and 2.5 wt. % PEGBio combinations.

The Electrical conductance of the PEGBio combinations was determined using the HR2 high resistance meter. Furthermore, testing of the PEGBio combinations material properties and their in-vitro impact on PC-12 cells was carried out, similarly to phase 1 of the thesis.

4.1 PEGBio material properties

4.1.1 Chemical properties

As mentioned in section 3.2.1 successful photopolymerisation of PEGDMA can be confirmed by the disappearance of the acrylate groups, in particular, the C-H bending of the $H_2C=CH-C=O$ group at 815 cm^{-1}, the CO-C stretching at 1167 cm^{-1}, and the C=C bending of the $CH_2=CH$ groups at 1637 cm^{-1} (Silverstein and Webster, 1998) can be seen to decrease when compared to PEGDMA monomer shown in Figure 3-12. The FTIR spectra for all five hydrogels with different bioglass concentrations were measured as per the method detailed in section 2.3.2, with results shown at day 0 in the unhydrated state, day 2, day 14 and day 28 in Figures 4-1 to 4-27. The chemical structure of the PEGDMA is shown inset with characteristic peaks at 2800-3200 cm^{-1} for CH stretching, 1520-1350 cm^{-1} for CH bending, 1500-1000 cm^{-1} attributed to C-O stretching and 2000-1500 cm^{-1} for C=O stretching, which correlates with the spectra shown in Figure 4-8. As shown in Figures 4-1 to 4-7, the two peaks at 815 cm^{-1} and 1167 cm^{-1} disappeared. However, the peak at 1637 cm^{-1} attributed to bending of the $CH_2=CH$ group was

present, this could be attributed to residual unreacted monomer being present in all samples from day 0 through to day 28 or due to the presence of C=C bonds which will occur at the very edge of the PEGDMA network. Comparing the peaks of PEGBio samples with those of PEGDMA samples showed there was no shift in peaks following photopolymerisation or during the subsequent 28 days in physiological solution. Since the peaks are indicative of chemical bonds present in the sample, and there were no alterations to the peaks present when comparing PEGBio samples to the PEGDMA samples, it can be concluded there was no chemical interaction between PEGDMA and bioglass during photopolymerisation or during the subsequent days spent in solution.
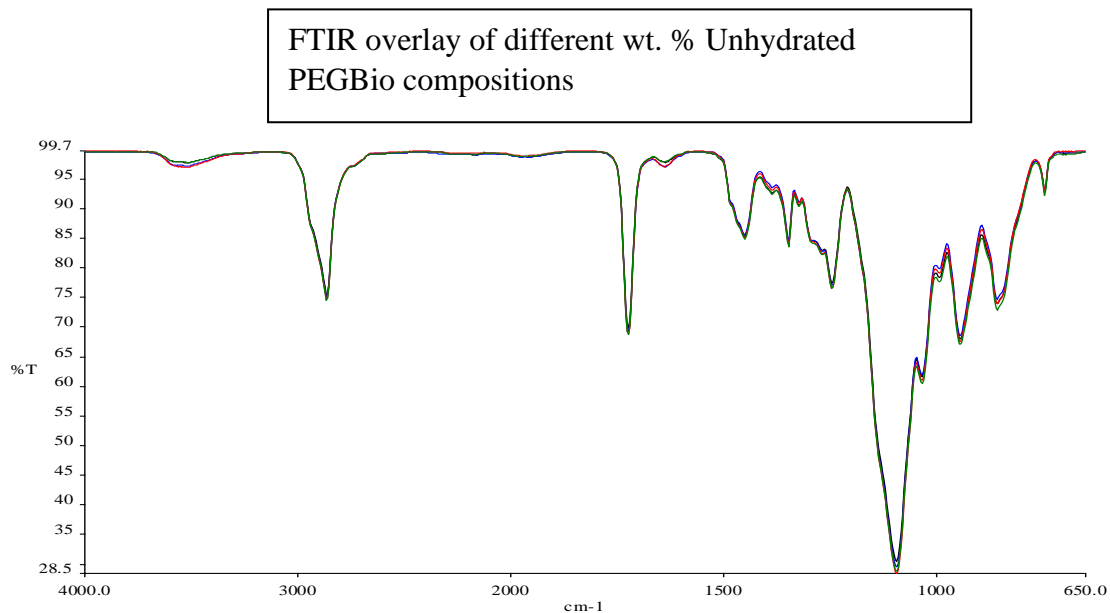
Figure 4-1 Day 0 combined FTIR of the 1 (Blue), 2.5 (Red), 3.5 (Green) and 5 wt. % (Black) PEGBio compositions
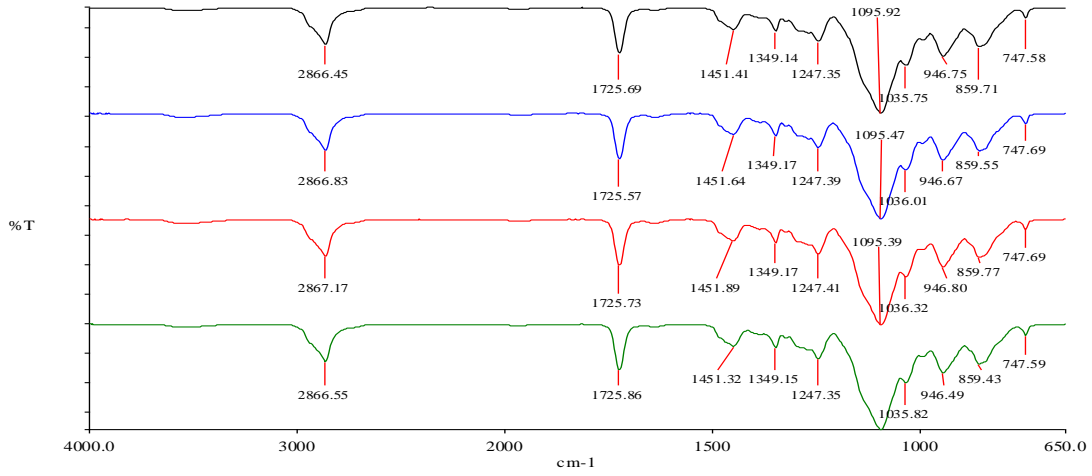
Figure 4-2 Day 0 labelled FTIR of the 1 (Blue), 2.5 (Red), 3.5 (Green) and 5 wt. % (Black) PEGBio compositions highlighting the different peaks associated with PEGBio spectra and highlighting the individual peaks for each PEGBio composition

Figure 4-3 Day 2 combined FTIR of the 1 (Green), 2.5 (Blue), 3.5 (Red) and 5 wt. % (Black) PEGBio compositions

FTIR of individual wt. % PEGBio compositions
following 2 days in PBS solution

%T

4000.0   3000   2000   1500   1000   650.0
                              cm-1
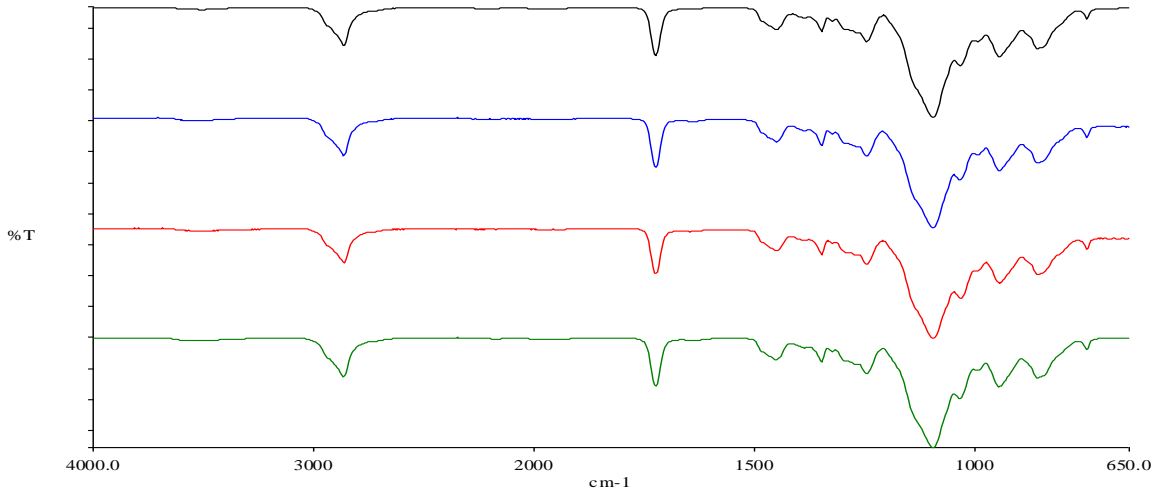
Figure 4-4 Day 2 FTIR of the 1 (Green), 2.5 (Blue), 3.5 (Red) and 5 wt. % (Black) PEGBio compositions highlighting the individual peaks for each

FTIR overlay of PEGBio wt. % compositions
following 14 days in PBS solution

%T

4000.0   3000   2000   1500   1000   650.0
                              cm-1
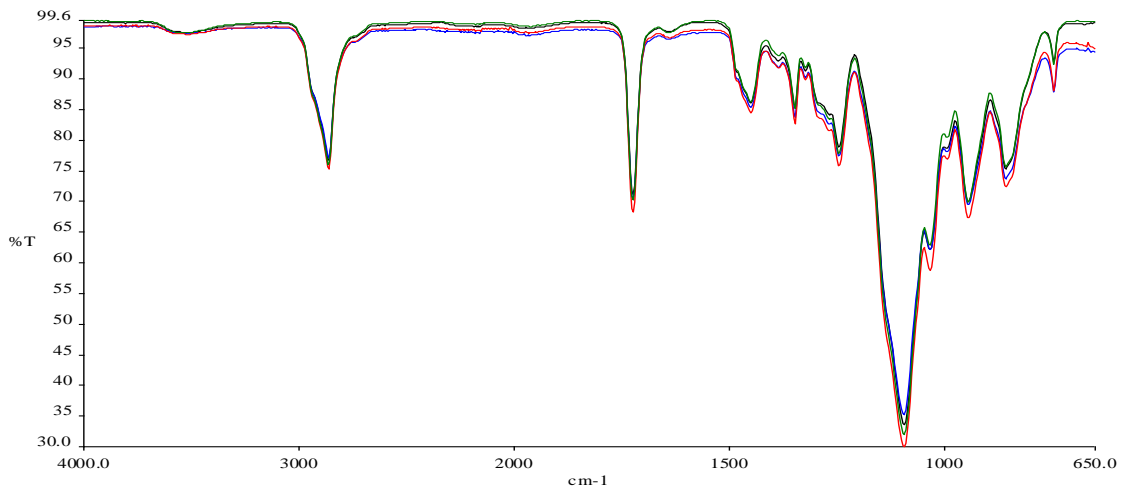
Figure 4-5 Day 14 combined FTIR of the 1 (Green), 2.5 (Red), 3.5 (Blue) and 5 wt. % PEGBio compositions

FTIR of individual PEGBio wt. % compositions
following 14 days in PBS solution
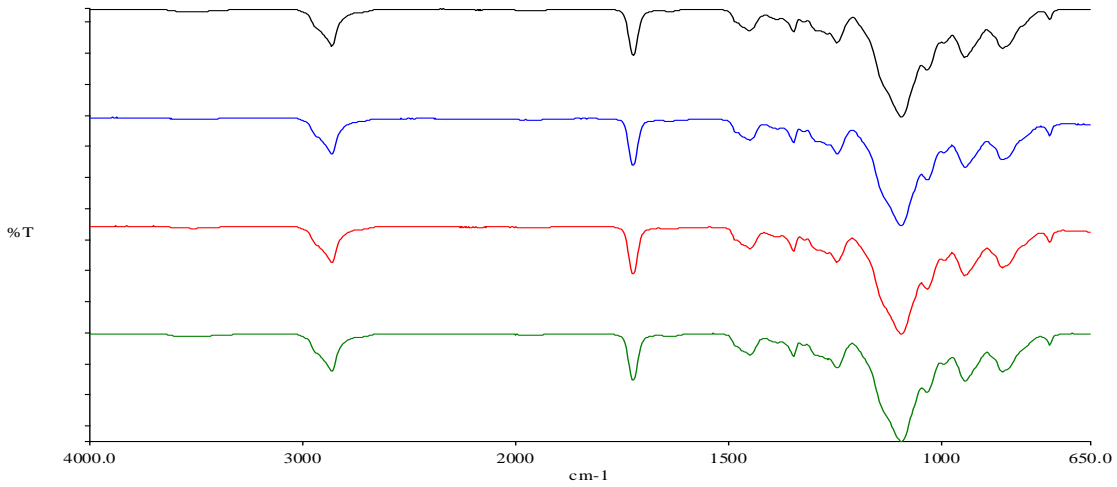
Figure 4-6 Day 14 FTIR of the 1 (Green), 2.5 (Red), 3.5 (Blue) and 5 wt. % PEGBio compositions highlighting the individual peaks for each

FTIR overlay of PEGBio wt. % compositions
following 28 days in PBS solution
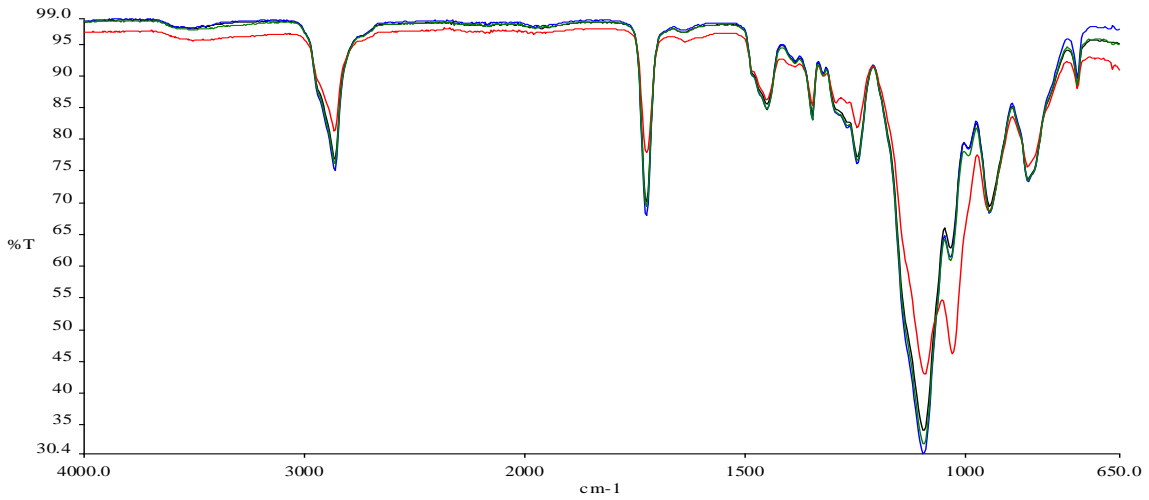
Figure 4-7 Day 28 combined FTIR of the 1 (Blue), 2.5 (Red), 3.5 (Green) and 5 wt. % (Black) PEGBio compositions

FTIR of individual PEGBio wt. % compositions following 28 days in PBS solution
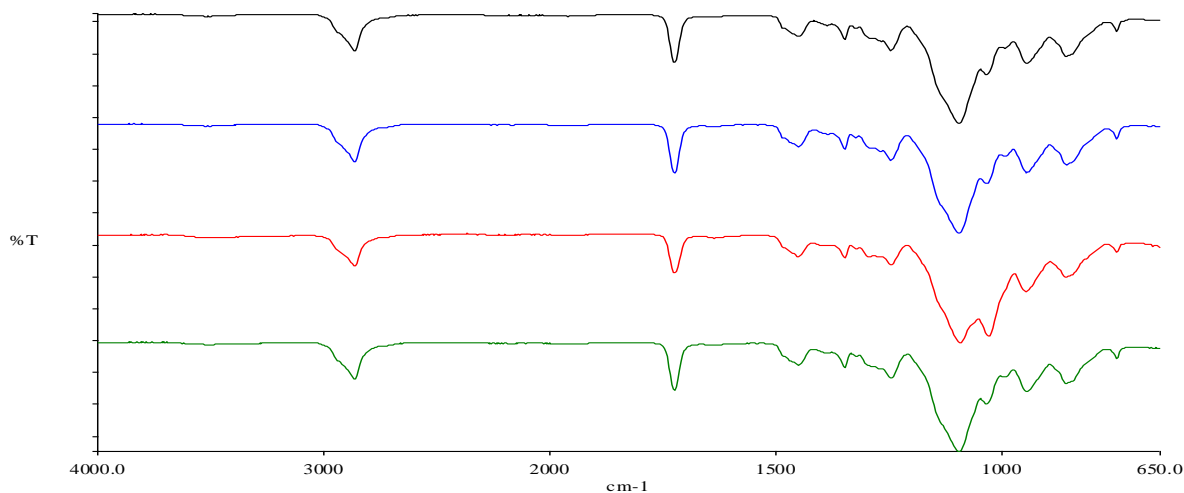
Figure 4-8 Day 28 labelled FTIR of the 1 (Blue), 2.5 (Red), 3.5 (Green) and 5 wt. % (Black) PEGBio compositions highlighting the different peaks associated with each

4.1.2 Swelling studies

The equilibrium water content of the PEGBio wt. %s of 0, 1, 1.5, 2.5 and 5% are shown in Figure 4-9. For day 0, there were significant differences recorded between the equilibrium water content values for 0 and 1.5 wt. %, 0 and 5 wt. %, 1 and 1.5 wt. %, 1 and 5 wt. %, 1.5 and 2.5 wt. %, 1.5 and 5 wt. % and the 2.5 and 5 wt. % samples. With a decrease in equilibrium water content occurring with an increase in bioglass wt. % with the 1% PEGBio having the highest equilibrium water content seeing a 30% increase from dried weight following swelling and the 5% PEGBio having the lowest resulting in an actual decrease in weight following swelling of almost 15% of its dry weight. This could be due to the bioglass occupying the space that would normally be taken up by PBS in the polymer network or a result of the bioglass inhibiting the UV from penetrating the sample, preventing a complete polymerisation of the PEG(600)DMA monomer. As there was a disappearance of the peaks associated with photopolymerisation in section 4.1.1 like what was seen in section 3.2.1, it is unlikely that the bioglass had prevented UV penetration of the samples. These results albeit to a greater degree

are mirrored in the mean swelling ratios shown in Figure 4-10, with the 1 wt. % having a swelling ratio of 56 and the 5 wt. % having a swelling ratio of 46. Thus it can be thought that bioglass takes up extra space within the PEGDMA polymer network, limiting the ability of the network to swell. These results compare quite well with the swelling ratios of the 50 wt. % samples (Q=56) in section 3.2.2 with all the 1% and 2.5% samples having a swelling ratio of 56 also. This indicates that the addition of bioglass in amounts below 2.5 wt. % does not interfere with the swelling of PEGDMA hydrogels. There is a significant decrease in swelling when the amount of bioglass increases beyond this point. Indicating that higher concentrations of bioglass affect the overall PEGBio swellability in a manner like the impact of increased crosslinking density. If this increase in bioglass inhibits cell adhesion in a manner similar to crosslinking as outlined by (Bryant and Anseth, 2002) then it can be concluded that PEGBio wt. %s greater than 2.5% are unsuitable for nerve guidance conduits.

Equilibrium water content for PEGBio composites
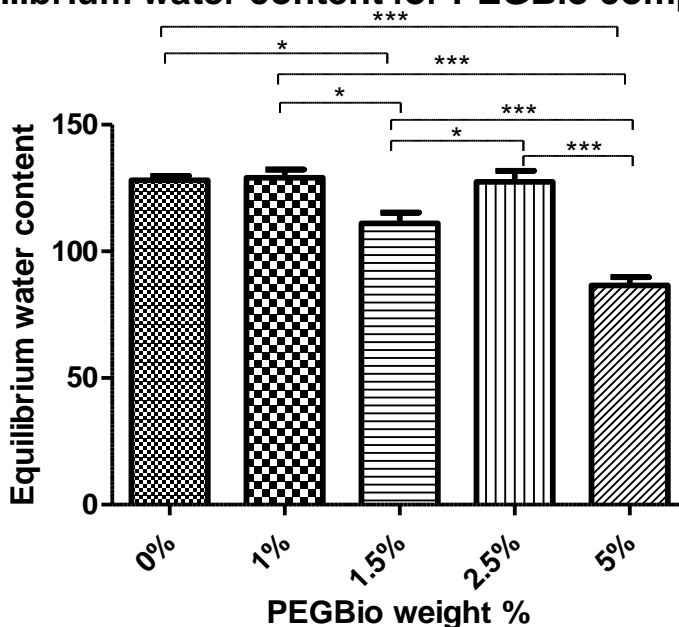
Figure 4-9 Equilibrium water content of differing Bioglass weight percentages, statistical analysis was carried out using Graphpad Prism 5 (n=5) with p-values of less than 0.05 being considered statistically significant (*p < 0.05, **p < 0.01 and ***p < 0.001)

Mean swelling ratio (Q) of different PEGBio composites
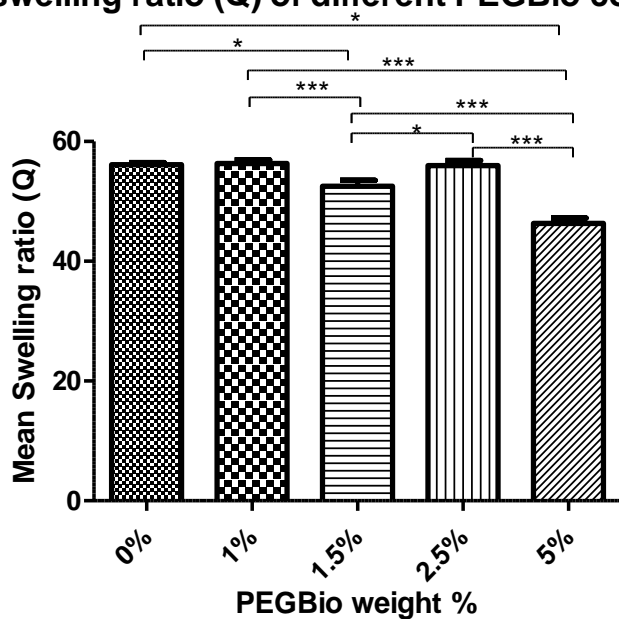
Figure 4-10 Mean swelling ratio of differing weight percentages of PEGBio, statistical analysis was carried out using Graphpad Prism 5 (n=5) with p-values of less than 0.05 being considered statistically significant (*p < 0.05, **p < 0.01 and ***p < 0.001)

4.1.3 Thermal properties

From Figures 4-11 to 4-15, the impact of bioglass on polymer properties can be seen. When looking at the data from days 0 to 28, it appeared that the addition of bioglass had a plasticising effect on the PEGDMA polymer. Only three PEGBio compositions recorded a Tg above -40°C being the 1% day 2, the 3.5% day 14 and the 5% day 2, with the highest Tg being the -39.5°C value recorded for the 3.5% day 14 result. When comparing these values to the results for 50 wt. % PEGDMA which is the base monomer to which bioglass was added the impact is evident. The values following bioglass addition maintained consistently lower Tg values, the lowest mean Tg value for 50 wt. % PEGDMA occurring after two days of immersion in physiological solution, with a mean Tg value of -39.33°C, higher than the highest glass transition temperature registered for any PEGBio sample.

When looking at the glass transition temperatures recorded for the unhydrated samples no clear pattern can be seen regarding the bioglass composites, the results recorded varied from a mean

temperature of -41.62° for the 3.5% samples to -43.64°C for the 5% samples. All results recorded were shown to be lower than the 50 wt. % PEGDMA polymer however there was not enough evidence for the results to be called significant.

When looking across all results, the glass transitions of PEGBio appeared to be higher overall following immersion in physiological solution for two days. This could be due to changes in the conformation of polymer chains caused by the higher mobility allowed to chains in the presence of water. After two days however the increase in Tg began to reverse, reaching the levels more in line with unhydrated samples. Further, as there was not a significant difference recorded when comparing the day 2 results of any bioglass percentage with their unhydrated, day 14 or day 28 counterparts or when comparing to the unhydrated samples, it can be concluded hydration did not have an impact on the thermal properties of PEGBio samples. This falls in line with the work of other researchers (Chiang and Fernandez-Garcia, 2003) who concluded that a decrease in Tg is caused only by the presence of free volume water in a sample. As all samples were vacuum dried prior to testing, no free volume water would be present to influence PEGBio Tg.

When looking at the glass transitions across the different bioglass percentages, it could be seen that at all days the samples containing bioglass were consistently lower than their PEGDMA counterpart as shown by comparing Figures 3-8 and 4-15. However when looking at the difference between bioglass percentages, there were no significant differences found across any of the bioglass percentages from 1% to 5% over the period of 28 days. Furthermore, when looking at the changes to Tg over the 28 day period for any of the bioglass percentages it could be seen that immersion in physiological solution did not impact Tg. Based on this information it could be concluded that bioglass did not significantly impact the chain mobility of PEGDMA and any difference recorded across the PEGBio composites could be attributed to background noise from the DSC.

Tg values of different unhydrated PEGBio weight percentages
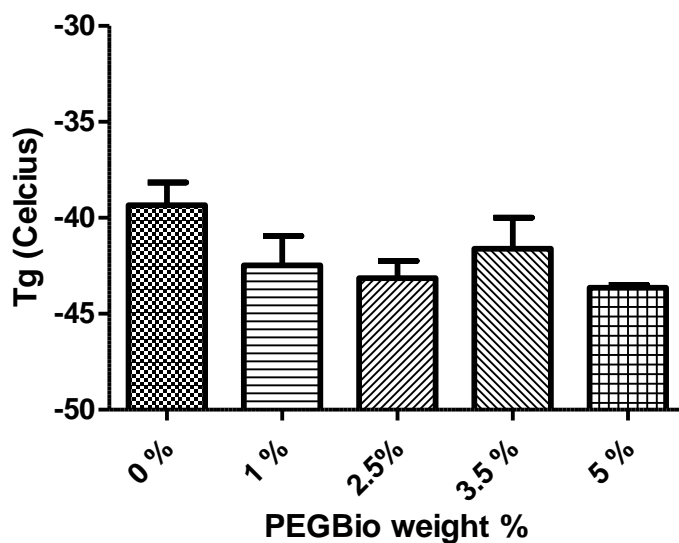
Figure 4-11 Glass transition temperatures of different PEGBio weight percentages measured in degrees Celsius in unhydrated samples, statistical analysis was carried out using Graphpad Prism 5 (n=2) with p-values of less than 0.05 being considered statistically significant (*p < 0.05, **p < 0.01 and ***p < 0.001)

Tg values at Day 2 of different PEGBio percentages
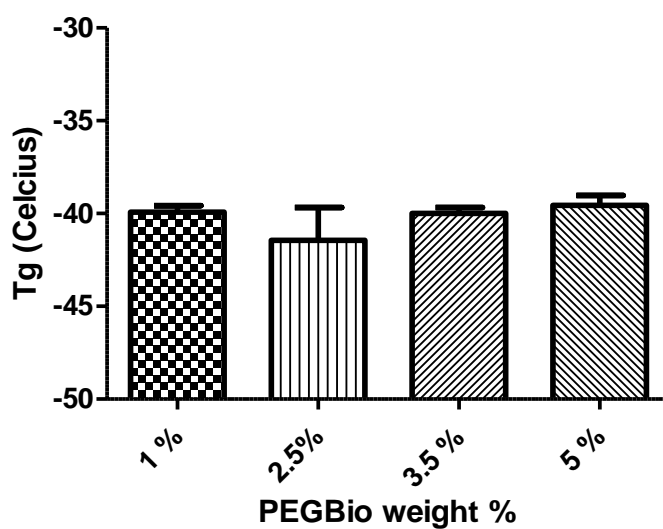
Figure 4-12 Glass transition temperatures of different PEGBio weight percentages measured in degrees Celsius after 2 days immersed in PBS solution, statistical analysis was carried out using Graphpad Prism 5 (n=2) with p-values of less than 0.05 being considered statistically significant (*p < 0.05, **p < 0.01 and ***p < 0.001)

Tg values at Day 14 of different PEGBio percentages
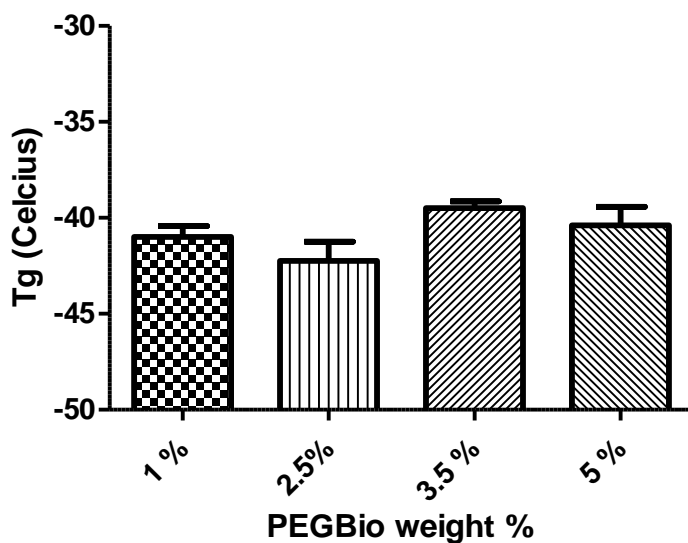
Figure 4-13 Glass transition temperatures of different PEGBio weight percentages measured in degrees Celsius after 14 days immersed in PBS solution, statistical analysis was carried out using Graphpad Prism 5 (n=5) with p-values of less than 0.05 being considered statistically significant (*p < 0.05, **p < 0.01 and ***p < 0.001)

Tg values at Day 28 of different PEGBio percentages
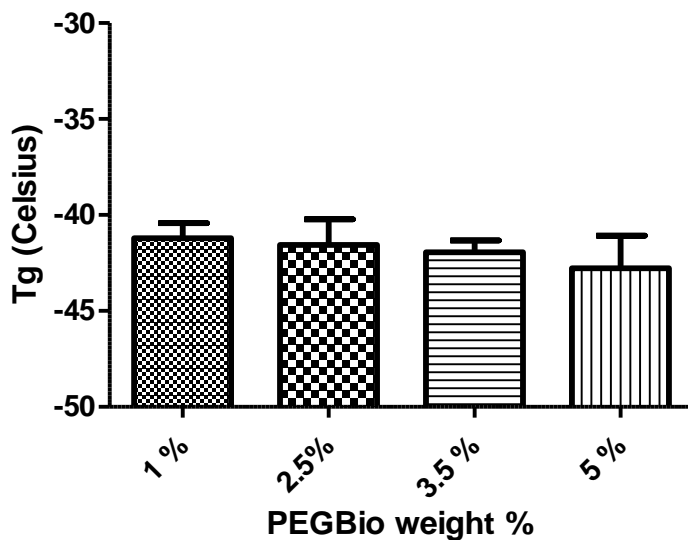
Figure 4-14 Glass transition temperatures of different PEGBio weight percentages measured in degrees Celsius after 28 days immersed in PBS solution, statistical analysis was carried out using Graphpad Prism 5 (n=2) with p-values of less than 0.05 being considered statistically significant (*p < 0.05, **p < 0.01 and ***p < 0.001)

Glass transition temperature (Tg) of PEGBio samples across all test days
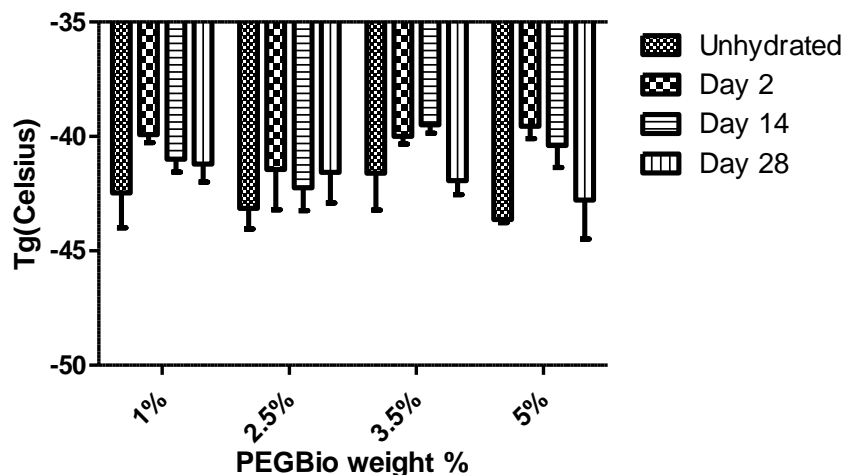
Figure 4-15 Glass transition temperatures of different PEGBio weight percentages measured in degrees Celsius across all time points following immersion in PBS

4.1.4 Mechanical strength

In a repeat of the results recorded in section 3.1.4 the 50 wt. % PEGDMA sample (recorded as 0 wt. % PEGBio) maintained its compressive strength up to 14 days however there was a drop from 6.1 MPa to 5 MPa for the day 28 measurement. This drop was not experienced by the PEGBio samples, showing that bioglass allows PEGDMA to maintain its mechanical stability over a greater length of time. Further the PEGBio results were very consistent over the 28-day period with a slight drop from 6.6 MPa to 6.1 MPa and 6.7 MPa to 5.6 MPa for the 1.5 and 5 wt. %s respectively. This is interesting as it would indicate that bioglass increases the compressive strength of PEGDMA at lower concentrations, however over time this compressive strength decreases if higher wt. %s of bioglass are used. Over time compressive modulus should decrease to facilitate the strengthening of peripheral nerves during regeneration, increasing the concentration of PEGBio could help tailor this property. Further as there was an increase of just 0.6 MPa for all PEGBio samples when compared with the compressive modulus of the 0 wt. %, a higher concentration of Bioglass is needed to improve mechanical properties.

As discussed in section 1.1.3, peripheral nerves start to deform at pressures as low as 6.7 kPa but their ultimate strain across a range species fell in the range of 1 to 12 MPa, the mechanical properties recorded across all PEGBio samples were approximately 1000 times the amount needed to start the process of deforming peripheral nerves. The work described by other researchers (Breuls, Jiya and Smit, 2008) indicate that such a degree of difference in mechanical properties could lead to suboptimal conditions for cell adhesion. However, the results fall within the range of the ultimate strain recorded for peripheral nerves across different species (Kwan *et al.*, 1992; Borschel *et al.*, 2003). Therefore, when looking to decide on a candidate for preparing a nerve guidance conduit a polymer with lower stiffness would be viewed more favourably than higher stiffness.
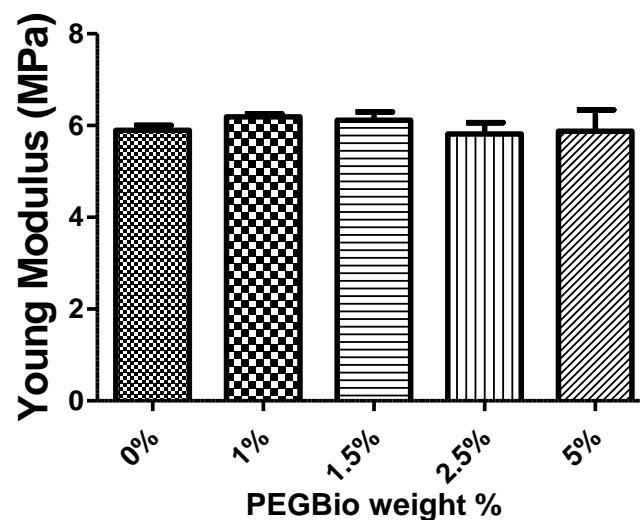
Figure 4-16 Data showing the impact of Bioglass weight percentage on the compressive properties in unhydrated PEGDMA 50 wt. % samples, statistical analysis was carried out using Graphpad Prism 5 (n=5) with p-values of less than 0.05 being considered statistically significant (*p < 0.05, **p < 0.01 and ***p < 0.001)

Compressive modulus calculated at 25% strain
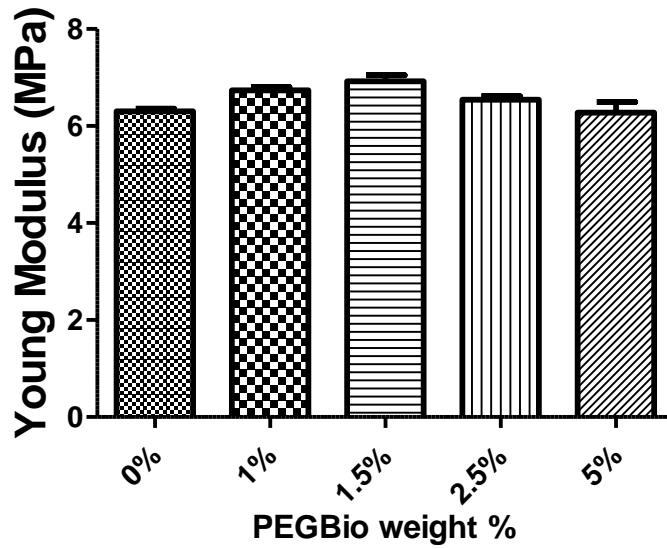
Figure 4-17 Data showing the impact of Bioglass weight percentage on the compressive properties of PEGDMA 50 wt. % samples after two days in physiological solution, statistical analysis was carried out using Graphpad Prism 5 (n=5) with p-values of less than 0.05 being considered statistically significant (*p < 0.05, **p < 0.01 and ***p < 0.001)

Compressive modulus calculated at 25% strain
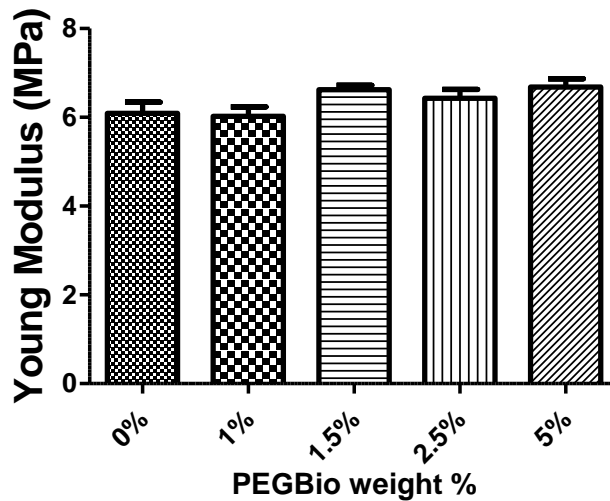
Figure 4-18 Data showing the impact of Bioglass weight percentage on the compressive properties of PEGDMA 50 wt. % samples after fourteen days in physiological solution, statistical analysis was carried out using Graphpad Prism 5 (n=5) with p-values of less than 0.05 being considered statistically significant (*p < 0.05, **p < 0.01 and ***p < 0.001)

Compressive modulus calculated at 25% strain
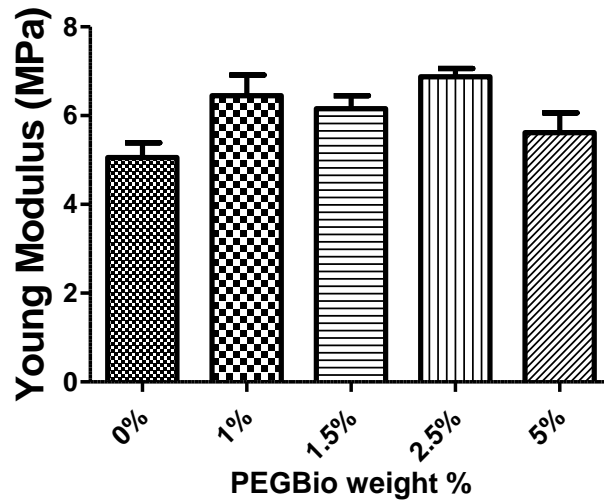
Figure 4-19 Data showing the impact of Bioglass weight percentage on the compressive properties of PEGDMA 50 wt. % samples after twenty-eight days in physiological solution, statistical analysis was carried out using Graphpad Prism 5 (n=5) with p-values of less than 0.05 being considered statistically significant (*p < 0.05, **p < 0.01 and ***p < 0.001)

Summary of Youngs modulus values across different test days
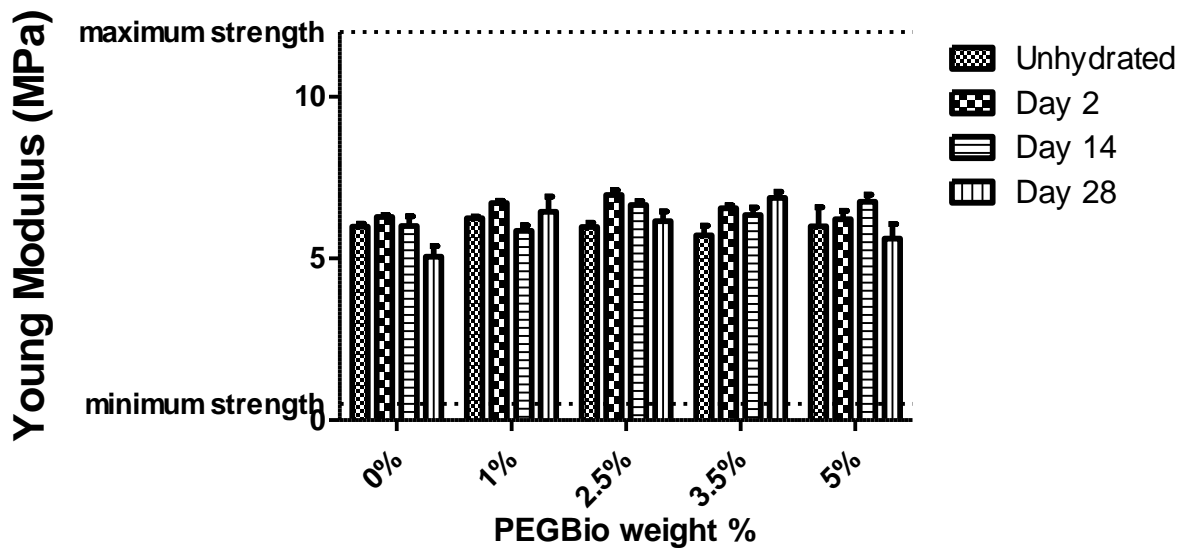
Figure 4-20 Summary of the impact to the compressive strength caused by Bioglass addition to PEGDMA 50 wt. % samples measured across a period of 28 days, Samples are given in groups based on wt. % bioglass present, with induvial columns representing 0, 2, 14 and 28 days in PBS solution at 37 degrees Celsius

4.1.5 Wettability measurement

It has been shown by others that the ideal wettability measurement for a polymer to be used in biomedical applications should be in the approximate range of 40° to 60° in order to maximise cell adhesion (Arima and Iwata, 2007; Dowling *et al.*, 2011). When viewing the changes to wettability measurement of PEGBio samples across days 0 to 28 (Figures 4-21 to 4-24) patterns could be seen to emerge across the different bioglass percentages.

Across days 0, 2 and 28 samples were shown to have increasing hydrophilicity the greater their respective bioglass concentration. For unhydrated samples shown in Figure 4-21 there was a significant difference between the 1% and the 5% bioglass samples highlighting the effect bioglass has on the increase in hydrophilicity. The differences between bioglass concentrations becomes clearer on day 2 in Figure 4-22, with the contact angle recorded for the 2.5 and 5 wt. %s being significantly lower than the 0, 1, and 1.5 wt. %s, falling to below the 40° wettability measurement. Wettability measurements on day 14 shown are in Figure 4-23 where all percentages experience a sharp increase in hydrophilicity, causing all wettability measurements except for the 5 wt. % PEGBio sample, to have lower contact angle values on day 14 than those recorded for days 0, 2 and 28.

Of note is the fact that the day 14 results for the different PEGBio samples match closely with the increase in hydrophilicity found in the PEGDMA samples, indicating there may be an underlying mechanism causing this change to hydrophilicity for the day 14 samples. For the day 28 results shown in Figure 4-24 no statistically significant difference was recorded between the different PEGBio samples, all PEGBio percentages did however, fall within the range of 40-60°, suggesting that over the 28-day period it could be seen that the different PEGBio percentages maintained their hydrophilicity.

It can be theorised that the bioglass provides a permanent rough surface creating a consistent level of hydrophilicity across which cell adherence would be aided hence based on the consistency of results the 1 wt. % and 2.5 wt. % samples are the most likely samples to utilise moving forward toward creating a nerve guidance conduit. This can be determined as both percentages maintain approximate wettability measurements of 40 to 60°.

Day 0 Measurement of Contact Angle
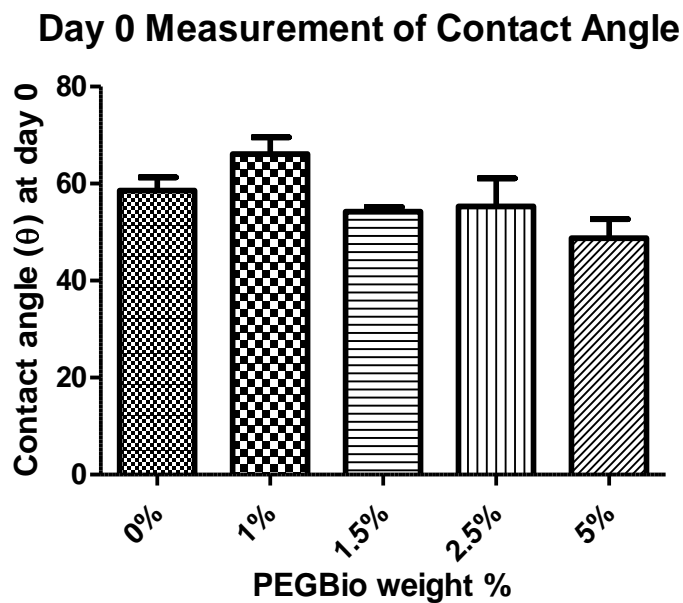
Figure 4-21 Mean contact angle results across the different unhydrated PEGBio weight percentages, statistical analysis was carried out using Graphpad Prism 5 (n=3) with p-values of less than 0.05 being considered statistically significant (*p < 0.05, **p < 0.01 and ***p < 0.001)
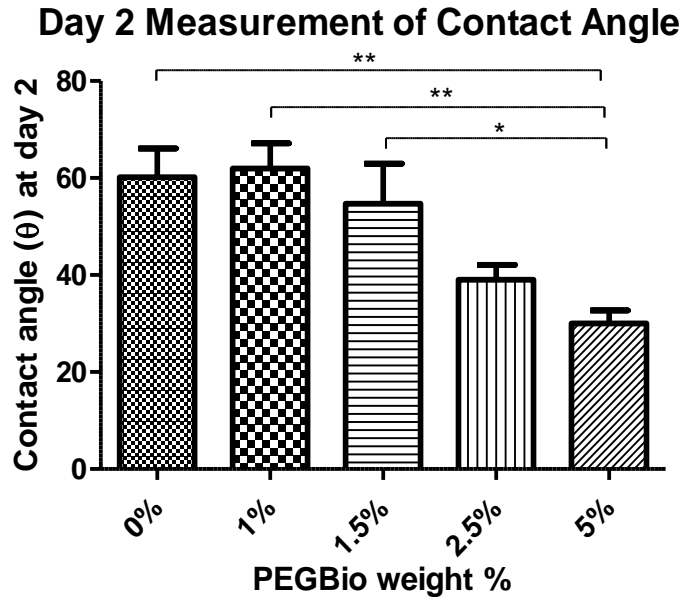
Figure 4-22 Mean contact angle results across the different PEGDMA weight percentages after 2 days in physiological conditions, statistical analysis was carried out using Graphpad Prism 5 (n=3) with p-values of less than 0.05 being considered statistically significant (*p < 0.05, **p < 0.01 and ***p < 0.001)
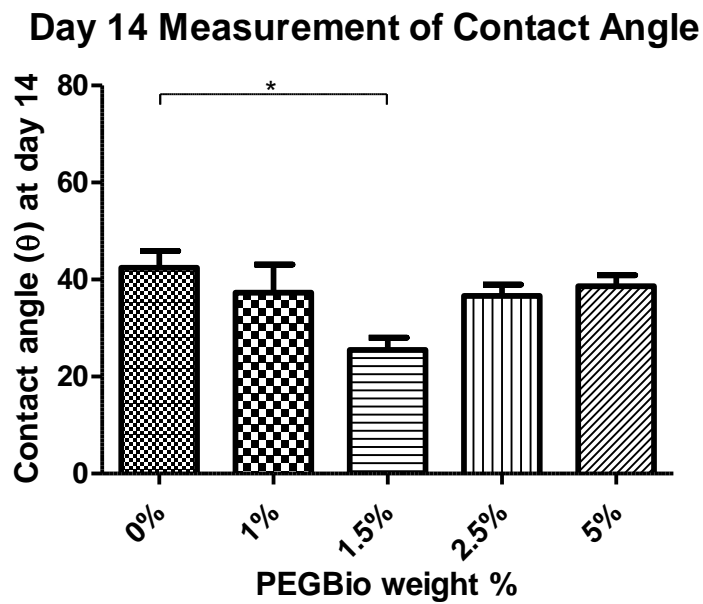
Figure 4-23 Mean contact angle results across the different PEGDMA weight percentages after 14 days in physiological conditions, statistical analysis was carried out using Graphpad Prism 5 (n=5) with p-values of less than 0.05 being considered statistically significant (*p < 0.05, **p < 0.01 and ***p < 0.001)

Day 28 Measurement of Contact Angle
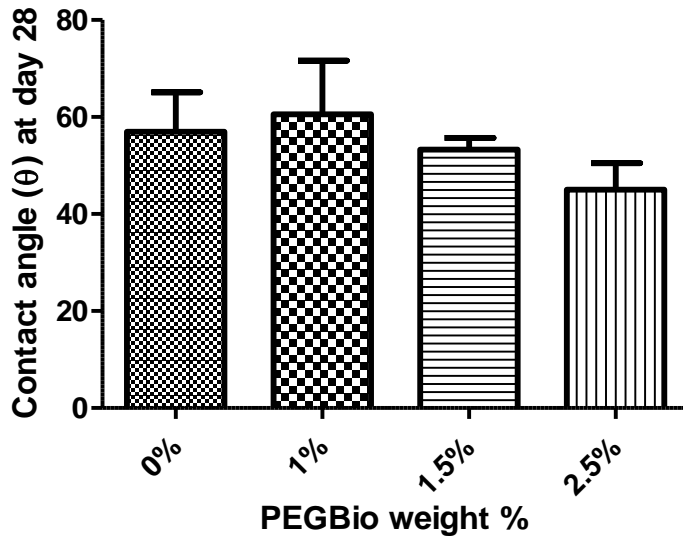
Figure 4-24 Mean contact angle results across the different PEGDMA weight percentages after 28 days, statistical analysis was carried out using Graphpad Prism 5 (n=3) with p-values of less than 0.05 being considered statistically significant (*p < 0.05, **p < 0.01 and ***p < 0.001)

4.1.6 Electrical properties

The measure of conductivity in a native peripheral nerve is approximately 5 milliSiemens per cm and for this reason, the conductivity of a peripheral nerve guidance conduit should be in the range of 5mS/cm (Runge *et al.*, 2010; Xu, Jeremy M Holzwarth, *et al.*, 2014) in order to achieve the criteria of electrical conductivity. In Figure 4-25 the 2.5 wt. % PEGBio samples provide conductivity in this approximate range. This trend continues when viewing the conductivity of the 2.5 wt. % samples in Figure 4-26 and 4-28. Across all timepoints only the 2.5 wt. % sample presents consistent conductivity values which are comparable with that of the native peripheral nerves. As such when based solely on conductivity the 2.5 wt. % samples provide the most promising results for a nerve guidance conduit.

Measurement of PEGBio wt % conductance (mS)
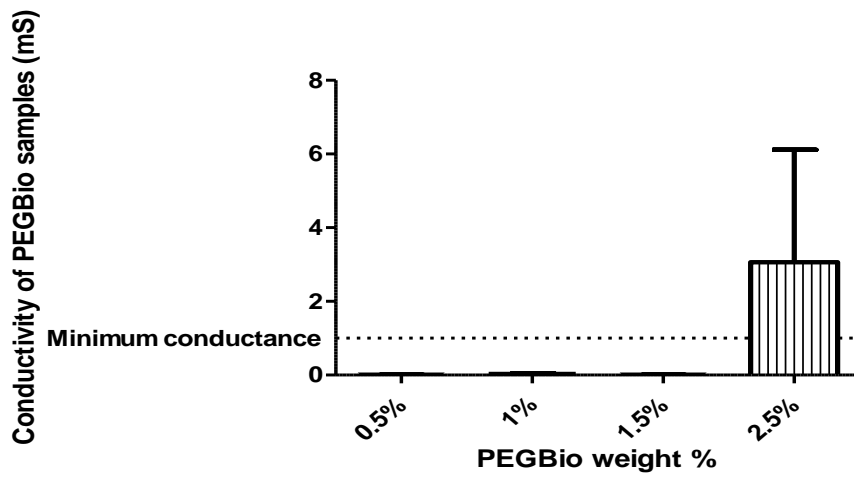
*Figure 4-25 Conductivity of various PEGBio concentrations in their unhydrated state measured in millisiemens, statistical analysis was carried out using Graphpad Prism 5 (n=3) with p-values of less than 0.05 being considered statistically significant (*p < 0.05, **p < 0.01 and ***p < 0.001)*

Day 2 measurement of PEGBio wt % conductance (mS)
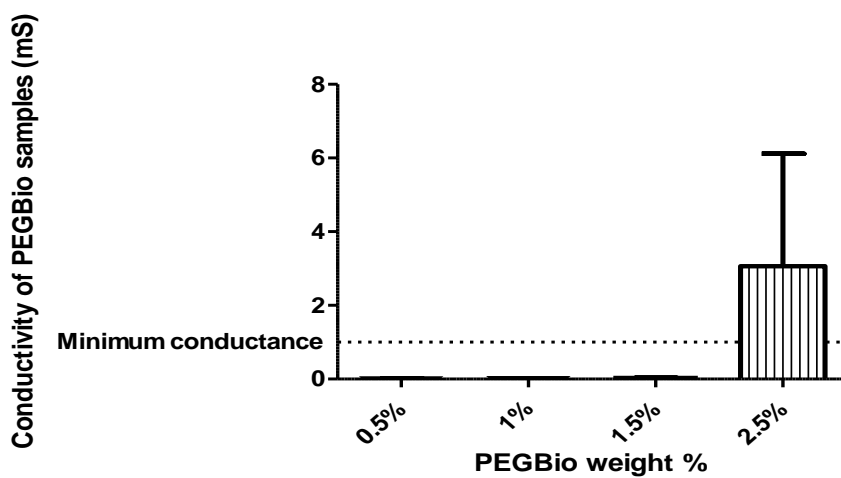
*Figure 4-26 Conductivity of various PEGBio concentrations following two days in PBS, measured in millisiemens, statistical analysis was carried out using Graphpad Prism 5 (n=3) with p-values of less than 0.05 being considered statistically significant (*p < 0.05, **p < 0.01 and ***p < 0.001)*

Day 14 measurement of PEGBio wt % conductance (mS)
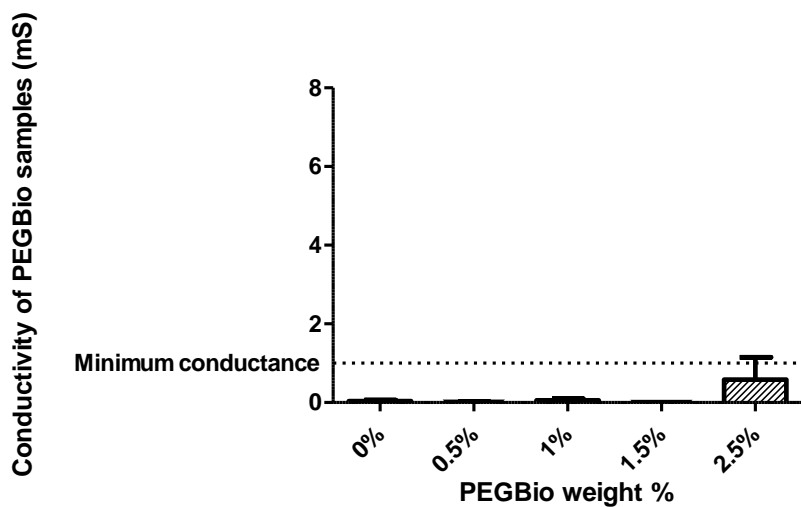
Figure 4-27 Conductivity of various PEGBio concentrations following fourteen days in PBS, measured in millisiemens, statistical analysis was carried out using Graphpad Prism 5 (n=3) with p-values of less than 0.05 being considered statistically significant (*p < 0.05, **p < 0.01 and ***p < 0.001)

Day 28 measurement of PEGBio wt % conductance (mS)
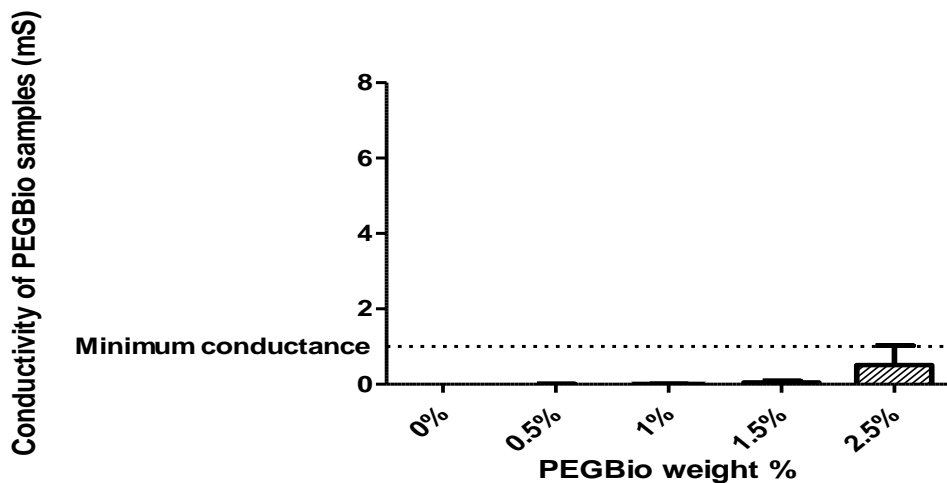
Figure 4-28 Conductivity of various PEGBio concentrations following twenty eight days in PBS, measured in millisiemens, statistical analysis was carried out using Graphpad Prism 5 (n=3) with p-values of less than 0.05 being considered statistically significant (*p < 0.05, **p < 0.01 and ***p < 0.001)

When looking at Figure 4-29, it could be seen that there are distinctive regions of smooth and rough polymer surfaces for the 0.5% and 1% PEGBio samples. This is representative of all PEGBio samples, where the smooth surface makes up approximately 25% of the polymer and the rougher surface the other 75%. It is thought that the cause of this differentiation is that during UV photopolymerisation there is a settling of the homogenised bioglass out of the PEGDMA solution. This line of thought is used for several reasons. The smooth region, closely resembles the surface of the 50 wt. % PEGDMA sample seen in Figure 3-15. The roughness of the samples is caused by the presence of large crystals which have an approximate average diameter of 40 µm, on comparison to the results of (Koudehi *et al.*, 2014) these crystals could be seen to match the approximate size of the bioglass samples they had prepared. Further, the large crystals appeared to increase in density going from lower to higher PEGBio percentages as can be seen in Figure 4-29. In Figure 4-30 it could be seen that there were also medium sized crystals (approximately 10µm in diameter) scattered throughout the polymer surface and small sized crystals (<1µm) which occurred in clusters. The medium sized crystals appeared to correspond with the PBS crystals seen in Figure 3-15 above whereas the small clusters of crystals are most likely photoinitiator spread throughout the sample. The small and medium crystals were spread evenly throughout the sample, being found in both the smooth and the rough parts of the PEGBio samples. In Figure 4-31 the different sized crystals can be seen more clearly.
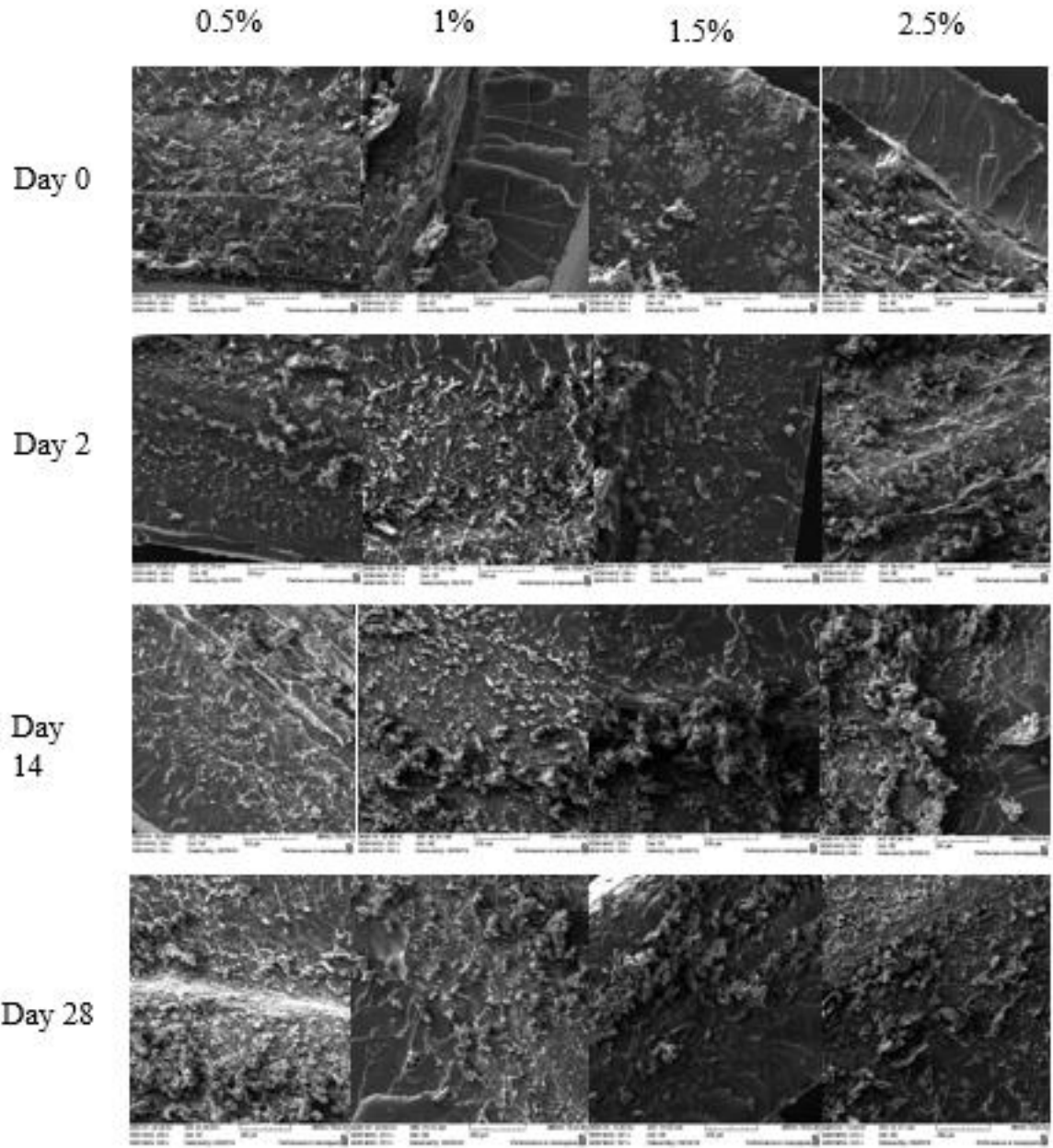
Figure 4-29 SEM (magnification 250x) of PEGBio sample surfaces taken for 0.5, 1, 1.5 and 2.5 Bioglass weight percentages following 0,2,14 and 28 days spent in physiological solution
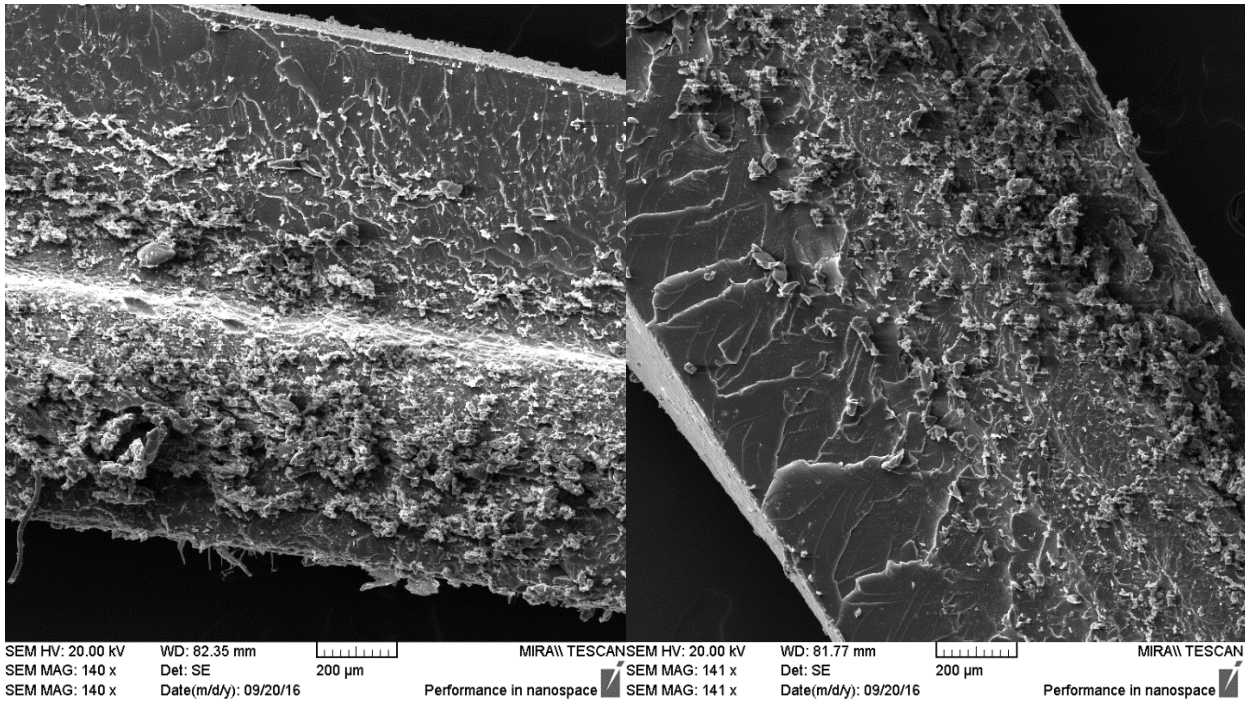
Figure 4-30 SEM (140X magnification) showing the cross section of the Day 28 0.5 and 1% PEGBio samples
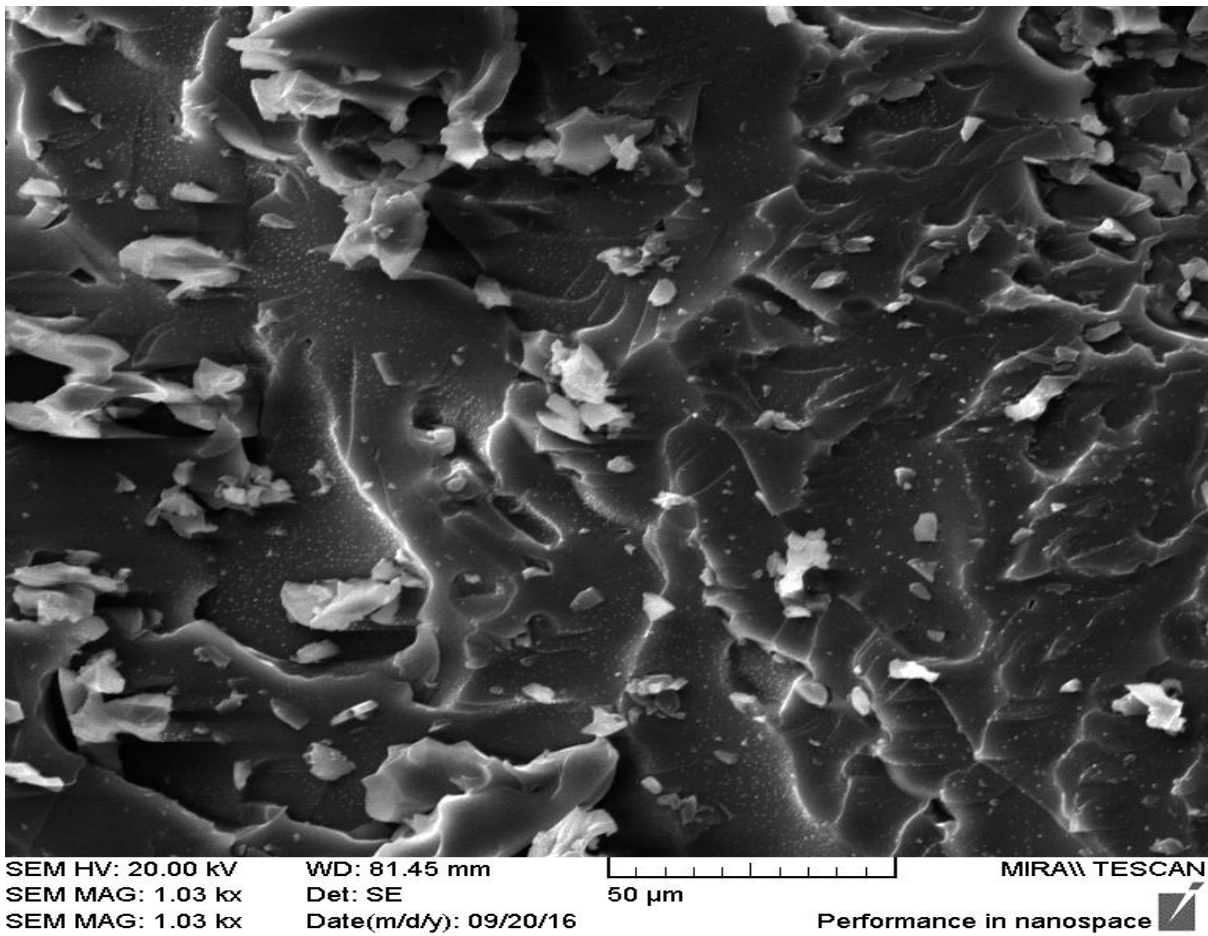
Figure 4-31 SEM (1KX magnification) showing the cross section of the day 28 1% PEGBio sample

4.2 PEGBio Cell Culture Studies

4.2.1 Direct contact

To determine whether the addition of bioglass to PEGDMA would result in a cytotoxic effect *in vitro*, a direct contact assay was set up as per Section 2.4.4. As shown in Figure 4-32, the standards outlined by ISO (ISO/EN10993-5, 2009) state that a drop in metabolic activity of greater than or equal to 30% can be considered a cytotoxic effect. Apart from the 0.5% PEGBio sample (69.76%) all PEGBio samples recorded a metabolic activity of greater than 70%. Highlighting there was no observed adverse effect to the metabolic activity of the cells grown in direct contact with the PEGBio hydrogels except for the 0.5% sample. From this it could be seen that when in direct contact with the polymer samples, there is no cytotoxic effect for the 1%, 1.5% and 2.5% PEGBio samples. From Figure 4-32 it could be seen that the 2.5 wt. % hydrogel provided the highest metabolic activity measurement in comparison to control.
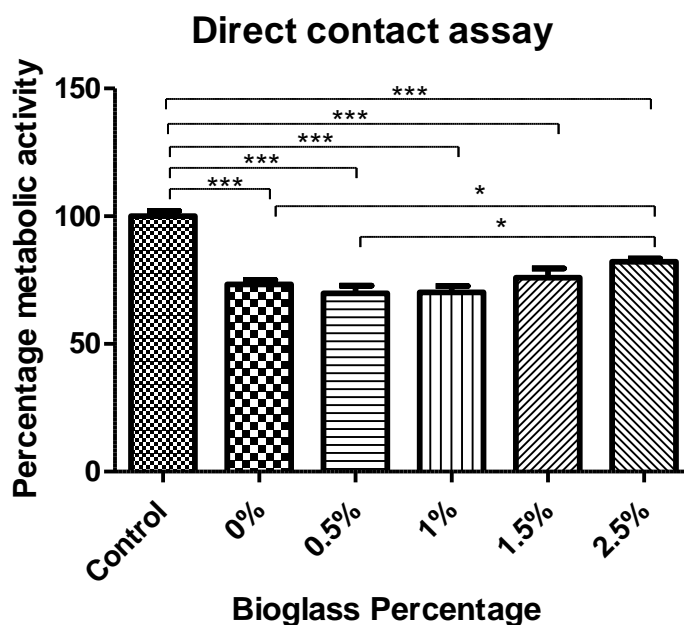
Figure 4-32 Direct contact assay comparing metabolic activity of PC-12 cells treated with different concentrations of PEGBio (With control being untreated well and 0% being PEGDMA with no bioglass) composites prepared as a percentage of control cells, statistical analysis was carried out using Graphpad Prism 5 (n=9) with p-values of less than 0.05 being considered statistically significant (*p < 0.05, **p < 0.01 and ***p < 0.001)

4.2.2 Neurite formation

Neurite forming cells were quantified and the length determined using ImageJ software, this data is presented in Table 4-1. From the data seen in Table 4-1, it can be determined that the NGF increased the differentiation of PC-12 cells into nerve like cells, with the number of neurite producing cells increasing from 0, to 17 after 22 hours and increasing to as many as 71 after 140 hours. When looking at neurite length, initially there is an increase in length, however upon reaching 106 µm in length the neurite length stops increasing, likely a combination of increasing number of neurite producing cells coming into contact with one another. Neurite formation over the days following nerve growth factor treatment of PC-12 cells can be seen in Figure 4-33. Watching the cells overtime the number of nerve like cells increased greatly through the differentiation of adherent PC-12 cells. Upon comparison the length of nerve like cells can be visually noted to increase day to day. The proliferation of PC-12 cells could be seen to decrease over the 6 days those cells were pictured. This is in agreement with what has already been understood of PC-12 cells post-nerve growth factor treatment (Fujita, Lazarovici and Guroff, 1989; Das, Freudenrich and Mundy, 2004). This section was used to confirm that it was possible to both attach and differentiate received PC-12 cells by addition of nerve growth factor treated media, highlighting their use as an *in vitro* cell line well suited to predicting the impact treatments may have on *in vivo* nerve cells. Of note is the fact that cells continued to differentiate for up to six days post treatment resulting in nerve like cells eventually interlocking to create a network of differentiated PC-12 cells. This continued differentiation indicates there is no cytotoxic nature associated with nerve growth factor treated media, as such it is likely that the addition of nerve growth factor would result in the continued differentiation of PC-12 cells if pictures had been taken at later timepoints.
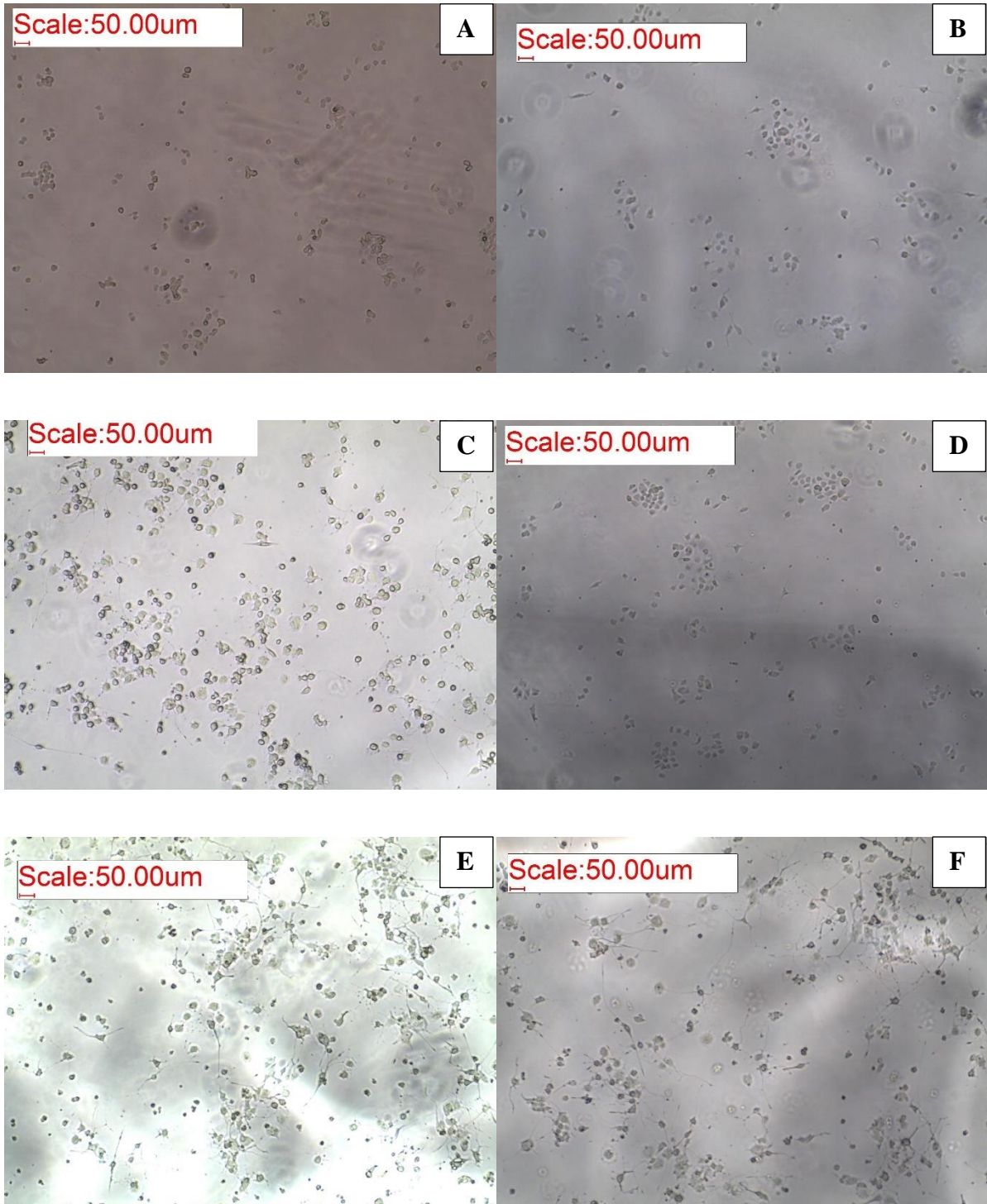
Figure 4-33 Pictures of PC-12 cells at x40 magnification showing (A) pre Nerve growth factor (NGF) treatment, (B) 5 hours post NGF treatment, (C) 22 hours post NGF treatment, (D) 91 hours post NGF treatment, (E) 117 hours post NGF treatment and (F) 140 hours post NGF treatment in well plate one of the 6-well plate used to demonstrate PC-12 cell differentiation. um in scale bar corresponds to μm

Table 4-1 Results of PEGDMA-thiol polymerisation check

Hours post NGF treatment (h)	Neurites formed (n)	Average neurite length (µm)
Pre-treatment (0)	0	0
5	12	23.56
22	17	41.18
91	29	106.03
117	43	95.39
140	71	95.56

4.2.3 PEGBio cell attachment

The pictures shown in Figure 4-34 showed attempts to monitor cell attachment in PEGBio samples. The purpose of this attachment and subsequent differentiation is to highlight the non-cytotoxic nature of PEGBio samples when encountering nerve like cells. The PEGBio samples coating of coll IV dissolved when placed in media. Coating the tissue culture well plates into which they have been placed; this allowed cells a more adherent surface to attach as tissue culture plastic is designed with cell attachment in mind. Further the addition of bioglass caused a decrease in the transparency of PEGBio samples, to such an extent that at higher concentrations polymers appeared to be black. The microscopy technique being used here relied on illuminating the polymer from below and taking photos from above, meaning that potential cells under the polymer surface could not be imaged. From the pictures shown, cells do not form a ring of inhibited growth around PEGBio samples however, with some even growing in contact with the hydrogels, providing indications that PEGBio samples do not leach cytotoxic material nor are they cytotoxic on contact.
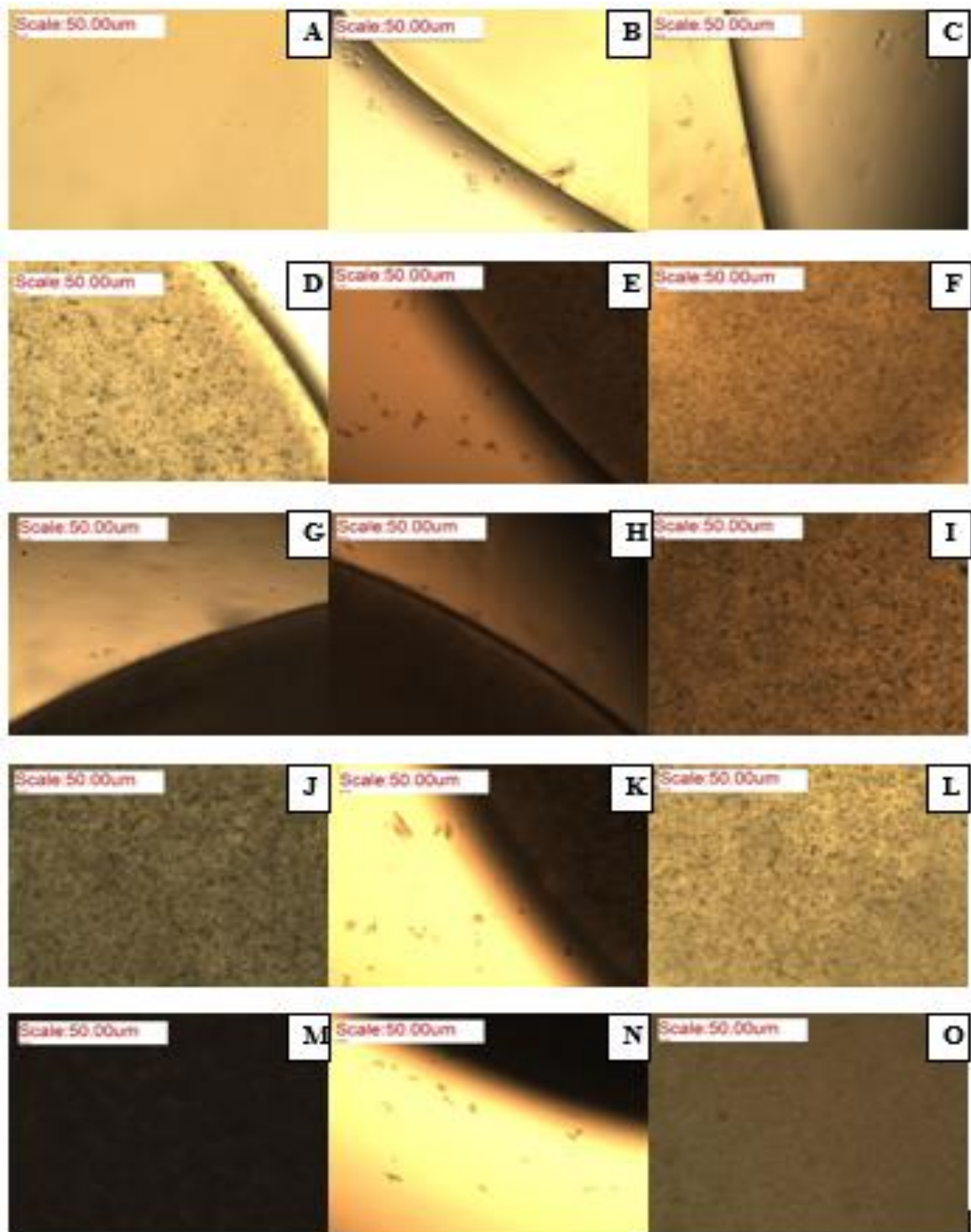
Figure 4-34 Cell attachment for multiple composites of PEGBio at x40 magnification. A = 0 % Bioglass and media on day 1 of attachment, B = Attachment in media surrounding 0 % bioglass on day two, C = Cellular attachment on 0 % bioglass polymer on day 2 of attachment. D = 0.5 % Bioglass and media on day 1 of attachment, E = Attachment in media surrounding 0.5 % bioglass on day two, F = Cellular attachment on 0.5 % bioglass polymer on day 2 of attachment. G = 1 % Bioglass and media on day 1 of attachment, H = Attachment in media surrounding 1 % bioglass on day two, I = Cellular attachment on 1 % bioglass polymer on day 2 of attachment. J = 1.5 % Bioglass and media on day 1 of attachment, K = Attachment in media surrounding 1.5 % bioglass on day two, L = Cellular attachment on 1.5 % bioglass polymer on day 2 of attachment. M = 2.5 % Bioglass and media on day 1 of attachment, B = Attachment in media surrounding 2.5 % bioglass on day two, C = Cellular attachment on 2.5 % bioglass polymer on day 2 of attachment. um in scale bar corresponds to µm

4.3 Summary

Like section 3, this section identifies the PEGBio wt. % which most closely matched the materials properties of the native peripheral nerve. In Section 4.1.1 it was again noted that photopolymerisation was conducted correctly by the disappearance of the peaks at 815 cm^{-1} and 1167 cm^{-1}. In Section 4.1.2 it could be seen that outside of the 5 wt. % and the 1.5 wt. % PEGBio samples, there was no significant differences between the different wt. % PEGBio samples and the 50 wt. % PEGDMA polymer. In Section 4.1.3 it was shown that bioglass wt. % did not have an impact on chain mobility, with no bioglass wt. % being significantly different to the 0 wt. % polymer. The mechanical strength results shown in Section 4.1.4 indicated that the addition of bioglass caused an increase in the stability of the samples over the 28-day period this a possible avenue through which the adhesion of cells to PEGDMA might be altered as polymer stiffness has been shown to play a role in cell adhesion (Chen, Yan and Zheng, 2018), it did not however impact the mechanical strength of the PEGDMA polymer. When looking at the wettability measurements of the PEGBio samples, only the 1.5 wt. % and 2.5 wt. % samples produced wettability measurements consistently in the range of 40° and 60° over the 28-day time period. Then when viewing the conductance of the samples in section 4.1.6 it could be seen that only the 2.5 wt. % sample presents consistent conductivity values which are comparable with that of the native peripheral nerves. This information pointed to the 2.5 wt. % sample as the best bioglass wt. % to use for a nerve guidance conduit. This evidence is further backed up by the results in section 4.2.1 where the 2.5 wt. % hydrogel treated PC-12 cells provided metabolic activity measurements most like control wells when conducting a direct contact assay. In sections 4.2.2 and 4.2.3 cells could be seen to grow in direct contact with PEGBio samples, further showcasing the non-cytotoxic nature of the PEGBio samples. This further shown in with no PEGBio concentration causing a decrease in metabolic activity of 30 % or more. Ultimately the 2.5 wt. % PEGBio samples were the only weight percentage which

achieved the desired conductivity, leading to the 2.5 wt. % concentration of bioglass was selected for use in future testing.

Chapter 5

Modification of PEGDMA hydrogels to increase biodegradability: addition of thiol monomers via click chemistry

5.0 Modification of PEGDMA hydrogels to increase biodegradability: addition of thiol monomers via click chemistry

Following the of identification of the 2.5 wt. % of bioglass as the weight to enhance PEGDMAs electrical conductance the focus of the thesis shifted to enhancing the degradability of PEGDMA. To achieve this aim, this phase of the thesis focused on the combination ten thiol-based monomers with the 50 wt. % PEGDMA samples. Once it was found that the combination of any thiols with the 50 wt. % PEGDMA samples resulted in immiscibility with the water leading to phase separation, the study switched to the use of 100 wt. % PEGDMA due to the similarity in properties and in-vitro impact on metabolic activity of cells. After switching to 100 wt. % PEGDMA, 10 different thiol-based monomers were mixed in 1:1 thiol to ene molar ratios with PEGDMA and selected for testing based on successful polymerisation.

The material properties of the successfully polymerised thiol-ene samples were determined similarly to previous sections with the addition tests looking at the thiol-ene hydrogels thermal and tensile properties (DMA) and chemical properties (RAMAN). As in phase 1, direct contact and elution assays were carried out to determine the in-vitro impact of the thiol-ene hydrogels, these tests were carried out on PC-12 cells and RT4-D6P2T (Schwann cells). Based off these tests an accelerated degradation study was carried out comparing the thiol-ene hydrogels rates of degradation to that of the base PEGDMA hydrogel.

Following 10 minutes exposure to UV light, it was found that three thiol-ene combinations produced a hydrogel - PEGDMA-PETMP, PEGDMA-DiPETMP and PEGDMA-GDMP. All other thiols were exposed to UV for an additional 30 minutes resulting in no formation of xerogel. Following removal from the UV chamber, unreacted monomers were stored in the dark for one week to observe whether self-polymerisation would occur. The ETTMP 1300-PEGDMA xerogels self-polymerised over time and were subsequently tested for their material properties. From the results in Table 5-1, it is difficult to predict whether successful polymerisation will occur as both the number of reactive groups present per monomer and the molecular weight of thiols varies greatly in successfully polymerised thiols. PEGDMA-PETMP, PEGDMA-DiPETMP and PEGDMA-GDMP have similar –SH group content to each other, however, these are also comparable to non-polymerised monomers such as TMPMP, and there are both monomers with higher and lower –SH content. However, it should be noted that no mercaptoacetates successfully polymerised and no thiol-based macromolecular monomer polymerised by UV exposure (PEGDMA-ETTMP 1300 polymerised over time). For comparison the main difference between GDMA and GDMP can be seen in Figure 5-1 (with the R group representing identical monomer structures), namely the extra carbon chain in the monomer backbone increasing the distance between the thiol and ester groups.

A

B
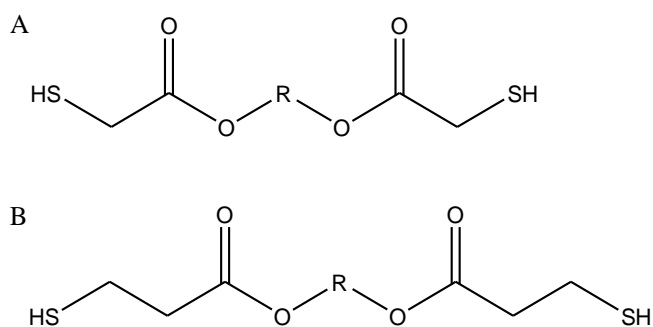
Figure 5-1 (A) Mercaptoacetate structure (B) Mercaptopropionate structure

Table 5-1 Results of PEGDMA-thiol polymerisation check

Thiol based monomer	Reactive groups	Molecular weight	SH content % (**Bock, 2012**)	Polymerisation success (Yes/No)
PETMP	4	489	26.0	Yes
DiPETMP	6	909	24.1	Yes
PETMA	4	433	29.5	No
ETTMP 700	3	700	13.5	No
ETTMP 1300	3	1300	7.1	Yes
TMPMP	3	399	24.0	No
TEMPIC	3	526	18.4	No
GDMA	2	210	30.5	No
GDMP	2	238	26.8	Yes
PCL4MP	4	1350	9.1	No

5.1.2 Chemical properties

FTIR results can be seen in Figure 5-2, across most samples there are no peaks at 815 cm^{-1} or the peak at 1167 cm^{-1}, indicative of C-H bending of the H$_2$C=CH-C=O group and C-O-C stretching respectively (Decker and Moussa, 1987; Wu *et al.*, 2010; Dobić, Filipović and Tomić, 2012), suggesting complete polymerisation occurred across all samples. In the PEGDMA-DiPETMP samples, there was a peak at 1142 cm^{-1} however, this peak can be explained by PEGDMA-DiPETMPs chemical structure containing a C-O-C bond at its centre (see Figure 1-4). With the GDMP and ETTMP 1300 samples, pronounced peaks were found at 1637 cm^{-1} (peak representative of the C=C bending of the CH$_2$=CH groups (Silverstein and

Webster, 1998)) indicating a large amount of PEGDMA monomer did not react with the thiol monomer. When considering PEGDMA-ETTMP 1300 polymerised over time instead of through UV exposure, there is an increased likelihood of PEGDMA-ETTMP 1300 self-polymerising with large amounts of PEGDMA remaining unreacted. No peak occurred in the 2550-2600 cm^{-1} range, indicating the disappearance of all S-H bonds, further evidence that complete thiol convergence had occurred (Coates, Ed and Coates, 2000) whereas the lack of peaks associated with the formation of the C-S-C bond during polymerisation falling in the 710-685 cm^{-1} range may be too weak to be detected by IR methods (Miller and Wlkins, 1952; Coates, Ed and Coates, 2000).
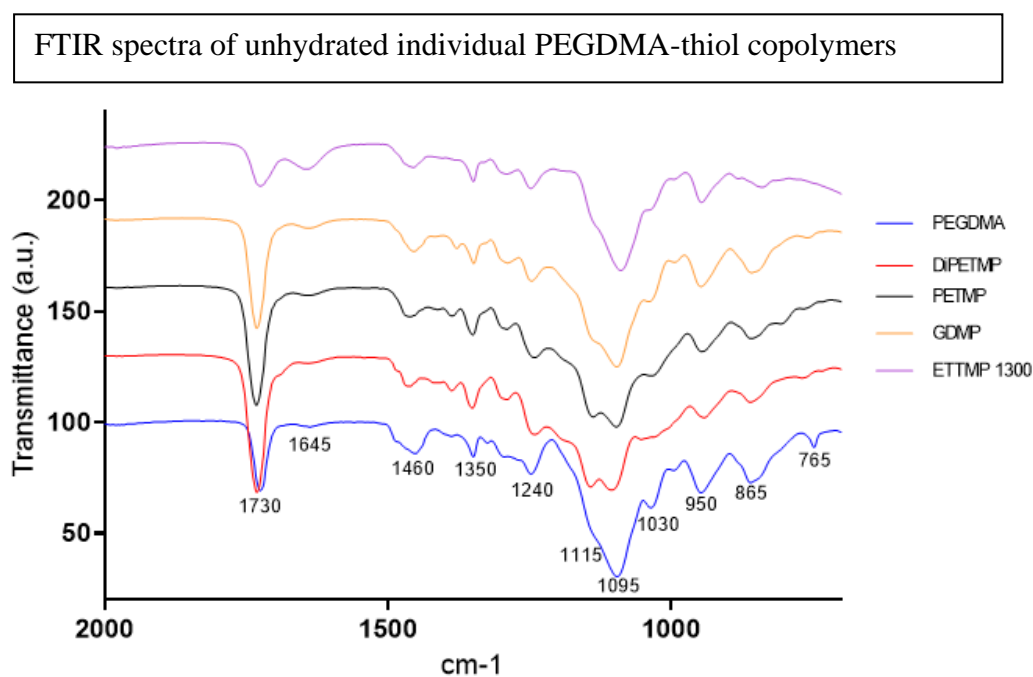
Figure 5-2 FTIR spectra for PEGDMA and PEGDMA-thiol samples post polymerisation

From testing in sections 5.1.3 to 5.1.6 it was determined that DiPETMP samples showed the most promise for future applications due to its similarity of compressive strength with PEGDMA, its degree of polymerisation and likelihood of enhanced degradability in comparison to other thiol copolymer networks. Further chemical characterisation was carried out via Raman spectroscopy of the PEGDMA and PEGDMA-DiPETMP polymerised samples

156

as shown in Figure 5-3. As can be seen, disappearance of the peak at 1640 cm^{-1} highlights the disappearance of all C=C bonds indicating the reaction between PEGDMA and DiPETMP resulted in a more complete crosslinking of the PEGDMA monomer than when PEGDMA was polymerised individually. Interestingly in contrast to this, the peaks at 940 and 2580 cm^{-1} suggests that there are still thiol bonds present throughout the monomer (Bazylewski, Divigalpitiya and Fanchini, 2017), indicating that DiPETMP did not fully polymerise when reacting with PEGDMA. This may be due to the polymerisation of DiPETMP samples locking the partially reacted DiPETMP in the polymer network. Preventing the continued polymerisation with further PEGDMA samples, this is possible as DiPETMP selectively reacts with PEGDMA as shown by the lack of peaks at 480-550 cm^{-1} associated with S-S bonding (Schulz and Baranska, 2007), whereas PEGDMA maintains the ability to react with either DiPETMP or other ene functionalities.
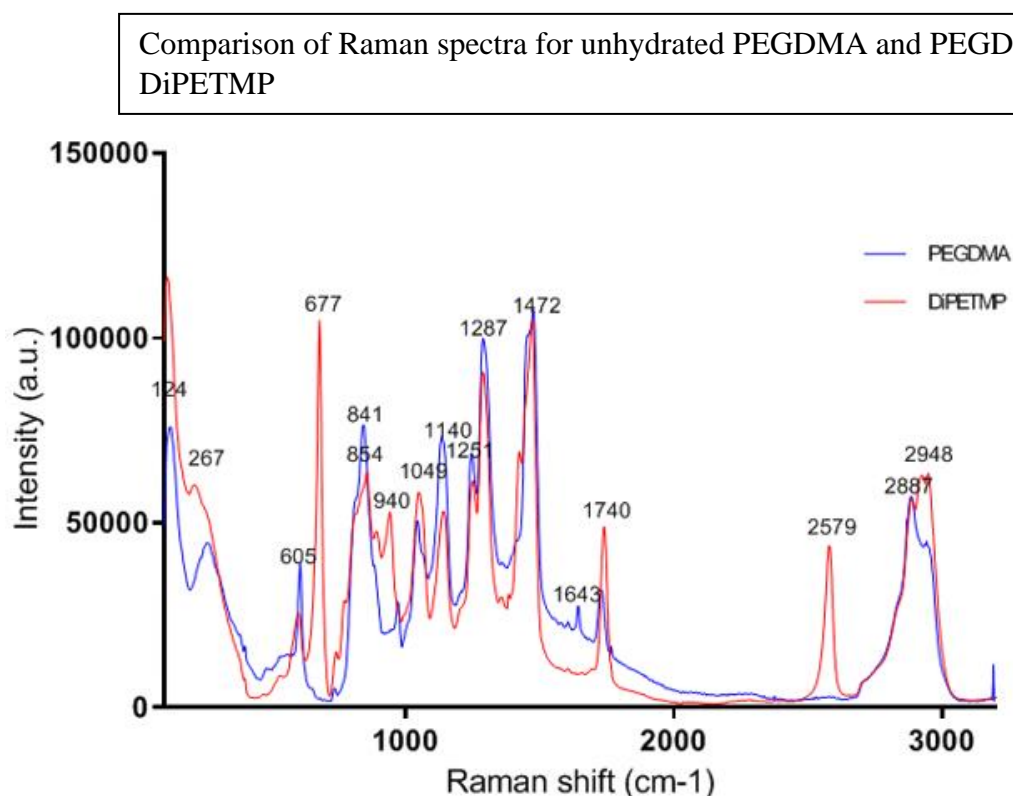
Figure 5-3 Raman spectra for PEGDMA and PEGDMA-DiPETMP samples

A typical glass transition temperature (Tg) for PEGDMA and PEGDMA-thiols can be seen in Table 5-2, with PEGDMAs mean Tg matching what was seen in section 3.2.3. Figure 5-4 showcased the typical DSC curves for each thiol-ene copolymer, of interest is that the samples which seemed most likely to be fully polymerised based on chemical characterisation had the highest Tg, namely PEGDMA, PEGDMA-DiPETMP and PEGDMA-PETMP with values of -40.51, -41.76 and -43.66°C respectively. This is likely due to there being more fully reacted polymer chains in these copolymers, thereby increasing the overall stiffness of the polymer network necessitating more energy to increase chain movement, resulting in a movement from a glassy to a rubbery state. This is supported by the Youngs modulus values in section 5.1.4 wherein the stiffer samples demonstrated higher Tg values. The thermal transitions determined via DSC were paralleled by the DMA thermograms shown in Figure 5-5, wherein PEGDMA had the highest Tg with PEGDMA-DiPETMP, PEGDMA-PETMP and PEGDMA-GDMP samples having progressively lower Tgs of -28.92, -34.51, -36.62 and -44.58 respectively. From Table 5-2 glass transitions determined via DMA were consistently lower than DSC determined Tgs, this is likely due to the difference in the way Tg is being calculated, with DSC measurement of glass transition identifying the beginning of the transition, whereas the Tan δ peak (used as determinant of Tg in DMA samples) corresponds more closely to a glass transitions midpoint than its beginning (TA Instruments, 1997; Menczel and Prime, 2009).

Of note is the appearance of a secondary tan δ peak for both the PETMP and DiPETMP samples as well as what appeared to be secondary tan δ peaks for PEGDMA and GDMP samples. These secondary peaks indicate that there are β relaxations occurring in these samples. This data matches what was observed in the DSC results in Figure 5-4 where there appeared to be β relaxations for PEGDMA-DiPETMP, PEGDMA-PETMP and PEGDMA-GDMP samples, as well as what could be a β

relaxation for PEGDMA. The DMA and DSC results for PEGDMA are interesting as the gap between the β relaxation and Tg is larger than all thiol samples in both tests, with PEGDMA occupying both the highest Tg values (representative of a polymers relaxation from glassy to rubbery state) and the lowest β relaxations (indicator of side chain motions in a polymer). Looking at results above 0 °C there did not appear to be any thermal events occurring in either pure PEGDMA or the thiol-based copolymers.

Table 5-2 Glass transition temperatures of thiol-PEGDMA copolymers (n=2)

Monomer of interest	DSC Mean Tg (°C)	DMA Mean Tg (°C)
PEGDMA	-39.04 ± 1.82	-28.92 ± 5.85
DiPETMP	-41.88 ± 0.95	-34.51 ± 4.07
PETMP	-43.47 ± 0.27	-36.62 ± 2.47
GDMP	-45.66 ± 0.13	-44.58 ± 0.76
ETTMP 1300	-49.86 ± 0.18	-
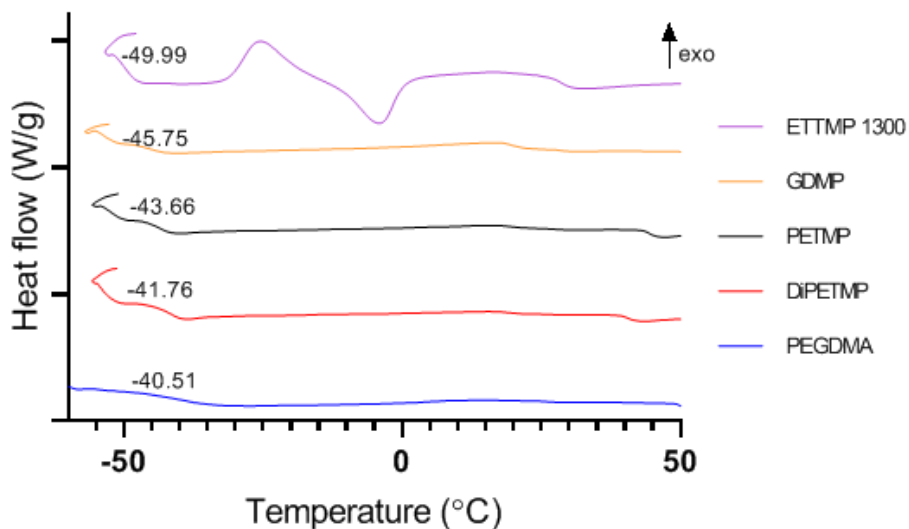
Figure 5-4 Differential scanning calorimetry thermogram highlighting the glass transition temperatures for PEGDMA and the different PEGDMA-thiol polymers
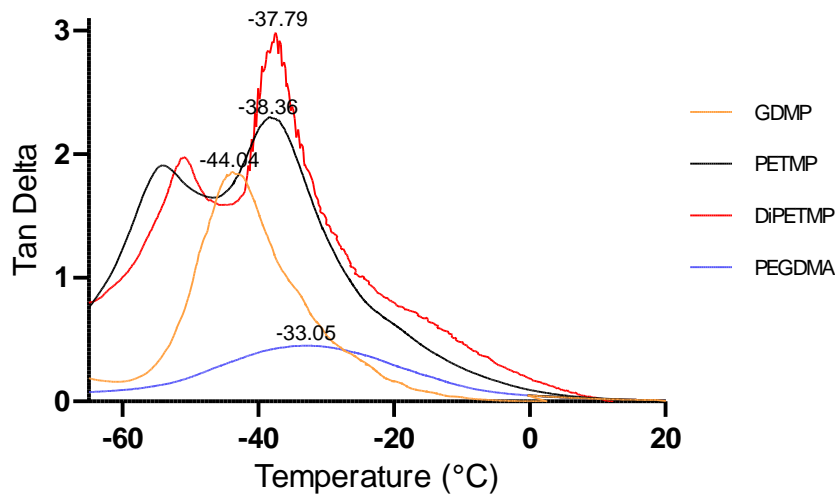
Figure 5-5 DMA thermogram of PEGDMA and thiol-ene based polymers

5.1.4 Mechanical properties

In Figure 5-6 the compressive strength at limit and Youngs modulus for each thiol-ene and

PEGDMA are shown. With comparison to 100 wt. % PEGDMA in section 3.2.4, the PEGDMA

results match very closely, highlighting consistency in the testing across testing phases. From

Figure 5-6 it could be seen that the addition of all thiols significantly decreased the stiffness of

PEGDMA xerogels with Youngs modulus values falling from 9.17 MPa for pure PEGDMA to

3.8, 3.9, 1.6 and 0.9 MPa for PEGDMA-DiPETMP, PEGDMA-PETMP, PEGDMA-GDMP

and PEGDMA-ETTMP 1300 respectively. It should also be noted that both the PEGDMA-

GDMP and PEGDMA-ETTMP 1300 have significantly lower stiffness values when compared

to PEGDMA-DiPETMP and PEGDMA-PETMP with PEGDMA-ETTMP 1300 samples also

having significantly lower compressive strength measurements, being approximately half the

stiffness and a third of the compressive strengths of the next weakest copolymer PEGDMA-

GDMP. Regarding compressive strength, the addition of thiols may end up benefitting the

cellular adhesion of samples, with both PEGDMA-DiPETMP and PEGDMA-PETMP

copolymers having compressive values matching closely with the lower end of the ideal 1 to

12 MPa compressive range being 1.09 and 1.24 MPa respectively. PEGDMA-GDMP and

PEGDMA-ETTMP 1300 however fall outside this range with values of 0.8 and 0.27 MPa. The PEGDMA samples were significantly stiffer and significantly stronger than thiol-ene samples. Interestingly there was a disparity within thiol-ene groupings with PEGDMA-DiPETMP and PEGDMA-PETMP both being significantly stiffer and significantly stronger than PEGDMA-GDMP and PEGDMA-ETTMP 1300 samples.
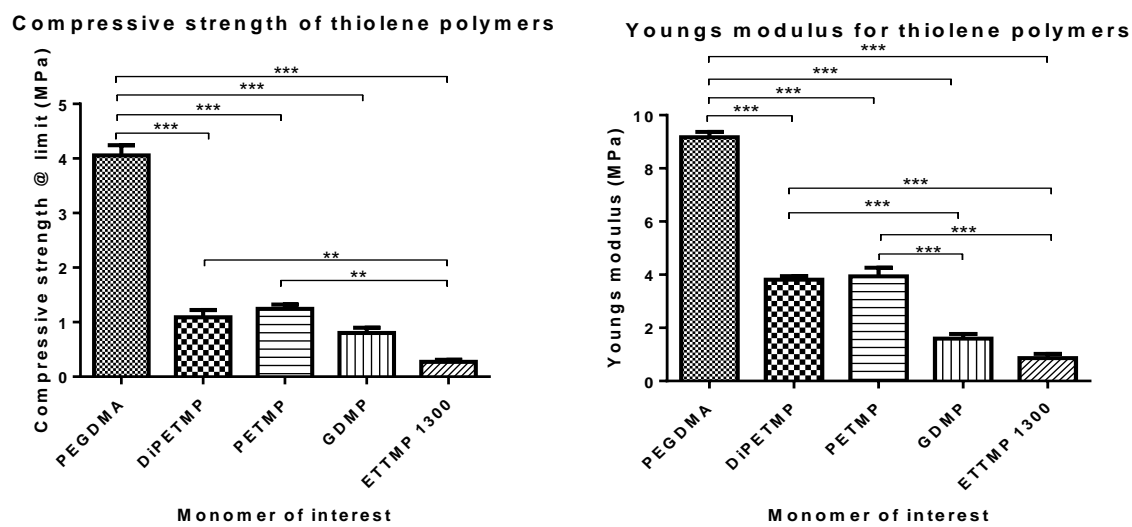
Figure 5-6 Compressive properties of PEGDMA-thiol copolymers showing (A) Compressive modulus at limit (MPa) and (B) Youngs modulus (MPa), statistical analysis was carried out using Graphpad Prism 7 (n=5) with p-values of less than 0.05 being considered statistically significant (*p < 0.05, **p < 0.01 and ***p < 0.001)

From the results in Figure 5-7, it could be seen that the inclusion of thiols reduced both the overall tensile strength at limit and tensile stiffness of PEGDMA xerogels in a similar manner to the effect thiol inclusion had on the compressive strength at limit and stiffness. Unlike in the compressive testing where PEGDMA-DiPETMP copolymers had values comparable to PEGDMA-PETMP, in Figure 5-7, the largest decreases in tensile strength and stiffness occurred with the PEGDMA-DiPETMP copolymer with compressive strength dropping from 3.46 MPa in PEGDMA to 1.67 MPa in PEGDMA-DiPETMP. PEGDMA, PEGDMA-PETMP and PEGDMA-GDMP exhibited results more closely matched with the mechanical properties seen in Figure 5-6, namely PEGDMA being the stiffest and strongest at limit, PEGDMA-PETMP having the values most like PEGDMA and PEGDMA-GDMP having values lower than both PEGDMA and PETMP.

161

Where these results differ is the comparative differences between samples in both tests. PEGDMA which had almost three times the compressive strength and stiffness compared to PEGDMA-PETMP (compressive strength 9.17 MPa to 3.94 MPa and stiffness 4.05 MPa to 1.09 MPa), dropped to less than twice the strength for tensile measurements (tensile strength 3.46 MPa to 3.02 MPa and stiffness 0.78 MPa to 0.36 MPa). Regarding PEGDMA-GDMP, the results are even more pronounced, with tensile strength values increasing from compressive values of 1.6 MPa to tensile strength at limit of 2.61 MPa meaning PEGDMA-GDMP samples go from having approximately one sixth the strength of PEGDMA samples to three quarters PEGDMAs strength. Considering the ideal 1 to 12 MPa range of tensile strength all tested samples met the minimum criteria of 1 MPa and fell in the lower end of that range, with DiPETMP having the tensile strengths most closely matching peripheral nerves prior to deformation.
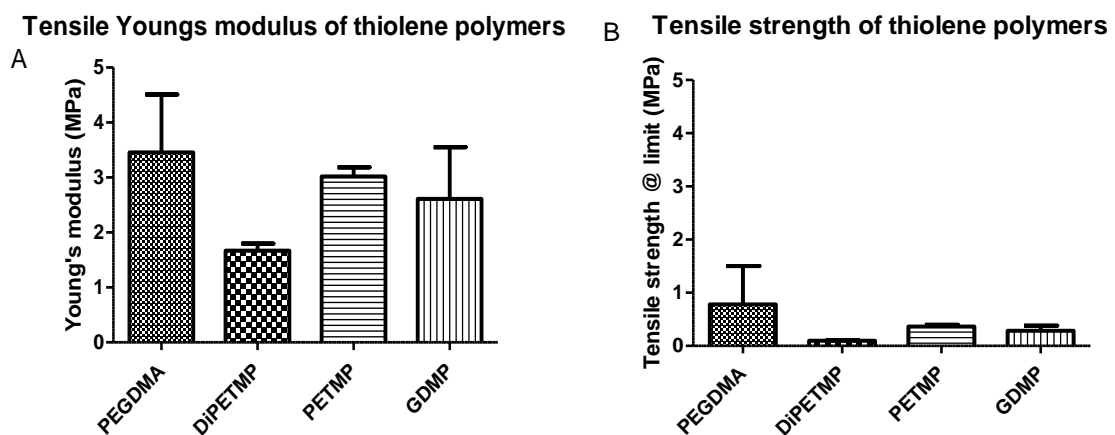
Figure 5-7 Dynamic mechanical analysis of PEGDMA and PEGDMA-thiol samples post polymerisation showing (A) Youngs Modulus and (B) Tensile strength at limit. Statistical analysis was carried out using Graphpad Prism 7 (n=3) with p-values of less than 0.05 being considered statistically significant (*p < 0.05, **p < 0.01 and ***p < 0.001)

5.1.5 Wettability measurements

Comparing the wettability of unhydrated 100 wt. % PEGDMA in section 3.2.5 with unhydrated PEGDMA in Figure 5-8 there appeared to be good consistency between tests, with mean wettability measurements of 47.88 and 41.65° respectively. Looking at the impact the introduction of thiols has on the wettability of PEGDMA, Figure 5-8 indicates an increase in hydrophobicity compared to pure PEGDMA across thiol-ene polymer composites. PEGDMA-PETMP and PEGDMA-GDMP samples were found to have wettability measurements of 65° and 61° respectively with PEGDMA-DiPETMP samples having a much more substantial increase in hydrophobicity trending up to 84° and being significantly different to all other thiolene copolymers. PEGDMA-ETTMP 1300s results again in contrasted those of the other thiols, increasing hydrophilicity rather than hydrophobicity with a wettability measurement of 30°. However, as the differences vary significantly between several of the thiol copolymers, it does open the possibility of selecting different thiols to tune the wettability of a hydrogel towards a specific desired hydrophilicity.
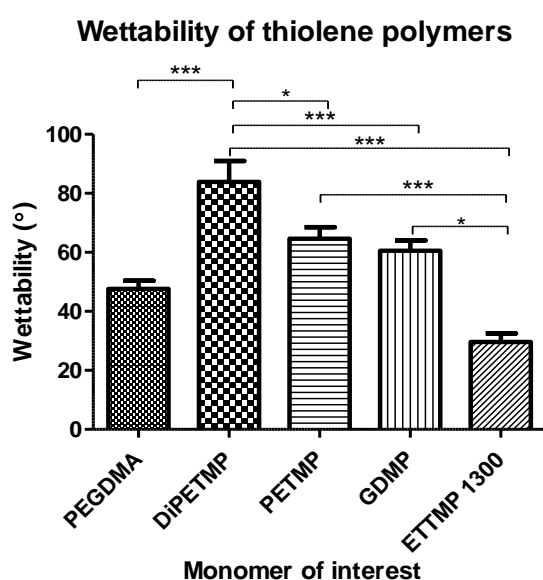
Figure 5-8 Wettability measurements of PEGDMA and PEGDMA-thiol samples, statistical analysis was carried out using Graphpad Prism 7 (n=3) with p-values of less than 0.05 being considered statistically significant (*p < 0.05, **p < 0.01 and ***p < 0.001)

5.1.6 Surface properties

The surface properties of the different samples were examined using SEM analysis and the results shown in Figure 5-9. When comparing the different thiol-ene hydrogels with pure PEGDMA it appears that the surface morphology is not affected by the introduction of thiol (except PEGDMA-ETTMP 1300) as the hydrogel morphologies of PEGDMA, PEGDMA-DiPETMP, PEGDMA-PETMP and PEGDMA-GDMP are very similar to one another. The morphology for PEGDMA-ETTMP 1300 was markedly different when compared with the other hydrogels, with small circular protrusions covering the surface of the sample. These bubbles are most likely air bubbles formed during the mixing of ETTMP 1300 and PEGDMA, which subsequently were trapped in the hydrogel as it polymerised over time. PEGDMA-ETTMP 1300s differences when compared with other hydrogels and the fact that there is unreacted PEGDMA present throughout the polymer led to the decision that further investigation of PEGDMA-ETTMP 1300 copolymers would not be pertinent. EDX analysis was carried out on all samples with carbon, oxygen and sulphur make up the majority of elemental responses across all samples.
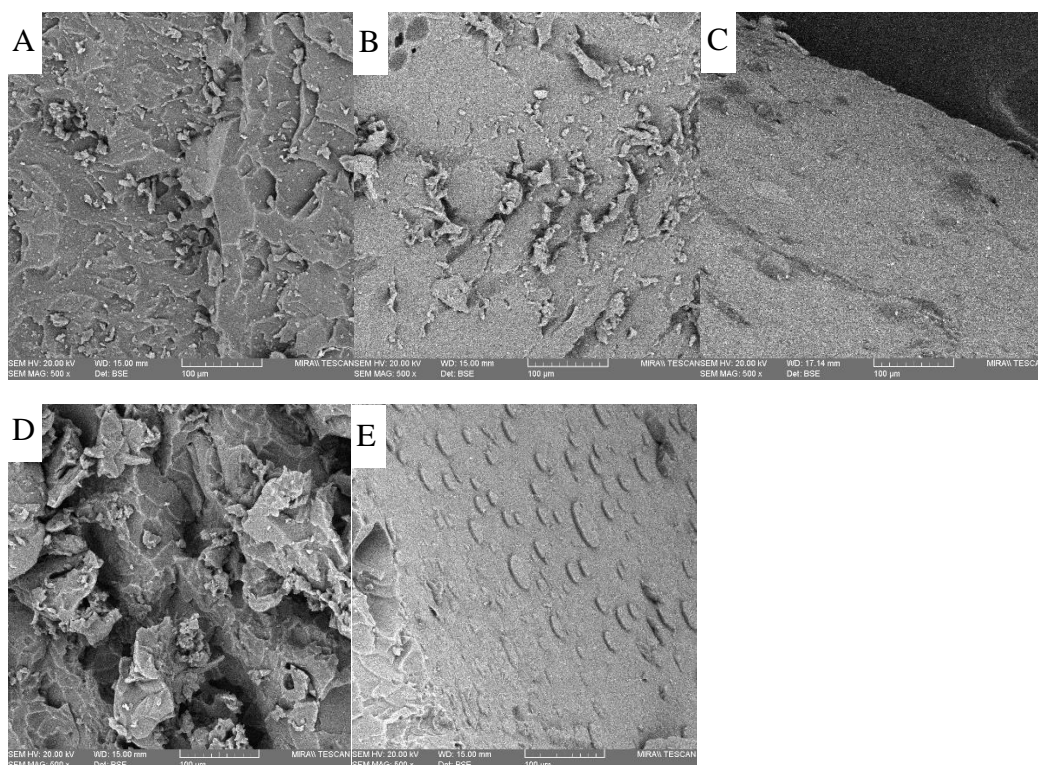
Figure 5-9 Scanning electron microscopy images of the surface topography of PEGDMA and PEGDMA-thiol hydrogels (A) PEGDMA, (B) DiPETMP, (C) PETMP, (D) GDMP and (E) ETTMP 1300

5.1.7 Swelling studies

Swelling ratio is an indicator of how tightly polymer networks are polymerised, with more considerable swelling showing greater freedom between polymer chains. In Figure 5-10 PEGDMA-DiPETMP and PEGDMA-PETMP which had similar stiffness values have different swelling ratios, the DiPETMP samples which have six functional groups compared to the PETMP samples four, are seen to have a swelling ratio of approximately 66 % that of PETMP (swelling ratio of 15.93 compared with 25.97). As the thiol-ene ratio is done in a 1:1 reactive group ratio, this could be put down to the -DiPETMP samples interacting with more PEGDMA linkages than the PETMP samples. Likely leading to faster rates of degradation as there would be less PEGDMA-PEGDMA polymer chains linkages throughout the gel, which would be resistant to breakdown. PEGDMA-GDMP copolymer networks have a comparable swelling ratio to PEGDMA (44.4 to 47.0) indicating both samples have similar degrees of polymer

network binding. With pure PEGDMA, the large degree of swellability comes from every reacting monomer possessing a long kinetic chain which gives the network freedom to expand. The PEGDMA-GDMP copolymer, on the other hand, has a much shorter chain length and would therefore restrict the swelling of the hydrogel. When comparing the gel fraction results, it becomes clear that there was a large amount of unreacted monomer left in the PEGDMA-GDMP hydrogel (13.8 % gel) when compared to the PEGDMA hydrogel (0.7 %), this more substantial degree of unreacted monomer could explain the comparability in swelling ratios between PEGDMA and PEGDMA-GDMP. The relationship between PEGDMA-GDMPs gel fraction and swelling ratio is mirrored by the DiPETMP and PETMP samples wherein the higher the gel fraction corresponded with a higher swelling ratio. Of note is the comparability of the gel fraction values to glass transition values wherein the higher gel fraction values resulted in lower Tg. Furthermore, the gel fraction values agreed with the previous results, reflecting which samples were most consistently polymerised, namely PEGDMA being the most confidently polymerised and PEGDMA-GDMP the least confident.
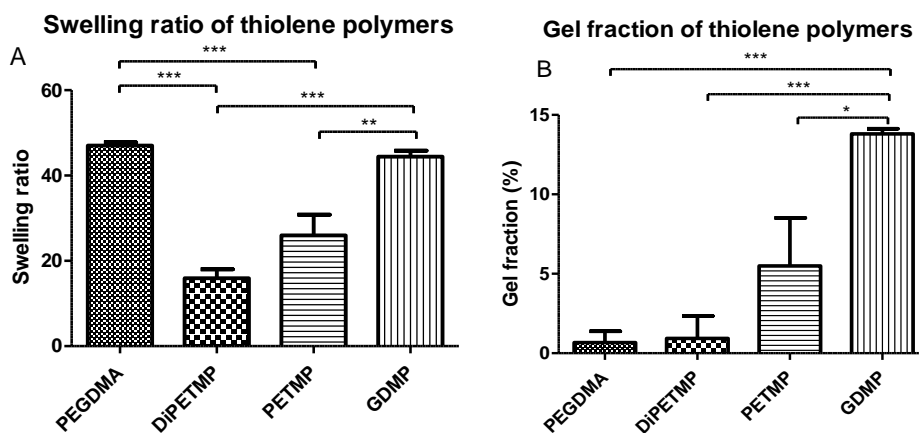
*Figure 5-10 Comparison between (A) the swelling characteristics and (B) the gel fraction values of PEGDMA and PEGDMA-thiol hydrogels, statistical analysis was carried out using Graphpad Prism 7 (n=5) with p-values of less than 0.05 being considered statistically significant (*p < 0.05, **p < 0.01 and ***p < 0.001)*

5.1.8 Accelerated degradation study

Accelerated degradation of PEGDMA and PEGDMA-DiPETMP samples stored in 5M NaOH and 5 mM NaOH are presented in Figure 5-11. When carrying out analysis of weight change with 5M NaOH the difference between PEGDMA and DiPETMP could be readily seen. With the PEGDMA samples there was no weight change from day 1 to the finish of the experiment (day 63) whereas PEGDMA-DiPETMP samples reached complete breakdown (to the extent that all gel had been converted to a liquid), within the first 24 hours of exposure. In 5 mM NaOH solutions a similar disparity between samples could be seen, where PEGDMA samples swelled to approximately 140 % the weight of day 0 samples and maintained that weight throughout the experiment.

During the first month, the properties of PEGDMA-DiPETMP in 5 mM NaOH did not change substantially, with the differences between PEGDMA and PEGDMA-DiPETMP being those determined previously throughout this study with the addition that PEGDMA-DiPETMP samples felt slightly stiffer in hand compared to pre 5mM NaOH immersion. After a month however, the mechanical properties of hydrogels started to steadily decrease noted by increasing degrees of softness when removing samples from solution and blotting dry. By day 63 samples had reached a state of complete breakdown with retrieval from solution invariably leading to damage to the hydrogel (see Table 5-3). Furthermore, attempts to blot dry PEGDMA-DiPETMP samples led to the complete breakdown of the hydrogel structure, as such samples were unable to be weighed accurately for day 63 testing, with one PEGDMA-DIPETMP sample (S5) having reached a state of being irretrievable from solution to be blotted dry.

5 mM NaOH allowed for a more gradual breakdown of hydrogel than 5M NaOH as thiol hydrogels breakdown is directly proportional to the increase in OH ions present (Shih and Lin, 2012), i.e. as 5 mM NaOH has a concentration of one-thousandth that of 5M NaOH, then the

rate of degradation should be 1000 times slower also. It is likely that as PEGDMA-DiPETMPs swelling increased there had been numerous bonds on the PEGDMA-DiPETMP sections of the monomer network broken through hydrolytic degradation, as the PEGDMA portions were resistant to degradation and there were still sections of PEGDMA-DiPETMP with intact structure then the initial outcome was increased hydrogel swelling. As more PEGDMA-DiPETMP bonds were broken, eventually the hydrogel would breakdown resulting in a gradual decrease in weight until complete breakdown was realised.
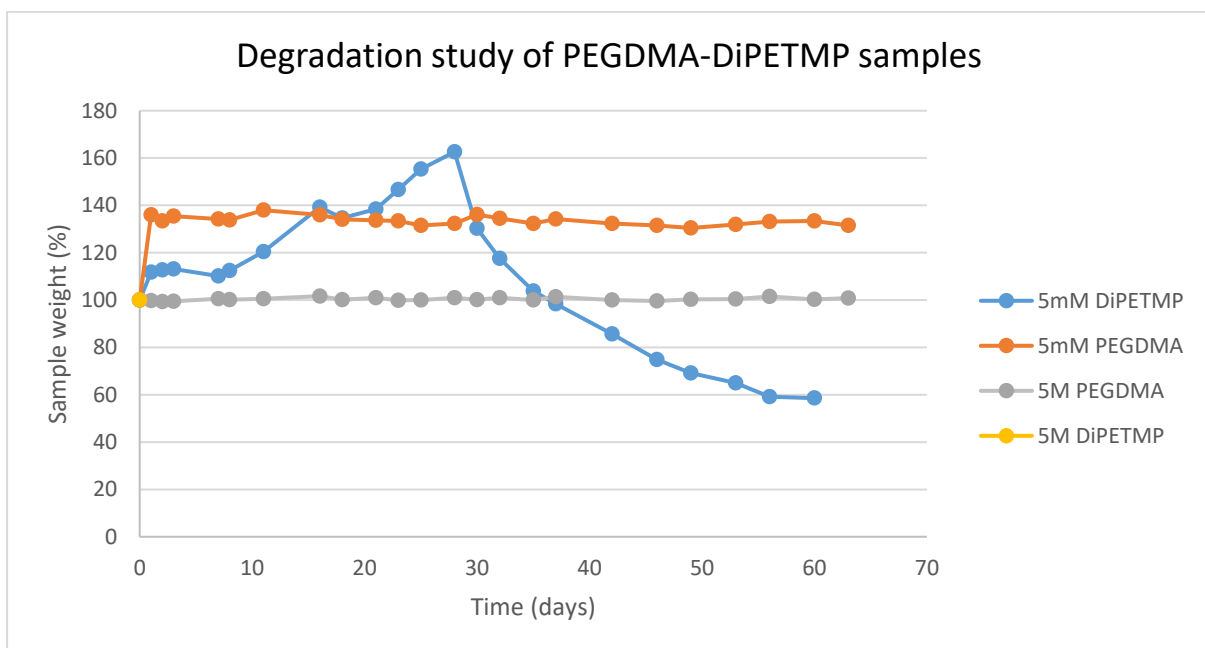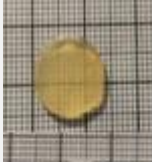
Figure 5-11 Degradation study of PEGDMA and DiPETMP samples stored in 1. 5M NaOH and 2. 5 mM NaOH at 37 °C, over a 63 day period

Table 5-3 Changes to hydrogel morphology during accelerated degradation study weeks 4 to 8

Monomer of Interest (NaOH concentration)	Week 4	Week 5	Week 6	Week 7	Week 8
PEGDMA (5 M)					
PEGDMA (5 mM)					
DiPETMP (5 mM)					

5.2 Cell culture

5.2.1 PC-12 cell metabolic activity comparison 24- and 48-hour post Direct contact and Elution assays

From the results shown in Figure 5-12 the impact of both PEGDMA and PEGDMA-DiPETMP on PC-12 cells could be seen to be positive. After 24 hours, PEGDMA-DiPETMP samples elucidated particularly beneficial outcomes, with metabolic activity values for elution and direct contact assays of 175 and 170% respectively when compared with control wells. This increase in metabolic activity was also present 48 hours post treatment particularly with direct contact samples where this increased to 206% of control wells. Across both timepoints, pure PEGDMA also displayed increased metabolic activity when compared with the untreated wells, however at both timepoints PEGDMA-DiPETMP samples outperformed their pure PEGDMA counterparts.
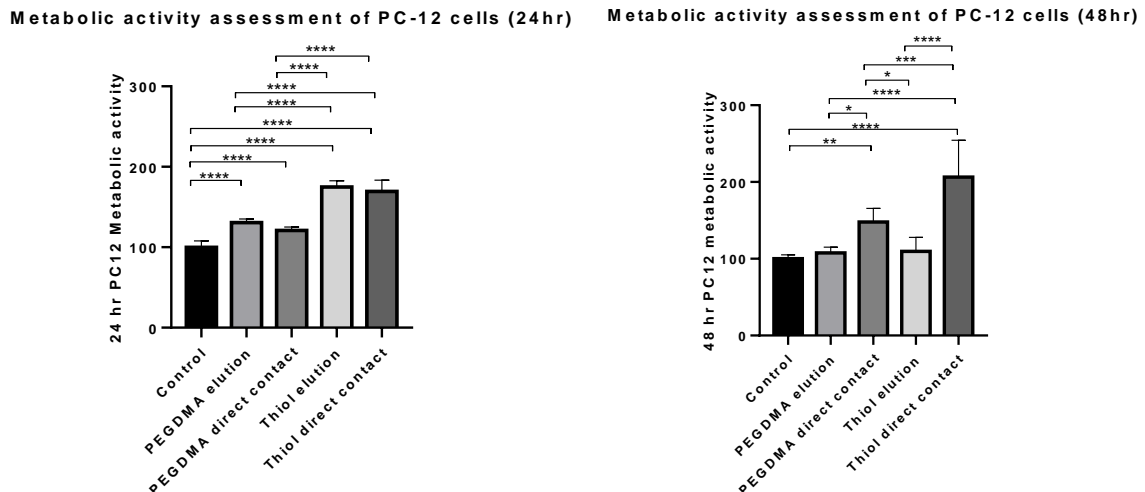
Figure 5-12 Metabolic activity measurement of PC-12 cells as a percentage of control (A) 24 hours and (B) 48 hours post treatment with either PEGDMA or DiPETMP-PEGDMA via direct contact or elution assay, statistical analysis was carried out using Graphpad Prism 7 (n=9) with p-values of less than 0.05 being considered statistically significant (*p < 0.05, **p < 0.01 and ***p < 0.001)

5.2.2 Schwann cell metabolic activity comparison 24- and 48-hour post Direct contact and Elution assays

Unlike in section 5.2.1 where PEGDMA-DiPETMP samples proved to greatly enhance the metabolic activity of PC-12 cells, their impact on Schwann cells proved to be more muted as shown in Figure 5-13, where all treatments (both PEGDMA and PEGDMA-DiPETMP) were shown to negatively impact cellular metabolic activity. This is particularly shown with pure PEGDMA samples where direct contact assays 24 hours post treatment results were shown to produce cytotoxic effects based on ISO standards (ISO/EN10993-5, 2009). These cytotoxic effects were not mirrored by PEGDMA-DiPETMP samples, where direct contact assays metabolic activity values of 97.53 and 79% that of control wells and in elution assays with 80.64 and 72.91% respectively. Although these results showed PEGDMA-DiPETMP did not boost SC metabolic activity in a manner like their impact on PC-12cells, they did maintain a non-cytotoxic impact over the 48-hour treatment period.
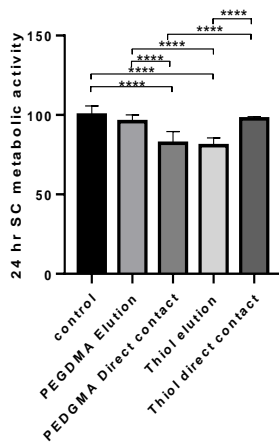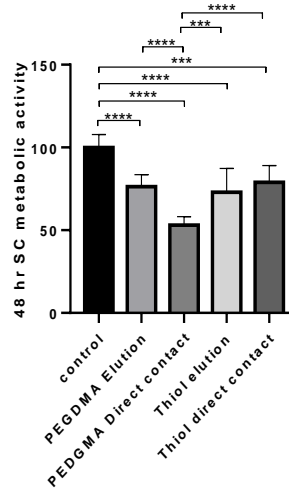
Figure 5-13 Cell metabolic activity measurement of PC-12 cells expressed as a percentage of untreated PC-12 cells (A) 24 hours, (B) 48 hours post treatment with either PEGDMA or DiPETMP-PEGDMA via direct contact or elution assay, statistical analysis was carried out using Graphpad Prism 7 (n=9) with p-values of less than 0.05 being considered statistically significant (*p < 0.05, **p < 0.01 and ***p < 0.001)

5.3 Summary

From an initial group of ten thiols, only four thiols were found to successfully polymerise with PEGDMA via either UV exposure or over time. All four of these thiols possessed mercaptopropionate functional groups with no monomer containing the mercaptoacetate functionality reacting with PEGDMA to produce a hydrogel. It has been shown that mercaptoacetates are less reactive than mercaptopropionates, which may explain why there was no formation of thiol-ene copolymers (Morgan, Magnotta and Ketley, 1977). However, it was also shown that the differences in curing rates between any -ene and either mercaptoacetate or mercaptopropionate was not significant (Morgan, Magnotta and Ketley, 1977). It is possible that the weight % of thiol per thiol monomer has an impact on the successful thiol-ene polymerisation, since three of the thiols which successfully underwent copolymerisation were all in the range of 24.1 to 26.8 weight %, but this is also unlikely since TMPMP has an -SH weight % of 24, which is only 0.1 % off the value for PEGDMA-DiPETMP. Regarding molecular weight, the weights of thiols which formed polymers with PEGDMA ranged from 238Da up to 1300Da, showing no sign that polymerisation was affected by Mw within this range. The same appears to be true for functional group numbers which ranged from 2 to 6 in hydrogel producing thiols, although it is worth noting that the thiols with higher numbers of functional groups (DiPETMP with 6 and PETMP with 4) would present consistently higher compressive strengths than those of GDMP (2 functional groups) and ETTMP 1300 (3 functional groups). Ultimately from the ten potential thiols identified to produce a degradable PEGDMA based nerve guidance conduit, this group was narrowed to 4 based on their successful polymerisation, namely DiPETMP, PETMP, GDMP and ETTMP 1300.

From section 5.1.4 it could be seen that a significant drop in stiffness followed the introduction of all thiol monomers. Through adjustments to the ratios of thiol-PEGDMA mixtures, there is potential to adjust these values to more suitably match their stiffness to that required of other

tissue engineering applications such as bone scaffolding or muscle cell differentiation (Even-Ram, Artym and Yamada, 2006; Das and Zouani, 2014). A possible explanation for the difference in mechanical strength of PEGDMA-thiol copolymer networks compared to PEGDMA hydrogels could be the degree of polymer homogeneity. In pure PEGDMA samples, the polymer architecture consists of a homologous repetition of PEGDMA monomers which have a long kinetic chain length, limiting their ability to disperse stress. As the polymer architecture of thiol-ene copolymer networks is more heterogeneous, this lends itself to lower degrees of brittleness when compared with methacrylate hydrogels (Ligon-Auer *et al.*, 2016; Ligon *et al.*, 2017). However, if this was true, ETTMP 1300 that has long kinetic chains should also have high degrees of stiffness and strength. This could be accounted for by the idea that ETTMP 1300 had an incomplete polymerisation leading to unreacted PEGDMA being present in both samples, as fully polymerised PEGDMA would have provided for stiffer hydrogels. Regarding the ideal nerve guidance conduit it was felt that PEGDMA-DiPETMP and PEGDMA-PETMPs mechanical properties matched most closely with those identified in section 1.3.

The introduction of thiols to the PEGDMA polymer network had a marked impact on wettability. Wettability is an important factor for the purposes of tissue engineering as samples that are too hydrophilic or too hydrophobic will inhibit cell attachment to their surface, with 40° to 60° being the ideal range for cellular adhesion (Arima and Iwata, 2007). Unlike the wettability values for pure PEGDMA hydrogels which fell within the preferred wettability range. The wettability measurements of PEGDMA-DiPETMP, PEGDMA-PETMP and PEGDMA-GDMP were found to be outside the ideal range for cellular adhesion, tissue engineering applications may be limited being too hydrophobic. To combat this a number of options are possible and have been explored with regard to other polymer networks including adding a more hydrophilic outer coating to the thiol-ene co-polymer or the addition of an

additive to improve wettability (Zhong, 1997; Otitoju, Ahmad and Ooi, 2018), also there is potential that when polymerised in the presence of bioglass (which in section 4.1.5 lowered wettability following inclusion in pure PEGDMA) this increase in PEGDMAs wettability will be limited.

The introduction of thiols can be seen to also impact glass transition temperature of PEGDMA as all thiols lowered the temperature needed to allow for the necessary chain relaxations. Supporting the idea that thiol-ene networks allow for softer hydrogels with a lower useful temperature range compared to methacrylate networks due to the effect thiol addition has on the overall heterogeneity of the polymer network (Ligon *et al.*, 2017). The ETTMP 1300 samples results did not match those for other thiols, producing a Tm peak close to 0 °C (indicating the presence of water, which is supported by a large O-H stretch peak at 3400 cm^{-1} in the FTIR spectra of ETTMP 1300 (Moffat *et al.*, 2011)) in the sample as well as a secondary Tg at 28 °C. This suggests that despite the 2 hour mixing prior to attempted polymerisation there are miscibility issues between PEGDMA and ETTMP 1300, allowing the two monomers to separate while they were curing over time and no longer being stirred. The evidence supporting ETTMP and PEGDMA having miscibility issues was further supported by the SEM images wherein PEGDMA-ETTMP 1300 samples appear to have bubbles appearing on its surface; these could be due to the previously mentioned presence of bubbles in PEGDMA-ETTMP 1300 mixtures or indeed a sign of the separation of ETTMP 1300 and PEGDMA. This, in addition to the observed shortcomings in performance compared to other thiol-ene polymers and failure to achieve complete polymerisation resulted in ETTMP-1300 being excluded from further investigation. The sole focus of this section of work then shifted to DiPETMP, PETMP and GDMP monomers.

From the study of gel fraction in section 5.1.7 PEGDMA-DiPETMP samples were shown to have the lowest degree of unreacted monomer, followed by PEGDMA-PETMP. PEGDMA-

GDMP thiol-ene networks were shown to have 13.8 % gel compared to PEGDMAs 0.7 %. When considering the previous FTIR results in section 5.1.2, it became clear that PEGDMA-DiPETMP and PEGDMA-PETMP were the most compatible hydrogels for reaction with PEGDMA, with both thiols providing opportunities to impact the mechanical properties and wettability of PEGDMA samples while also improving their degradability.

When looking further at the mechanical properties of thiol-ene samples, the lower tensile strength of PEGDMA-DiPETMP samples shown in Figure 5-7 compared to other thiol-ene copolymers is unexpected as the PEGDMA-DiPETMP copolymers appeared up to this point to most closely match PEGDMA hydrogel. Furthermore, with a gel fraction percentage of 0.9 % PEGDMA-DiPETMP samples were second to only PEGDMA polymer networks in confidence of polymerisation. As tensile strength is directly related to crosslinking (Pedro *et al.*, 2007), PEGDMA-DiPETMP was predicted to have increased tensile strength compared to hydrogels with lower degrees of crosslinking, such as PEGDMA-GDMP. Furthermore, SEM samples do not indicate any porosity within the sample, which could cause localised stresses and decrease PEGDMA-DiPETMP samples overall strength (Liu, Won and Ma, 2006). Regardless of tensile properties, PEGDMA-DiPETMP mechanical performance and thermal properties more closely matched with PEGDMA than either PEGDMA-GDMP or PEGDMA-PETMP furthermore PEGDMA-DiPETMPs Raman analysis agrees with previous chemical and gel fraction characterisations, based on this, PEGDMA-DiPETMP samples were selected as the ideal copolymer to continue testing.

When analysing degradation it was found through the addition of DiPETMP, thiol copolymer networks achieved complete breakdown following immersion in 5 mM NaOH for 9 weeks and 5 M NaOH in less than 24 hours. Compared with no change in sample size or weight when pure PEGDMA samples were placed in 5 M and 5 mM NaOH for the same period of time.

Thus, highlighting PEGDMA-DiPETMPs ability to improve degradability of PEGDMA based hydrogels.

With cell metabolic activity in mind PEGDMA-DiPETMP samples showed good promise as shown in section 5.2.1 boosting metabolic activity of PC-12 cells at both 24- and 48-hours post direct contact, outperforming pure PEGDMA which also boosted the PC-12 cells metabolic activity. A similar outcome of PEGDMA-DiPETMP outperforming PEGDMA was seen in the Elution assay, albeit to a greater degree as shown in section 5.2.1. When comparing the metabolic activity of Schwann cells post treatment it could be seen that although these results showed PEGDMA-DiPETMP did not boost SC metabolic activity in a manner similar to their impact on PC-12 cells, they did maintain a non-cytotoxic impact over the 48-hour treatment period.

Chapter 6

Modification of PEGDMA hydrogels to increase bioactivity: addition of API combinations

6.0 Modification of PEGDMA hydrogels to increase bioactivity: addition of API combinations

With the modifications to enhance conductance and degradability identified, phase 4 of the thesis focused on enhancing the bioactivity of the degradable PEGDMA-DiPETMP hydrogel to best enhance the peripheral nerve repair process. With this goal in mind three drugs capable of interacting with the four main pathways of peripheral nerve repair (N-acetyl cysteine, Ibuprofen and Progesterone) were identified. When looking to utilise these drugs to enhance bioactivity it was important to understand their drug synergy and drug release rates.

Drug synergy was determined over three stages of high throughput screening using the Alamar blue assay on well plates with post drug treatment timepoints of 24, 48 and 72 hours. Stage one utilised both Schwann cells and PC-12 cells with three two-drug combinations (NAC-Ibu, Ibu-Prog or Prog-NAC) with concentrations based on a pre-study literature review. Stage two of testing utilised Schwann cells and the same three two-drug combinations with concentrations based on stage one outcomes. Stage three returned to the use of both Schwann cells and PC-12 cells and was based on stage two outcomes, in this phase a fixed concentration of was used with varying concentrations of NAC and Prog. Based on the cell response in this phase of testing the final concentrations of NAC, Ibu and Prog were determined.

The drug release rates of NAC, Ibu and Prog were an important consideration for a peripheral nerve guidance conduit. As the combination of NAC, Ibu and Prog had overlapping UV absorption spectra, HPLC was used, with system of suitability determination as well as sensitivity determination being carried out prior to drug release study. To determine their release rates 1mg/ml concentrations of NAC, Ibu and Prog were added to PEGDMA-DiPETMP and polymerised. Post polymerisation these polymers were placed into 50ml McCartney bottles and submerged in PBS-SDS solutions maintained at sink conditions. Aliquots were removed and replaced until complete drug release had occurred determined via HPLC analysis.

Following determination of drug release, release rate models for the three drugs were determined as were their modes of drug release.

6.1 Drug synergy optimisation

6.1.1 Initial drug combinations

6.1.1.1 Ibu-NAC combinations

6.1.1.1.1 Schwann cell response

From the initial NAC-Ibu tests shown in Figure 6-1 it could be seen that the Schwann cells experienced cytotoxic responses for concentrations of Ibuprofen above 1200 µM. With the metabolic activity of Schwann cells treated with 2400 µM being below 30% of the control well regardless of the NAC concentration with which it was combined. The 1200 µM Ibu concentrations also appeared to initially induce a cytotoxic effect in Schwann cells which appeared to be counteracted by the presence of NAC. Both the 0 µM and 2.758 µM NAC concentrations when combined with the 1200 µM Ibu concentration resulted in a loss of metabolic activity greater than 30% of the control wells, a result only observed with one NAC concentration above this amount (11.0325 µM with a metabolic activity % of 68.496%). This impact on the proliferation of Schwann cells may continue to be seen to a lesser extent with the 600 µM Ibuprofen concentrations where metabolic activity values fell in the range of 89 to 97% for 7 of the combination wells. Interestingly the combination of NAC and Ibu drug concentrations did appear to be more conductive for cellular proliferation than either drug alone. When Schwann cells were treated with NAC alone only two concentrations (22.065 and 44.13 µM) were shown to increase cellular metabolic activity more than the control well. Whereas all drug combinations of NAC and Ibu (with Ibu in the 32.5-300 µM range) where shown to have an increase on the metabolic activity of Schwann cells (ranging from 100 to 170% of the control well).

After 48 hours exposure it was again found that the higher Ibuprofen concentrations indicated a cytotoxic response particularly at the 2400 µM concentration as can be seen in Figure 6-2. It could be seen that the higher NAC concentrations particularly the 88.26 and 176.52 µM concentrations were found to improve the Schwann cells metabolic activity across most Ibuprofen concentrations including the 1200 and 2400 µM, this trend continued into the 72-hour post-treatment results shown in Figure 6-3. The lower NAC concentrations also improved cellular activity of Schwann cells, however when combined with higher Ibuprofen concentrations (in the 150 to 1200 µM concentration range) they were found to lower overall metabolic activity at 48-hour and 72-hour measurements post treatment. When viewing their impact as singular drug concentrations it was found that the Ibuprofen concentrations continued to inhibit the cellular activity of Schwann cells compared to the control wells however it was seen that across all NAC concentrations there was an increase in cellular activity compared to control wells. When viewing the 72-hour post-treatment readings it was again found that Ibuprofen inhibited cellular activity whereas with NAC concentrations the higher concentrations appeared to boost cellular activity when used individually.

Figure 6-1 Schwann cell 24-hour response to initial Ibuprofen and N-acetyl cysteine combinations (n=4), results are normalised to untreated control well
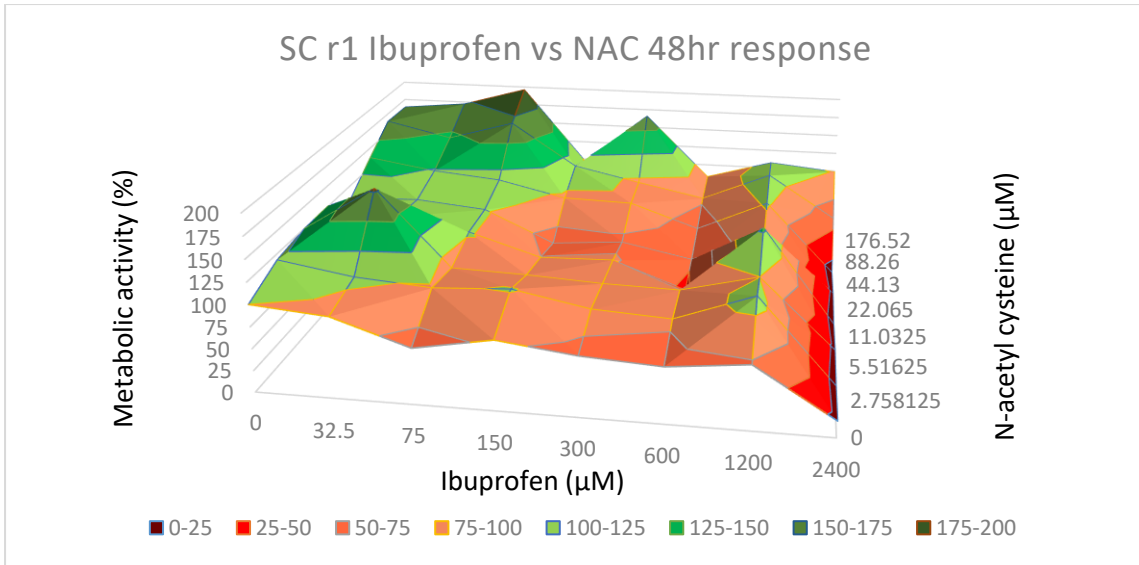
Figure 6-2 Schwann cell 48-hour response to initial Ibuprofen and N-acetyl cysteine combinations (n=4), results are normalised to untreated control well
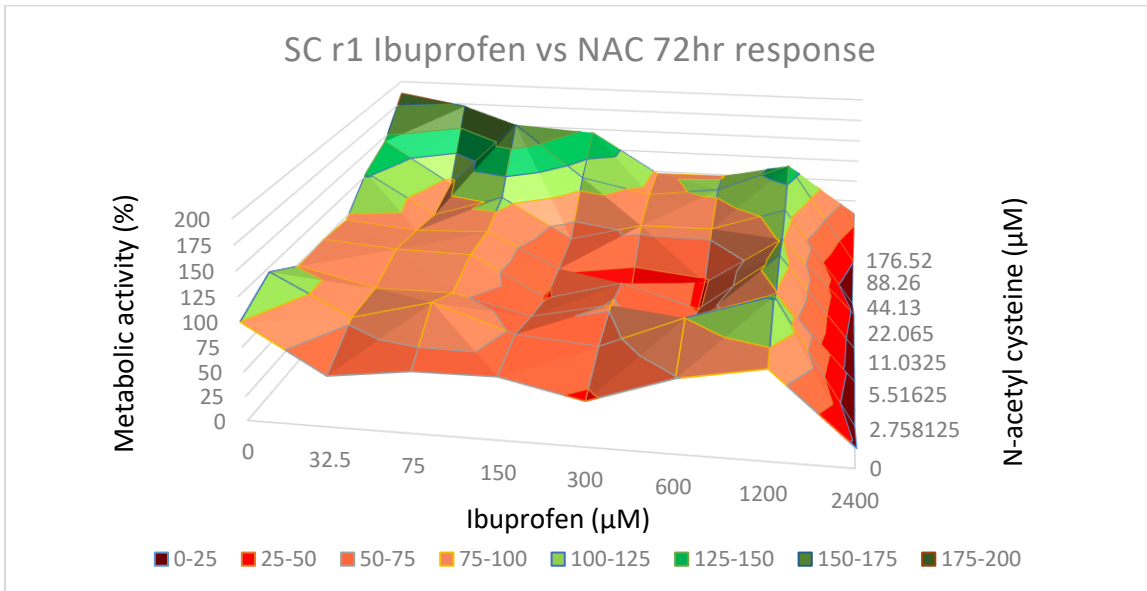
Figure 6-3 Schwann cell 72-hour response to initial Ibuprofen and N-acetyl cysteine combinations (n=4), results are normalised to untreated control well

6.1.1.2 PC-12 cell response

In Figure 6-4 the PC-12 cells responds to NAC and Ibu concentrations similarly to the response seen with Schwann cells, namely that the higher Ibuprofen concentrations appear to cause an inhibitory effect on PC-12 cell proliferation particularly when combined with low NAC concentrations or no NAC at all. Unlike the Schwann cells no drug combination of NAC and Ibuprofen caused a cytotoxic impact in PC-12 cells after 24 hours. The closest result to a cytotoxic response being the 1200 µM Ibuprofen concentration with no NAC treatment, which recorded a metabolic activity measurement of 71.2% of the control well. Based on this information it appears that the PC-12 cells are more robust in responding to Ibu-NAC drug combinations. For PC-12 cells 48 hours after treatment, the higher NAC concentrations had a detrimental effect on cellular proliferation. Interestingly in a contrast to what was seen with the Schwann cells, the PC-12s cells treated with NAC and Ibuprofen were more likely exhibit a cytotoxic response than PC-12 cells treated with either drug alone. This is shown particularly at the 176.52 µM NAC concentration where all combinations with Ibuprofen inhibited cellular metabolic activity and the 88.26 µM NAC combination where 5 of the 7 combinations with Ibuprofen inhibited cellular activity. Like what was previously seen with Schwann cells the higher Ibuprofen concentrations were more likely to inhibit cellular activity than lower Ibuprofen concentrations with all cytotoxic responses being recorded at Ibu concentrations higher than 150 µM.

In Figure 6-5 the 48-hour results show that the higher NAC concentrations inhibited PC-12 cell proliferation when in combination with higher Ibu concentrations. This trend was particularly evident with the 88.26 µM and the 176.52 µM NAC concentrations which both caused cytotoxic responses when combined with higher Ibu concentrations. NAC treatments at 2.758125 and 5.51625 µM treatments maintained a consistent increase in PC-12 cell proliferation, whereas higher NAC concentrations inhibited PC-12 proliferation. This contrasts

with what was seen with the Schwann cell treatments where the highest NAC concentration (176.52 µM) maintained the most positive result. In Figure 6-6 there appears to a decrease in metabolic activity 72-hours post exposure.

Figure 6-4 PC-12 cell 24-hour response to initial Ibuprofen and N-acetyl cysteine combinations (n=4), results are normalised to untreated control well
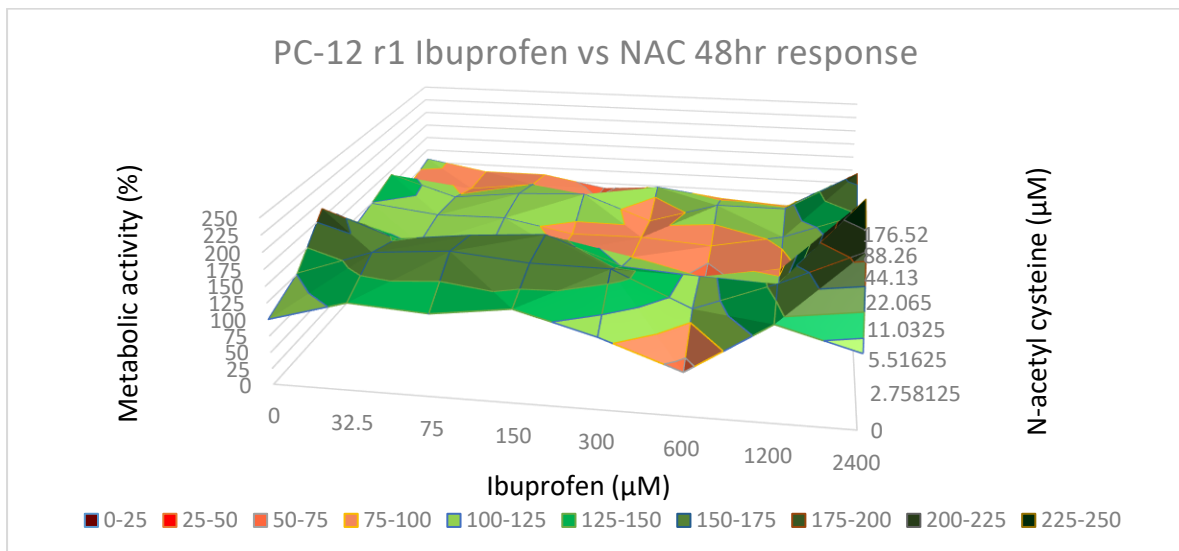
Figure 6-5 PC-12 cell 48-hour response to initial Ibuprofen and N-acetyl cysteine combinations (n=4), results are normalised to untreated control well
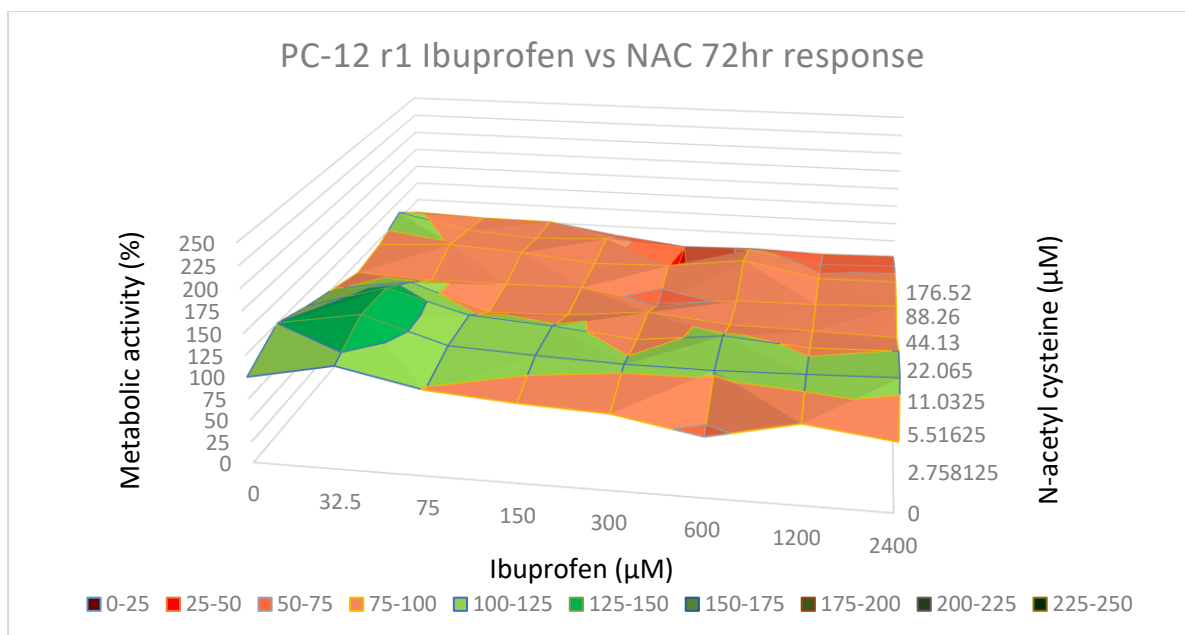
Figure 6-6 PC-12 cell 72-hour response to initial Ibuprofen and N-acetyl cysteine combinations (n=4), results are normalised to untreated control well

6.1.1.2 Prog-Ibu combinations

6.1.1.2.1 Schwann cell response

When viewing the impact of Prog and Ibu concentrations on Schwann cells in Figure 6-7 all combinations produced a positive impact on cellular proliferation with higher progesterone levels having an increased effect on cellular proliferation. The impact of Ibuprofen metabolic activity proliferation did not appear to be concentration dependent, producing near uniform responses across all concentrations. In Figure 6-8 there was a marked decrease in cellular activity with all Prog and Ibu concentrations presenting a decrease in cellular activity compared to control well. This overall effect contributed to an emerging pattern where the greater concentrations of either drug caused a cytotoxic response with the outcomes being the inverse of what was seen in the 24-hour treatment responses. The results for 72 hours post treatment in Figure 6-9 showed a similar response to 48 hours, namely cells which had greatest proliferative effect after 24-hour treatment continued to experience greatest decrease in metabolic activity

with many Prog-Ibu combinations particularly the higher concentration combinations experiencing cytotoxicity.

Figure 6-7 Schwann cell 24-hour response to initial Progesterone and Ibuprofen combinations (n=4), results are normalised to untreated control well

Figure 6-8 Schwann cell 48-hour response to initial Progesterone and Ibuprofen combinations (n=4), results are normalised to untreated control well
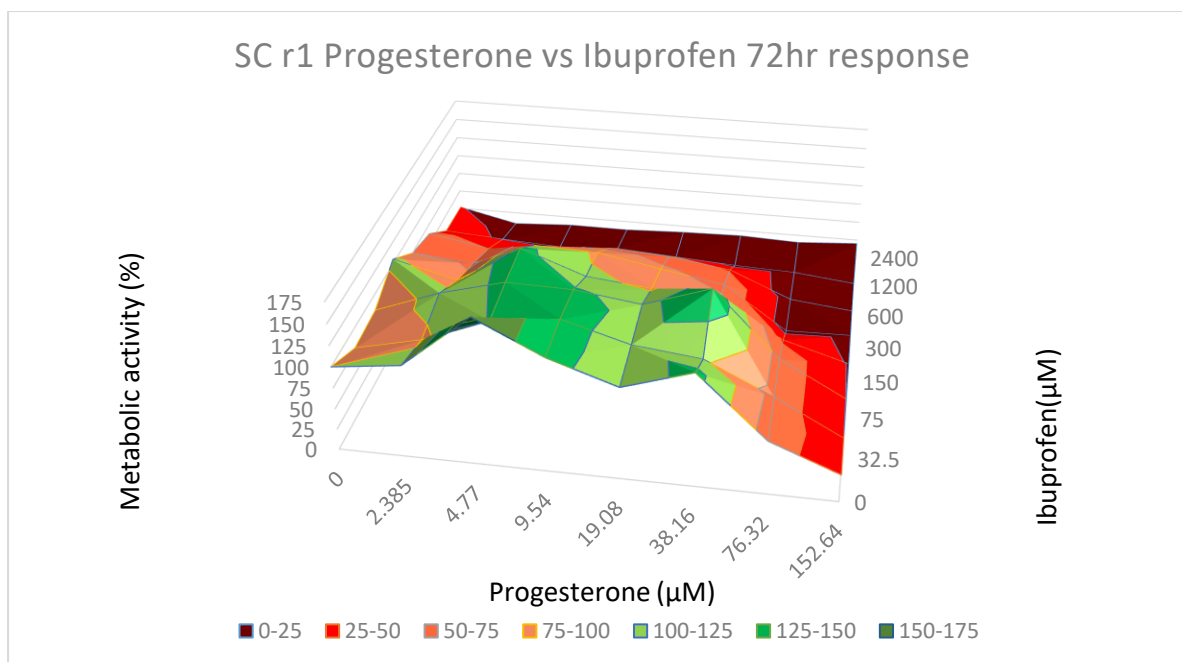
Figure 6-9 Schwann cell 72-hour response to initial Progesterone and Ibuprofen combinations (n=4), results are normalised to untreated control well

6.1.1.2.2 PC-12 cell response

The effect of Prog-Ibu combinations on PC-12 cells shown in Figure 6-10 to 6-12 contrast to the outcome of the NAC-Ibu treatments of PC-12 cells shown from 6-4 to 6-6. Namely that here PC-12 cells appeared to be much more sensitive to the effect higher Ibuprofen concentrations. This effect is shown particularly when high Ibu concentrations are combined with lower Prog concentrations, in a similar manner to how the Schwann cells reacted (i.e.: lower concentration combinations provided the best cellular response). 48 hours post treatment a similar pattern to what was seen in the Schwann cell treatments occurred, wherein the concentration combinations which provided the best cellular response displayed cytotoxicity after further incubation. In contrast to Schwann cells however is the general effect of Prog-Ibu combinations, as PC-12 cells underwent a proliferative effect at lower concentrations showing again that PC-12 cells appear to be less sensitive to drug combinations. Higher drug concentrations of both Prog and Ibu appeared to inhibit cellular activity particularly the 152.64 μM concentration which produced a cytotoxic response across all combinations with

Ibuprofen. 72 hours post treatment saw results mirror what was seen with the 48-hour SC and PC-12 responses and the SC 72-hour responses with low Ibu concentrations continuing to produce a proliferative effect in PC-12 cells with most Prog concentrations. The 150 and 300 µM concentrations appeared to produce the best effect on PC-12 cells, giving a proliferative response across all Prog concentrations whereas higher Ibu concentrations appeared to inhibit PC-12 cellular activity. This was especially prevalent in combination with the 152.64 µM NAC concentration, producing a cytotoxic response similar to the 48-hour responses.
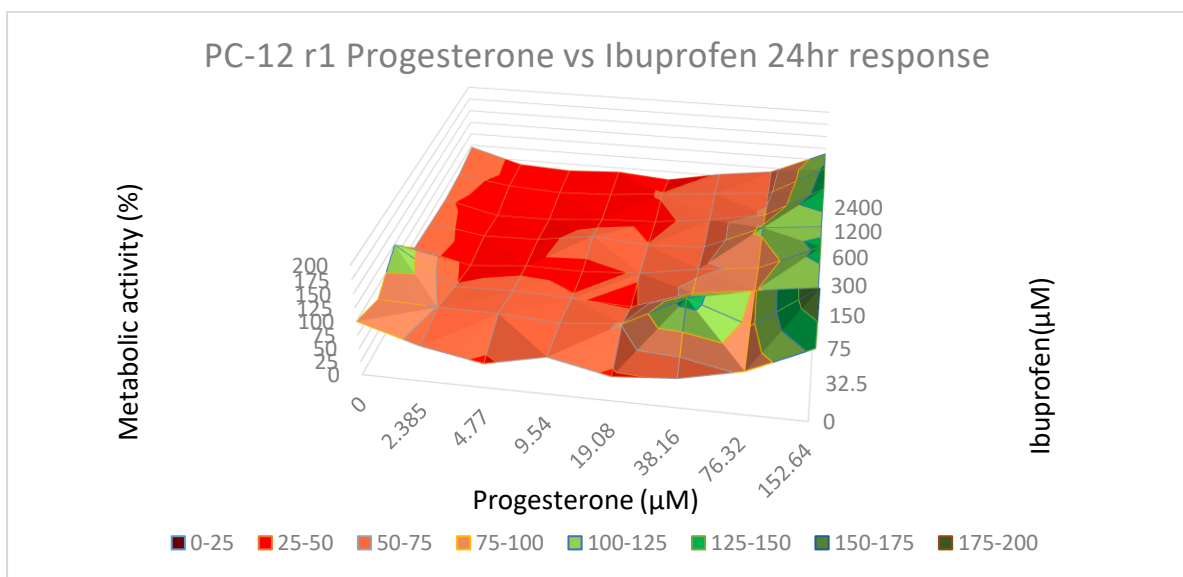
Figure 6-10 PC-12 cell 24-hour response to initial Progesterone and Ibuprofen combinations (n=4), results are normalised to untreated control well
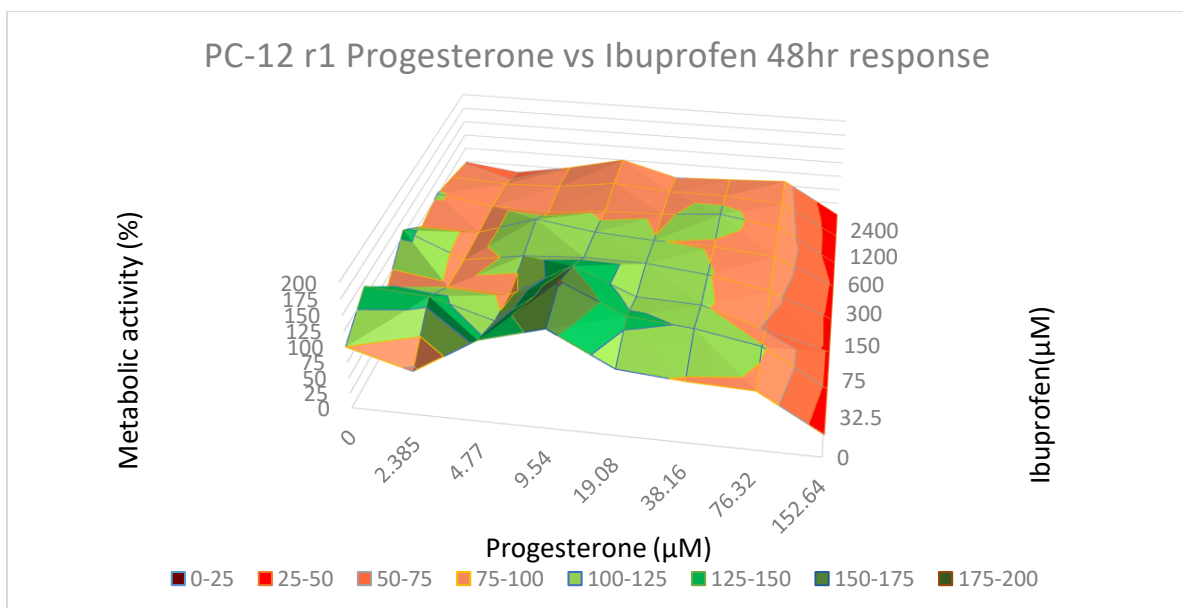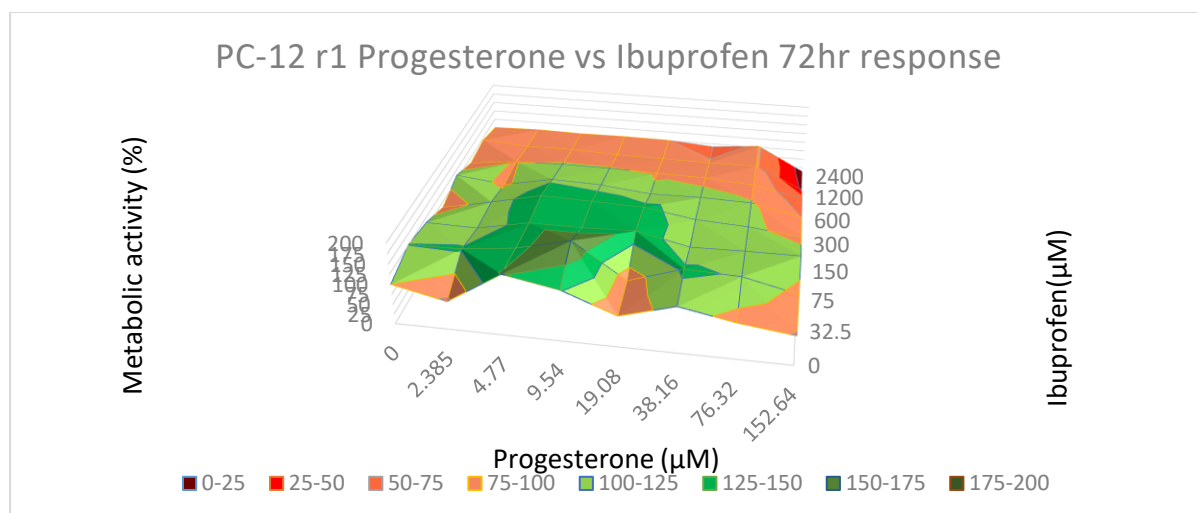
Figure 6-12 PC-12 cell 72-hour response to initial Progesterone and Ibuprofen combinations (n=4), results are normalised to untreated control well

6.1.1.3 NAC-Prog combinations

6.1.1.3.1 Schwann cell response

Based on Figure 6-13, 24-hour post treatment there was no cytotoxic response for any of the Prog-NAC combinations or for either drug individually. It should be noted that the most inhibitive effects were seen when cells were treated with either drug individually or with the lowest concentration combination of both drugs. Potentially due to synergistic effects Prog-NAC combinations have on one another as higher NAC concentrations produce a proliferative effect in Schwann cells especially in combination with mid to high Prog concentrations. In Figure 6-14 with an extra day post treatment, in general all concentrations of NAC provided a proliferative effect to the Schwann cells, this is especially shown with the higher NAC concentrations, indicating the potential for a higher NAC concentration to possibly show a better response. Higher Prog concentrations appeared to inhibit cellular proliferation 48 hours post treatment, however when combined with higher NAC concentrations there is an increased proliferative response, in general however lower Prog concentrations have a better impact on cellular proliferation. In Figure 6-15 following 72 hours treatment, low NAC concentrations

were shown to cause a slightly inhibitory effect on SC proliferation paralleling 24-hour responses. A similar response occurs with higher NAC concentrations however none of the 176.52 µM treated wells experienced a cytotoxic response. In Prog treatments, the proliferative effect seen with Schwann cells appears to be more common with lower concentrations, contrasting what was seen in the 24-hour responses to progesterone treatments.
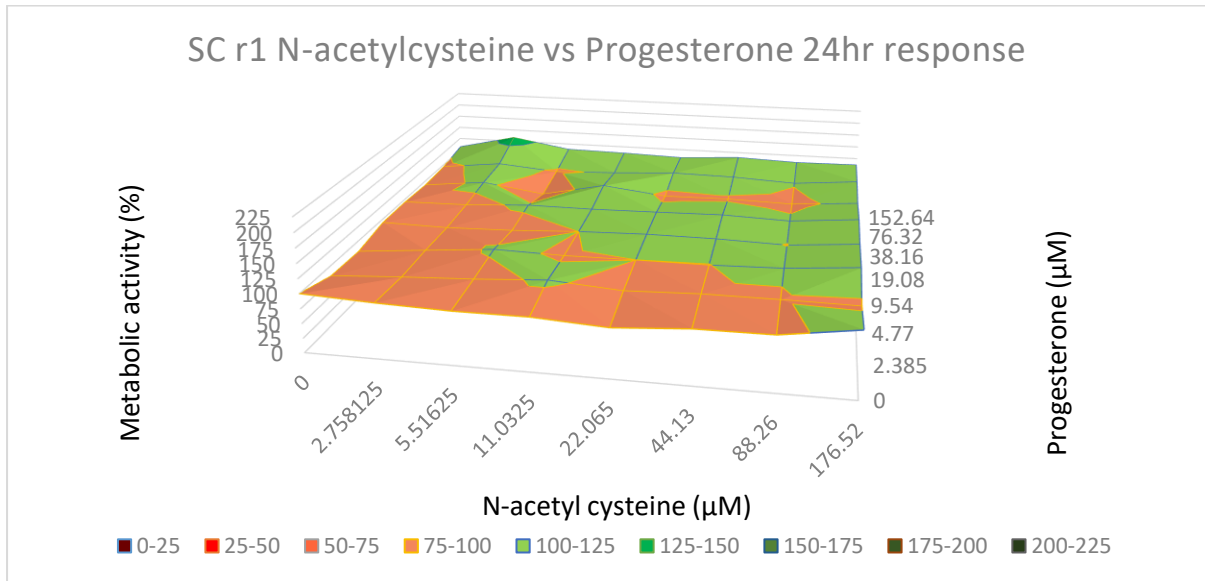
Figure 6-13 Schwann cell 24-hour response to initial Progesterone and N-acetyl cysteine combinations (n=4), results are normalised to untreated control well
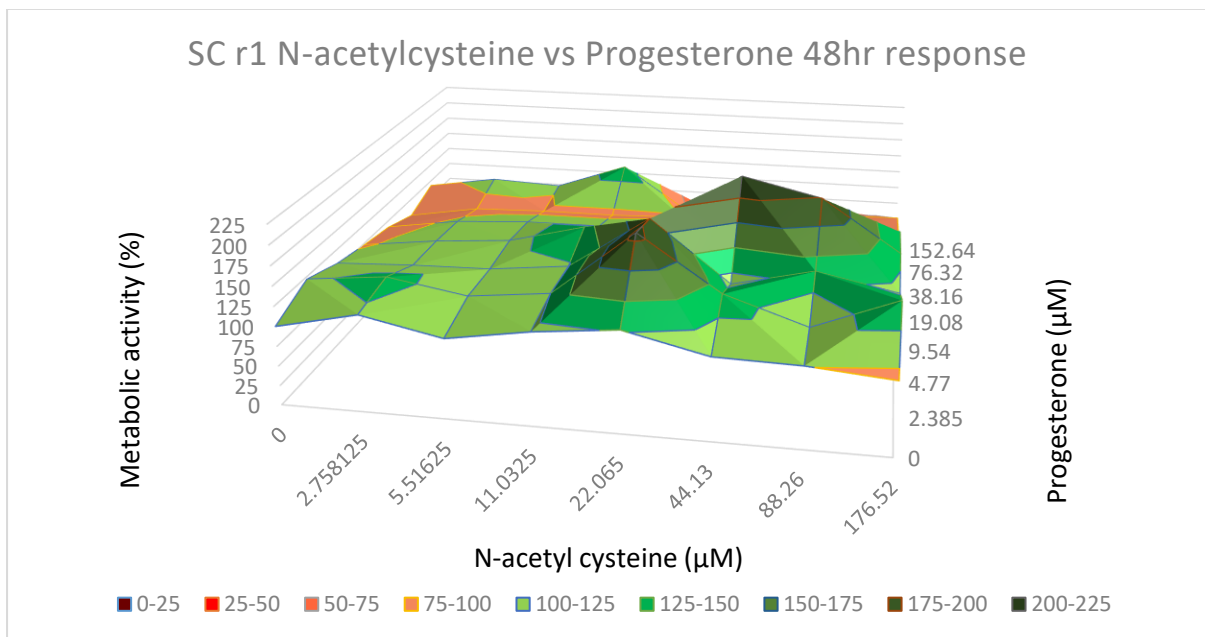
Figure 6-14 Schwann cell 48-hour response to initial Progesterone and N-acetyl cysteine combinations (n=4), results are normalised to untreated control well
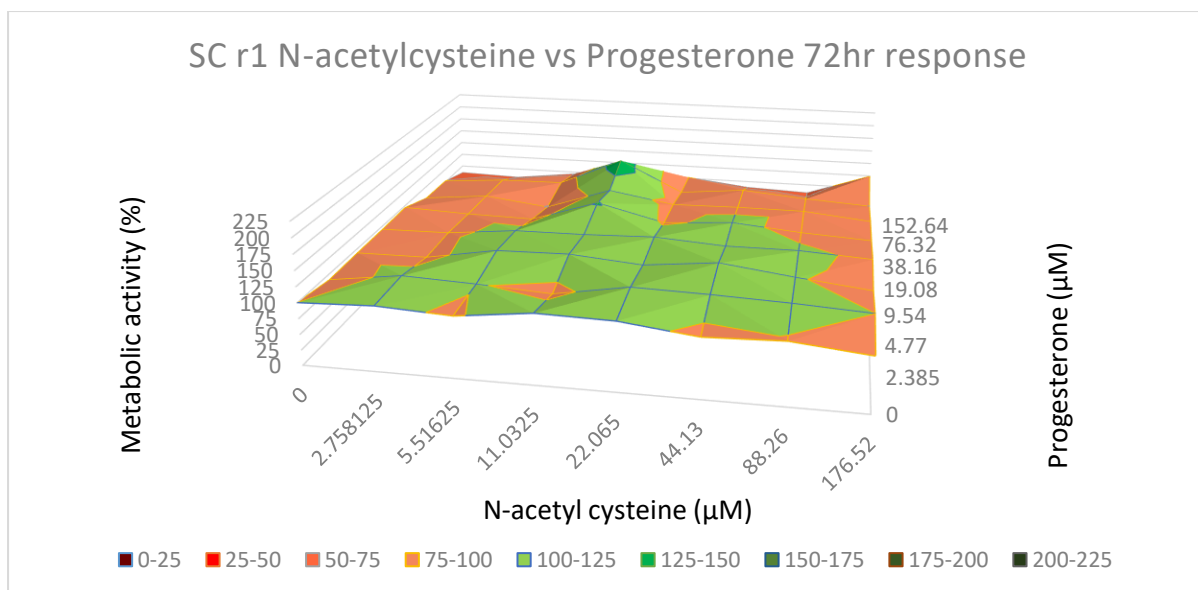
Figure 6-15 Schwann cell 72-hour response to initial Progesterone and N-acetyl cysteine combinations (n=4), results are normalised to untreated control well

6.1.1.3.2 PC-12 cell response

In Figure 6-16 the impact of NAC and progesterone combinations on PC-12 cells can be seen, there is an initially proliferative effect shown with higher Prog concentrations, indicating that higher concentrations may have a greater impact on proliferation. In NAC treatments there was no clear pattern to their effect on PC-12 cellular proliferation apart from the 176.52 µM NAC concentration which produced a cytotoxic response with all Prog concentrations below the 19.08 µM concentration. After the initial boost to proliferation there is a drop-off in cellular activity for higher prog concentrations whereas at lower prog concentrations all combinations with NAC produce a proliferative effect in PC-12 cells. Regarding NAC there was no clear pattern to its effects on PC-12 cells in combination with progesterone, with each individual concentration recording a proliferative effect with multiple progesterone concentrations.

As shown in Figure 6-18 after 72 hours a large number NAC and Prog combinations displayed a proliferative effect except for higher concentration combinations. With the higher NAC-Prog concentrations PC-12 cells displayed a slightly inhibitive response 72 hours post treatment. In general, the responses were comparable to what was seen in Figure 6-17 with 48-hour

responses where there was no clear pattern to discern the effect of different cellular concentrations. Interestingly there was a contrast between 24- and 72-hour results, namely that high progesterone and NAC concentrations produced the greatest proliferative response in the 24-hour post treatment results whereas for the 72 hour results the opposite was seen with lower NAC-Prog concentrations producing greater proliferative effects.
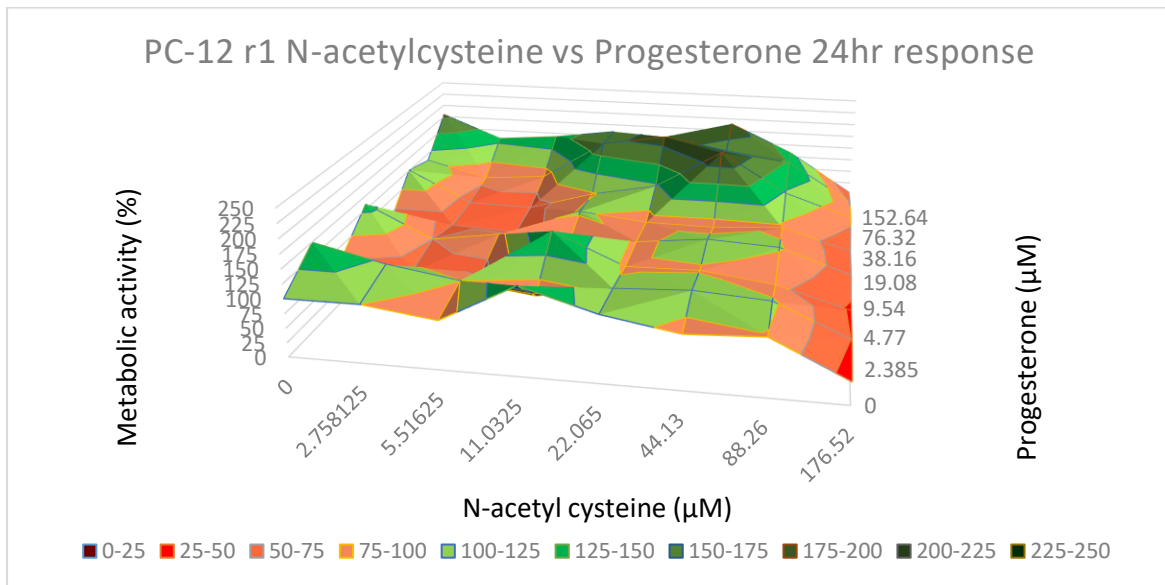
Figure 6-16 PC-12 cell 24-hour response to initial Progesterone and N-acetyl cysteine combinations (n=4)
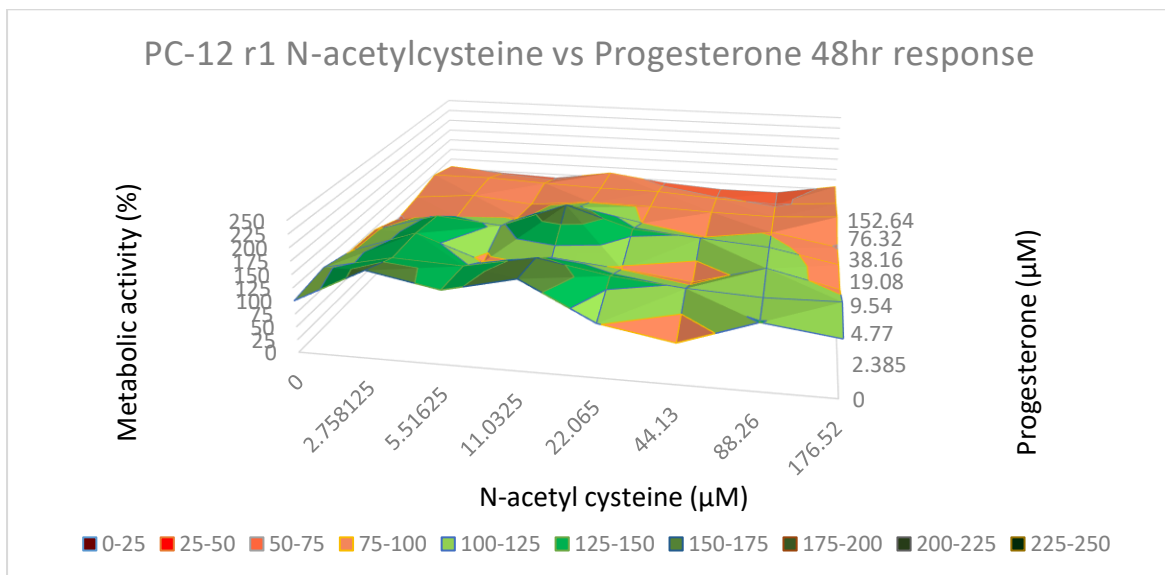
Figure 6-17 PC-12 cell 48-hour response to initial Progesterone and N-acetyl cysteine combinations (n=4), results are normalised to untreated control well
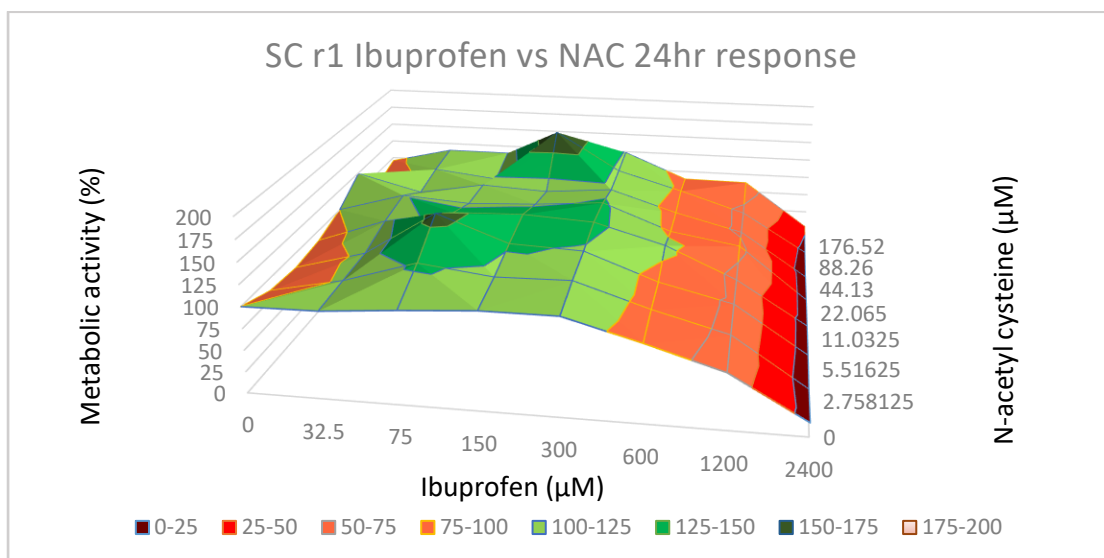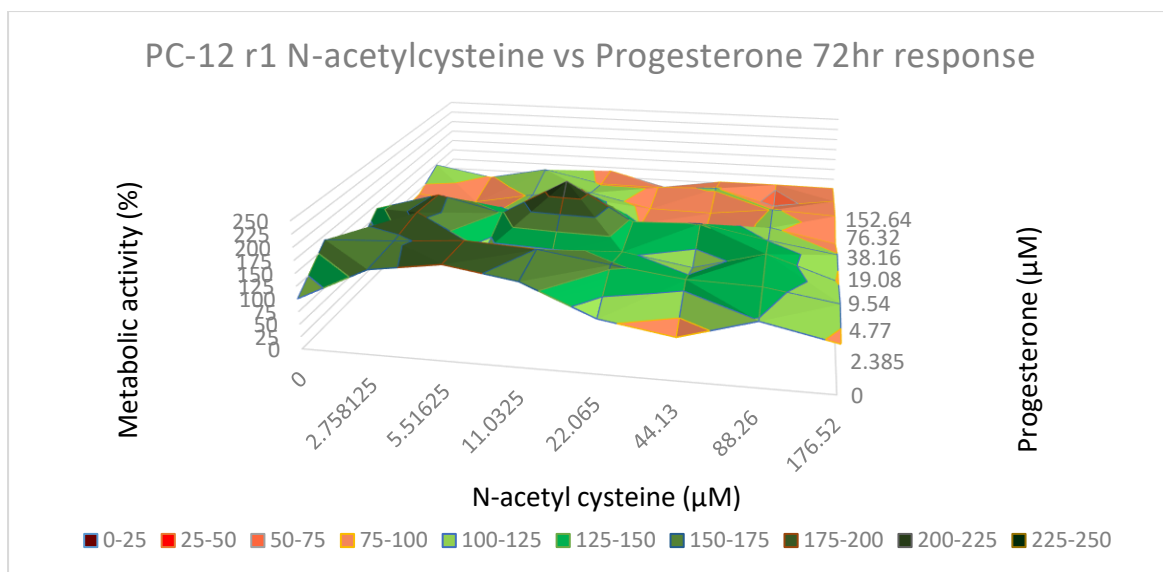
Figure 6-18 PC-12 cell 72-hour response to initial Progesterone and N-acetyl cysteine combinations (n=4), results are normalised to untreated control well

6.1.2 Second drug combinations

6.1.2.1 Ibu-NAC combinations

Consistent with the results from the first treatments of PC-12 cells and Schwann cells the biggest decrease in metabolic activity occurred when cells were treated singularly with either Ibu or NAC. In Figure 6-19 all combinations of NAC and Ibu demonstrated no clear pattern associated with the combinations of NAC and Ibu other than a generally positive impact on metabolic activity of Schwann cells (with the lowest recorded value being 93% of the control well) and that the highest concentrations of NAC and Ibu appeared to provide the biggest improvement to metabolic activity.

48 hours post treatment the 176.52 µM NAC concentration showed an inhibition of Schwann cell proliferation across most combinations with Ibuprofen including cytotoxic responses at Ibu concentrations ranging from 32.5 to 150 µM concentrations. The 176.52 µM concentration was the only NAC concentration to produce a cytotoxic response after 48 hours treatment, doing so with multiple Ibu concentrations as shown in Figure 6-20. In general, the responses

to NAC-Ibu concentrations continued to be positive, indicating good cellular growth in response to the NAC-Ibu concentrations.

Figure 6-21 highlighted that 72-hour post treatment metabolic activity in most treatment wells underwent a decline in comparison to the control well with only the 450 µM Ibu concentration continuing to provide a proliferative effect with a cytotoxic response being recorded across most combinations and all combination wells of NAC-Ibu producing an inhibition of cellular activity 72 hours post treatment. This was not expected and can be explained by one of the four NAC 0 µM, Ibu 450 µM replicate wells having exceptionally high metabolic activity measurements, increasing the average disproportionately (with the aberrant well removed values fall to 90 % of the control well, more in line with other treatments).
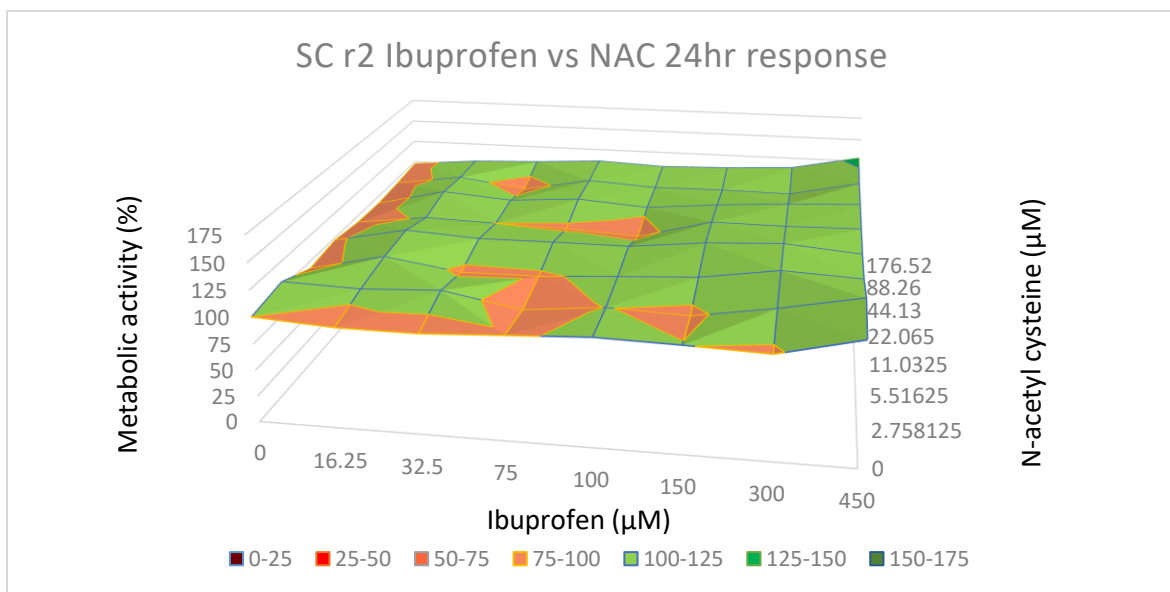
Figure 6-19 Schwann cell 24-hour response to second Ibuprofen and N-acetyl cysteine combinations (n=4), results are normalised to untreated control well
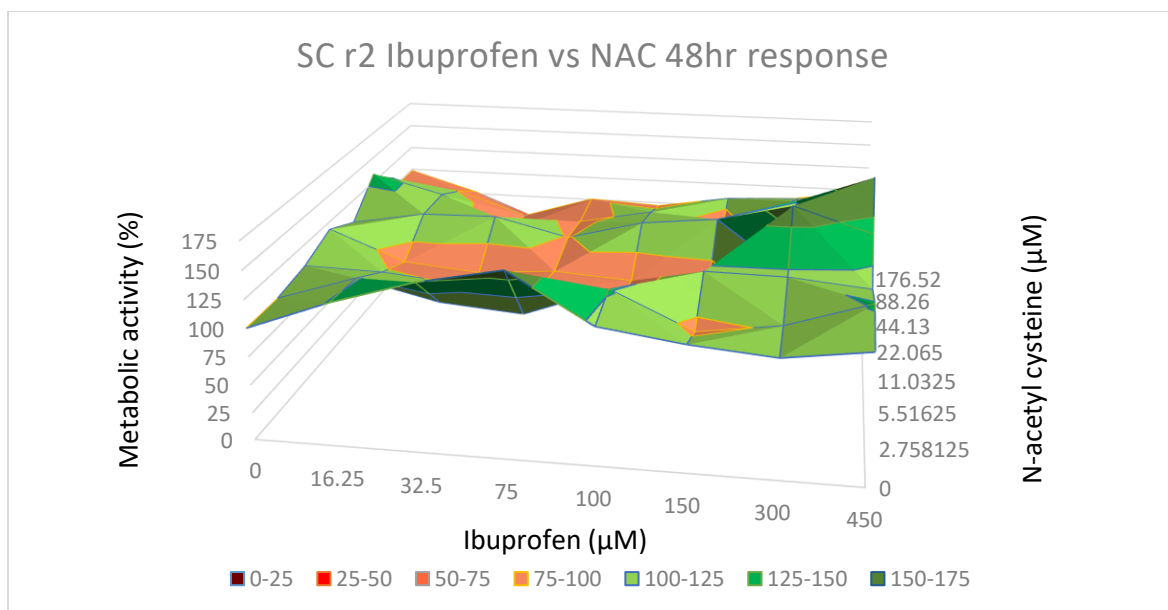
Figure 6-20 Schwann cell 48-hour response to second Ibuprofen and N-acetyl cysteine combinations (n=4), results are normalised to untreated control well
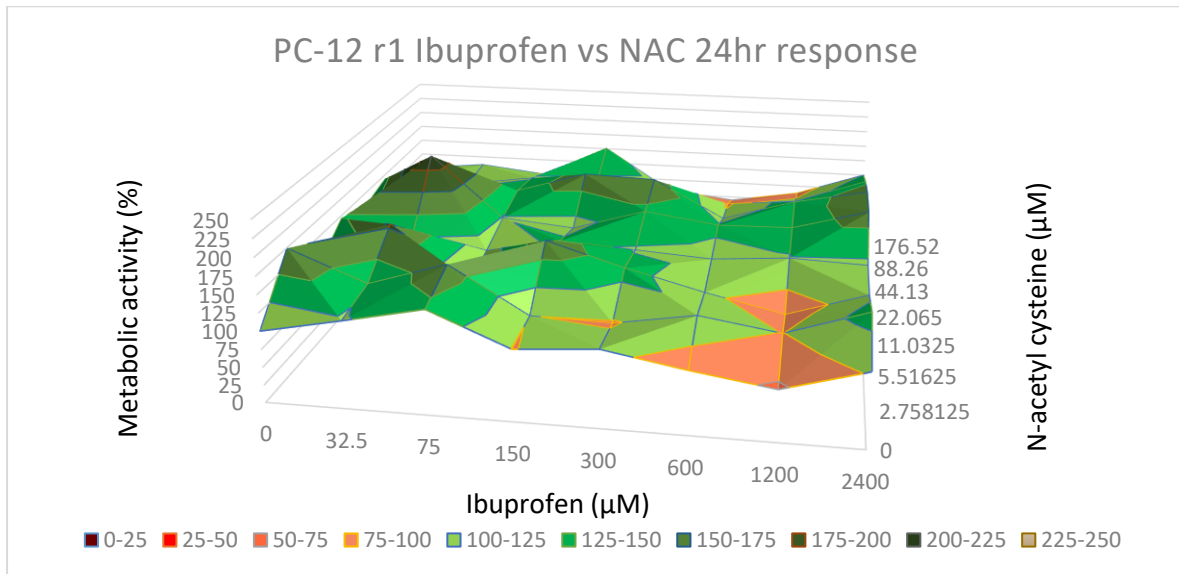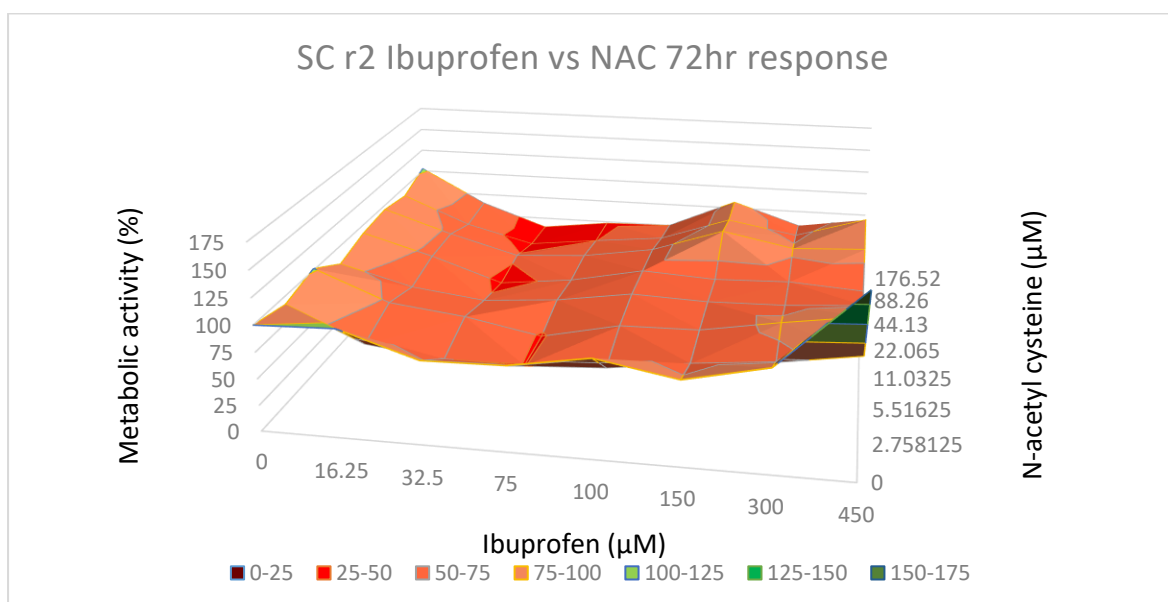

Figure 6-21 Schwann cell 72-hour response to second Ibuprofen and N-acetyl cysteine combinations (n=4), results are normalised to untreated control well

6.1.2.2 Prog-Ibu combinations

In Figure 6-22, after 24 hours treatment all drug combinations produced a proliferative effect on Schwann cells. This effect was particularly shown with the higher Prog concentrations and all Ibu concentrations, reaching between 2.35 and 2.6 times the metabolic activities of the control well with no inhibition of cellular growth was indicated across any concentration. No

wells were found to inhibit cellular activity, therefore the closest to inhibition was found with the lowest metabolic activity, this was recorded for wells treated with Prog and no Ibu treatment. From Figure 6-23 48 hours exposure cytotoxicity appeared to occur across most Ibu-Prog combinations, this was potentially due to a combination of factors namely using up all nutrients in well and contact inhibition. The only well showing proliferation was the Prog treated wells with no Ibu treatment, which had the lowest metabolic activity measurement after 24-hour treatment, lending credence to the idea that cells are either reaching limit of confluence in well, using up all nutrients within the 24 hour period of incubation or a combination of both. In Figure 6-24, after 72 hours exposure cytotoxicity was consistent with what was seen following 48 hours exposure with the only change being the wells treated with Prog also undergoing a decrease in metabolic activity, potentially due to the same effect seen with other wells (i.e.: using up all nutrients in well and contact inhibition).
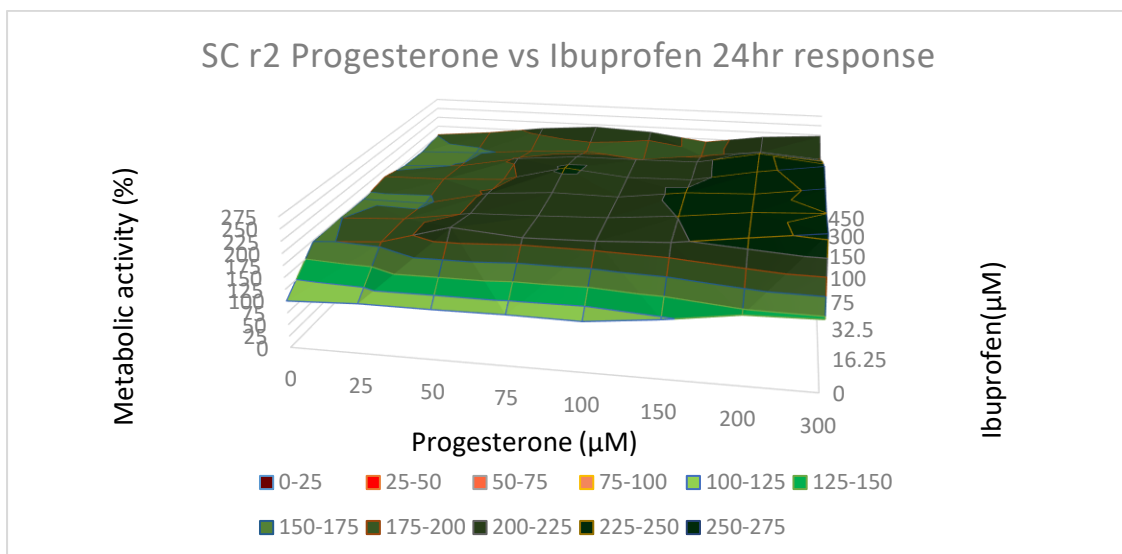
Figure 6-22 Schwann cell 24-hour response to second Progesterone and Ibuprofen combinations (n=4), results are normalised to untreated control well
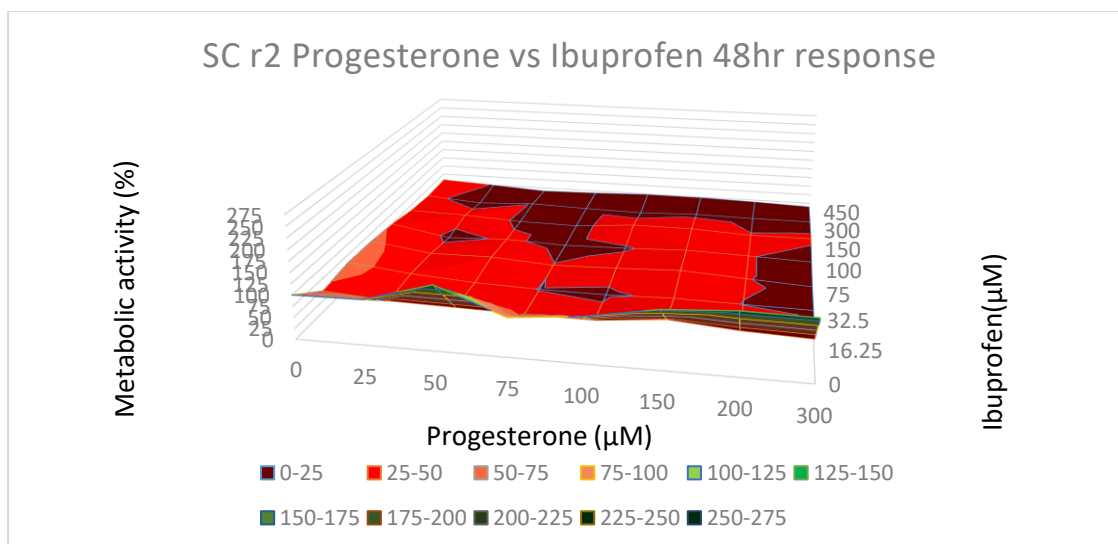
Figure 6-23 Schwann cell 48-hour response to second Progesterone and Ibuprofen combinations (n=4), results are normalised to untreated control well
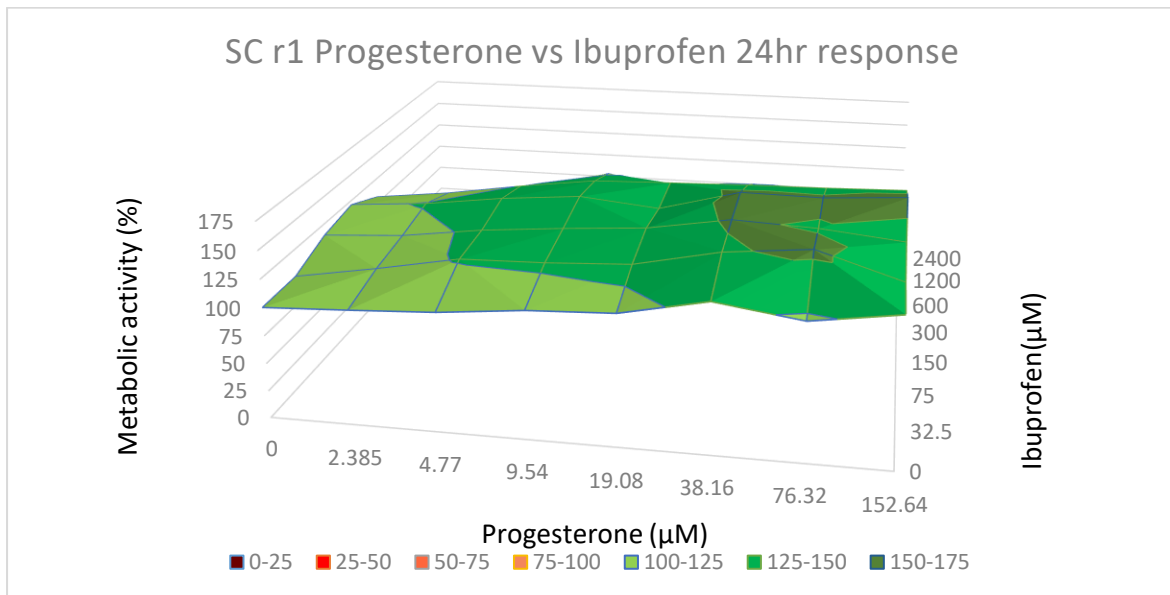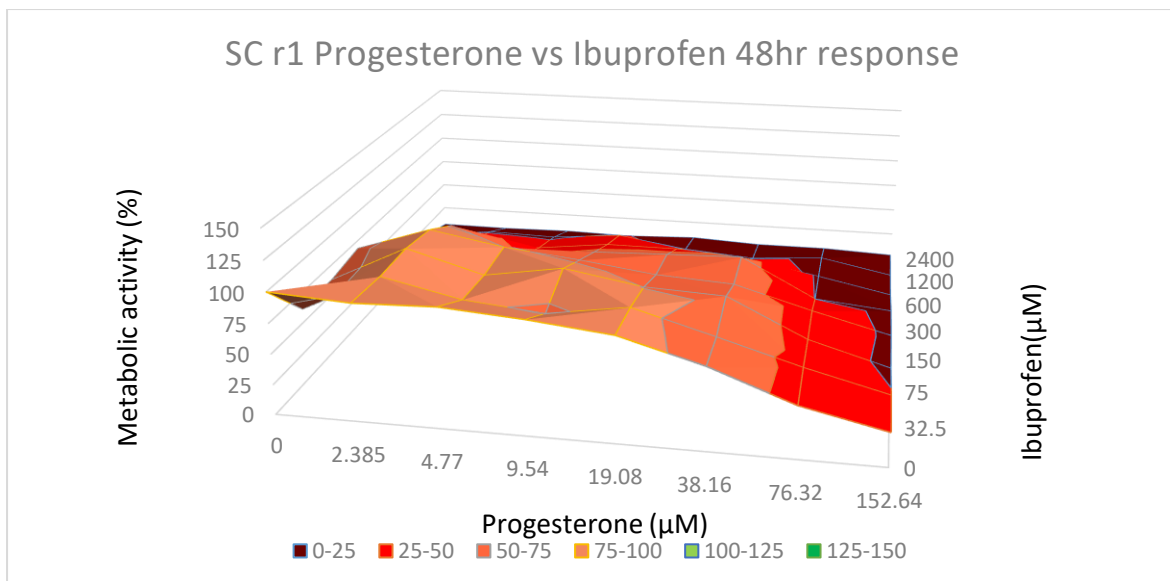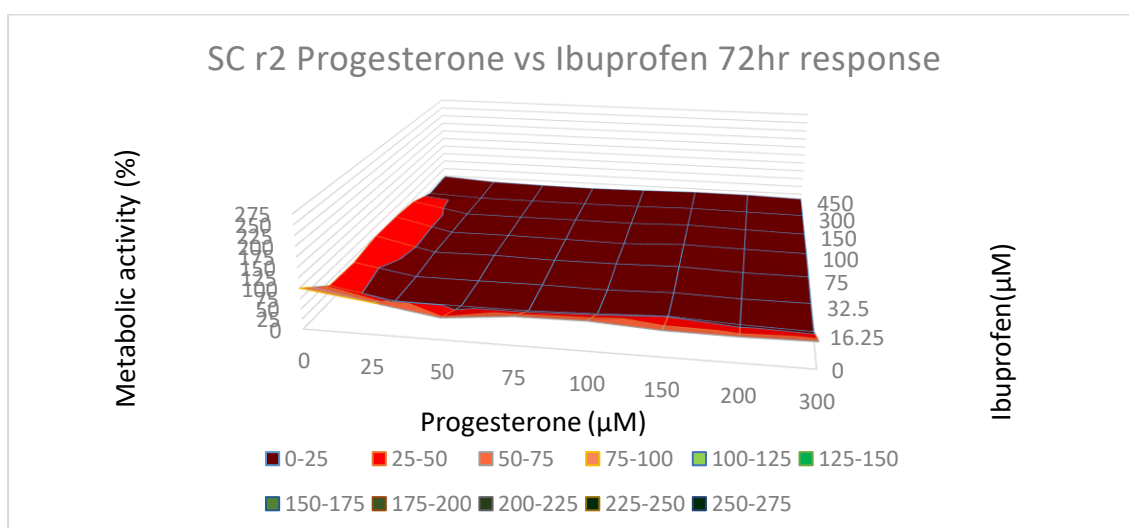

Figure 6-24 Schwann cell 72-hour response to second Progesterone and Ibuprofen combinations (n=4), results are normalised to untreated control well

6.1.2.3 NAC-Prog combinations

Figure 6-25 showed that 24 hours post treatment, all NAC concentrations produced a proliferative effect when combined with the different Prog concentrations. Interestingly there was inhibitory effect seen when Schwann cells were treated solely with NAC like what has been seen with previous NAC treatments. Progesterone in the range of 2.385 µM to 152.64 µM were consistently shown to produce a proliferative response in combination with NAC reaching metabolic activity values between 1.23 and 2.17 times the untreated control well. Like what

was seen in Figures 6-22 to 6-24, only wells which recorded inhibitive response initially were shown to produce a proliferative response after 48 hours exposure as shown in Figure 6-26, supporting the idea of contact inhibition/nutrient usage. These outcomes were repeated in the 72-hour results shown in Figure 6-27.
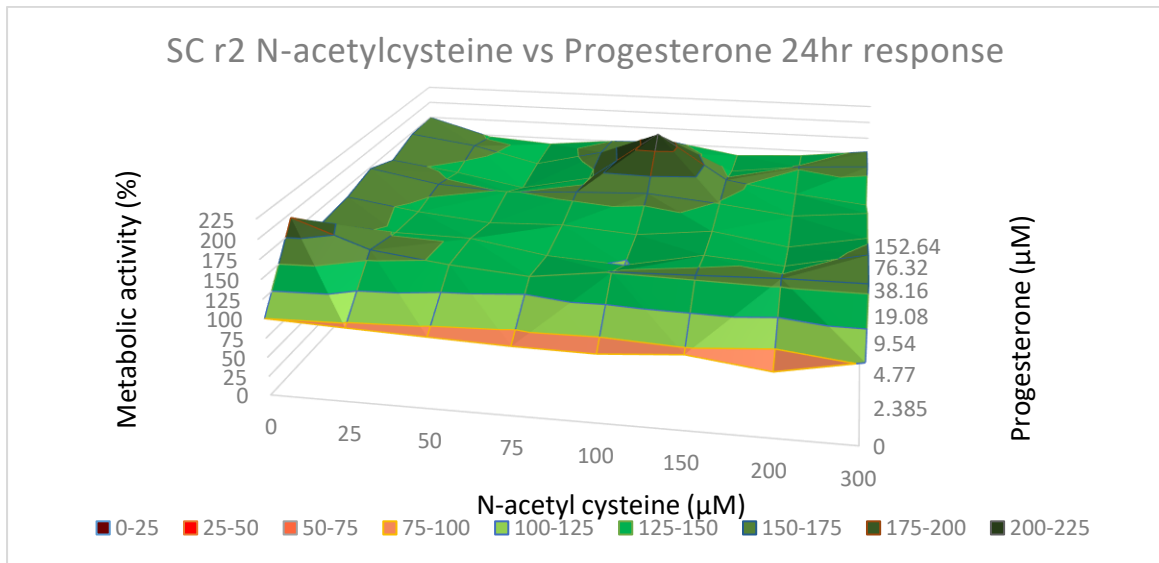
Figure 6-25 Schwann cell 24-hour response to second N-acetyl cysteine and Progesterone combinations (n=4), results are normalised to untreated control well
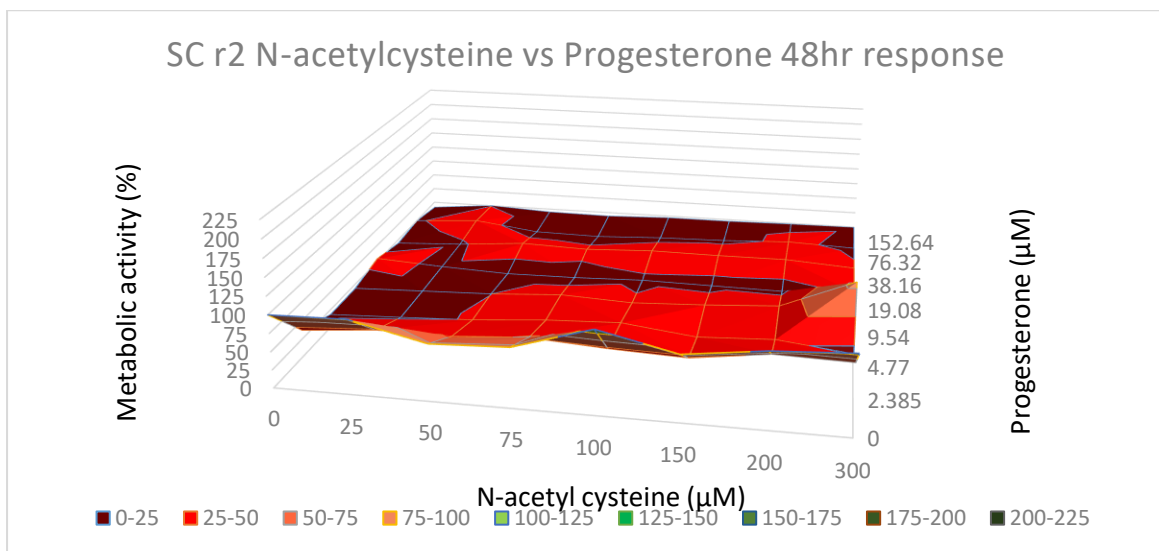
Figure 6-26 Schwann cell 48-hour response to second N-acetyl cysteine and Progesterone combinations (n=4), results are normalised to untreated control well
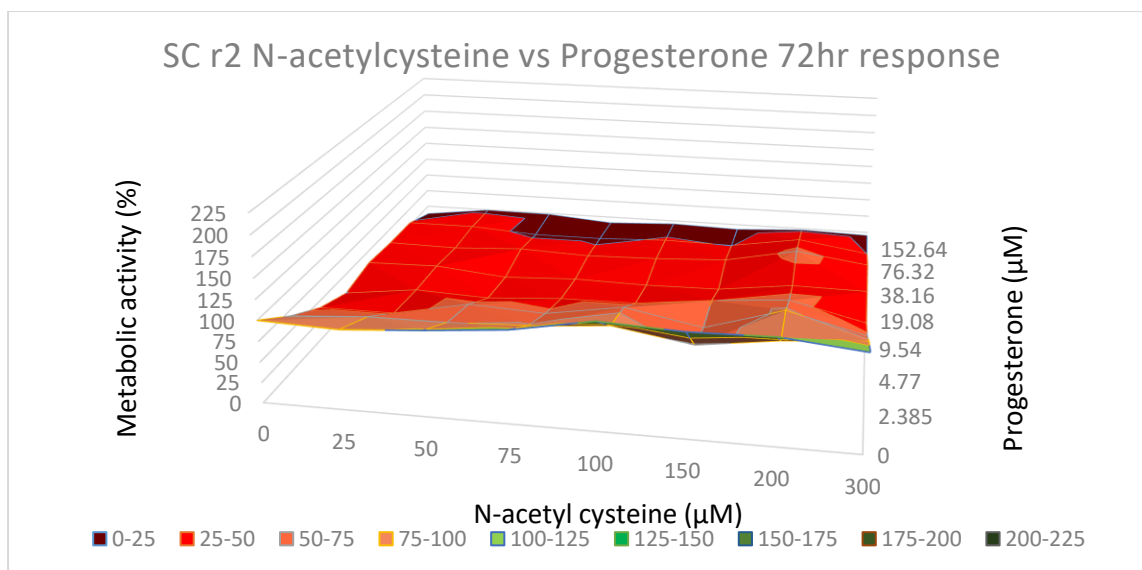
Figure 6-27 Schwann cell 72-hour response to second N-acetyl cysteine and Progesterone combinations (n=4), results are normalised to untreated control well

6.1.2.4 24 hour synergy

In order to determine the best drug combinations to use for the final cell treatments a synergy finding software (SynergyFinder) created by Ianevski *et al*. was utilised (Ianevski *et al.*, 2017). As discussed in section 1.6.1, this software employs a zero interaction policy (ZIP) approach created by Yadav et al.(Yadav *et al.*, 2015). Using two drugs independent dose response curves the software determines the relative shift in expected cell viability when the drugs are combined. This deviation from the expected dose response curves gives two delta (δ) scores (one for each dose response curve) which when averaged gives a summary of the interaction between drugs which in turn allows for the determining of the most efficient drug concentrations to improve cellular metabolic activity. To this end the 24-hour results for Schwann cells treated with the Ibu-NAC, Prog-Ibu and NAC-Prog combinations were analysed utilising SynergyFinder software with the results shown in Figures 6-28 to 6-30, wherein negative delta scores showed increased synergy of drug combinations.

In Figure 6-28 highlighting Ibu-NAC combinations, NAC concentrations did not appear to impact overall synergies, with negative δ values occurring across all concentrations and no

discernible differences in the impact made by individual concentrations. For Ibu the most synergistic effects occur when using the 450 µM concentration with δ scores lower than -13 recorded for all 450 µM Ibu combinations. Interestingly the lowest Ibu concentration also performed well, with negative δ scores occurring in all combinations of 16.25 µM Ibu with NAC (indicating good synergy), only giving non-synergistic effects in the well treated solely with Ibuprofen.

In Figure 6-29 showing Prog-Ibu combinations, Ibu had even greater synergy, producing negative delta scores with all Prog combinations. In Prog-Ibu combinations, excellent synergies occurred across all drug combinations with the 16.25 µM Ibuprofen showing good synergies, having δ values ranging from -71.91 to -158.02 when combined with the increasing Prog concentrations. In other Ibu concentrations, it was seen that after the 100 µM concentration there appeared to be a gradual decrease in synergy with Prog, while still maintaining a positive outcome overall. From Figure 6-30 the synergy of NAC when in combination with Prog could be seen, based on δ values recorded for NAC-Prog concentrations the drug combination with the highest synergy was the 100 µM NAC and 38.16 µM Prog concentrations with a δ value of -117.73. From the synergy seen between the 100 µM NAC and 38.16 µM Prog concentrations as well as considering the 16.25 µM Ibu concentrations excellent synergies with both NAC and Prog, the concentrations of NAC, Ibu and Prog for the final drug treatments were determined.

With the final drug combinations in mind the most synergistic NAC concentration was already situated in the centre of the plate, therefore requiring no change. For Progesterone the most synergistic value is one concentration treatment higher than the middle concentration (being 38.16 µM) and the greater values (values higher than 9.5 µM) provide better delta scores in general compared to the Progesterone values at or below 9.5 µM. Therefore, the Progesterone concentrations were adjusted as shown in Table 6-1, increasing the concentrations so that the

lowest Progesterone concentration is above 9.5 µM and the 40 µM concentration occupies the middle well.
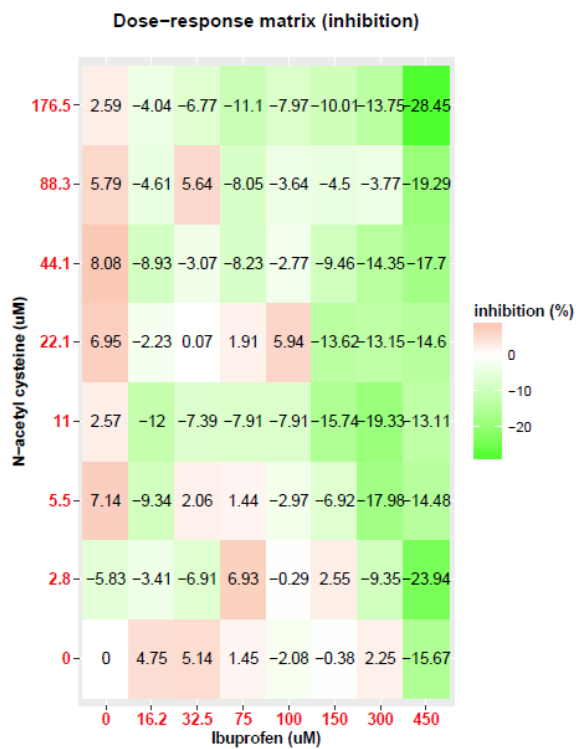
Figure 6-28 Synergies of NAC and Ibu combinations on Schwann cells (shown in Figure 6-19), visualised as δ-scores 24 hours post treatment, greater δ-scores indicate greater synergy

Dose–response matrix (inhibition)

Progesterone (uM)								
152.6	−74.75	−47	−40.04	−49.86	−53.03	−36.75	−41.83	−53.17
76.3	−71.94	−58.54	−34.93	−58.2	−62.7	−39.19	−51.2	−56.98
38.2	−57.36	−43.57	−25.58	−45.88	117.73	54.61	−39.12	−28.48
19.1	−72.52	−54.66	−49.1	−54.44	−58.32	−49.33	−37.71	−47.59
9.5	−60.02	−44.95	−35.17	−38.6	−31.31	−42.38	−26.98	−45.66
4.8	−54.84	−47.96	−46.59	−29.79	−23.69	−43.75	−36.29	−57.75
2.4	−94.32	−58.84	−46.21	−38.01	−50.83	−53.68	−56.88	−57.43
0	0	4.17	7.78	11.27	12.58	5.09	17.66	−1.96
	0	25	50	75	100	150	200	300

N–acetyl cysteine (uM)

inhibition (%): 0, −40, −80
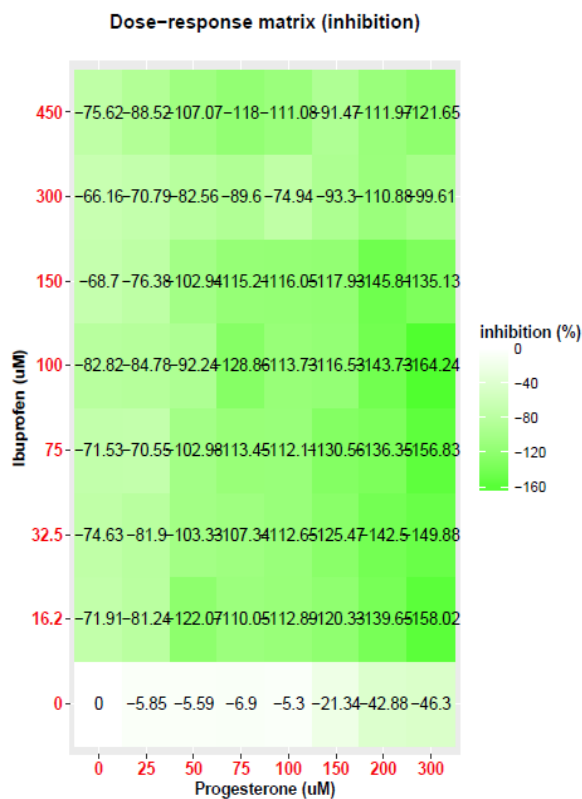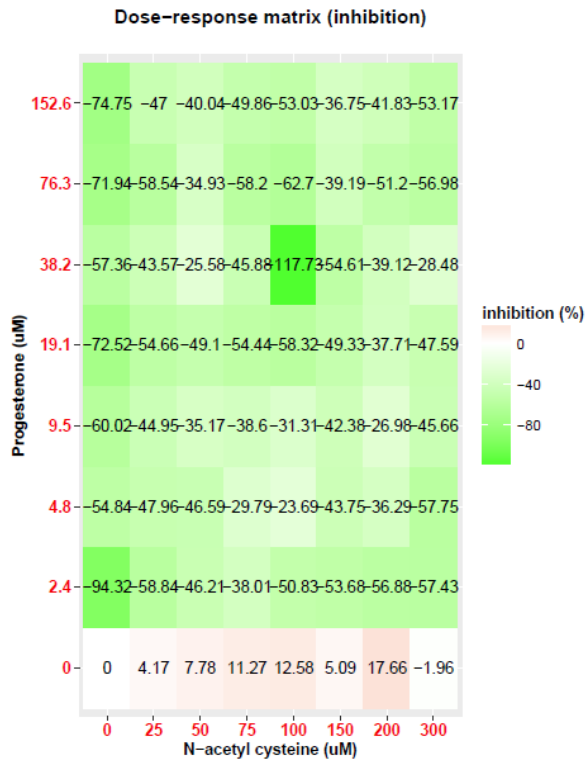
Figure 6-30 Synergies of Prog and NAC combinations on Schwann cells (shown in Figure 6-25), visualised as δ-scores 24 hours post treatment, greater δ-scores indicate greater synergy

Table 6-1 Changes made to progesterone concentrations for final drug combination treatments

Drug Concentration	Original Prog concentration (μM)	New Prog Concentration (μM)
1	0	0
2	2.4	10
3	4.8	20
4	9.5	30
5	19.1	40
6	38.16	80
7	76.3	125
8	152.6	200

6.1.3 Final drug combinations

6.1.3.1 Schwann cell response plus synergy

Figure 6-31 demonstrates the impact of the combinations of NAC, Ibu and Prog on the metabolic activity of Schwann cells 24 hours post treatment is shown. Across all combinations there was a marked increase in cellular metabolism with some combinations producing metabolic activity increases 3 times higher than control well, with the 75 µM NAC, 16.25 µM Ibu and 30 µM Prog combination showing good synergy, producing metabolic activity values 3.5 times greater than the control. When analysing the synergy between drugs via δ score in Figure 6-32, there were similarly positive outcomes across all treatments with no combination demonstrating antagonistic behaviour between drugs. When determining the best drug combination based on synergy again the 75 µM NAC, 16.25 µM Ibu and 30 µM Prog combination was highlighted as producing the most synergistic impact on SC proliferation.
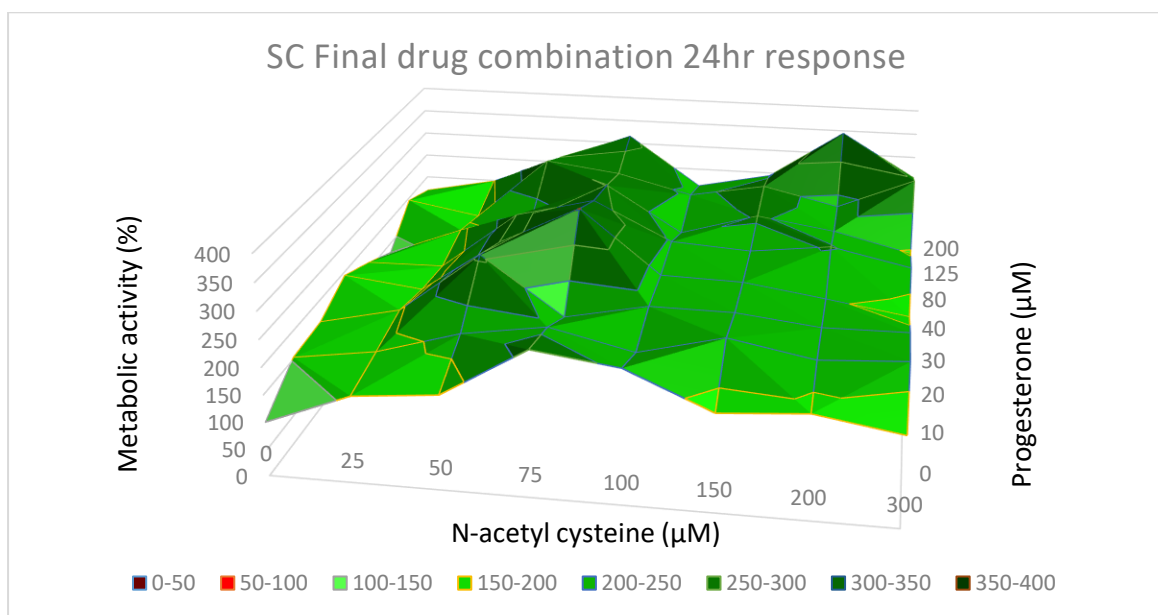
Figure 6-31 Impact of final drug combinations on cellular activity of Schwann cells 24 hours post treatment (n=4), results are normalised to untreated control well and fixed Ibu concentration of 16.25 µM is in all drug combination wells
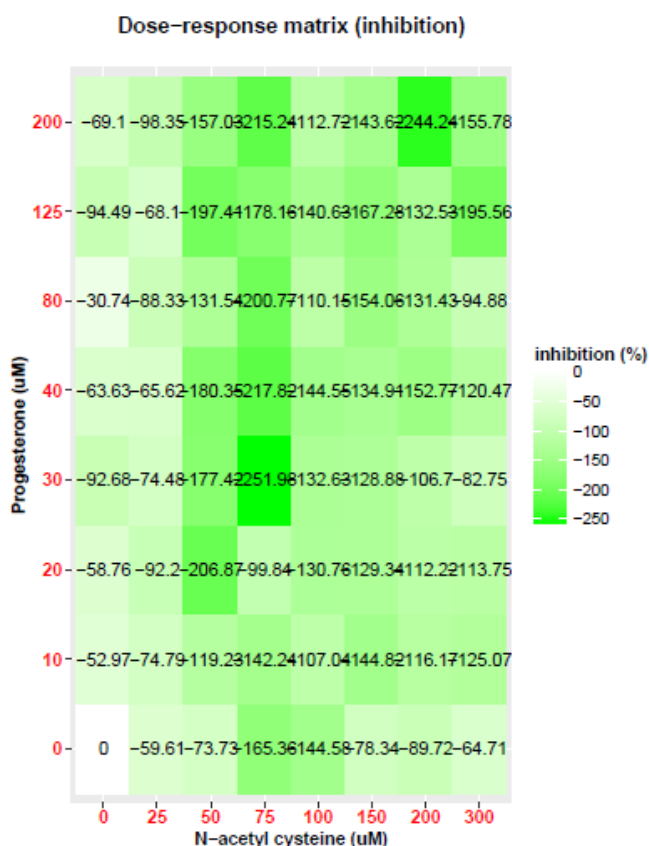
Figure 6-32 Synergy of final drug combinations on the cellular activity of Schwann cells, visualised as δ scores 24 hours post treatment

6.1.3.2 PC-12 cell response plus synergy

Following the treatment of PC-12 cells with NAC, Ibu and Prog concentrations, Figure 6-33 shows their impact 24 hours post treatment. Unlike SC response in section 6.1.3.1, the impact of drug combinations on PC-12 cells is more muted with many wells exhibiting lower viability than the control wells, with the lowest metabolic activity recorded being 79% of the control (it is important to note that this is not considered cytotoxic, with the ISO definition of cytotoxicity being considered lower than 70% of the control well (ISO/EN10993-5, 2009)). When looking at drug combinations which produced a positive impact on cellular activity there were several, notably the 300 µM NAC, 16.25 µM Ibu and 200 µM Prog combination produced the greatest increase in cellular activity (1.4 times the control well), indicating PC-12 cells responded better to higher drug concentrations, which is consistent with the results seen in initial drug

treatments. This is particularly evident for the treatments with 200 µM which saw the most consistent increases in cellular activity. Notably the 75 µM NAC, 16.25 µM Ibu and 30 µM Prog combination, which showed the greatest promise in Schwann cells also produced a proliferative effect in the treatment of PC-12 cells, with metabolic activity increasing to 1.15 times the control well. Importantly this also shows up when viewing the synergy between drugs, with the 75 µM NAC, 16.25 µM Ibu and 30 µM Prog combination producing a value of -14.34. Which although less pronounced than the impact in Schwann cells still showcased an improved synergistic effect between NAC, Ibu and Prog on the cellular activity of PC-12 cells.
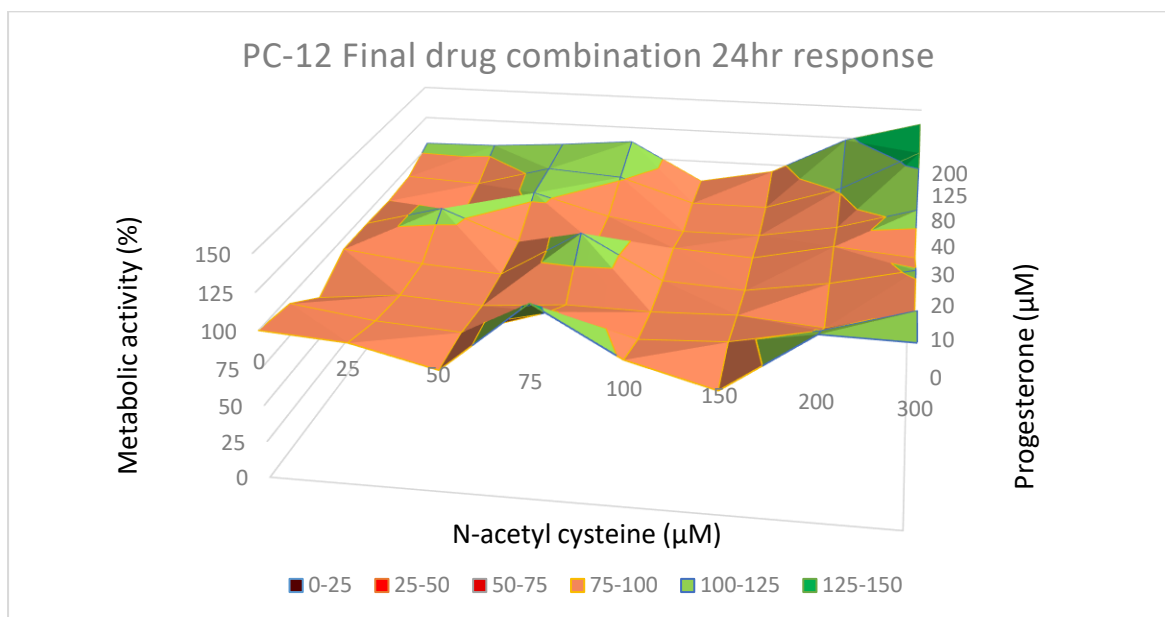
Figure 6-33 Impact of final drug combinations on cellular activity of PC-12 cells 24 hours post treatment (n=4), results are normalised to untreated control well and fixed Ibu concentration of 16.25 µM is in all drug combination wells
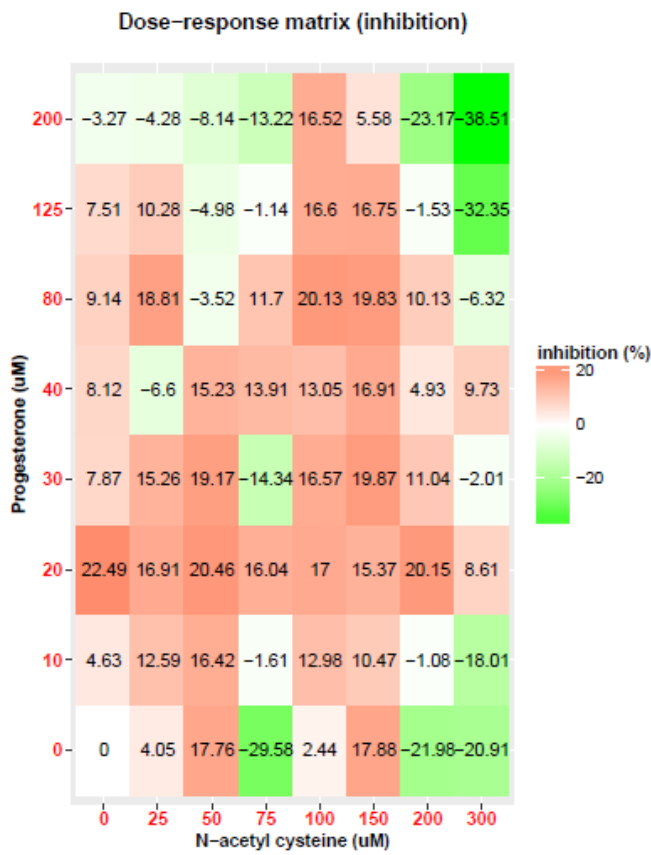
Figure 6-34 Synergy of final drug combinations on the cellular activity of PC-12 cells, visualised as δ scores 24 hours post treatment

6.2 Drug release

6.2.1 LOD and LOQ

To carry out drug release studies the sensitivity of the adapted HPLC method was determined and shown in Table 6-2. Using the S/N ratio the limit of detection for both Ibuprofen (Ibu) and Progesterone (Prog) was determined to be 0.001 mg/ml representing very good sensitivity, N-Acetyl Cysteine (NAC) had a lower sensitivity of 0.02 mg/ml which while 5 times less than the sensitivity of Ibu and Prog still represented good sensitivity. The limit of quantification was also determined, with Ibu having the lowest accurately quantifiable concentration of 0.002 mg/ml with Prog and NAC having values of 0.008 and 0.04 mg/ml respectively. From these results the sensitivity of the HPLC technique was highlighted particularly for Ibu and Prog with deviation in peak area for drug concentrations of approximately 0.01 mg/ml being less than 1%.

Table 6-2 LOD and LOQ values for NAC, Ibu and Prog

Drug	LOD	LOQ	Deviation (% of peak area)
N-acetylcysteine	0.02 mg/ml	0.04 mg/ml	1.003
Ibuprofen	0.001 mg/ml	0.002 mg/ml	0.511
Progesterone	0.001 mg/ml	0.008 mg/ml	0.784

6.2.2 Validation of methods

From Tables 6-3 and 6-4, the resolution values of all drug comparisons are at 3.182 (determined from the peaks for Ibuprofen and Progesterone) or above demonstrating a clear separation of drugs, readily clearing the usual resolution criteria of 1.5 to 2 (Shabir, 2003; Huber, 2010; Bhanot, 2013). When considering Asymmetry, Tables 6-3 and 6-4 also showcased the low degree of peak tailing across the singular drugs, dual drug peaks and 3 drug combinations peaks for both Ibu and Prog, with asymmetry values all falling within the 0.8 to 1.2 range commonly considered acceptable for peak symmetries, (CHROMacademy, no date). NAC samples did not fall in this ideal symmetry range however with all NAC peaks being at 1.32 or higher, indicating the potential to optimize this method for increased NAC

sensitivity efficiency, this is backed up when looking at theoretical plates where NAC falls well below the efficiency threshold of 2000 plates reaching between 359 and 377 plates (Shabir, 2004; Bhanot, 2013). In contrast both Ibuprofen and Progesterone readily cleared this efficiency metric with the lowest efficiency in either drug being 2518 for Ibu, when prepared in combinations with either NAC, Prog or both.When examining the variation in peak area, all deviations were within the 2% relative standard deviation (RSD), well within the standard requirements for intra assay precision measurements (The United States Pharmacopeia, 2015). The HPLC technique utilised also demonstrated excellent linearity with no r^2 value below 0.96 apart from NAC and Prog in the NACProg combination where r^2 values of 0.94 and 0.93 respectively, highlighting the accuracy of the method being utilised. Indeed this accuracy appears to be exemplified in the three drug combination where the lowest recorded r^2 value was 0.9954 for the NAC standard curve. When examining the equations of the line for each drug there does appear to be some impact particularly on Prog, with Prog showing a steeper curve when in the presence of either NAC or Ibu compared to its single drug equation.

Headings added, table was included to show the changes in conc.

Have added note to legend stating which drug matrix they correspond to

Table 6-3 System of suitability outcomes for NAC, Ibu and Prog in single and dual drug combinations

Drug	Resolution	Asymmetry	Theoretical plates	Precision (%)[a]	Equation of Line	Peak area Linearity (r^2 value)
NAC (single)	-	1.32	377	0.548545	Y=7E+06x	0.9715
Ibu (single)	-	1.14	4672	0.9117	Y=2E+07x	1
Prog (single)	-	1.03	5410	0.671723	Y=8E+06x	0.9988
NAC (NACIbu)	7.782	1.28	363	-	Y=7E+06x	0.969
Ibu (NACIbu)		1.03	2518	-	Y=2E+07x	1
NAC (NACProg)	11.162	1.46	359	-	Y=8E+06x	0.9416
Prog (NACProg)		1.07	4046	-	Y=1E+07x	0.9301
Ibu (IbuProg)	3.182	1.09	2518	-	Y=2E+07x	0.9995
Prog (IbuProg)		1.05	4045	-	Y=2E+07x	0.9884

Table 6-4 System of suitability outcomes for NAC, Ibu and Prog in a three-drug combination

Drug	Resolution	Asymmetry	Theoretical plates	Precision (%)[a]	Equation of Line	Peak area Linearity (r^2 value)
NAC and Ibu (NACIbuProg)	8.213					
NAC and Prog (NACIbuProg)	11.109					
Ibu and Prog (NACIbuProg)	3.565					
NAC (NACIbuProg)		1.72	367	1.453103	Y=6E+06x+23370	0.9954
Ibu (NACIbuProg)		1.08	2518	0.396643	Y=2E+07x	1
Prog (NACIbuProg)		1.13	4044	0.093622	Y=2E+07x	0.9999

6.2.3 Drug release

When examining the rates of drug release, there was a remarkable consistency for each drug across all combinations. NAC showcased the quickest rates of release undergoing complete release 1 day (24 hours) after immersion in McCartney bottles. This rate of release was shown to occur whether NAC was a single drug, in combination with Ibu, in combination with Prog or in combination with both Ibu and Prog, as shown across Figures 6-35, 6-36, 6-37 and 6-39. This consistency in rates of release occurred with both Ibu and Prog samples, indeed all drugs showcased remarkable consistency in rates of release. The key difference between drugs was shown to be the time needed to reach complete drug release, with Ibuprofen reaching complete release after 3 days (72 hours) in all combinations and Progesterone reaching complete release in all combinations after 21 days (504 hours). From figures 6-35, 6-36, 6-38 and 6-39 it could be seen that Ibuprofen consistently reached approximately 100% of release from PEGDMA-DiPETMP hydrogels, with final drug release values of 99.96, 101.44, 103.31 and 107.51 respectively all within the accepted differences from calculated max value of 15% outlined by USP standards (U.S. Pharmacopoeial Convention, 2011). Progesterone showed excellent consistency with Prog single, IbuProg and NACIbuProg combinations having final release values within 15% of calculated maximum, the NACProg combination did not meet these criteria however, which could be due to the decreased linearity associated with NACProg samples (r^2 of 0.93, compared to other Prog combinations with r^2 values between 0.98 and 0.99). Different to Ibu and Prog, NAC does not demonstrate consistency at complete release with there being a variance from 58.17% of calculated max for the NAC single drug release curve up to 165.35% of calculated max for the NAC release curve in three drug combination.
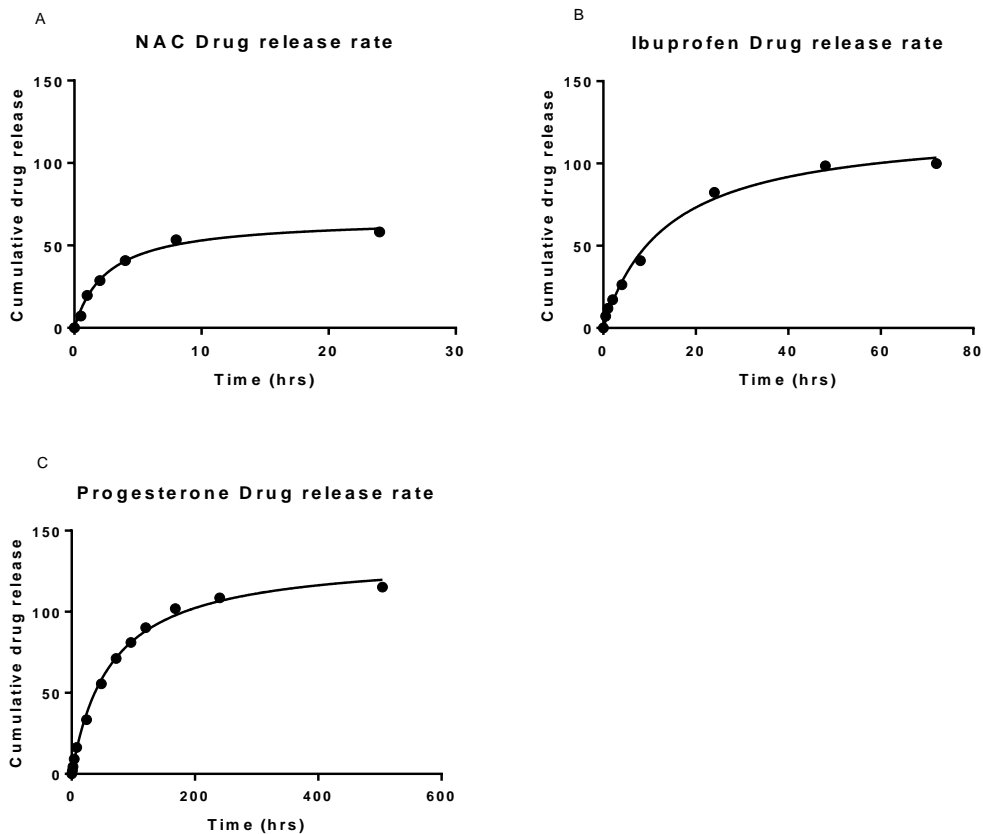
Figure 6-35 Cumulative release curves for (A) N-acetyl cysteine singular (B) Ibuprofen singular and (C) Progesterone singular prepared in PEGDMA-DiPETMP copolymers (n=4)
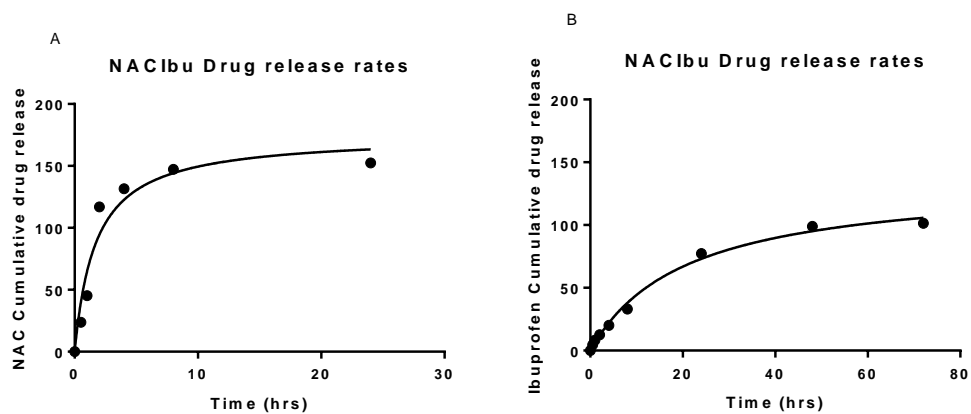
Figure 6-36 Cumulative release curves for (A) N-acetyl cysteine from NACIbu tablets and (B) Ibuprofen from NACIbu tablets (n=4)
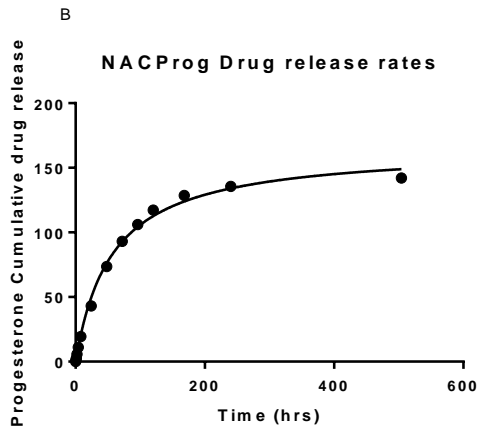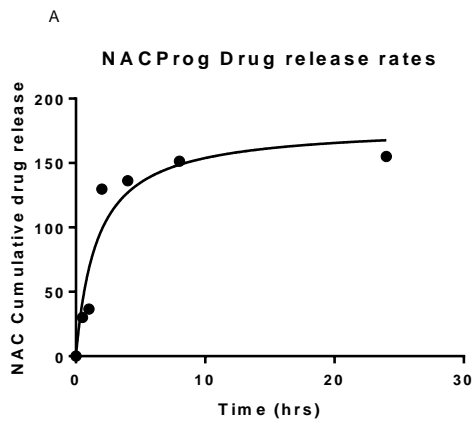
Figure 6-37 Cumulative release curves for (A) N-acetyl cysteine from NACProg tablets and (B) Progesterone from NACProg tablets (n=4)
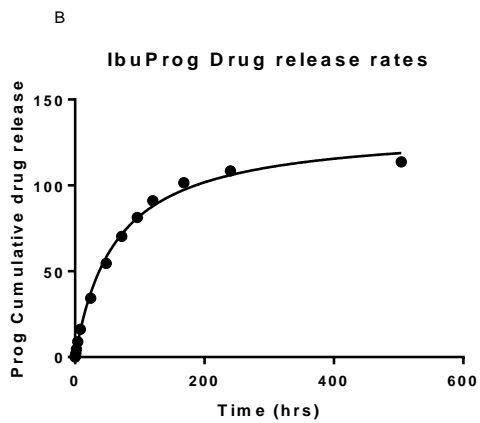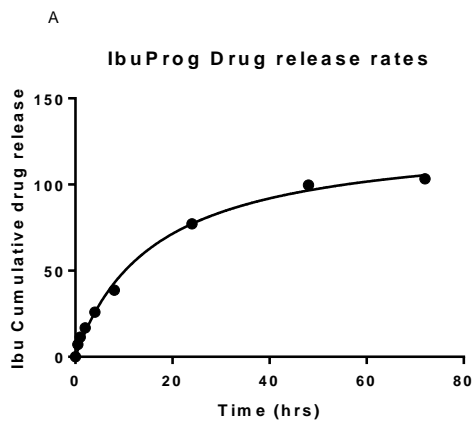
Figure 6-38 Cumulative release curves for (A) Ibuprofen from IbuProg tablets and (B) Progesterone from IbuProg tablets (n=4)

C

N A C I b u P r o g D r u g r e l e a s e r a t e s
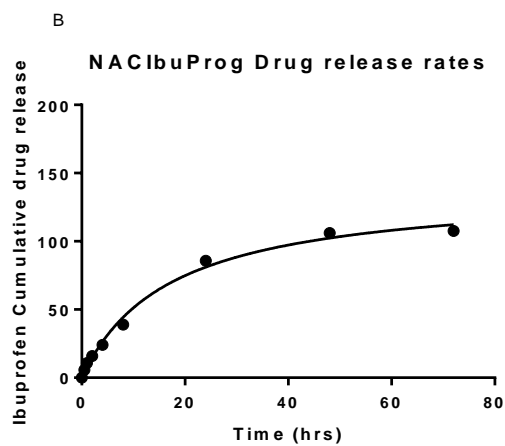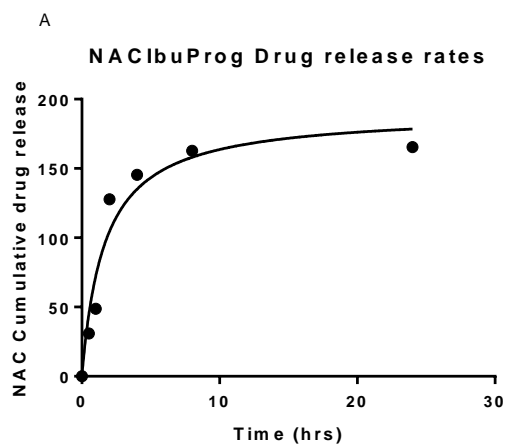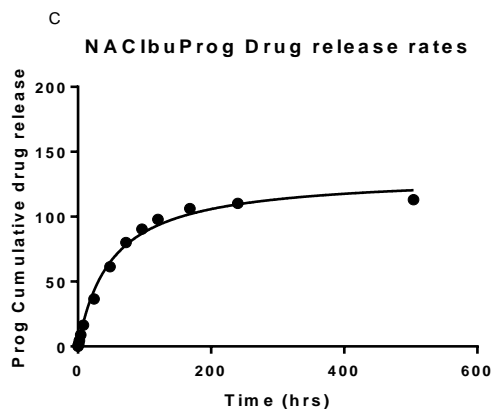
Figure 6-39 Cumulative release curves for (A) N-acetyl cysteine (B) Ibuprofen and (C) Progesterone prepared in a three drug combination in PEGDMA-DiPETMP copolymers (n=4)

6.2.4 Release kinetics

Using goodness of fit modelling shown in Table 6-5 all three drugs were shown to follow the Korsmeyer-Peppas model of drug release indicating NAC, Ibu and Prog conformed to the type of drug release expected from drugs embedded in a polymeric system. From the modes of drug transport shown in Table 6-5 it could be seen that the size of the drugs likely played a key role in determining rates of drug release with the larger Progesterone molecule falling into the super case II type transport (dependent entirely on the swelling of the molecule/polymer erosion) and the smaller Ibuprofen molecule classified in the non-fickian release (semi dependent on diffusion and semi dependent on erosion). There is potential for this impact to occur with NAC, as NAC with the quickest release is also the smallest molecule.

Table 6-5 In vitro release kinetics and model of drug transport

Drug	Release rate model (r^2 value)	n value	Mode of drug release
NAC (single)	Korsmeyer-peppas (0.845)	NA	NA
Ibu (single)	Korsmeyer-Peppas (0.9989)	0.6162	Non-Fickian
Prog (single)	Korsmeyer-Peppas (0.9509)	0.938	Super case II
NAC (NACIbu)	Korsmeyer-peppas (0.789)	NA	NA
Ibu (NACIbu)	Korsmeyer-Peppas (0.9885)	0.6952	Non-Fickian
NAC (NACProg)	Korsmeyer-peppas (0.8303)	NA	NA
Prog (NACProg)	Korsmeyer-Peppas (0.9509)	0.938	Super case II
Ibu (IbuProg)	Korsmeyer-Peppas (0.9912)	0.6015	Non-Fickian
Prog (IbuProg)	Korsmeyer-Peppas (0.9559)	0.907	Super case II
NAC (NACIbuProg)	Korsmeyer-peppas (0.7658)	NA	NA
Ibu (NACIbuProg)	Korsmeyer-Peppas (0.9848)	0.6692	Non-Fickian
Prog (NACIbuProg)	Korsmeyer-Peppas (0.9567)	0.9359	Super case II

The ideal combination of NAC, Ibu and Prog was determined via three stages of testing with the goal of enhanced synergy between drugs. In the initial phase of testing drug concentrations were determined based on literature and studied for their impact on the cellular activity of Schwann cells and PC-12 cells. From this initial study it was determined that higher Ibu concentrations (600 µM and above) would produce cytotoxic responses in Schwann cells as indicated by the low metabolic activity in wells treated with these concentrations 24 hours post treatment. This cytotoxic impact was confirmed by the metabolic activity of wells failing to recover 48 hours post treatment which was common for other drug concentrations. Whereas PC-12 cells did not experience the same adverse effect with higher Ibu concentrations, in fact having positive metabolic outcomes when exposed to Ibu concentrations above 600 µM. This positive effect extended to all Ibu concentrations however and was particularly evident in lower Ibu concentrations of 32.5 µM which showed a positive metabolic activity when combined with lower NAC concentrations up to and including 72 hours post treatment measurements. Prog caused increased cellular proliferation at higher concentrations, particularly when used in combination with Ibu, this trend was shown in both SC and PC-12 cells 24 hours post treatment where a similar but less defined trend occurred with NAC combinations also. Whereas NAC did not demonstrate a clear impact on cellular activity when in combination with Ibu or Prog it was shown to have interesting protective properties against the higher Ibu concentrations, wherein the maximum NAC concentration (176.52 µM) was the only concentration which did not produce a cytotoxic effect when in combination with 1200 µM Ibu in Schwann cells, which showed a negative impact on SC activity 24 hours post treatment but a positive outcome 48 hours post treatment. The overall goal of this study was to boost the cellular activity of both PC-12 cells and Schwann cells using combinations of NAC, Ibu and Prog. With the only clear correlation between both PC-12 cells and Schwann cells being the impact of Prog (higher Prog

concentrations boosting cellular proliferation) and the indistinct impact of NAC on cellular proliferation, the second phase of testing was carried out with the focus shifting to Schwann cells. This was done to narrow the focus of drug combinations to a single cell line, with Schwann cells being selected over PC-12 cells as PC-12s were shown in section 5.2.1 to have better responses to the thiol-ene hydrogels and demonstrating decreased sensitivity to drug combinations.

Following analysis of secondary drug combinations, it was determined that the cytotoxic effects seen in Schwann cells following 48 and 72 hours of exposure were most likely due to the impact of contact inhibition and nutrient depletion caused by increased proliferation of Schwann cells (Abercrombie, 1979). The focus of the second phase of testing therefore, shifted to the impact of drug combinations on SC proliferation 24 hours post treatment and to assist in optimising the drug combinations of NAC, Ibu and Prog using SynergyFinder software. After optimising the concentrations in the first two runs, Ibu now gave a positive response across its entire concentration range particularly when combined with Prog concentration achieving metabolic activities more than twice what was seen with the untreated control. When combined with NAC the impact of Ibuprofen was less pronounced, however all combinations of Ibu and NAC reached at least 93% viability after 24 hours exposure, with the general response being a proliferative effect compared to the untreated control. From these results it can be determined that there is a strong synergistic effect between Ibu and both NAC and Prog across all concentrations. Based on its impact in combination with Prog and NAC, the 16.25 µM Ibu concentration was selected to be used in combination with all treatment wells in the final testing phase, with fixed NAC and Prog concentrations selected for final phase testing.

With the final drug combinations being optimised for Schwann cells proliferation (as per the second drug combinations focus solely on SC response) it is unsurprising that there was a generalised proliferative effect occurring across all combinations. Unlike the initial and second

drug combinations where there was a common thread of single drug treatments having lowered proliferation compared to the control well, this does not occur in the final drug combination most likely due to the presence of 16.25 µM Ibu in all wells except for the control meaning there are no single dose wells. When considering the synergies of the drugs, there was a combination which clearly had greater synergy than other concentrations being the 75 µM NAC and 30 µM Prog combination with a synergy score of -251.98, although it was notable that all drug treatments produced negative delta scores (indicative of increased synergy) in the final drug combination consistent with what would be expected following two previous optimisations of drug concentrations. This trend of the 75 µM NAC and 30 µM Prog combination being shown to have increased synergy was also found when looking at their impact on PC-12 cells which in most of the lower NAC and Prog concentrations experienced inhibition of cellular activity. Potentially this increased rate of inhibition could be attributed to the optimisation of the drug concentrations towards SC responses, this is supported by the general trend for increased synergy to occur when using the higher concentration ranges of NAC and Prog. This correlates with Initial drug combination testing outcomes where PC-12 cells responded better to higher drug concentrations. As the 75 µM NAC, 16.25 µM Ibu and 30 µM Prog combination produced a positive outcome on cellular proliferation and demonstrated increased synergy in both cell lines, the 75 µM NAC, 16.25 µM Ibu and 30 µM Prog combination was selected as the drug concentration for the testing in the final nerve guidance conduit.

As there was a requirement to develop a HPLC method capable of separating N-acetyl cysteine, Ibuprofen and Progesterone it became imperative to determine the suitability of this new method. Following analysis of the results in sections 6.2.1 to 6.2.3 the authors determined the technique to be highly sensitive capable of discerning the release rates and endpoints for NAC, Ibu and Prog release. The HPLC technique utilised also demonstrated excellent linearity with no r^2 value below 0.98 being

recorded highlighting the accuracy of the method being utilised for Ibu, Prog and IbuProg solutions, however it could be further optimised for NAC quantifications.

Section 6.2.3 outlined the release rates of NAC, Ibu and Prog from PEGDMA-DiPETMP hydrogels, of note from this testing was the consistency of release when prepared separately or combined, indicating that the drugs release rates were not impacted by their combinations with one another. Ibuprofen was shown to have a release rate seven times faster than Progesterone (full release in 3 days as opposed to 21 days), whereas NAC had the quickest release, occurring within 24 hours (1 day) of placement in McCartneys. There are several factors with the potential to cause the disparate release rates seen in section 6.2.3 including polarity/binding, Mw/size, crystallinity, and solubility/hydrophobicity the values for these factors are outlined in Table 6-6.

Table 6-6 Potential factors to impact drug release rates of N-acetyl cysteine, Ibuprofen and Progesterone

Drug	Mw (g/mol)	Hydrophilicity (log kow)	Water solubility (mg/ml)	Crystallinity
N-acetyl Cysteine	163.19	-0.66 (0.21878)	100	Crystalline powder (Tm 109.5 C)
Ibuprofen	206.28	3.97 (9332.54301)	21	Crystalline solid (Tm 157 C)
Progesterone	314.46	3.87 (7413.10241)	0.00881	Crystalline powder (Tm 121-132 C)

Previously it was highlighted that there was the potential for altering the release rates of diclofenac sodium and dexamethasone based on their interactions with a PEGDMA-PPGDA copolymer (Barron *et al.*, 2016) wherein the larger more acidic dexamethasone was shown to elute faster than the smaller basic diclofenac sodium due to their interactions with the PEGDMA-PPGDA copolymer namely due to the weak binding of hydrogens along the polymer chain to the electronegative chlorine atoms found in diclofenac. Considering the electronegative oxygen molecules found on the polymer chains of PEGDMA there was potential for hydrogen bonding and van der waals forces to take place between the polymer chain and Ibuprofen or Progesterone, this is unlikely however as no atoms present in any

of the three drugs (as shown in Figure 6-40) has a big enough discrepancy in electronegativity to produce hydrogen bonding, for example Na which is not present would have produced hydrogen bonding due to large gap in electronegativity between Na (0.93) and O (3.43). With regard to crystallinity all drugs are crystalline in nature so crystallinity is unlikely to play a large role in release rates. Initially hydrophilicity was considered as a potential factor in drug release rates as NAC the most hydrophilic (log Kow value less than 10 (considered very hydrophilic)) drug had the fastest release rates, it was determined however, that hydrophilicity was unlikely to greatly impact drug release profiles, as Ibu, the most hydrophobic drug had a release profile closer to NACs, occurring in 3 days compared to Progs 21 days. With Ibu and Progs log Kow values being between 10 (very hydrophilic) and 10000 (very hydrophobic). Furthermore testing was carried out under sink conditions making it unlikely for solubility to play a part in release rates, leading to MW/size likely having the greatest effect on drug dissolution rates. This is demonstrated clearly with the largest Progesterone molecule having the slowest release, NAC which is the smallest drug being the quickest and Ibu being the middle drug in terms of both size and release rates.
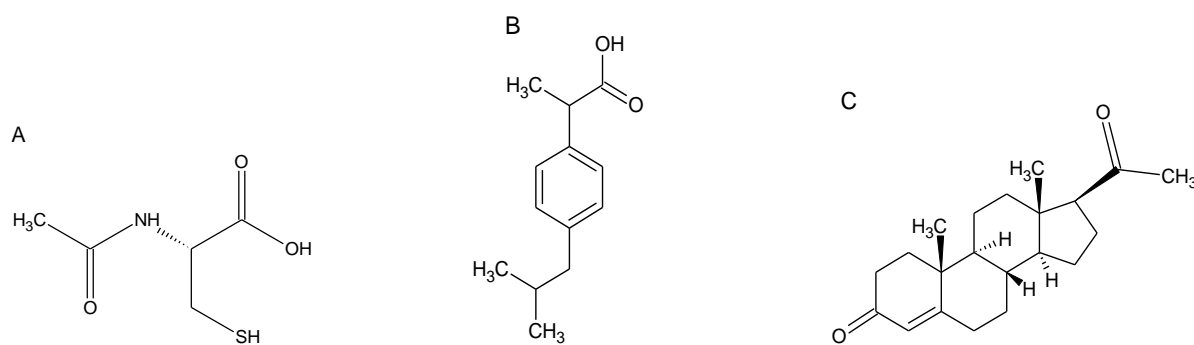
Figure 6-40 Chemical structures of (A) N-acetyl Cysteine (B) Ibuprofen and (C) Progesterone

Section 6.2.4 further characterised the release profiles of all three drugs, wherein each was shown to follow the Korsemeyer-Peppas model of drug release (polymeric system release). As all drugs were found to follow the same mode of drug release, the method of drug transport was investigated. Drug transport mechanisms were determined for both Ibu and Prog as outlined by others previously (Dash *et al.*, 2010; Guerra-Ponce *et al.*, 2016) to discern the cause of differing release rates. Calculation of n values from Korsemeyer-Peppas model proved impractical for NAC, as NAC only provided two data

points before achieving drug release greater than 60% (the cut-off point for preparing a Korsemeyer-Peppas plot), therefore calculations of n values would not be accurate for NAC. From the drug transport mechanisms, it was confirmed that MW/size was the determining factor in drug release rates from PEGDMA-DiPETMP hydrogels.

It was an important consideration for this thesis to determine the release rates of NAC, Ibu and Prog from PEGDMA-DiPETMP hydrogels, it was determined that NAC, Ibu and Prog reach complete drug release after 1, 3 and 21 days respectively. This provides a key option in treating peripheral nerve injuries, with controlled release of drugs being possible by utilising drugs of differing molecular weights/sizes. Regarding NAC, Ibu and Prog, this creates a situation wherein the release of drugs can be sequestered, with the goal of boosting peripheral nerve repair by interacting with the different nerve repair mechanisms in a controlled manner over time.

Chapter 7

Modification of PEGDMA towards final performance of hydrogel

7.0 Modification of PEGDMA towards final performance of hydrogel

For the final performance of modified PEGDMA two main objectives were identified. One was to determine the impact of stereolithography on the properties of PEGDMA and in doing so predict its potential impact on 3D printing. Following this a final composition of PEGDMA, DiPETMP, Bioglass and the drugs NAC, Ibu and Prog was prepared determined by the previous phases of testing (referred to as PEGCombo). Following polymerisation the properties of PEGCombo were determined over a 28 day period under both physiological and accelerated degradation conditions.

7.1 UV vs SLA materials properties

7.1.1 Swelling studies

In this section, hydrogel swelling ratios provided an indication of how tightly polymer networks were cured, with greater swelling being associated with greater freedom between polymer chains. In Figure 7-1 the swelling ratios and gel fractions of UV chamber and SLA samples were shown. The swelling ratios UV and SLA printed samples were shown to be significantly different at 47.0 and 41.7 respectively, indicating that the SLA fabricated hydrogels have less chain freedom compared to UV chamber samples. With respect to gel fraction results, both processes resulted in an unreacted monomer percentage below 5%, with results of 99.3% and 97.6% for UV chamber and SLA samples respectively.
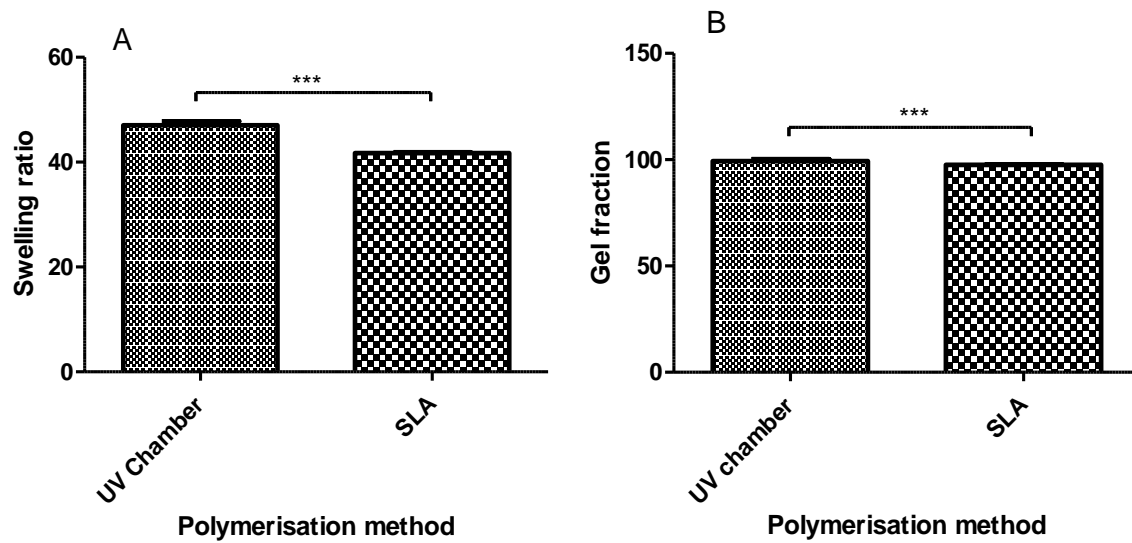
Figure 7-1 Comparison between (A) the swelling characteristics and (B) the equilibrium water content of UV chamber polymerised PEGDMA hydrogels and SLA polymerised PEGDMA hydrogels, statistical analysis was carried out using Graphpad Prism 7 (n=5) with p-values of less than 0.05 being considered statistically significant (*p < 0.05, **p < 0.01 and ***p < 0.001)

To further confirm curing was completed FTIR analysis was carried out as shown in Figure 7-2 Both UV chamber and SLA hydrogels resulted in a loss of peaks at 815 cm^{-1} and 1167 cm^{-1}, indicative of C=CH bending and C-O bonding respectively(Decker and Moussa, 1987; Colthup, Daly and Wiberley, 1990; Wu *et al.*, 2010), when compared with FTIRs of PEGDMA monomer. There is a small peak present at 1637 cm^{-1} associated with CH=CH bonding(Coates, Ed and Coates, 2000), highlighting the presence of unreacted monomer in both the UV chamber and SLA hydrogels. This agrees with what was seen in gel fraction results wherein less than 3% of PEGDMA present in both UV chamber and SLA hydrogels was unreacted gel.
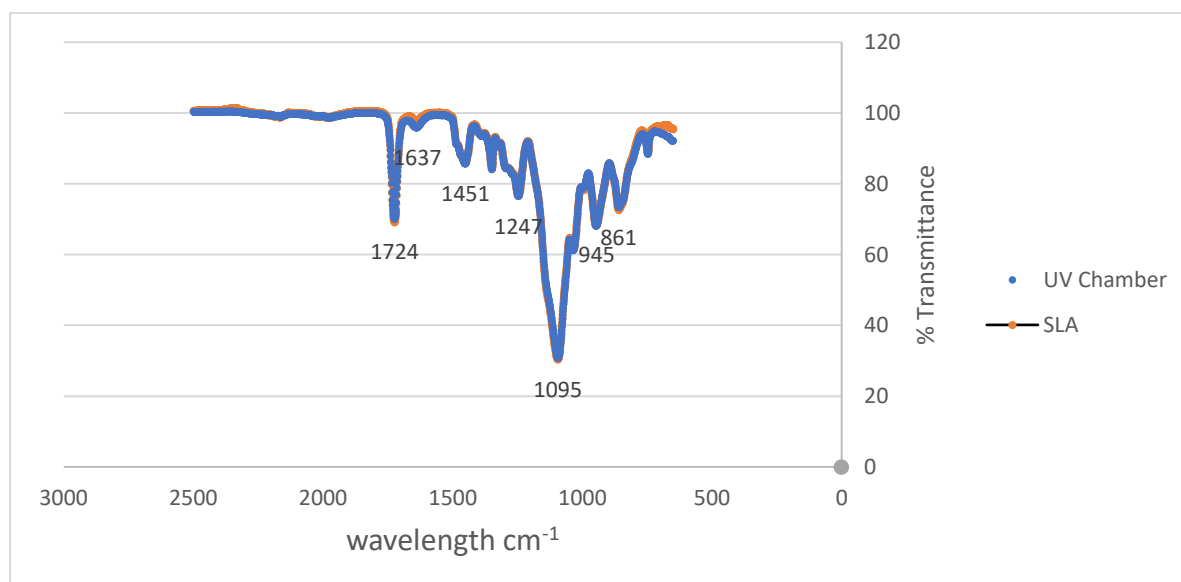
Figure 7-2 FTIR spectra of PEGDMA polymers post polymerisation prepared via UV chamber and SLA

7.1.3 Dynamic mechanical analysis

The tensile stiffness of a matrix upon which cells are attached is a very important factor for both cell proliferation and cell differentiation (Discher, Janmey and Wang, 2005; Hadjipanayi, Mudera and Brow, 2009). From the tensile testing results shown in Figure 7-3 SLA samples were shown to have slightly higher tensile stiffness when compared with UV chamber samples with Youngs modulus values of 15.5MPa and 19.9MPa respectively. These values are not mirrored with tensile strength at limit where UV samples were shown to have almost four times the tensile strength of SLA prepared samples with values of 1.84MPa and 0.54MPa respectively. Thermal analysis results shown in Figure 7-4 provided a similar outlook regarding the differences in stiffness values between UV chamber and SLA samples. Based on storage modulus measurements, there was a decrease in stiffness for UV chamber hydrogels at -57.7°C whereas with SLA hydrogels the same decrease was not seen until -48.1°C, indicating a higher degree of stiffness in SLA samples compared to UV chamber samples. The peak of loss modulus values for both UV chamber and SLA samples were much closer being -38.2°C and -39°C respectively and Tan δ values similarly were close at -22.8°C and -23.8°C. With the Tan δ peak corresponding more closely to a glass transitions midpoint than its beginning and loss modulus peak corresponding more closely to the beginning of the glass transition (Menczel and Prime, 2009) it appears that the thermal behaviour of PEGDMA hydrogels are not affected by the change in curing process.
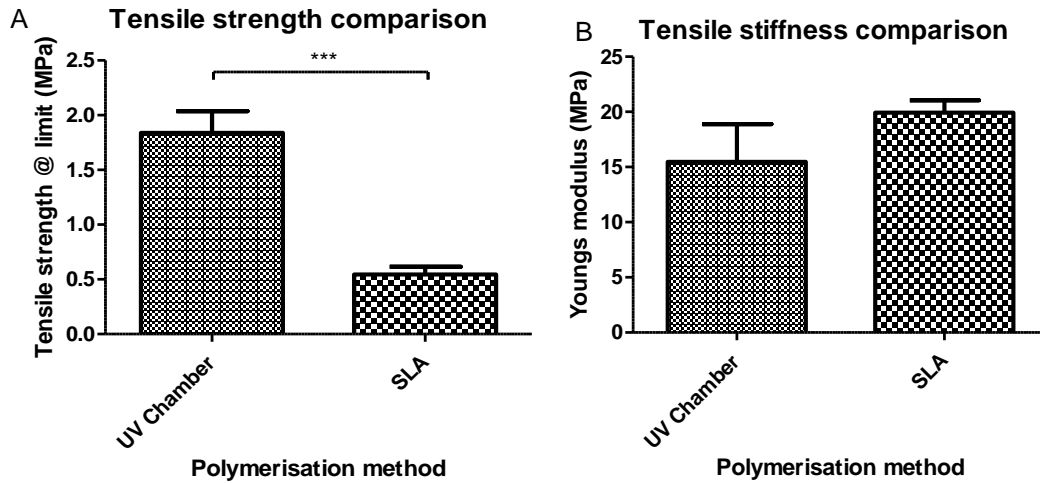
Figure 7-3 Dynamic mechanical analysis results showing (A) the tensile strength at limit and (B) Youngs modulus for unhydrated SLA and UV chamber polymerised PEGDMA samples, statistical analysis was carried out using Graphpad Prism 7 (n=5) with p-values of less than 0.05 being considered statistically significant (*p < 0.05, **p < 0.01 and ***p < 0.001)
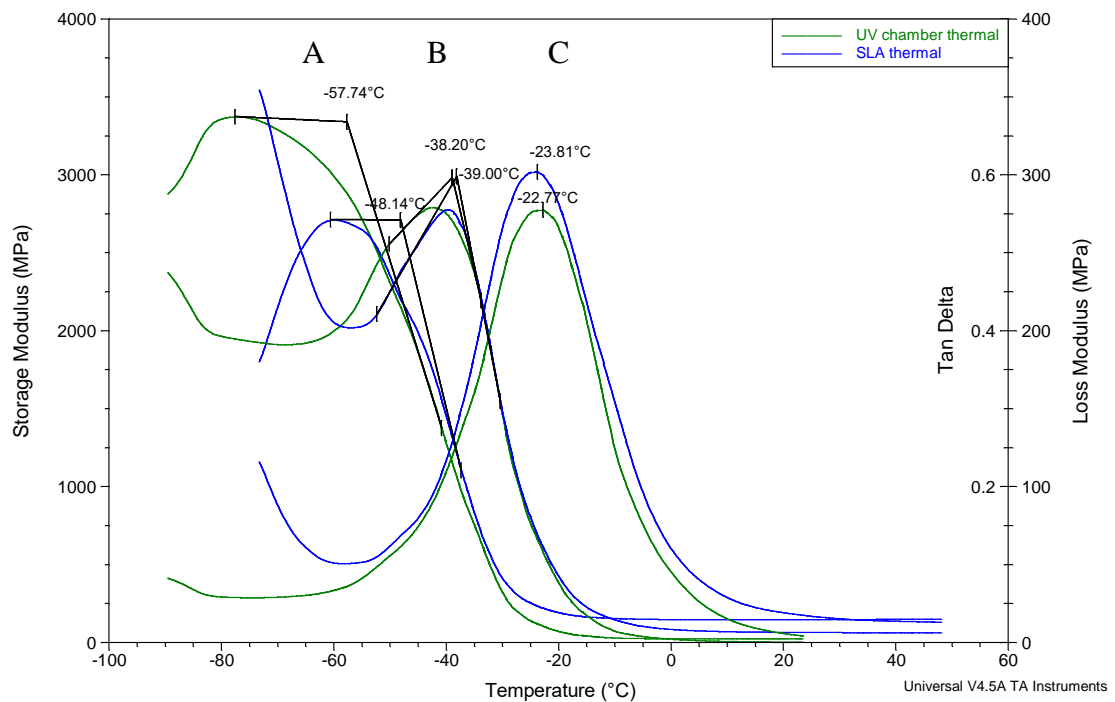
Figure 7-4 Dynamic mechanical analysis results showing (a) the storage modulus (G'), (b) the loss modulus (G'') and (c) tan delta for both PEGDMA samples prepared via UV chamber and PEGDMA hydrogels prepared by SLA.

Table 7-1 Mean Tg of PEGDMA hydrogels determined from DMA

Polymer	Mean Tg (°C)
PEGDMA (UV	-42.5 ±0.7
PEGDMA	-41.7 ±0.3

7.1.4 Compression testing

Similarly to what was seen with tensile Youngs modulus measurements in section 7.1.3 The compressive Youngs modulus values shown in Figure 7-5 (B) had SLA hydrogels with increased stiffness values when compared to UV chamber samples with Youngs modulus values of 13.01MPa and 8.26MPa respectively. Also seen in Figure 7-5 (A) were compressive strength values of 3.73MPa for UV chamber samples and 4.08MPa for SLA samples with no significant differences showcasing the comparability of the overall strength PEGDMA samples.
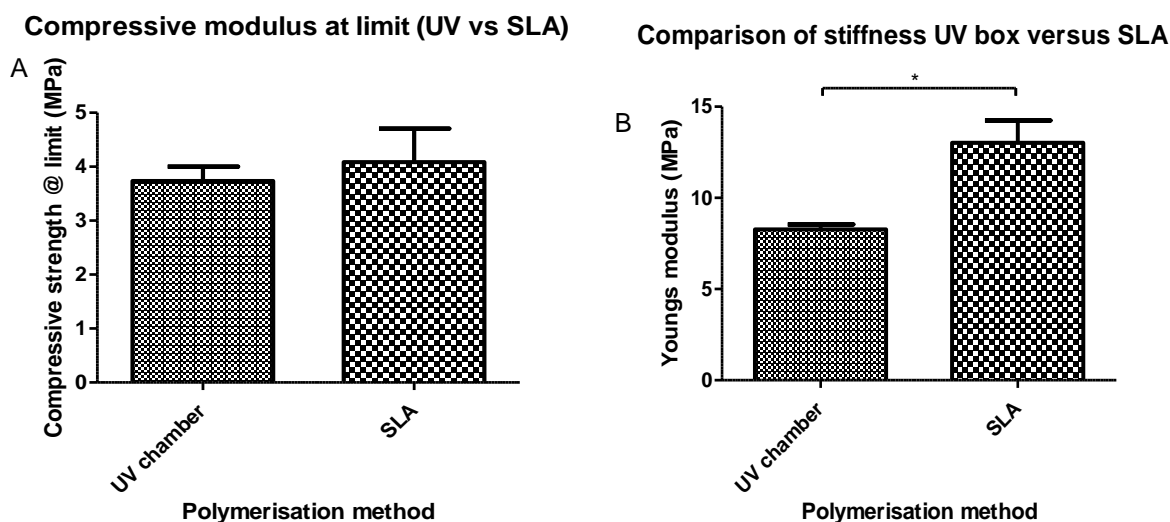
Figure 7-5 Compressive properties of PEGDMA (UV chamber) and PEGDMA (SLA) hydrogels) showing (A) Compressive strength at limit and (B)Youngs modulus, statistical analysis was carried out using Graphpad Prism 7 (n=3) with p-values of less than 0.05 being considered statistically significant (*p < 0.05, **p < 0.01 and ***p < 0.001)

7.1.5 Wettability measurements

In Figure 7-6 the wettability of UV chamber and SLA hydrogels were compared. Wettability is an important consideration for biomedical applications as it can have a significant impact on the ability of cells to attach to a polymers surface with ideal cell adhesion occurring with contact angle measurements between 40° and 60°(Arima and Iwata, 2007). It was thought that the layer-by-layer polymerisation process would create minor imperfections on the surface of SLA samples causing a decrease in overall wettability compared to UV chamber samples(Wenzel, 1936). This was confirmed with UV chamber samples having a wettability measurement of 47.6° significantly more hydrophobic than SLA samples at 30.6°.

Comparison of wettability (UV vs SLA)
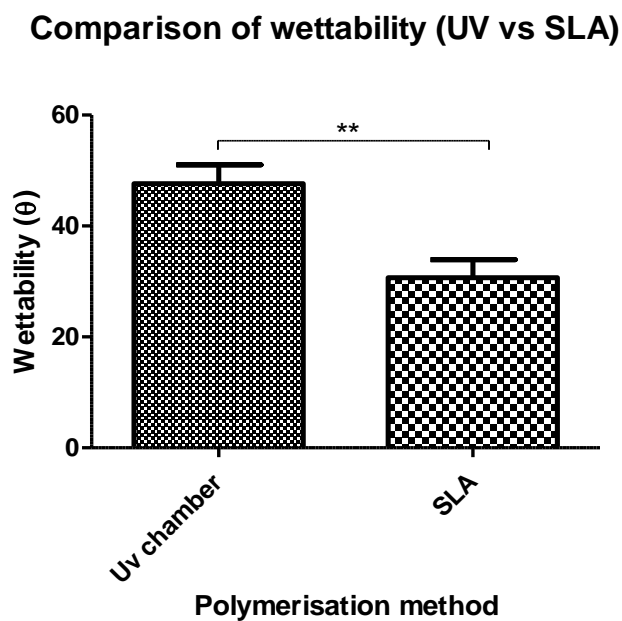
Figure 7-6 Wettability measurements of UV chamber based PEGDMA hydrogels and SLA based PEGDMA hydrogels, statistical analysis was carried out using Graphpad Prism 7 (n=5) with p-values of less than 0.05 being considered statistically significant (*p < 0.05, **p < 0.01 and ***p < 0.001)

7.1.6 Thermal properties

The thermal transitions of UV chamber and SLA polymerised PEGDMA samples were found to be within degree of one another as shown in Table 7-2. A similar comparability was seen in section 7.1.3 where the glass transition temperatures based on loss modulus and Tan delta were also found to be within a degree of one another. Confirming the results seen with loss modulus and Tan delta in section 7.1.3 the glass transition temperatures were found to be within a degree of each other, the UV chamber samples Tg values were slightly lower than the SLA samples, at -42.5°C and -41.7°C respectively. Figure 7-7 further highlights the similarities in thermal properties of UV and SLA polymerised PEGDMA with the DSC thermograms being near identical.

Table 7-2 Thermal properties of PEGDMA hydrogels prepared via UV chamber and SLA polymerisation

Polymer	Mean tg (°C)
PEGDMA (UV chamber)	-42.5 ±0.7
PEGDMA (SLA)	-41.7 ±0.3
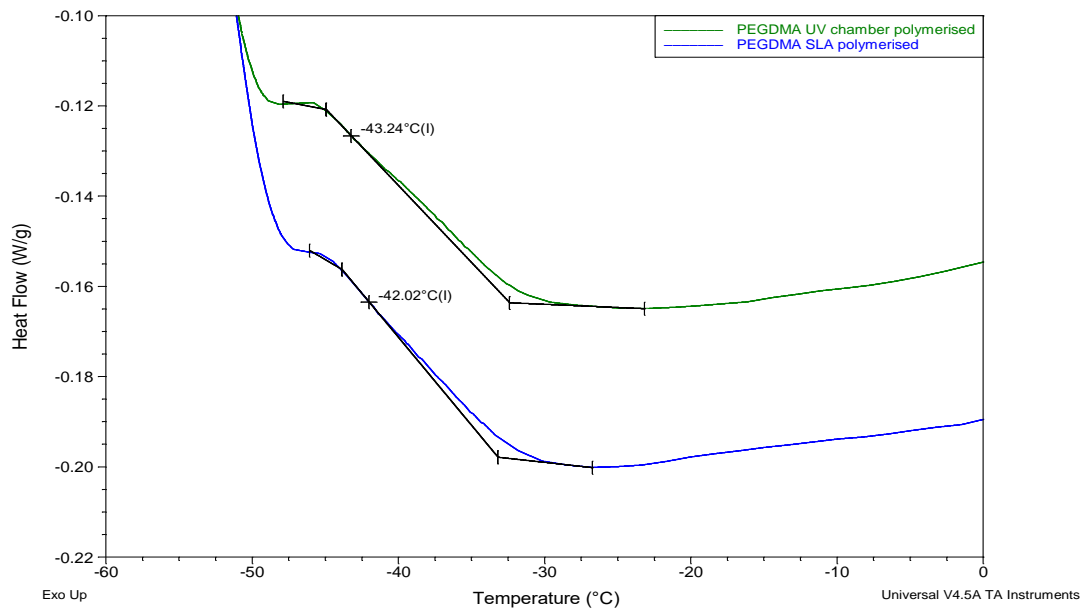
Figure 7-7 DSC thermograms highlighting the glass transition temperatures for PEGDMA samples prepared via UV chamber and SLA polymerisation

7.2 PEGCombo materials properties

7.2.1 SLA of PEGCombo

Although promising for the personalisation of nerve guidance conduits due to its high control over resolutions, as well as potential to improve material properties of PEGCombo as outlined in sections 7.1 and 7.3, SLA of the PEGCombo formulation did not produce the desired control over the 3D architecture necessary for producing an ideal nerve guidance conduit. Instead undergoing rapid polymerisation while placed on the SLA resin tank, polymerising in an uncontrolled fashion which due to the nature of the thiol-ene reaction polymerised the entire batch of PEGCombo as shown in Figure 7-8.
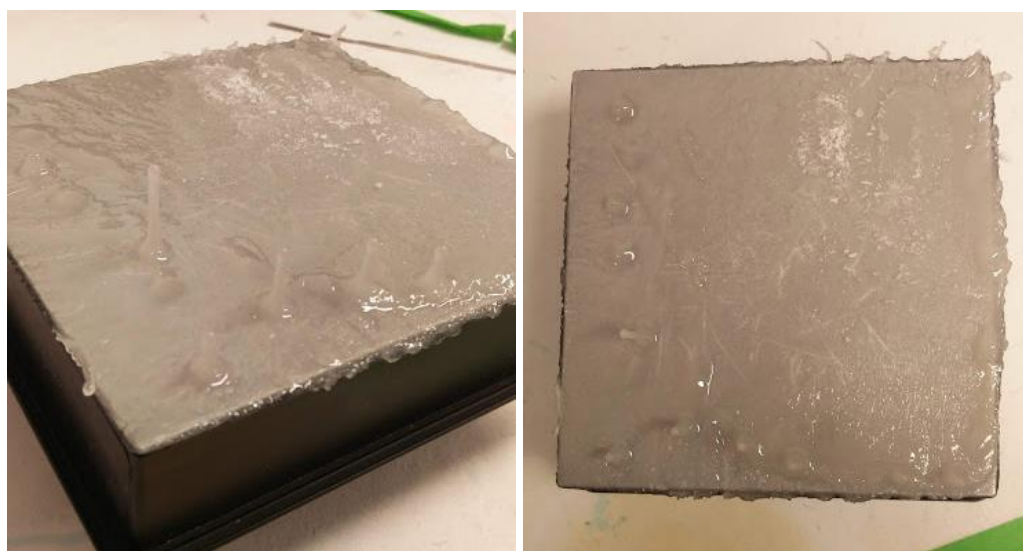
Figure 7-8 Outcome from attempts to print PEGCombo samples with controlled architecture via the use of a formlabs Form2 SLA

7.2.2 Chemical properties

In Figure 7-9 highlighting FTIR spectra for PEGCombo samples over a 28-day period there is an absence of peaks at 815 cm^{-1} and 1167 cm^{-1} as well as the near complete removal of the peak at 1637 cm^{-1} (associated with C-H bending of H$_2$C=CH-C=O group, C-O-C stretching and bending of the CH$_2$=CH group respectively). Based off the disappearance of these peaks it could be said with relative confidence that polymerisation had been completed post UV

chamber exposure in PEGCombo samples. The size of the 1730 cm^{-1} peak associated with the ester bonds (Coates, Ed and Coates, 2000) was noticeably decreased in day 28 NaOH samples compared to day 28 PBS. PEGCombo polymerisation was further verified by the Raman spectra in Figures 7-10, 7-11, 7-12 and 7-13, namely by the disappearance of the peak at 1640 cm^{-1} associated with C=C bonds, highlighting the absence of C=C peaks. Similarly to section 5.1.2 there were peaks at 940 and 2580 cm^{-1} associated with S-H bonding which decreased over time. There was a gradual appearance of peaks at 401 cm^{-1} and also at 1420cm^{-1} over the 28 day time period following immersion in either PBS or NaOH with the 401 cm^{-1} peak going from non-existent at day 0 to the most prominent peak present in either PBS or NaOH immersed samples at day 28. With the 401 cm^{-1} peak being associated with C-N-C bending and the 1420 being associated with carboxylic acid O-H bending (Lambert, 1987), both features of NAC these peaks are likely associated with the presence of NAC in PEGCombo. Concurrently over the 28 day period of testing there was a decrease in peak size of the 1470 cm^{-1} peak and of the 678 cm^{-1} peak. The peak at 678 cm^{-1} likely corresponds to C-S stretching (Lambert, 1987), indicating a decrease in C-S bonds following immersion in PBS or NaoH over time, with intensity drops from 100000au at day 0 to 40000au at day 28 (in both NaOH and PBS samples). The 1470 cm^{-1} peak in Raman and the 1460 cm^{-1} peak in FTIR represent either CH$_2$ or CH$_3$ bonding, with both peaks undergoing decreases over time, there appears to be a decrease in C-H chains in the PEGCombo hydrogel, likely highlighting the breakdown of PEGCombo over time.

FTIR of final composition in fingerprint region
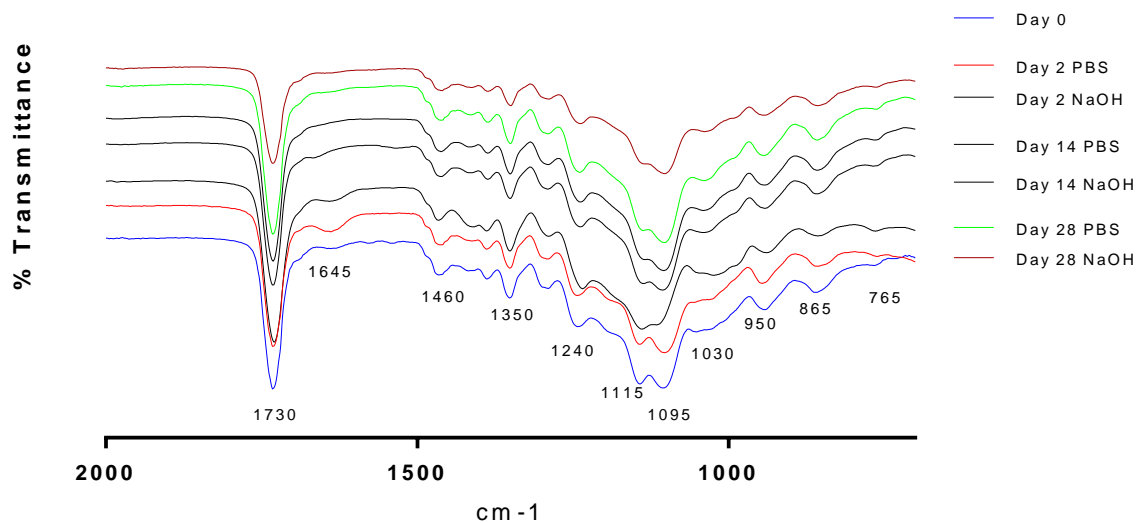
Figure 7-9 FTIR analysis in the 2000-650 cm^{-1} range for PEGCombo samples stored in PBS or NaOH over a 28 day period

Raman analysis of unhydrated final composition material
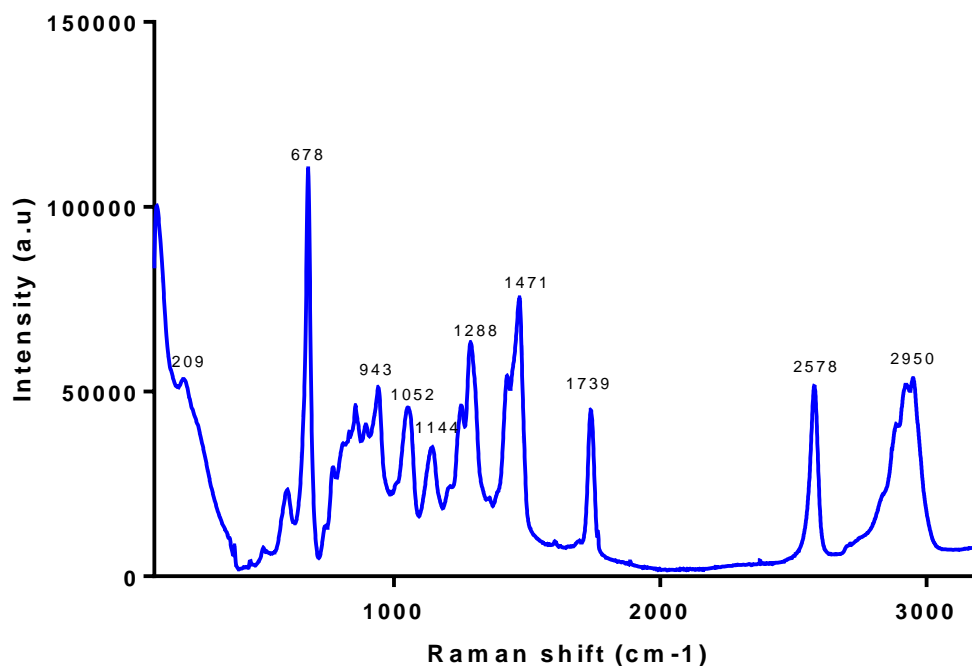
Figure 7-10 Raman analysis in the 3200-100 cm^{-1} range for freshly polymerised PEGCombo samples
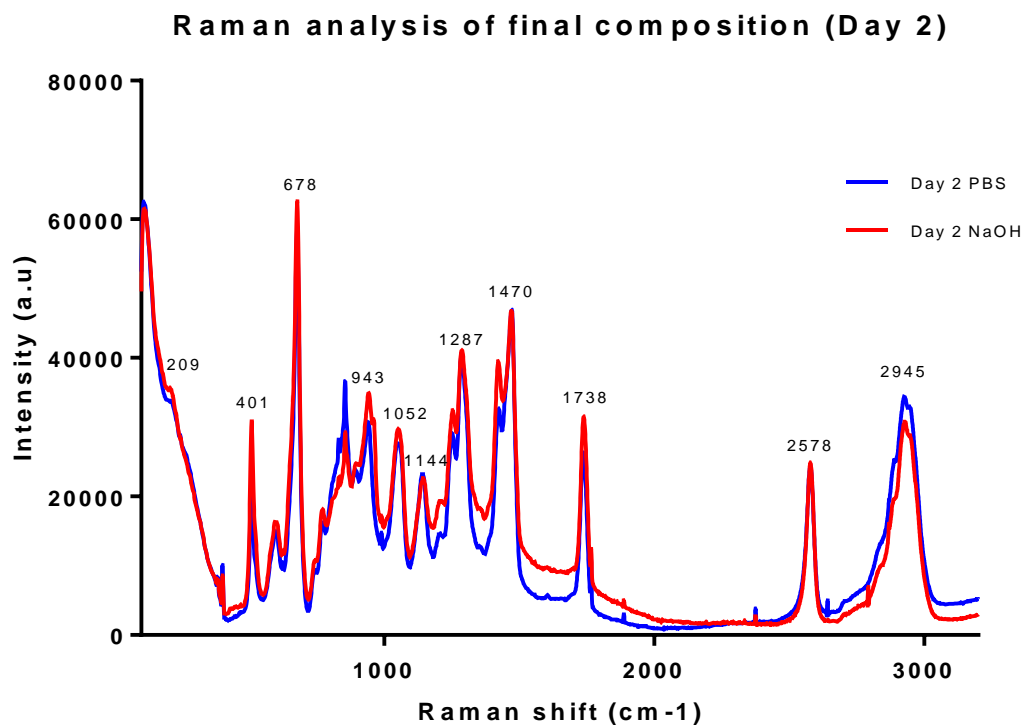
Figure 7-11 Raman analysis in the 3200-100 cm^{-1} range for PEGCombo samples stored in PBS or NaOH for 2 days
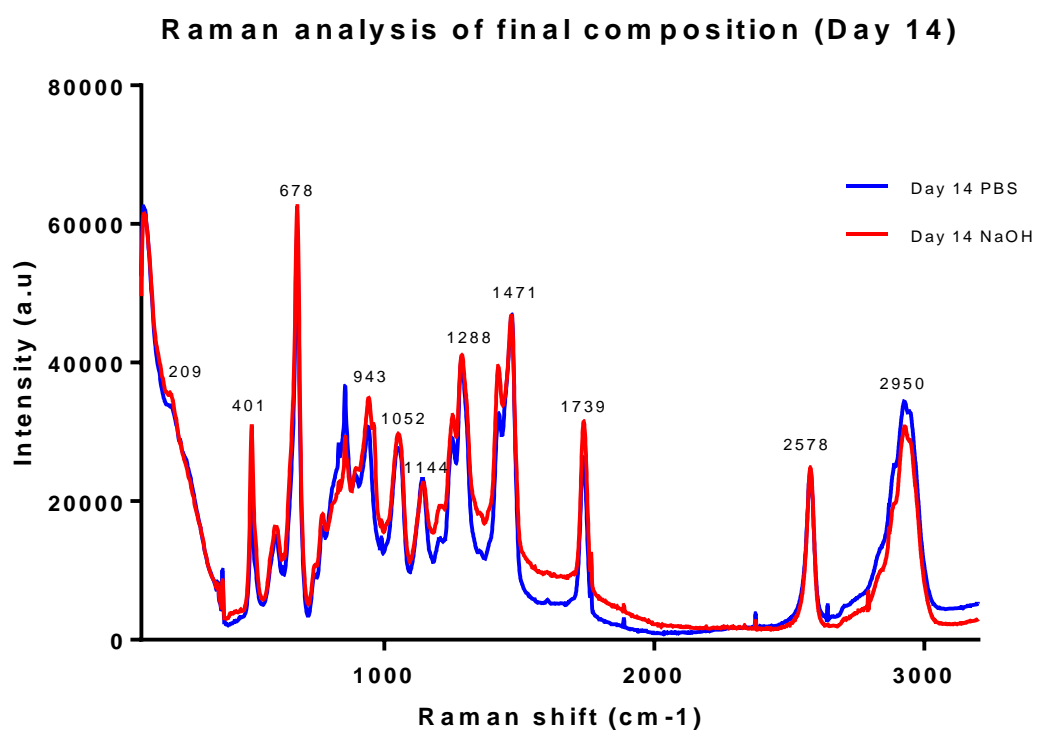
Figure 7-12 Raman analysis in the 3200-100 cm^{-1} range for PEGCombo samples stored in PBS or NaOH for 14 days

233
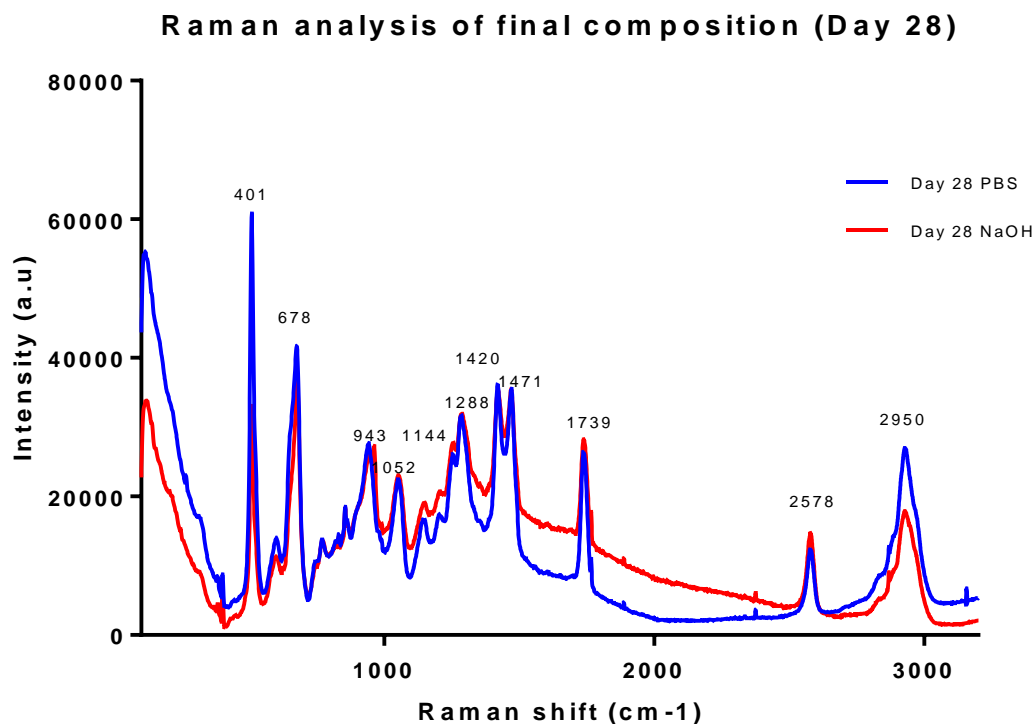
Figure 7-13 Raman analysis in the 3200-100 cm^{-1} range for PEGCombo samples stored in PBS or NaOH for 28 days

7.2.3 Thermal properties

From Figure 7-14 the glass transitions for PEGCombo over a 28-day period calculated using DSC can be seen. From these results it could be seen that glass transition temperature for PEGCombo began at -42.5°C and increased over time to -31.6°C in day 28 NaOH immersed samples and -32.6°C in PBS immersed samples. While there is a general increase in Tg over time, this increase becomes significant at day 28 with day 28 NaOH immersed samples being significantly different to every sample except day 28 PBS immersed samples. Day 28 PBS immersed samples also had significantly increased Tgs, however they did not have significant differences compared to either day 14 results. The results for Tg calculated from tensile DMA shown in Figure 7-16 correlated well with DSC results, with both sections showing DMA determined Tgs were higher than their DSC determined counterparts. Also, in a similar manner to DSCs there is a general trend toward increasing Tgs with increased time immersed in either PBS or NaOH solutions, with Tgs going from -33.74°C in PEGCombo at day 0 to -19.39°C

234

and -25.52°C in Day 28 NaOH and PBS immersed PEGCombo samples respectively. When looking purely at PBS immersed PEGCombo samples the increase in Tg is shown to occur after 2 days immersion and remain consistent across day 14 and 28 tests with values of -21.38°C, -22.08°C and -25.52°C, indicating that PEGCombo undergoes an increase to chain stiffness following PBS immersion however the increase does not change greatly over a 28-day period. With NaOH immersion there was an initial decrease in Tg, however with an increase in Tg at every subsequent timepoint, by day 28 NaOH immersed PEGCombo samples had higher Tgs than the PBS immersed samples.
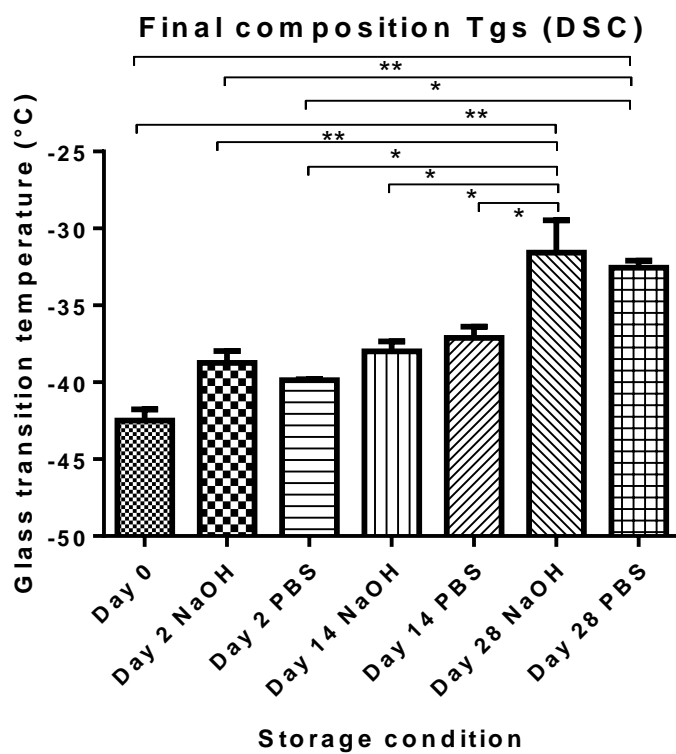
Figure 7-14 Glass transition temperatures for PEGCombo samples stored in PBS or NaOH over a 28 day period determined by DSC, statistical analysis was carried out using Graphpad Prism 7 (n=2) with p-values of less than 0.05 being considered statistically significant (*p < 0.05, **p < 0.01 and ***p < 0.001)
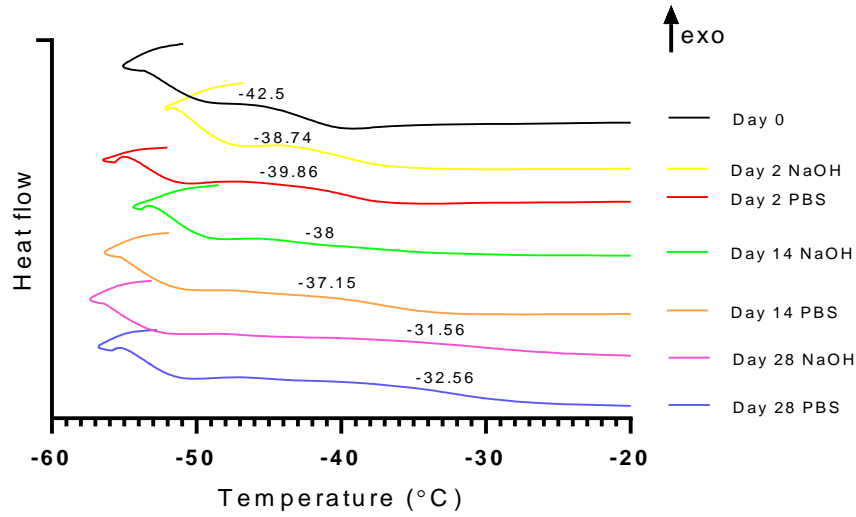
*Figure 7-15 Sample thermograms for PEGCombo samples stored in PBS or NaOH for 0, 2, 14 and 28-day periods determined by DSC analysis*
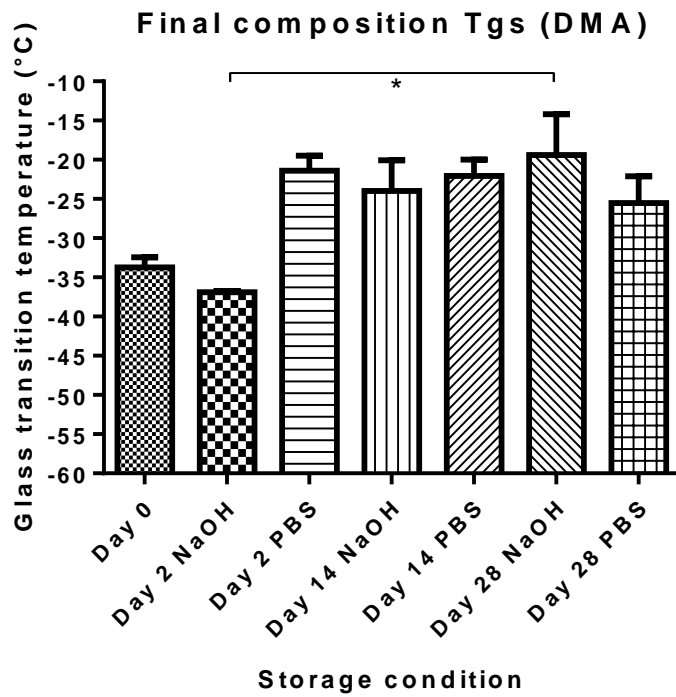
Figure 7-16 Glass transition temperatures for PEGCombo samples stored in PBS or NaOH over a 28 day period determined by DMA

7.2.4 Mechanical properties

Figure 7-17 showcases mechanical strength of PEGCombo samples as well as compressive stiffness of PEGCombo samples over a 28 day period under normal (PBS) and accelerated degradation (5mM NaOH) rates. When considering compressive strength PEGCombo samples remain consistent up to day 14 of testing in both standard and accelerated degradations, with compressive values for day 0 PEGCombo samples of 1.2 MPa. NaOH immersed samples then have values of 1.25 MPa and 1.08 MPa for days 2 and 14 respectively, with PBS immersed samples having similar values of 1.16 MPa and 1.1 MPa. PEGCombo samples stored in both degradation conditions undergo an increase in compressive testing at day 28 of testing with NaOH immersed samples having compressive strength of 2.4 MPa and PBS immersed samples being 1.71 MPa. A similar trend is followed when determining PEGCombos stiffness over 28 days with Youngs modulus values between 2.13 MPa and 2.32 MPa for both NaOH and PBS samples over days 0, 2 and 14. For day 28, PBS immersed PEGCombo maintained stiffness comparable to earlier stiffness values (2.23 MPa) whereas NaOH samples underwent a significant increase in stiffness (7.42 MPa).

In Figure 7-18 the tensile strength and stiffness of PEGCombo samples under normal (PBS) and accelerated degradation (5mM NaOH) conditions over a 28 day period. Similarly to compression testing there was an increase in tensile stiffness of PEGCombo samples following immersion in PBS or 5mM NaOH going from an initial tensile Youngs modulus of 1.06 MPa in day 0 PEGCombo to values up to 8.88 MPa in day 28 PBS stored samples a greater than eightfold increase in stiffness. After the increase in stiffness seen in day 2 samples neither NaOH or PBS stored samples followed a clear pattern regarding trends in stiffness with PBS stored PEGCombo going from 6.14 MPa to 5.62 MPa and then 8.88 MPa for days 2, 14 and 28. PEGCombo similarly had no clear pattern going from 2.31 MPa to 5.61 MPa and then 5.26 MPa for days 2, 14 and 28 respectively. PEGCombos tensile strength values similarly to tensile

stiffness did not demonstrate a clear trend in values over time, with the exception that again day 0 PEGCombo samples were notably weaker (0.053 MPa) compared to later days of testing (0.098 to 0.158 MPa), indicating that upon swelling there is an increase in the tensile strengths of PEGCombo samples.
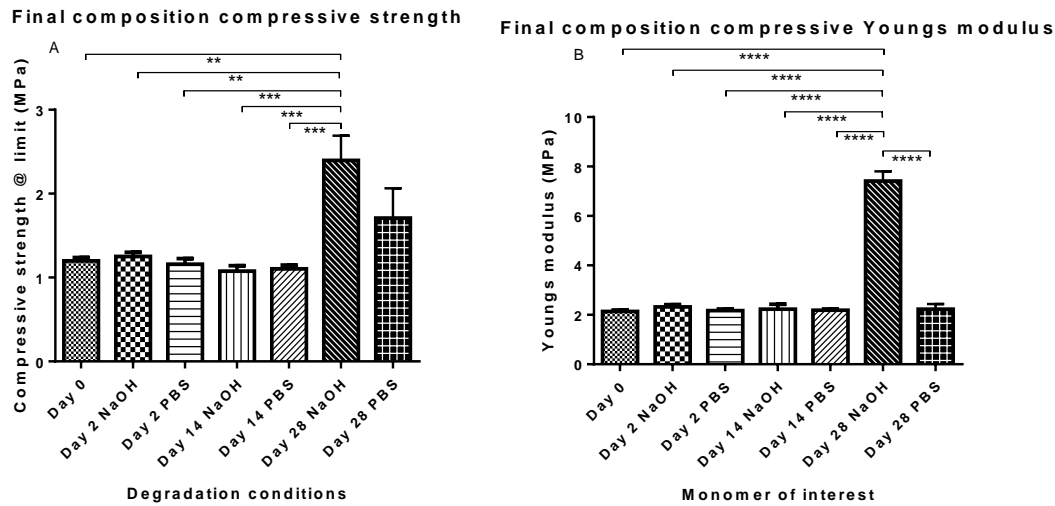
Figure 7-17 Data showing (A) Compressive strength at limit and (B) Compressive Youngs modulus values for PEGCombo samples following immersion in PBS or 5 mM NaOH over a 28 day period, statistical analysis was carried out using Graphpad Prism 7 (n=5) with p-values of less than 0.05 being considered statistically significant (*p < 0.05, **p < 0.01, ***p < 0.001 and ****p < 0.0001)
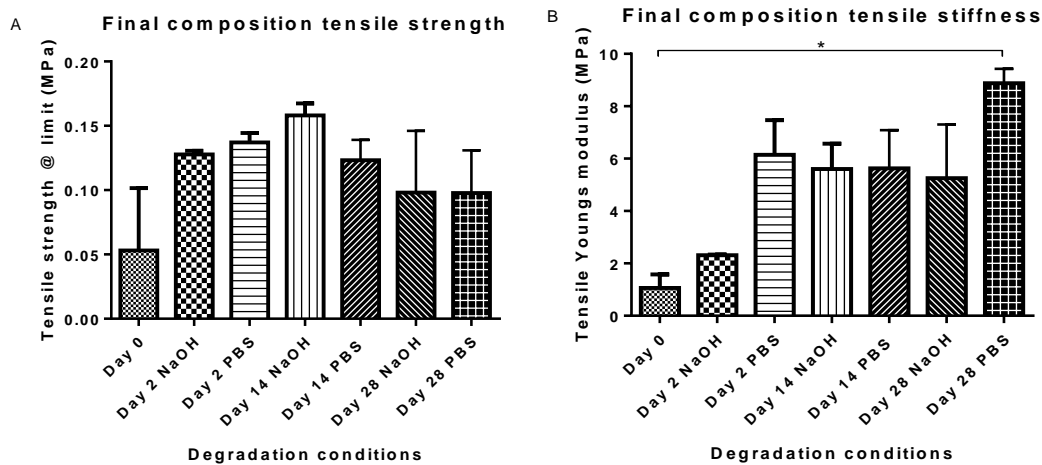
Figure 7-18 Data showing (A) Tensile strength at limit and (B) Tensile Youngs modulus values for PEGCombo samples following immersion in PBS or 5 mM NaOH over a 28 day period, statistical analysis was carried out using Graphpad Prism 7 (n=5) with p-values of less than 0.05 being considered statistically significant (*p < 0.05, **p < 0.01 and ***p < 0.001)

7.2.5 Wettability measurements

In Figure 7-19 the changes in wettability of PEGCombo samples over a 28 day period are shown for normal and accelerated degradation conditions. With both conditions there was a clear trend for wettability to increase over time. In the accelerated conditions PEGCombo can be seen to undergo a steady decrease in wettability going from 103.56° to 90.90°, 77.88° and 66.15° for days 2, 14 and 28 in NaOH respectively. A similar trend occurs in PBS stored samples although it is noteworthy to highlight the increase in wettability is more pronounced for PBS stored samples than NaOH stored samples. This was shown with values for days 2, 14 and 28 of 85.15°, 53.92° and 45.83° respectively. While the day 14 and day 28 PBS stored samples fell in the 40 to 60° range considered ideal for cellular attachment by Arima et al. or the 65° suggested by Dowling (Arima and Iwata, 2007; Dowling *et al.*, 2011), all NaOH stored samples as well as PEGCombo day 0 and PBS day 2 were outside this range with PEGCombo day 0 and NaOH stored day 2 being considered hydrophobic rather than hydrophilic.

Final composition wettability
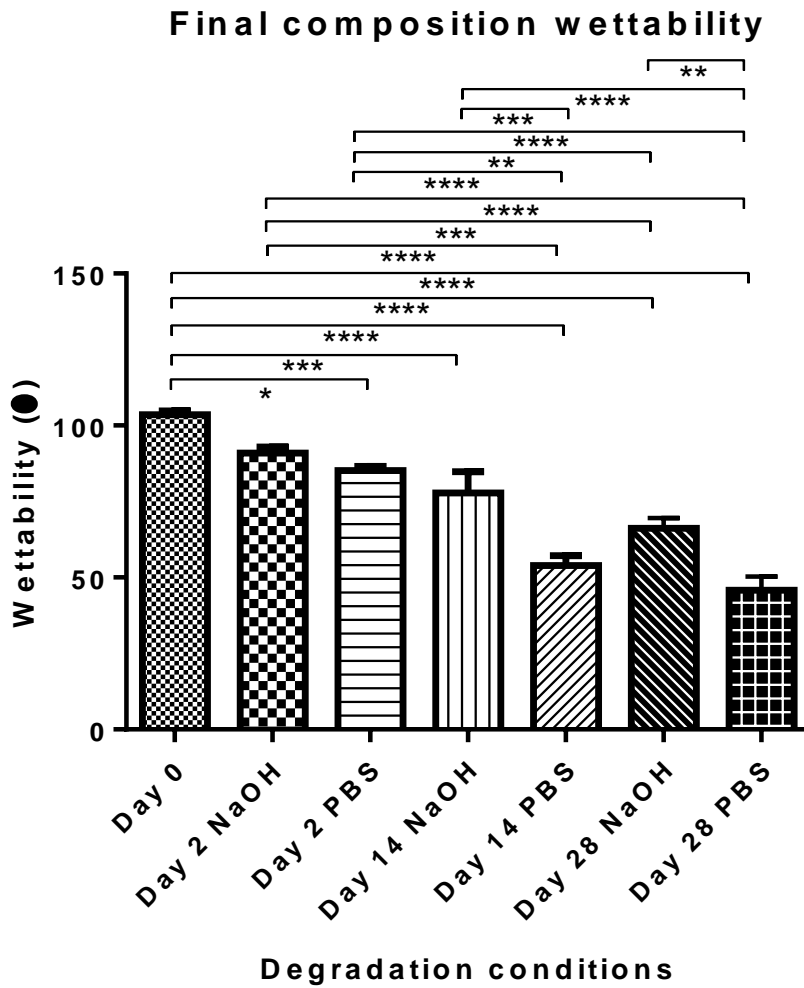
Figure 7-19 Wettability measurements for PEGCombo samples stored in PBS or NaOH over a 28 day period, statistical analysis was carried out using Graphpad Prism 7 (n=15) with p-values of less than 0.05 being considered statistically significant (*p < 0.05, **p < 0.01, ***p < 0.001 and ****p < 0.0001)

7.2.6 Surface properties

The surface properties of PEGCombo samples following exposure to physiological conditions or accelerated degradation conditions over 28 days were determined by SEM analysis, with images shown in Figure 7-20. In contrast to earlier SEMs there are several key differences to be noted. When compared with 2.5 wt. % bioglass SEMs in section 4.1.7 and the thiol samples in section 5.1.6 there is a clear increase in smoothness across PEGCombos surface. With only day 0 and day 2 NaOH immersed samples having similar degrees of roughness to that seen in

sections 4.1.7 and 5.1.6, it is still possible to identify bioglass in all samples however they appear to occur in smaller amount than would be expected when comparing with earlier tests.
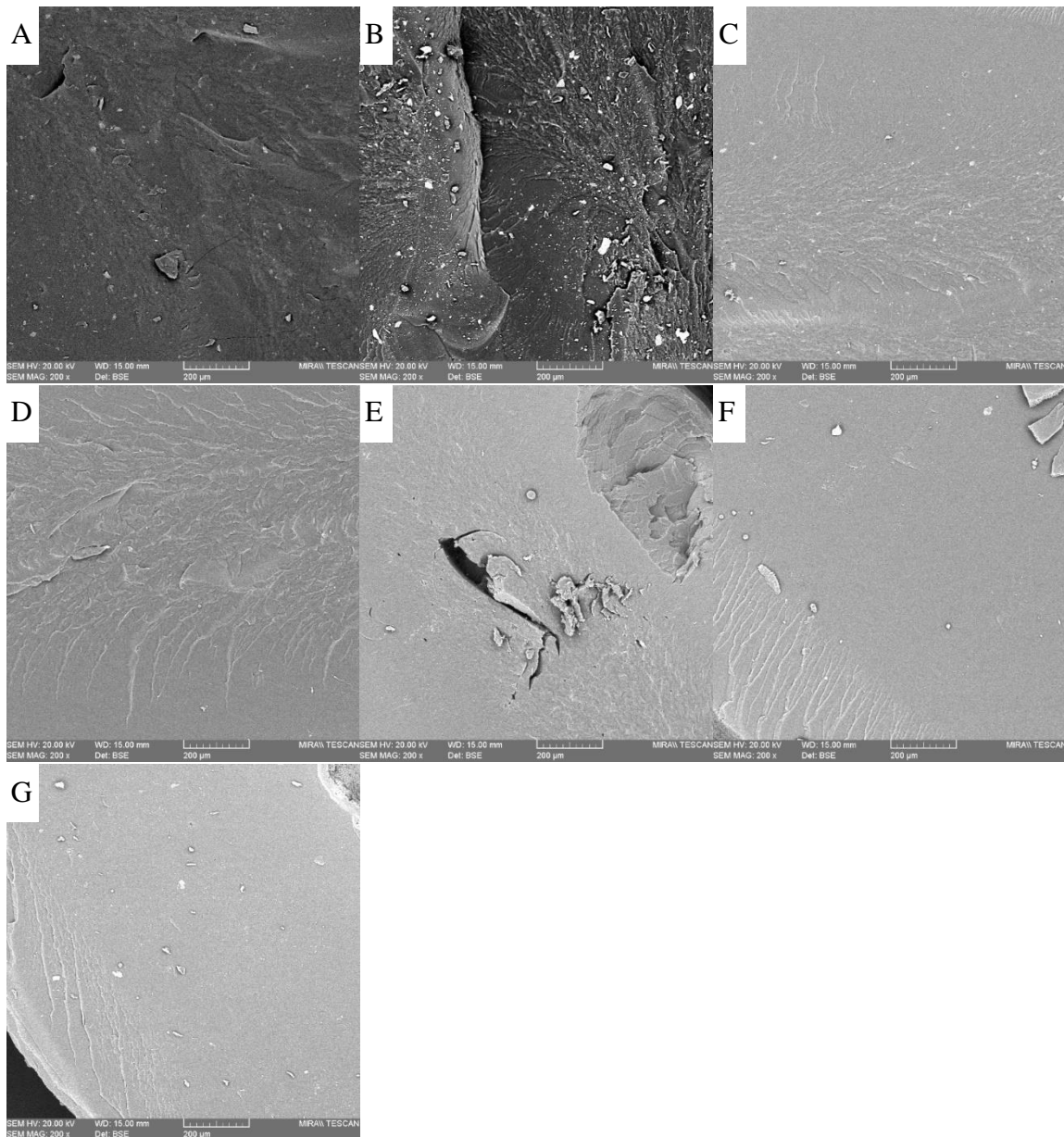
Figure 7-20 Scanning electron microscopy images (Magnification 200x) of the surface topography of PEGCombo hydrogels at (A) Day 0, (B) Day 2 in NaOH (C) Day 2 in PBS, (D) Day 14 in NaOH, (E) Day 14 in PBS, (F) Day 28 in NaOH and (G) Day 28 in PBS

7.2.7 Swelling studies

Gel fraction results provided a reliable method of determining the degree of unreacted material following polymerization (Wong, Ashton and Dodou, 2015) with Table 7-3 showing that upwards of 98% of PEGCombo was reacted following UV exposure, showcasing remarkably high polymerisation compared to similar works (Killion *et al.*, 2013) and agreeing with FTIR and Raman results discussed in section 7.2.2 which indicated a high degree of polymerisation occurred. When comparing PEGCombos swelling ratio (Q=16.3) with previous phases, PEGCombo most closely matched the PEGDMA-DiPETMP result (Q=15.93), with 100 wt. % PEGDMA and 2.5 wt. % PEGBio having much higher swelling ratios (Q=38 and Q=55.98 respectively). Likely due to PEGDMA and DiPETMP being the largest components by weight in the PEGCombo composition.

Table 7-3 Swelling and gel fraction values for PEGCombo samples

	Swelling ratio	Gel fraction
Final drug combo	16.3±0.82	1.17±0.38

7.2.8 Degradation study

In Figure 7-21 the weights of PEGCombo samples as a percentage of their day 0 weights is given for accelerated degradation and simulated physiological conditions. In Figure 5-11 where the PEGDMA-DiPETMP samples stored in 5mM NaOH were shown to steadily increase in weight up to a maximum after 30 days, after which there was a steady drop in weight until it was no longer tenable to remove and weigh samples. Contrasting this PEGCombo samples instead steadily increase in weight over the first two weeks and then hold a consistent for an extended period of time up to day 56. After day 56 the next weighing of PEGCombo samples at day 77 underwent a sharp increase in weight and a notable drop in mechanical strength when handled. This drop in mechanical strength was more apparent at day 84 of testing where

samples had advanced signs of breaking down with a large drop in weight. Subsequent attempts to weigh PEGCombo samples stored in 5mM NaOH resulted in the samples breaking and therefore accurate weighing became untenable. Samples placed in physiological underwent an initial increase in weight reaching between 125 and 130% of day 0 weights after 5 days immersion and maintained this weight throughout the 127 days of testing.
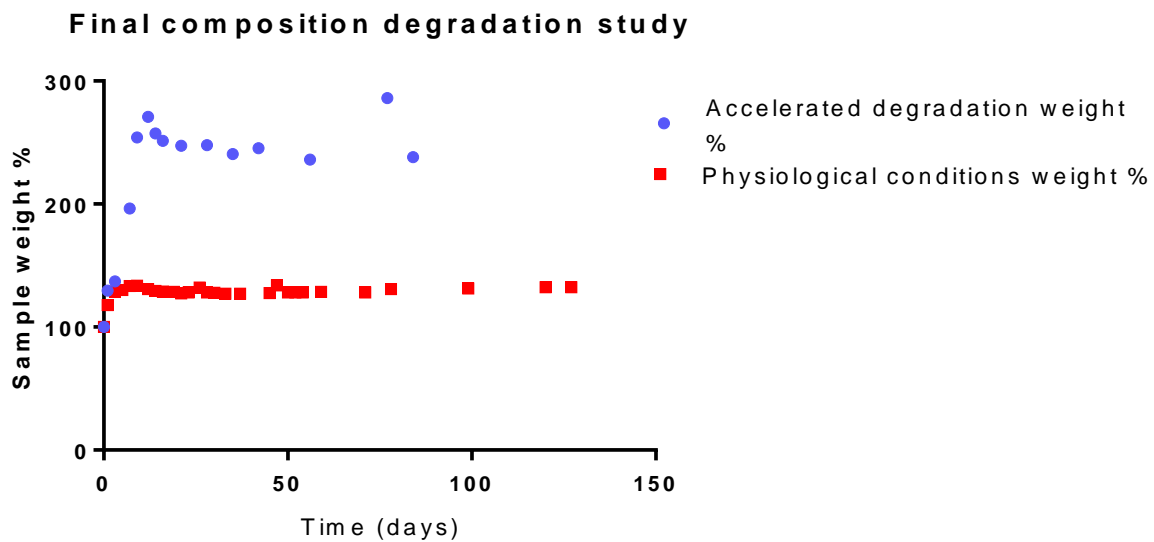
Figure 7-21 Degradation study of PEGCombo samples stored in 5M NaOH (Accelerated degradation conditions) and PBS (Physiological conditions) over a 127 day period

7.2.9 Conductivity

The addition of 2.5 wt. % bioglass to enhance the conductivity of PEGCombo was shown to work in Figure 7-22. Similarly to section 4.1.6 the conductance of day 0 samples were below the ideal threshold of 5 mS/cm although they were somewhat comparable (Runge *et al.*, 2010; Xu, Jeremy M. Holzwarth, *et al.*, 2014). After immersion in physiological solutions however, PEGCombo samples were shown to exceed the values required for nerve guidance conduits reaching 12.386 mS/cm and 13.898 mS/cm respectively. Day 28 conductivity measurements drastically dropped off when compared to earlier measurements with a value of 0.009 mS/cm. What was apparent in NaOH stored samples was a sharp decrease in conductance following

immersion going from 0.995 mS/cm in day 0 samples to 0.009 mS/cm, 0.005 mS/cm, and 0.007 mS/cm for days 2, 14 and 28 respectively.
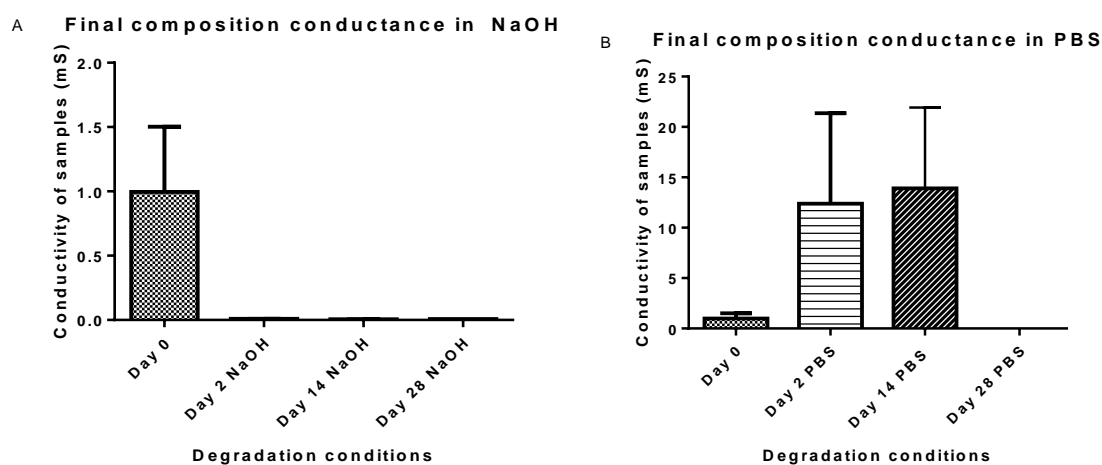
Figure 7-22 Showing conductivity of PEGCombo samples under (A) Accelerated degradation and (B) Simulated physiological conditions over a 28 day period, statistical analysis was carried out using Graphpad Prism 7 (n=3) with p-values of less than 0.05 being considered statistically significant (*p < 0.05, **p < 0.01 and ***p < 0.001)

7.3 Summary

In the first part of this study a side-by-side comparison of the properties of UV chamber cured and SLA fabricated PEGDMA hydrogels was made with the goal of predicting how SLA may impact the properties of the final prepared polymer for nerve repair.

The swelling ratio results in Figure 7-1 showed that the SLA polymerised PEGDMA had a significantly lower swelling ratio when compared to UV chamber samples which indicated that a more tightly crosslinked polymer network was found in the SLA polymerised samples (Omidian *et al.*, 1994; Pacios *et al.*, 2007). This is further shown through analysis of both thermal characterisations and through wettability measurement. In section 7.1.3 the glass transition temperatures, indicative of the temperature needed to achieve chain relaxation was slightly higher in SLA samples. This result was repeated in section 7.1.6 where again the SLA samples required slightly higher temperatures to undergo a glass transition. Regarding the potential impact on the final polymer there is likely to be very little as the nature of the thiol-

ene chemical reaction would have led to increased polymer network crosslinking regardless. This also lends itself to thiol-ene networks being softer and having a lower useful temperature range than methacrylate networks (Ligon *et al.*, 2017). For some a lower modulus would be inhibitory, it may however prove beneficial to our project as the stiffness of our samples post SLA have been higher than traditional polymerisations.

With wettability it was shown in Figure 7-6 that the UV chamber samples were more hydrophobic than the SLA samples with values of 30.6 and 47.6° respectively. Considering swellability is higher in the more hydrophobic UV chamber samples than the more hydrophilic SLA samples, it was indicated that a greater degree of chain freedom occurred in UV chamber samples. It was thought that further hydrogels prepared through SLA fabrication would experience a similar shift in wettability measurements, becoming more hydrophilic than UV cured polymerised counterparts.

Through analysis of mechanical testing, it was also indicated that there was greater chain freedom in UV chamber samples as they were shown to be significantly less compressively stiff. From these results it could be assumed that there was a greater degree of curing in SLA cured samples, this is not however backed up by either chemical analysis or gel fraction results. Both FTIR and gel fraction highlight the high degree of curing efficiency in both polymerisation processes. Interestingly gel fraction results imply that although SLA polymerised samples were shown to have a high degree of polymerisation efficiency, they were also of a lower efficiency than UV chamber samples, with approximately four times the amount of gel fraction present in SLA hydrogels compared to UV chamber samples (0.67% compared to 2.42%). Under these circumstances, it appears that despite having less polymerised material, the SLA polymerised samples have a greater degree of crosslinking density, impacting on polymer chain movement. It should be noted that most SLA curing processes including the one described above have a post-cure process wherein samples which have been printed are cleaned

of unreacted monomer and placed into a UV chamber for 10 minutes, effectively giving these samples a second curing. There is potential for this approach to produce several of the above differences due to overcuring the polymer, this is unlikely to be the case however as upon polymerisation the samples were not subject to the warping that would typically be associated with overcuring of a hydrogel (Arcaute, Mann and Wicker, 2006).

Another potential cause of these differences in properties can be assumed based on SLAs process of polymerisation. Namely that there are imperfections throughout the SLA fabricated hydrogels caused by the nature of its layer-by-layer curing process. Through this layer-by-layer curing localised regions of unreacted monomer are formed which affect the overall strength of the hydrogel. In theory the UV chamber posture would polymerise these pockets of unreacted monomer however there is credence lent to this theory by the increased presence of unreacted monomer in SLA samples as outlined in section 7.1.1. By examining the differences between the compressive and tensile results it would be thought that the greater crosslinking density indicated by swelling and thermal analysis would lead to greater tensile strengths in the SLA samples (Zhao, Yu and Dong, 2016). This is true of the tensile stiffness values shown in section 7.1.3 however it does not hold true for tensile strength at limit where although both samples have much lower tensile strengths compared to tensile stiffness, the SLA polymerised samples were significantly weaker than UV chamber polymerised samples. In contrast to the tensile results compressive Youngs modulus and compressive strength at limit values are relatively close in value to one another with SLA samples experience a smaller drop off from their stiffness values, moreover they maintain higher compressive strength values than UV chamber samples which would be expected with greater crosslinking densities. As the effect of layer-to-layer imperfections would be felt less under compressive strains than tensile strains the results shown in sections 7.1.3 and 7.1.4 further highlight the likelihood of unreacted monomer present in SLA polymerised hydrogels. A more likely cause of the contrast in the

expected tensile properties may be due to the print direction of samples. All samples were printed based on Form2 software recommendations, with uniform x, y, and z orientations. It has been established by others that print orientation, particularly z-orientation, has an impact on the mechanical properties of 3D printed components (Quan and Cotton, 2017). The work of Mueller described identical outcomes to our study, wherein the tensile stiffness was minimally impacted by the print direction due to the effect not occurring until the bonds were broken, whereas there was a drastic decrease in the tensile strength (Mueller and Shea, 2015).

This study found that both polymerisation methods were successful in forming PEGDMA based hydrogels with less than 3% of PEGDMA monomer from either process being unreacted, the wettability of PEGDMA samples was found to be significantly increased in SLA polymerised samples an outcome likely due to slight differences in surface uniformity of SLA samples being rougher than traditionally polymerised samples. SLA was also found to significantly increase the stiffness of PEGDMA samples compared to UV chamber samples while no significant impact on the thermal properties of samples was noted nor was there a difference in chemical properties between samples. These potential impacts on properties would likely synergise well with the properties of a PEGDMA-DiPETMP hydrogel containing electroactive bioglass as well as biological factors.

In the second part of this phase of testing the study focused on the analysis of PEGCombo samples With the notable decrease in size of the FTIR $1730cm^{-1}$ peak associated with the ester bonds in day 28 NaOH samples compared to day 28 PBS samples there is evidence to support the idea of ester bond breakages being the source of polymer degradation conforming with the expected degradation process (Shih and Lin, 2012). The confirmation of polymerisation in Figure 7-9 provided strong evidence of the viability of the composition of PEGCombo for future applications, indicating no interactions between its disparate components prevented its polymerisation, this was further confirmed with gel fraction analysis

in Table 7-3. With the lack of peaks in the 480-550 cm^{-1} range and the presence of peaks at 940 and 2580 cm^{-1} there is similarity to the results in section 5.1.2, namely that DiPETMP appears to be partially reacting with PEGDMA and becoming embedded in the polymer network prior to complete reaction. With the 940 cm^{-1} and 2580 cm^{-1} peaks decreasing over time going from days 0 to 28, there is an indication that S-H bonds are breaking down over time.

The bioglass appeared to initially have a large impact on the thermal properties of PEGCombo samples, with the day 0 Tg for PEGCombo (-42.5°C) matching very closely with the Tg recorded for 2.5 wt. % PEGBio at day 0 (-43.14°C). Interestingly where PEGBio samples maintained consistent Tgs below 40°C over time, the results for PEGCombo Tgs increased over time with day 28 samples stored in NaOH and PBS having Tgs of -31.56°C and -32.56°C respectively. Based off this increase in Tg there appeared to be an increase in the overall stiffness of the polymer network following immersion in either PBS or NaOH, with NaOH appearing to cause the greater increase in stiffness due to its more rapid hydrolytic degradation of the ester bond in the PEGCombo polymer network. Glass transition temperatures determined by DMA follow a similar pattern to section 5.1.3, with Tgs being lower than DSC calculated Tgs at -19.39°C and -25.52°C in Day 28 NaOH and PBS PEGCombo samples compared with Tgs of -31.56°C and -32.56°C calculated by DSC. This trend occurs across all corresponding Tgs between DSC and DMA results and is attributed to DSC Tgs identifying the glass transition at the beginning of the transition, whereas the DMA samples Tg corresponds to the midpoint of the transition(TA Instruments, 1997; Menczel and Prime, 2009). With PEGCombo samples undergoing an increase in Tg following immersion in PBS and NaOH it was determined that immersion in solutions resulted in increased polymer chain stiffness for PEGCombo samples due to their breakdown in solution similarly to section 5.1.8 where an initial increase in stiffness preceded the breakdown of PEGDMA-DiPETMP

samples. With the NaOH immersed samples undergoing greater increases in Tg over time likely being due to NaOH solution degrading PEGCombo faster than PBS solution.

Due to the changes to polymer chain stiffness in section 7.2.3 it would be predicted that a gradual increase in stiffness would occur in the NaOH immersed samples, this however does not occur, instead stiffness values for NaOH immersed samples remain constant until Day 28 when the Youngs modulus values for PEGCombo samples increased from 2.23 MPa to 7.42 MPa with all other Youngs modulus values in the in the range of 2.13 MPa (Day 0) up to a maximum of 2.32 MPa (Day 2 NaOH). With the inclusion of DiPETMP in PEGCombo it was expected that a decrease in polymer stiffness would occur as in section 5.1.4 where any thiol addition lowered the stiffness of PEGDMA, and DiPETMPs addition brought the overall stiffness of PEGDMA down from 9.17 MPa to 3.82 MPa at Day 0. In PEGCombo samples with most stiffness values being below 2.5 MPa it is likely that the addition of bioactive factors and electroactive bioglass in conjunction with DiPETMP contributed to PEGCombos lower than expected polymer stiffness. This lowering of stiffness values is likely conducive to the goal of preparing a nerve guidance conduit as PEGCombo still falls in the 1-12 MPa range highlighted as being ideal for nerve repair and being in the range of 2-2.5 MPa are likely more conductive to axonal regrowth (Balgude *et al.*, 2001; Flanagan *et al.*, 2002; Georges *et al.*, 2006). Values for compressive strength at limit while following a similar pattern to compressive Youngs modulus values, also fit the ideal criteria for nerve repair and axonal regrowth with values in the range of 1.08 MPa (PBS day 14) up to 2.4 MPa (NaOH day 28). With the goal of reaching a tensile strength of between 0.5 and 12 MPa similar to native peripheral nerves (Rydevik *et al.*, 1990), it was found that although stiffness values for PEGCombo samples did fall in this range, the stiffness values did not. Instead tensile strength values were found to be as low as 0.05 MPa, a tenth of the minimum tensile strength. Further adjustments to the PEGCombo composite will need to be made in the future to improve its

tensile properties. With greater time under physiological and accelerated degradation conditions PEGCombo samples underwent increases compressive and tensile stiffness.

It was initially thought Day 0 wettability measurements would even out quite closely to the ideal wettability range. Considering the initial wettability of PEGDMA 100 wt. % at Day 0 was 47.68° in section 3.2.5 it was felt that the wettability of PEGCombo would fall roughly into the 40 to 60° range possibly skewing to above the 60° end becoming slightly more hydrophobic than intended. This was thought as the addition of DiPETMP to PEGDMA resulted in PEGDMAs wettability increasing to 83.9° and the addition of bioglass 2.5 wt. % resulted in PEGDMAs wettability changing to 55.33°. The idea being PEGDMAs wettability would be an average of these wettability measurements. With the Day 0 PEGCombo wettability instead increasing to a hydrophobic 103.56°, it became clear that both bioglass and DiPETMP increased the wettability of PEGCombo independently to the extent it was no longer considered hydrophilic at Day 0. This creates a potential need for an additional component to be added to PEGCombo to increase hydrophilicity of the overall composite for its use as a nerve guidance conduit. While there was initially an issue with being too hydrophobic, over time the wettability of PEGCombo improved, with day 14 and 28 samples in physiological solution fitting the ideal range for cellular attachment (Arima and Iwata, 2007), with this in mind a possible surface coating to temporarily lower wettability may provide a workable solution. Several such coatings are already commonplace with the likes of polyvinylpyrrolidone (PVP), polyacrylamide (PAM) and polysaccharides being used since the 1980s (Mehta and Mehta, 2019) and provide a number of options for improving wettability.

From Table 7-3 it is apparent that the gel fraction for PEGCombo is slightly lower than that seen for pure PEGDMA-DiPETMP in section 5.1.7, where less than 1% of PEGDMA-DiPETMP was unreacted gel potentially due to bioglass impacting polymerisation. Considering gel fraction was maintained above 95% however, this drop was unlikely to affect

the other hydrogel properties of PEGCombo samples with other researchers considering gel fractions above 80% to be polymerised successfully (Yoshii *et al.*, 1999). The similarity between PEGCombos swelling ratio and PEGDMA-DiPETMPs swelling ratio makes sense when considering the overall similarity in compositions between both preparations, with the greatest difference being the 2.5 wt. % of bioglass which in section 4.1.2 was established to not impact the swelling ratio of polymerised samples.

Regarding the degradation study, it became apparent that although PEGCombo underwent degradation, it did so at a slower pace than what was seen with pure PEGDMA-DiPETMP, taking approximately 2.5 times as long to reach breakdown. Unlike the PEGDMA-DiPETMP study where there was a steady decrease in weight the breakdown of PEGCombo once reached was much more rapid. Potentially the addition of bioglass or the drugs NAC, Ibu and Prog could have influenced the degradation profile of PEGCombo but the mechanism by which this was done is unclear and would likely require further characterisation. It is noteworthy that PEGCombo samples placed in PBS did not undergo any distinct breakdown during testing maintaining a consistent swelling weight of between 125 and 130% their weight at day 0 of testing, with this in mind, despite showing degradability of our PEG based composition, it is likely that for the advancement of this compositions use in nerve guidance conduits changes to thiol-ene ratio would be necessitated to change degradation rates by increasing the presence of degradable ester bonds, with alterations to thiol ratios being common practice by others (Lowe, 2014).

With the criteria of conductance in the 5 mS/cm range PEGCombo samples readily achieved these results when stored in physiological conditions for at least the first two weeks of immersion, indicating PEGCombos viability in carrying electrical signals between severed nerve endings. Between days 14 and 28 in PBS solution, PEGCombo underwent a rapid decrease in conductance, with day 28 conductance values being comparable to samples

exposed to accelerated degradation conditions. In a study of rat sciatic nerve regeneration over a 10 mm gap by Yeh et al. it was shown that a period of 14 days electrical stimulation starting from day 14 post injury provided the greatest repair of nerve damage. With successful repair occurring in 70% of rats exposed to electrical stimulation from day 15 to day 29, compared with 30% of untreated rats recoverin and 60% of rats treated from day 1 to day 15 (Yeh *et al.*, 2010). Considering the biological signalling to induce nerve repair begins to steadily decrease from day 14 post injury without external influences (Önger *et al.*, 2017), it may be advantageous to insert the PEGCombo based nerve guidance conduit 14 days post injury. Allowing for a synergistic impact between the effects of NAC, Ibu and Prog release boosting the molecular pathways and the enhanced electrical conductivities boost to peripheral nerve repair.

Chapter 8

Conclusions

8.1 Introduction

The aim of this study was to develop a PEGDMA based hydrogel suitable for the fabrication of a peripheral nerve guidance conduit. To do this several phases of testing were undertaken with the aim of improving the properties of PEGDMA more suitable for the idealised nerve guidance conduit.

8.2 Conclusion

Initial testing was conducted on four different monomer concentrations (25, 50, 75 and 100 wt. %) of PEGDMA (600) stored in physiological solutions at 37°C over a 28-day period to simulate changes *in vivo*. After that, the material properties were examined after 0, 2, 14 and 28 days for their swelling characteristics, wettability, surface topography, chemical properties, polymer morphology, mechanical properties, and cellular response. From this testing the feasibility of PEGDMAs use as a nerve guidance conduit was assessed with particular attention put toward the compressive strength (aiming for a strength between 1 and 12 MPa), ease of manufacture (aiming to demonstrate easily replicable manufacture through UV polymerisation) and biocompatibility (to ensure no adverse cellular response occurs *in vivo*) and wettability (40 to 60° range for enhanced cellular attachment). From this data, it was decided that the 50 and 100 wt. % PEGDMA hydrogels were most suited to replicate the conditions of peripheral nerve tissue due to their good mechanical strength (falling in the range of 3 to 4 MPa), ease and reliability of manufacture (demonstrated with all wt. %s), wettability matching the idealised range for cellular attachment and being non-cytotoxic to the nerve-like PC-12 cell line. Initially 50 wt. % was selected to continue with due to decreased material costs. While the base 50 wt. % PEGDMA met several of the criteria identified for peripheral nerve guidance conduits, it did not have the conductive properties to match those of the peripheral nerve as PEGDMA is known to be conductively inert. It was determined that a material was needed to increase the conductivity of PEGDMA, as such a boron doped bioactive glass,

Bioglass45S5 known to enhance electrical properties was identified as an additive for 50% PEGDMA.

Electrical stimulation has been previously shown to enhance nerve regeneration and decrease the rates of muscle atrophy commonly seen post peripheral nerve injury due to a lack of signals reaching beyond the injury site. To facilitate enhanced nerve regeneration and decrease muscular atrophy during the repair process, we set out to enhance the conductance of the PEGDMA hydrogel to a rate matching the current state of the art which is in the range of 1 to 15 mS/cm, preferably around 5 mS/cm which is the conductance of native peripheral nerves. To do this, initial boron doped bioglass wt. %s of 2.5 wt. %, 5 wt. %, 10 wt. % and 20 wt. % were added to PEGDMA, over the course of several tests these percentages were continually lowered to 0.5 wt. %, 1 wt. %, 1.5 wt. % and 2.5 wt. % due to a combination of incomplete polymerisations and subpar mechanical performances. The materials properties of these PEGBio composites were tested with an emphasis on maintaining the desired properties which had been previously achieved in the initial testing and determining if boron doped bioglass enhanced the conductivity of 50 wt. % PEGDMA. When looking specifically at conductance it was found that only the 2.5 wt. % bioglass samples experienced enhanced conductance going from 7 µS/cm (0.007 mS/cm) in the 0.5 wt. % bioglass up to 3 mS/cm for days 0 and 2 of testing and approximately 0.5 mS/cm for days 14 and 28 in the 2.5 wt. % bioglass samples. The 2.5 wt. % also maintained the desired wettability measurements where other wt. %s were found to have wettability outside the desired range during the 28 days of testing taken, furthermore as all bioglass compositions were shown to be non-cytotoxic to PC-12 cells the 2.5 wt. % bioglass was identified to successfully enhance the conductance of PEGDMA for use as a peripheral nerve guidance conduit.

Following the identification of bioglass to enhance the conductance, the focus of the project shifted to the degradability of the material. One of PEGDMAs major drawbacks is its

lack of degradability this can be a major drawback for peripheral nerve repair where biodegradable materials have been found to have better long-term outcomes for nerve repair. To tackle this limitation 10 thiol monomers were copolymerised with PEGDMA in 1:1 thiol to ene ratios. The addition of thiols was identified as its inclusion allowed for hydrolytic degradation to break down the PEGDMA-Thiol copolymer. After initial miscibility issues between thiols and the water needed to prepare 50 wt. % PEGDMA it was decided to switch to 100 wt. % PEGDMA based hydrogels as the properties for 100 wt. % and 50 wt. % samples were comparable and the change removed the issue of thiol-water miscibility. Successfully polymerised thiol-ene copolymers were then characterised to determine the ideal copolymer for peripheral nerve repair. As in the previous two sections the focus was initially on testing PEGDMAs mechanical, thermal, and chemical properties in combination with the additive (in this case thiol monomers), with the selected thiol being based on how it improved or maintained PEGDMAs desirable properties. With this end-goal two thiol monomers were found to have improved the properties of PEGDMA specifically maintaining PEGDMAs mechanical strength while also having comparable thermal properties, PETMP and DiPETMP. Ultimately the thiol-based monomer DiPETMP was selected due to its increased novelty against the comparatively more studied PETMP. Following copolymerisation, PEGDMA-DiPETMP based hydrogels were found to have greatly increased degradability compared with pure PEGDMA hydrogels. Subsequent cytotoxicity testing of PEGDMA-DiPETMP samples showed that the improvement of PEGDMAs degradability did not cause increased cytotoxicity via either direct contact or elution assays. In fact, PEGDMA-DiPETMP direct contact assays in PC-12 cells were instead shown to have a two-fold increase in cellular proliferation and in Schwann cells were shown to have comparable proliferation rates to pure PEGDMA hydrogels. With this knowledge DiPETMP was successfully identified as a suitable additive to enhance the degradability of PEGDMA.

With adjustments made to PEGDMA to enhance both electrical conductance and degradability, the focus of the project shifted to the addition of biological factors, namely N-acetyl cysteine (NAC), Ibuprofen (Ibu) and Progesterone (Prog) to enhance peripheral nerve repair. For a nerve guidance conduit to have improved clinical outcomes in the repair of damaged nerves the use of factors which boosted outcomes associated with nerve repair including cytoskeletal assembly, neurite outgrowth and neuronal survival. Through combining the drugs NAC, Ibu and Prog each of four major pathways of peripheral nerve repair, namely the Pl3K/Akt pathway, the Ras-ERK pathway, the Rho-ROK pathway and the cyclic AMP pathway are positively affected resulting in the enhancement of nerve repair. It was thought that through this combination of NAC, Ibu and Prog, a synergistic effect might occur. For this chapter two objectives associated with NAC, Prog and Ibu were identified, first, determining the most synergistic combination of drugs for the enhancement of peripheral nerve repair and second, determining the rates of release for NAC, Ibu and Prog once added to PEGDMA-DiPETMP copolymers to establish whether PEGDMA-DiPETMP hydrogels could accurately deliver NAC, Ibu and Prog *in vivo*. With the objective of determining the most synergistic combination of NAC, Ibu and Prog a high-throughput testing procedure was prepared to identify potential synergies produced by combining NAC, Ibu and Prog. With this in mind the cell lines RT4-D6P2T (Schwann) and PC-12 (Rat adrenal gland) cells were treated initially with dual drug combinations and ultimately with a 3 drug combination to identify the combination of NAC, Ibu and Prog concentrations which provided the most beneficial impact on cellular proliferation. After 3 rounds of screening the most synergistic drug combination was determined to be 75 µM NAC, 16.25 µM Ibu and 30 µM Prog. With the aim of determining the release rates of these drugs from PEGDMA-DiPETMP hydrogels a novel HPLC process was developed which could separate, identify, and determine the rates of release for each drug through the adaption of pre-existing USP methods. Their rates of drug release when

incorporated separately and in combination with one another was investigated. All drug release rates were found to be independent of one another with release kinetic analysis finding drug size to be the determining factor in release rates. It was determined that NAC had the fastest release rate, fully releasing in 1 day, Ibuprofen was slower than NAC but had a faster release rate than Progesterone, reaching full release after 3 days. Progesterone required 21 days to reach complete drug release. With the knowledge that the drugs NAC, Ibu and Prog when incorporated into PEGDMA-DiPETMP hydrogels could provide a sustained release over three weeks capable of impacting the nerve repair process, leading to the addition of all three drugs for at concentrations of 75 µM NAC, 16.25 µM Ibu and 30 µM Prog to enhance the peripheral nerve repair process over a 3 week period.

Having established methods to enhance the conductivity, degradation, and biological activity of PEGDMA hydrogels, the final section of work identified two aims to be achieved for the preparation of a nerve guidance conduit. Firstly to ascertain a technique capable of controlling the 3D architecture of PEGDMA, if a nerve guidance conduit is to be prepared control of its architecture can allow for the tailoring of the conduit to match the injury site. Secondly to prepare a final print of PEGDMA enhanced by the additions determined throughout this study with the aim of demonstrating the feasibility of a finalised print for peripheral nerve repair. With the goal of controlling PEGDMAs 3D architecture the use 3D printing technique stereolithography (SLA) was investigated to determine if SLA could allow for spatial control of the PEGDMAs polymerisation and if SLA impacted the overall properties of PEGDMA the peripheral nerve guidance conduits. SLA was employed as it allowed for control of polymer synthesis at very high resolution making possible the creation of tissue engineered devices with microarchitecture similar to the tissues they are replacing. SLAs rapid method of polymerisation also lends itself to the improved viability of encapsulated cells, should they be added. From the subsequent testing SLA fabricated hydrogels were shown to

maintain similar thermal and chemical properties to UV cured hydrogels while having increased compressive and tensile stiffness as well as increased hydrophilicity most likely due to the increased exposure to UV light SLA samples received compared to traditionally cured samples. With SLAs potential to increase the tensile stiffness of PEGDMA based hydrogels as well as allowing for control over PEGDMAs architecture, while maintaining thermal and chemical impacts of PEGDMA, it was determined SLA was a suitable process to prepare the final PEGDMA based combination in this study and an ideal additive. To continue from the initial aim, the second aim looked to utilise SLA to polymerise a composite of PEGDMA, DiPETMP, Bioglass and the drugs NAC, Ibu and Prog (PEGCombo). It was found that due to the nature of the thiol-ene reaction it was not possible to control PEGCombos rate of polymerisation, consequently, attempts to control polymer architecture be pushed back to future studies. Following this PEGCombo samples were polymerised using UV polymerisation as previously and its properties were determined. From this it was determined that while PEGCombo had the compressive strength, conductivity and controlled release of drugs required for a nerve guidance conduit, further alterations would be needed to improve PEGCombos tensile strength, wettability as well as degradability.

Considering this study enabled the formulation of a PEGDMA based hydrogel, which was shown to be conductive, degradable, and capable of controlled delivery of biological factors over a biologically relevant timeframe, there are several future investigations which could build upon and improve this work with the end goal of a clinically relevant peripheral nerve guidance conduit in mind:

- The addition of a thiol-ene reaction stabiliser to improve control over the thiol-ene reaction allowing for SLA applications potentially addressing the issues of both improving the hydrophilicity and increasing the tensile strength of the final PEGCombo composition.

- Investigating alternative options to improve control over the architecture of PEGCombo composites should the SLA route need replacing.

- Carrying out in-depth analysis of the impact PEGCombo has on RT4-D6P2T (Schwann) and PC-12 (Rat adrenal gland) cells with the potential for a follow-up *in vivo* study.

Chapter 9

References

9.0 Bibliography

Abercrombie, M. (1979) 'Contact inhibition and malignancy', *Nature*, 281(5729), pp. 259–62. Available at: http://www.ncbi.nlm.nih.gov/pubmed/551275.

Agnew, S. P. and Dumanian, G. A. (2010) 'Technical Use of Synthetic Conduits for Nerve Repair', *Journal of Hand Surgery*. Elsevier Inc., 35(5), pp. 838–841. doi: 10.1016/j.jhsa.2010.02.025.

Ahn, H. S. *et al.* (2015) 'Carbon-nanotube-interfaced glass fiber scaffold for regeneration of transected sciatic nerve', *Acta Biomaterialia*. Acta Materialia Inc., 13, pp. 324–334. doi: 10.1016/j.actbio.2014.11.026.

Aimetti, A. A., Machen, A. J. and Anseth, K. S. (2009) 'Poly(ethylene glycol) hydrogels formed by thiol-ene photopolymerization for enzyme-responsive protein delivery', *Biomaterials*. Elsevier Ltd, 30(30), pp. 6048–6054. doi: 10.1016/j.biomaterials.2009.07.043.

Allodi, I., Udina, E. and Navarro, X. (2012) 'Specificity of peripheral nerve regeneration: Interactions at the axon level', *Progress in Neurobiology*. Elsevier Ltd, 98(1), pp. 16–37. doi: 10.1016/j.pneurobio.2012.05.005.

Almansoori, A. A. *et al.* (2020) 'Tantalum – Poly (L-lactic acid) nerve conduit for peripheral nerve regeneration', *Neuroscience Letters*. Elsevier, 731(November 2019), p. 135049. doi: 10.1016/j.neulet.2020.135049.

Anandagoda, N. *et al.* (2012) 'Hyaluronan hydration generates three-dimensional meso-scale structure in engineered collagen tissues', *Journal of the Royal Society, Interface / the Royal Society*, 9(75), pp. 2680–2687. doi: 10.1098/rsif.2012.0164.

Annabi, N. *et al.* (2010) 'Controlling the Porosity and Microarchitecture of Hydrogels for Tissue Engineering', *Tissue Engineering Part B: Reviews*, 16(4), pp. 371–383.

Annabi, N. *et al.* (2014) '25th anniversary article: Rational design and applications of hydrogels in regenerative medicine', *Advanced Materials*, pp. 85–124. doi: 10.1002/adma.201303233.

Arcaute, K., Mann, B. K. and Wicker, R. B. (2006) 'Stereolithography of three-dimensional bioactive poly(ethylene glycol) constructs with encapsulated cells', *Annals of Biomedical Engineering*, 34(9), pp. 1429–1441. doi: 10.1007/s10439-006-9156-y.

Arima, Y. and Iwata, H. (2007) 'Effect of wettability and surface functional groups on protein adsorption and cell adhesion using well-defined mixed self-assembled monolayers', *Biomaterials*, 28(20), pp. 3074–3082. doi: 10.1016/j.biomaterials.2007.03.013.

Arslantunali, D. *et al.* (2014) 'Peripheral nerve conduits: technology update.', *Medical devices (Auckland, N.Z.)*, 7, pp. 405–24. doi: 10.2147/MDER.S59124.

ASTM-D638-14 (2014) 'Standard Test Method for Tensile Properties of Plastics', *ASTM Standards*, 08, pp. 1–15.

Atkins, S. *et al.* (2006) 'Scarring impedes regeneration at sites of peripheral nerve repair', *NeuroReport*, 17(12), pp. 1245–1249. doi: 10.1097/01.wnr.0000230519.39456.ea.

Awad, A. *et al.* (2018) 'Reshaping drug development using 3D printing', *Drug Discovery Today*. Elsevier Ltd, (17). doi: 10.1016/j.drudis.2018.05.025.

Bäckström, S. *et al.* (2012) 'Tailoring Properties of Biocompatible PEG-DMA Hydrogels with UV Light', *Materials Sciences and Applications*, 03(June), pp. 425–431. doi: 10.4236/msa.2012.36060.

Baier Leach, J. *et al.* (2003) 'Photocrosslinked hyaluronic acid hydrogels: natural, biodegradable tissue engineering scaffolds', *Biotechnology and bioengineering*, 82(5), pp. 578–589. doi: 10.1002/bit.10605.

Balgude, A. P. *et al.* (2001) 'Agarose gel stiffness determines rate of DRG neurite extension in 3D cultures', *Biomaterials*, 22(10), pp. 1077–1084. doi: 10.1016/S0142-9612(00)00350-1.

Barron, V. *et al.* (2015) 'Evaluation of the Early In Vivo Response of a Functionally Graded Macroporous Scaffold in an Osteochondral Defect in a Rabbit Model', *Annals of Biomedical Engineering*. doi: 10.1007/s10439-015-1473-6.

Barron, V. *et al.* (2016) 'Development of chemically cross-linked hydrophilic-hydrophobic hydrogels for drug delivery applications', *European Polymer Journal*, 75, pp. 25–35. doi: 10.1016/j.eurpolymj.2015.10.033.

Bazylewski, P., Divigalpitiya, R. and Fanchini, G. (2017) 'In situ Raman spectroscopy distinguishes between reversible and irreversible thiol modifications in l-cysteine', *RSC Advances*. Royal Society of Chemistry, 7(5), pp. 2964–2970. doi: 10.1039/c6ra25879d.

Belkas, J. S., Shoichet, M. S. and Midha, R. (2004) 'Peripheral nerve regeneration through guidance tubes.', *Neurological research*, 26, pp. 151–160. doi: 10.1179/016164104225013798.

Bhanot, D. (2013) *How to calculate System Suitability in Chromatography*, *Chromatography*.

Bock, B. (2012) 'BrunoBock catalogue', (1907), pp. 1–11.

Boerboom, A. *et al.* (2017) 'Molecular mechanisms involved in schwann cell plasticity', *Frontiers in Molecular Neuroscience*, 10(February), pp. 1–18. doi: 10.3389/fnmol.2017.00038.

Borschel, G. H. *et al.* (2003) 'Mechanical properties of acellular peripheral nerve', *Journal of Surgical Research*, 114(2), pp. 133–139. doi: 10.1016/S0022-4804(03)00255-5.

Bowman, C. N. and Kloxin, C. J. (2008) 'Toward an Enhanced Understanding and Implementation of Photopolymerization Reactions', *American Institute of Chemical Engineers*, 54(11), pp. 2775–2795. doi: 10.1002/aic.

Bracco, G. and Holst, B. (2013) *Surface science techniques*, *Springer Series in Surface Sciences*. doi: 10.1007/978-3-642-34243-1.

Brandl, F., Sommer, F. and Goepferich, A. (2007) 'Rational design of hydrogels for tissue engineering: Impact of physical factors on cell behavior', *Biomaterials*, 28(2), pp. 134–146. doi: 10.1016/j.biomaterials.2006.09.017.

Breuls, R. G. M., Jiya, T. U. and Smit, T. H. (2008) 'Scaffold stiffness influences cell behavior: opportunities for skeletal tissue engineering.', *The open orthopaedics journal*, 2, pp. 103–9. doi: 10.2174/1874325000802010103.

Browning, M. . *et al.* (2014) 'Determination of the in vivo degradation mechanism of PEGDA hydrogels', *Journal of Biomedical Materials Research A*, 102(12), pp. 4244–4251. doi:

10.1002/jbm.a.35096.

Brushart, T. M. *et al.* (1995) 'Dispersion of regenerating axons across enclosed neural gaps', *Journal of Hand Surgery*, 20(4), pp. 557–564. doi: 10.1016/S0363-5023(05)80267-9.

Bryant, S. J. and Anseth, K. S. (2002) 'Hydrogel properties influence ECM production by chondrocytes photoencapsulated in poly(ethylene glycol) hydrogels', *Journal of Biomedical Materials Research*, 59, pp. 63–72. doi: 10.1002/jbm.1217.

Bulman, S. *et al.* (2012) 'Enhancing the MSC Therapeutic Response: Cell Localization and Support for Cartilage Repair', *Tissue engineering. Part B, Reviews*. doi: 10.1089/ten.TEB.2012.0101.

Bunting, S. *et al.* (2005) 'Bioresorbable Glass Fibres Facilitate Peripheral Nerve Regeneration', *Hand Surgery*, 30B(3), pp. 242–247.

Buwalda, S. J. *et al.* (2014) 'Hydrogels in a historical perspective: From simple networks to smart materials', *Journal of Controlled Release*. Elsevier B.V., 190, pp. 254–273. doi: 10.1016/j.jconrel.2014.03.052.

Caillaud, M. *et al.* (2019) 'Peripheral nerve regeneration and intraneural revascularization', *Neural Regeneration Research*, 14(1), pp. 24–33. doi: 10.4103/1673-5374.243699.

Carlson, G. D. and Gorden, C. (2002) 'Current developments in spinal cord injury research', *The Spine Journal*, 2, pp. 116–128.

Catapano, J. *et al.* (2017) 'N -acetylcysteine prevents retrograde motor neuron death after neonatal peripheral nerve injury', *Plastic and Reconstructive Surgery*, 139(5), pp. 1105e-1115e. doi: 10.1097/PRS.0000000000003257.

Catrina, S. and Madduri, S. (2013) 'Nerve conduit scaffolds for discrete delivery of two neurotrophic factors', *European Journal of Pharmaceutics and Biopharmaceutics*, 85(1), pp. 139–142. doi: 10.1016/j.ejpb.2013.03.030.

Chamberlain, L. J. *et al.* (2000) 'Connective tissue response to tubular implants for peripheral nerve regeneration: The role of myofibroblasts', *Journal of Comparative Neurology*, 417(4), pp. 415–430. doi: 10.1002/(SICI)1096-9861(20000221)417:4<415::AID-CNE3>3.0.CO;2-9.

Chan, K. M. *et al.* (2014) 'Improving peripheral nerve regeneration: From molecular mechanisms to potential therapeutic targets', *Experimental Neurology*. Elsevier Inc., 261, pp. 826–315. doi: 10.1016/j.expneurol.2014.09.006.

Chang, J. Y. *et al.* (2009) 'Highly permeable genipin-cross-linked gelatin conduits enhance peripheral nerve regeneration', *Artificial Organs*, 33(12), pp. 1075–1085. doi: 10.1111/j.1525-1594.2009.00818.x.

Chen, L., Yan, C. and Zheng, Z. (2018) 'Functional polymer surfaces for controlling cell behaviors', *Materials Today*. Elsevier Ltd, 21(1), pp. 38–59. doi: 10.1016/j.mattod.2017.07.002.

Cheng, C. *et al.* (2008) 'Activated RHOA and peripheral axon regeneration', *Experimental Neurology*. Academic Press, 212(2), pp. 358–369. doi: 10.1016/j.expneurol.2008.04.023.

Cheng, Y. *et al.* (2020) '3D structured self-powered PVDF/PCL scaffolds for peripheral nerve

regeneration', *Nano Energy*. Elsevier Ltd, 69, p. 104411. doi: 10.1016/j.nanoen.2019.104411.

Chew, S. Y. *et al.* (2007) 'Aligned protein-polymer composite fibers enhance nerve regeneration: A potential tissue-engineering platform', *Advanced Functional Materials*, 17(8), pp. 1288–1296. doi: 10.1002/adfm.200600441.

Chhabra, A. *et al.* (2014) 'Peripheral nerve injury grading simplified on MR neurography: As referenced to Seddon and Sunderland classifications.', *The Indian journal of radiology & imaging*. Medknow Publications and Media Pvt. Ltd., 24(3), pp. 217–24. doi: 10.4103/0971-3026.137025.

Chiang, M. Y. M. and Fernandez-Garcia, M. (2003) 'Relation of swelling and Tg depression to the apparent free volume of a particle-filled, epoxy-based adhesive', *Journal of Applied Polymer Science*, 87(9), pp. 1436–1444. doi: 10.1002/app.11576.

Chierzi, S. *et al.* (2005) 'The ability of axons to regenerate their growth cones depends on axonal type and age, and is regulated by calcium, cAMP and ERK', *European Journal of Neuroscience*, 21(8), pp. 2051–2062. doi: 10.1111/j.1460-9568.2005.04066.x.

Chikarakara, E. *et al.* (2015) 'In vitro fibroblast and pre-osteoblastic cellular responses on laser surface modified Ti-6Al-4V', *Biomedical Materials (Bristol)*. IOP Publishing, 10(1), p. 15007. doi: 10.1088/1748-6041/10/1/015007.

Chiriac, S. *et al.* (2011) 'Experience of using the bioresorbable copolyester poly(DL-lactide-e-caprolactone) nerve conduit guide NeurolacTM for nerve repair in peripheral nerve defects: Report on a series of 28 lesions', *The Journal of hand surgery, European volume*, 37(4), pp. 342–349. doi: 10.1177/17531934114226.

Chowdhury, S. M. and Hubbell, J. A. (1996) 'Adhesion prevention with ancrod released via a tissue-adherent hydrogel', *The Journal of Surgical Research*, 61(1), pp. 58–64. doi: 10.1006/jsre.1996.0081.

Christie, K. J. and Zochodne, D. (2013) 'Peripheral axon regrowth: New molecular approaches', *Neuroscience*. IBRO, 240, pp. 310–324. doi: 10.1016/j.neuroscience.2013.02.059.

CHROMacademy (no date) *The Theory of HPLC: Chromatographic Parameters*, *Crawford Scientific*. Available at: http://www.chromacademy.com/index.html (Accessed: 19 February 2020).

Ciardelli, G. and Chiono, V. (2006) 'Materials for peripheral nerve regeneration', *Macromolecular Bioscience*, 6(1), pp. 13–26. doi: 10.1002/mabi.200500151.

Coates, J., Ed, R. A. M. and Coates, J. (2000) 'Interpretation of Infrared Spectra , A Practical Approach Interpretation of Infrared Spectra , A Practical Approach', *Encyclopedia of Analytical Chemistry*, pp. 10815–10837.

Collier, J. H. *et al.* (2000) 'Synthesis and characterization of polypyrrole-hyaluronic acid composite biomaterials for tissue engineering applications', *Journal of biomedical materials research*, 50(4), pp. 574–584.

Colthup, N. B., Daly, L. H. and Wiberley, S. E. (1990) *Introduction To Infrared and Spectroscopy*. Third edit. London: Academic Press. doi: http://dx.doi.org/10.1016/B978-0-

08-091740-5.50003-X.

Coronel, M. F. *et al.* (2011) 'Progesterone Prevents Nerve Injury-Induced Allodynia and Spinal NMDA Receptor Upregulation in Rats', *Pain Medicine*, 12(8), pp. 1249–1261. doi: 10.1111/j.1526-4637.2011.01178.x.

Cramer, N. B. *et al.* (2003) 'Thiol - Ene Photopolymerization Mechanism and Rate Limiting Step Changes for Various Vinyl Functional Group Chemistries', *Macromolecules*, 36(21), pp. 7964–7969. doi: 10.1021/ma034667s.

Cruise, G. M. *et al.* (1998) 'A sensitivity study of the key parameters in the interfacial photopolymerization of poly(ethylene glycol) diacrylate upon porcine islets', *Biotechnology and Bioengineering*, 57, pp. 655–665. doi: 10.1002/(SICI)1097-0290(19980320)57:6<655::AID-BIT3>3.0.CO;2-K.

Cruise, G. M. *et al.* (1999) 'In vitro and in vivo performance of porcine islets encapsulated in interfacially photopolymerized poly(ethylene glycol) diacrylate membranes', *Cell Transplantation*, 8(3), pp. 293–306.

Cruise, G. M., Scharp, D. S. and Hubbell, J. A. (1998) 'Characterization of permeability and network structure of interfacially photopolymerized poly(ethylene glycol) diacrylate hydrogels', *Biomaterials*, 19(14), pp. 1287–1294.

Daly, W. *et al.* (2012) 'A biomaterials approach to peripheral nerve regeneration: bridging the peripheral nerve gap and enhancing functional recovery', *Journal of The Royal Society Interface*, 9(November 2011), pp. 202–221. doi: 10.1098/rsif.2011.0438.

Daly, W. T. *et al.* (2012) 'The effect of intraluminal contact mediated guidance signals on axonal mismatch during peripheral nerve repair', *Biomaterials*, 33(28), pp. 6660–6671. doi: 10.1016/j.biomaterials.2012.06.002.

Das, K. P., Freudenrich, T. M. and Mundy, W. R. (2004) 'Assessment of PC12 cell differentiation and neurite growth: A comparison of morphological and neurochemical measures', *Neurotoxicology and Teratology*, 26, pp. 397–406. doi: 10.1016/j.ntt.2004.02.006.

Das, R. K. and Zouani, O. F. (2014) 'A review of the effects of the cell environment physicochemical nanoarchitecture on stem cell commitment', *Biomaterials*. Elsevier Ltd, 35(20), pp. 5278–5293. doi: 10.1016/j.biomaterials.2014.03.044.

Dash, S. *et al.* (2010) 'Kinetic modeling on drug release from controlled drug delivery systems', *Acta Poloniae Pharmaceutica - Drug Research*, 67(3), pp. 217–223.

Davies, N. M. (1998) 'Clinical pharmacokinetics of ibuprofen. The first 30 years', *Clinical Pharmacokinetics*. Springer, 34(2), pp. 101–154. doi: 10.2165/00003088-199834020-00002.

Decker, C. and Moussa, K. (1987) 'Photopolymerization of multifunctional monomers in condensed phase ', *Journal of Applied Polymer Science*, 34(4), pp. 1603–1618. doi: 10.1002/app.1987.070340420.

Dhariwala, B. *et al.* (2004) 'Rapid Prototyping of Tissue-Engineering Constructs , Using', *Tissue Engineering*, 10(9), pp. 1316–1322.

Dicko, A., Mayer, L. D. and Tardi, P. G. (2010) 'Use of nanoscale delivery systems to maintain

synergistic drug ratios in vivo', *Expert Opinion on Drug Delivery*, 7(12), pp. 1329–1341. doi: 10.1517/17425247.2010.538678.

Ding, T. *et al.* (2011) 'Rapid repair of rat sciatic nerve injury using a nanosilver-embedded collagen scaffold coated with laminin and fibronectin', *Regenerative Medicine*, 6(4), pp. 437–447. doi: 10.2217/rme.11.39.

Discher, D. E., Janmey, P. and Wang, Y. (2005) 'Tissue Cells Feel and Respond to the Stiffness of Their Substrate', *Materials and Biology*, 310(5751), pp. 1139–1143.

Dobić, S. N., Filipović, J. M. and Tomić, S. L. (2012) 'Synthesis and characterization of poly(2-hydroxyethyl methacrylate/itaconic acid/poly(ethylene glycol) dimethacrylate) hydrogels', *Chemical Engineering Journal*, 179, pp. 372–380. doi: 10.1016/j.cej.2011.10.083.

Dowling, D. P. *et al.* (2011) 'Effect of Surface Wettability and Topography on the Adhesion of Osteosarcoma Cells on Plasma-modified Polystyrene.', *Journal of biomaterials applications*, 26(3), pp. 327–347. doi: 10.1177/0885328210372148.

Dreesmann, L. *et al.* (2009) 'Nerve fibroblast impact on Schwann cell behavior', *European Journal of Cell Biology*, 88(5), pp. 285–300. doi: 10.1016/j.ejcb.2009.01.001.

Drug Approval Package: Acetadote (Acetylcysteine) NDA #021539 (no date). Available at: https://www.accessdata.fda.gov/drugsatfda_docs/nda/2004/21-539_Acetadote.cfm (Accessed: 28 March 2020).

DWS LAB - XFAB (no date). Available at: http://dwslab.com/xfab/?v=d2cb7bbc0d23 (Accessed: 5 August 2018).

DWS XFAB review - plug-and-play resin 3D printer (SLA) (no date). Available at: https://www.aniwaa.com/product/3d-printers/dws-xfab/ (Accessed: 5 August 2018).

Dyck, P. J. *et al.* (1990) 'Structural alterations of nerve during cuff compression.', *Proceedings of the National Academy of Sciences of the United States of America*, 87(24), pp. 9828–9832. doi: 10.1073/pnas.87.24.9828.

Elzinga, K. *et al.* (2015) 'Brief electrical stimulation improves nerve regeneration after delayed repair in Sprague Dawley rats', *Experimental Neurology*. Elsevier Inc., 269, pp. 142–153. doi: 10.1016/j.expneurol.2015.03.022.

Emel, E. *et al.* (2011) 'Effects of insulin-like growth factor–I and platelet-rich plasma on sciatic nerve crush injury in a rat model', *Journal of Neurosurgery*, 114(2), pp. 522–528. doi: 10.3171/2010.9.JNS091928.

Entekhabi, E. *et al.* (2021) 'Fabrication and in vitro evaluation of 3D composite scaffold based on collagen/hyaluronic acid sponge and electrospun polycaprolactone nanofibers for peripheral nerve regeneration', *Journal of Biomedical Materials Research - Part A*, 109(3), pp. 300–312. doi: 10.1002/jbm.a.37023.

Evangelista, M. S. *et al.* (2015) 'Single-lumen and multi-lumen poly(ethylene glycol) nerve conduits fabricated by stereolithography for peripheral nerve regeneration in vivo', *Journal of Reconstructive Microsurgery*, 31(5), pp. 327–335. doi: 10.1055/s-0034-1395415.

Evans, G. R. (2001) 'Peripheral nerve injury: a review and approach to tissue engineered constructs.', *The Anatomical record*, 263(January), pp. 396–404. doi: 10.1002/ar.1120.

Even-Ram, S., Artym, V. and Yamada, K. M. (2006) 'Matrix Control of Stem Cell Fate', *Cell*. Cell Press, 126(4), pp. 645–647. doi: 10.1016/J.CELL.2006.08.008.

FabPro 1000 | 3D Systems (no date). Available at: https://www.3dsystems.com/3d-printers/fabpro-1000 (Accessed: 5 August 2018).

FDA Briefing Document NDA 021945 Hydroxyprogesterone Caproate Injection (trade name Makena) Bone, Reproductive, and Urologic Drugs Advisory Committee (BRUDAC) Meeting (2019).

Flanagan, L. a *et al.* (2002) 'Neurite branching on deformable substrates.', *Neuroreport*, 13(18), pp. 2411–2415. doi: 10.1097/00001756-200212200-00007.

Form 2: Desktop Stereolithography (SLA) 3D Printer | Formlabs (no date). Available at: https://formlabs.com/3d-printers/form-2/ (Accessed: 5 August 2018).

Francisco, U. of C. S. (2019) *Serum progesterone*. Available at: https://www.ucsfhealth.org/medical-tests/serum-progesterone (Accessed: 26 September 2021).

Frostick, S. P., Yin, Q. and Kemp, G. J. (1998) 'Schwann cells, neurotrophic factors, and peripheral nerve regeneration', *Microsurgery*, 18(7), pp. 397–405. doi: 10.1002/(SICI)1098-2752(1998)18:7<397::AID-MICR2>3.0.CO;2-F.

Fu, Q., Hue, J. and Li, S. (2007) 'Nonsteroidal Anti-Inflammatory Drugs Promote Axon Regeneration via RhoA Inhibition', *Journal of Neuroscience*, 27(15), pp. 4154–4164. doi: 10.1523/JNEUROSCI.4353-06.2007.

Fujita, K., Lazarovici, P. and Guroff, G. (1989) 'Regulation of the differentiation of PC12 pheochromocytoma cells', *Environmental Health Perspectives*, 80, pp. 127–142. doi: 10.1289/ehp.8980127.

Gaudet, A. D., Popovich, P. G. and Ramer, M. S. (2011) 'Wallerian degeneration: Gaining perspective on inflammatory events after peripheral nerve injury', *Journal of Neuroinflammation*, 8, pp. 1–13. doi: 10.1186/1742-2094-8-110.

Gaudin, R. *et al.* (2016) 'Approaches to peripheral nerve repair: Generations of biomaterial conduits yielding to replacing autologous nerve grafts in craniomaxillofacial surgery', *BioMed Research International*, 2016. doi: 10.1155/2016/3856262.

Georges, P. C. *et al.* (2006) 'Matrices with compliance comparable to that of brain tissue select neuronal over glial growth in mixed cortical cultures.', *Biophysical journal*. Elsevier, 90(8), pp. 3012–3018. doi: 10.1529/biophysj.105.073114.

Good, D. W. and George, T. (2001) 'Neurotrophin-3 inhibits HCO3- absorption via a cAMP-dependent pathway in renal thick ascending limb', *American Journal of Physiology - Cell Physiology*, 281(6 50-6), pp. 1804–1811. doi: 10.1152/ajpcell.2001.281.6.c1804.

Gordon, T. (2014) 'Neurotrophic factor expression in denervated motor and sensory Schwann cells: Relevance to specificity of peripheral nerve regeneration', *Experimental Neurology*. Elsevier Inc., 254, pp. 99–108. doi: 10.1016/j.expneurol.2014.01.012.

Greene, L. A. and Tischler, A. S. (1976) 'Establishment of a noradrenergic clonal line of rat adrenal pheochromocytoma cells which respond to nerve growth factor', *Proceedings of the*

National Academy of Sciences of the United States of America, 73(7), pp. 2424–2428. doi: 10.1073/pnas.73.7.2424.

Grehan, L. *et al.* (2014) 'The development of hot melt extruded biocompatible controlled release drug delivery devices', *International Journal of Polymeric Materials and Polymeric Biomaterials*, 63(9), pp. 476–485. doi: 10.1080/00914037.2013.854218.

Griffin, J. W. *et al.* (2013) 'Peripheral Nerve Repair and Reconstruction', *Journal of Bone and Joint Surgery America*, 95, pp. 2144–2151.

Grinsell, D. and Keating, C. P. (2014) 'Peripheral nerve reconstruction after injury: a review of clinical and experimental therapies.', *BioMed research international*. Hindawi Publishing Corporation, 2014, p. 698256. doi: 10.1155/2014/698256.

Gu, J. *et al.* (2012) 'Surgical repair of a 30 mm long human median nerve defect in the distal forearm by implantation of a chitosan–PGA nerve guidance conduit', *Journal of tissue engineering and regenerative medicine*, 6, pp. 163–168. doi: 10.1002/term.

Gu, X. *et al.* (2011) 'Construction of tissue engineered nerve grafts and their application in peripheral nerve regeneration', *Progress in Neurobiology*. Elsevier Ltd, 93(2), pp. 204–230. doi: 10.1016/j.pneurobio.2010.11.002.

Gu, X., Ding, F. and Williams, D. F. (2014) 'Neural tissue engineering options for peripheral nerve regeneration', *Biomaterials*, 35(24), pp. 6143–6156. doi: 10.1016/j.biomaterials.2014.04.064.

Guerra-Ponce, W. L. *et al.* (2016) 'In vitro evaluation of sustained released matrix tablets containing ibuprofen: A model poorly water-soluble drug', *Brazilian Journal of Pharmaceutical Sciences*, 52(4), pp. 751–760. doi: 10.1590/S1984-82502016000400020.

Habibovic, P. *et al.* (2006) 'Predictive value of in vitro and in vivo assays in bone and cartilage repair--what do they really tell us about the clinical performance?', *Advances in Experimental Medicine and Biology*, 585, pp. 327–360.

Hadjipanayi, E., Mudera, V. and Brow, R. A. (2009) 'Close dependence of fibroblast proliferation on collagen scaffold matrix stiffness', *Journal of tissue engineering and regenerative medicine*, 13(2), pp. 512–520. doi: 10.1002/term.

Haftek, J. and Thomas, P. K. (1968) 'Electron-microscope observations on the effects of localized crush injuries on the connective tissues of peripheral nerve.', *Journal of anatomy*, 103(2), pp. 233–243.

Han, D. K. and Hubbell, J. a (1997) 'Synthesis of Polymer Network Scaffolds from l -Lactide and Poly(ethylene glycol) and Their Interaction with Cells', *Macromolecules*, 30(97), pp. 6077–6083. doi: 10.1021/ma970302u.

Hardy, J. G., Lee, J. Y. and Schmidt, C. E. (2013) 'Biomimetic conducting polymer-based tissue scaffolds', *Current opinion in biotechnology*, 24(5), pp. 847–854. doi: 10.1016/j.copbio.2013.03.011.

Healy, A. V. *et al.* (2019) 'Additive manufacturing of personalized pharmaceutical dosage forms via stereolithography', *Pharmaceutics*, 11(645), pp. 1–20. doi: 10.3390/pharmaceutics11120645.

Hill-West, J. L. *et al.* (1994) 'Prevention of postoperative adhesions in the rat by in situ photopolymerization of bioresorbable hydrogel barriers', *Obstetrics and Gynecology*, 83(1), pp. 59–64.

Hiraga, A. *et al.* (2006) 'Rho-kinase inhibition enhances axonal regeneration after peripheral nerve injury.', *Journal of the peripheral nervous system : JPNS*, 11(3), pp. 217–24. doi: 10.1111/j.1529-8027.2006.00091.x.

Hoffner, S. E., Svenson, S. B. and Källenius, G. (1987) 'Synergistic effects of antimycobacterial drag combinations on Mycobacterium avium complex determined radiometrically in liquid medium', *European Journal of Clinical Microbiology*, 6(5), pp. 530–535. doi: 10.1007/BF02014241.

Hong, M. H. *et al.* (2018) 'Controlled Release of Growth Factors from Multilayered Fibrous Scaffold for Functional Recoveries in Crushed Sciatic Nerve', *ACS Biomaterials Science and Engineering*, 4(2), pp. 576–586. doi: 10.1021/acsbiomaterials.7b00801.

Houlton, J. *et al.* (2019) 'Therapeutic potential of neurotrophins for repair after brain injury: A helping hand from biomaterials', *Frontiers in Genetics*, 10(JUL). doi: 10.3389/fnins.2019.00790.

Huang, J. *et al.* (2012) 'Electrical stimulation to conductive scaffold promotes axonal regeneration and remyelination in a rat model of large nerve defect', *PloS one*, 7(6), p. e39526. doi: 10.1371/journal.pone.0039526.

Huang, L. *et al.* (2018) 'A compound scaffold with uniform longitudinally oriented guidance cues and a porous sheath promotes peripheral nerve regeneration in vivo', *Acta Biomaterialia*. Acta Materialia Inc., 68, pp. 223–236. doi: 10.1016/j.actbio.2017.12.010.

Huber, L. (2010) *Validation of analytical methods*. doi: 10.3989/gya.2002.v53.i1.295.

Hull, C. W. (1984) 'Apparatus for production of three-dimensional objects by stereolithography'. United States Patent Office. Available at: https://patents.google.com/patent/US4575330A/en (Accessed: 23 June 2018).

Hurley, D. *et al.* (2019) 'An investigation of the inter-molecular interaction, solid-state properties and dissolution properties of mixed copovidone hot-melt extruded solid dispersions', *Journal of Drug Delivery Science and Technology*. Elsevier, 53(June), p. 101132. doi: 10.1016/j.jddst.2019.101132.

Hutmacher, D. W. (2000) 'Scaffolds in tissue engineering bone and cartilage', *Biomaterials*. (Orthopaedic Polymeric Biomaterials: Applications of Biodegradables), 21(24), pp. 2529–2543. doi: 10.1016/S0142-9612(00)00121-6.

Hynes, T. (2013) *Mayfield: Anatomy of the Human Spine*. Available at: http://www.mayfieldclinic.com/PE-AnatSpine.htm#.VhJ77N9VhBc (Accessed: 5 October 2015).

Ianevski, A. *et al.* (2017) 'SynergyFinder: A web application for analyzing drug combination dose-response matrix data', *Bioinformatics*, 33(15), pp. 2413–2415. doi: 10.1093/bioinformatics/btx162.

Ibuprofen Drug Facts Label | FDA (no date). Available at: https://www.fda.gov/drugs/postmarket-drug-safety-information-patients-and-

providers/ibuprofen-drug-facts-label (Accessed: 28 March 2020).

Ide, C. (1996) 'Peripheral nerve regeneration', *Neuroscience Research*, 25(2), pp. 101–121. doi: 10.1016/S0168-0102(96)01042-5.

Ifkovits, J. L. and Burdick, J. A. (2007) 'Review: Photopolymerizable and Degradable Biomaterials for Tissue Engineering Applications', *Tissue Engineering*, 13(10), pp. 2369–2385. doi: 10.1089/ten.2007.0093.

Ilfeld, B. M., Preciado, J. and Trescot, A. M. (2016) *Novel cryoneurolysis device for the treatment of sensory and motor peripheral nerves, Expert Review of Medical Devices*. doi: 10.1080/17434440.2016.1204229.

INTEGRA (2005) 'The latest innovation in peripheral nerve protection NeuraWrap Nerve Protector', *Growth (Lakeland)*, pp. 1–4.

Invitrogen (no date) *alamarBlue assay*.

Van Irene, C. Y. and Greene, L. A. (1998) 'Prevention of PC12 cell death by N-acetylcysteine requires activation of the Ras pathway', *Journal of Neuroscience*, 18(11), pp. 4042–4049. doi: 10.1523/jneurosci.18-11-04042.1998.

Islam, A. *et al.* (2016) 'Fabrication and performance characteristics of tough hydrogel scaffolds based on biocompatible polymers', *International Journal of Biological Macromolecules*, 92, pp. 1–10. doi: 10.1016/j.ijbiomac.2016.07.010.

ISO/EN10993-5 (2009) 'Biological evaluation of medical devices', *International Standard ISO 10993-5 Biological evaluation of medical devices - Part 5: Tests for cytotoxicity: in vitro methods*, 3 Ed, p. 42.

Itai, S. *et al.* (2020) 'Cell-encapsulated chitosan-collagen hydrogel hybrid nerve guidance conduit for peripheral nerve regeneration', *Biomedical Microdevices*. Biomedical Microdevices, 22(4). doi: 10.1007/s10544-020-00536-x.

J, N. *et al.* (1998) 'Analysis of upper and lower extremity peripheral nerve injuries in a population of patients with multiple injuries', *The Journal of trauma*. J Trauma, 45(1), pp. 116–122. doi: 10.1097/00005373-199807000-00025.

Jessen, K., R, M. and Lloyd, A. (2015) 'Schwann cells: Development and Role in Nerve Repair', *Cold Spring Harbor perspectives in biology.*, 7(7), pp. 1–16. doi: 10.1101/cshperspect.a020487.

Kang, S. *et al.* (2003) 'Topical n-acetyl cysteine and genistein prevent ultraviolet-light-induced signaling that leads to photoaging in human skin in vivo', *Journal of Investigative Dermatology*. Blackwell Publishing Inc., 120(5), pp. 835–841. doi: 10.1046/j.1523-1747.2003.12122.x.

Kehoe, S., Zhang, X.F. and Boyd, D. (2012) 'FDA approved guidance conduits and wraps for peripheral nerve injury: A review of materials and efficacy', *Injury*, 43(5), pp. 553–572. doi: 10.1016/j.injury.2010.12.030.

Kehoe, S., Zhang, X. F. and Boyd, D. (2012) 'FDA approved guidance conduits and wraps for peripheral nerve injury: A review of materials and efficacy', *Injury*. Elsevier Ltd, 43(5), pp. 553–572. doi: 10.1016/j.injury.2010.12.030.

Khademhosseini, A. and Langer, R. (2007) 'Microengineered hydrogels for tissue engineering', *Biomaterials*, 28(34), pp. 5087–5092. doi: 10.1016/j.biomaterials.2007.07.021.

Khaing, Z. Z. *et al.* (2011) 'High molecular weight hyaluronic acid limits astrocyte activation and scar formation after spinal cord injury', *Journal of neural engineering*, 8(4), p. 046033. doi: 10.1088/1741-2560/8/4/046033.

Khaing, Z. Z. and Schmidt, C. E. (2012) 'Advances in natural biomaterials for nerve tissue repair', *Neuroscience letters*, 519(2), pp. 103–114. doi: 10.1016/j.neulet.2012.02.027.

Khalili, A. A. and Ahmad, M. R. (2015) 'A Review of cell adhesion studies for biomedical and biological applications', *International Journal of Molecular Sciences*, 16(8), pp. 18149–18184. doi: 10.3390/ijms160818149.

Killion, J. a. *et al.* (2013) 'Hydrogel/bioactive glass composites for bone regeneration applications: Synthesis and characterisation', *Materials Science and Engineering C*. Elsevier B.V., 33(7), pp. 4203–4212. doi: 10.1016/j.msec.2013.06.013.

Killion, J. A. *et al.* (2011) 'Mechanical properties and thermal behaviour of PEGDMA hydrogels for potential bone regeneration application', *Journal of the Mechanical Behavior of Biomedical Materials*, 4(7), pp. 1219–1227. doi: 10.1016/j.jmbbm.2011.04.004.

Killion, J. A. *et al.* (2012) 'Modulating the mechanical properties of photopolymerised polyethylene glycol-polypropylene glycol hydrogels for bone regeneration', *Journal of Materials Science*, 47(18), pp. 6577–6585. doi: 10.1007/s10853-012-6588-7.

Kim, D. H. *et al.* (1993) 'Comparison of macropore, semipermeable, and nonpermeable collagen conduits in nerve repair', *Journal of Reconstructive Microsurgery*, 9(6), pp. 415–420. doi: 10.1055/s-2007-1006750.

Kim, K. *et al.* (2010) 'Stereolithographic bone scaffold design parameters: osteogenic differentiation and signal expression.', *Tissue engineering. Part B, Reviews*, 16(5), pp. 523–39. doi: 10.1089/ten.TEB.2010.0171.

Kim, Y.-P. *et al.* (2012) 'Phosphate glass fibres promote neurite outgrowth and early regeneration in a peripheral nerve injury model.', *Journal of tissue engineering and regenerative medicine*, 9(3), pp. 236–46. doi: 10.1002/term.1626.

Kimpinski, K. and Mearow, K. (2001) 'Neurite growth promotion by nerve growth factor and insulin-like growth factor-1 in cultured adult sensory neurons: Role of phosphoinositide 3-kinase and mitogen activated protein kinase', *Journal of Neuroscience Research*, 63(6), pp. 486–499. doi: 10.1002/jnr.1043.

Kingston, R. E. *et al.* (1989) 'Synergistic effects of cis-platinum and cystosine arabinoside on ovarian carcinoma cell lines, demonstrated by dual-parameter flow cytometry', *Gynecologic Oncology*, 32(3), pp. 282–287. doi: 10.1016/0090-8258(89)90625-2.

Kiziltan, M. E. *et al.* (2007) 'Peripheral neuropathy in patients with diabetes mellitus presenting as Bell's palsy', *Neuroscience Letters*, 427, pp. 138–141. doi: 10.1016/j.neulet.2007.09.029.

Knott, E. P., Assi, M. and Pearse, D. D. (2014) 'Cyclic AMP signaling: A molecular determinant of peripheral nerve regeneration', *BioMed Research International*. Hindawi Publishing Corporation, 2014. doi: 10.1155/2014/651625.

Koenig, H. L., Gong, W. H. and Pelissier, P. (2000) 'Role of progesterone in peripheral nerve repair.', *Reviews of reproduction*, 5, pp. 189–199. doi: 10.1530/ror.0.0050189.

Koudehi, M. F. *et al.* (2014) 'Preparation and evaluation of novel nano-bioglass/gelatin conduit for peripheral nerve regeneration', *Journal of Materials Science: Materials in Medicine*, 25(2), pp. 363–373. doi: 10.1007/s10856-013-5076-1.

Kwan, M. K. *et al.* (1992) 'Strain, stress and stretch of peripheral nerve. Rabbit experiments in vitro and in vivo.', *Acta orthopaedica Scandinavica*, 63(3), pp. 267–272. doi: 10.3109/17453679209154780.

Lackington, W. A., Ryan, A. J. and O'Brien, F. J. (2017) 'Advances in Nerve Guidance Conduit-Based Therapeutics for Peripheral Nerve Repair', *ACS Biomaterials Science and Engineering*, 3(7), pp. 1221–1235. doi: 10.1021/acsbiomaterials.6b00500.

Lallo, A. *et al.* (2018) 'The combination of the PARP inhibitor olaparib and the WEE1 Inhibitor AZD1775 as a new therapeutic option for small cell lung cancer', *Clinical Cancer Research*. American Association for Cancer Research Inc., 24(20), pp. 5153–5164. doi: 10.1158/1078-0432.CCR-17-2805.

Lam, C. X. F. *et al.* (2008) 'Dynamics of in vitro polymer degradation of polycaprolactone-based scaffolds: Accelerated versus simulated physiological conditions', *Biomedical Materials*, 3(3). doi: 10.1088/1748-6041/3/3/034108.

Lambert, J. B. (1987) *Introduction to organic spectroscopy*. Macmillan.

LaPorte, R. J. (1997) *Hydrophilic Polymer Coatings for Medical Devices*. 1st edn. Edited by T. P. Company. CRC Press.

LCD Photon|3D printer|ANYCUBIC 3D Printer- Think Big, Make Bigger (no date). Available at: http://www.anycubic3d.com/products/show/1022.html (Accessed: 5 August 2018).

Leach, J. B. *et al.* (2004) 'Development of photocrosslinkable hyaluronic acid-polyethylene glycol-peptide composite hydrogels for soft tissue engineering', *Journal of biomedical materials research. Part A*, 70(1), pp. 74–82. doi: 10.1002/jbm.a.30063.

Lee, C. Y. *et al.* (2014) 'Characterization of the Network Structure of PEG Diacrylate Hydrogels Formed in the Presence of N-Vinyl Pyrrolidone', *Macromolecular Reaction Engineering*, 8, pp. 314–328. doi: 10.1002/mren.201300166.

Lee, D. C. *et al.* (2017) 'Neural stem cells promote nerve regeneration through IL12-induced Schwann cell differentiation', *Molecular and Cellular Neuroscience*. Elsevier B.V., 79, pp. 1–11. doi: 10.1016/j.mcn.2016.11.007.

Lee, H. J. *et al.* (2006) 'Collagen mimetic peptide-conjugated photopolymerizable PEG hydrogel', *Biomaterials*, 27(30), pp. 5268–5276. doi: 10.1016/j.biomaterials.2006.06.001.

Lee, K. Y. and Mooney, D. J. (2001) 'Hydrogels for Tissue Engineering', *Chemical Reviews*, 101(7), pp. 1869–1880. doi: 10.1021/cr000108x.

Lee, S. J. *et al.* (2017) 'Fabrication of a Highly Aligned Neural Scaffold via a Table Top Stereolithography 3D Printing and Electrospinning', *Tissue Engineering - Part A*, 23(11–12), pp. 491–502. doi: 10.1089/ten.tea.2016.0353.

Lehmann, M. *et al.* (1999) 'Inactivation of rho signaling pathway promotes CNS axon

regeneration', *Journal of Neuroscience*, 19(17), pp. 7537–7547. doi: 10.1523/jneurosci.19-17-07537.1999.

Leonelli, E. *et al.* (2007) 'Progesterone and its derivatives are neuroprotective agents in experimental diabetic neuropathy: A multimodal analysis', *Neuroscience*, 144(4), pp. 1293–1304. doi: 10.1016/j.neuroscience.2006.11.014.

Li, R. *et al.* (2020) 'Growth factors-based therapeutic strategies and their underlying signaling mechanisms for peripheral nerve regeneration', *Acta Pharmacologica Sinica*. Springer US, (November 2019), pp. 1–12. doi: 10.1038/s41401-019-0338-1.

Ligon-Auer, S. C. *et al.* (2016) 'Toughening of photo-curable polymer networks: A review', *Polymer Chemistry*, 7(2), pp. 257–286. doi: 10.1039/c5py01631b.

Ligon, S. C. *et al.* (2017) 'Polymers for 3D Printing and Customized Additive Manufacturing', *Chemical Reviews*, 117(15), pp. 10212–10290. doi: 10.1021/acs.chemrev.7b00074.

Lin, G. *et al.* (2016) 'Brain-derived neurotrophic factor promotes nerve regeneration by activating the JAK/STAT pathway in Schwann cells', *Translational Andrology and Urology*. AME Publishing Company, 5(2), pp. 167–175. doi: 10.21037/tau.2016.02.03.

Lin, H. *et al.* (2005) 'The Effect of Cross-Linking on Gas Permeability in Cross-Linked Poly(Ethylene Glycol Diacrylate)', *Macromolecules*, 38(20), pp. 8381–8393. doi: 10.1021/ma0510136.

Lin, H. *et al.* (2006) 'Transport and structural characteristics of crosslinked poly(ethylene oxide) rubbers', *Journal of Membrane Science*, 276(1–2), pp. 145–161. doi: 10.1016/j.aca.2006.03.068.

Liu, B. *et al.* (2019) 'Myelin sheath structure and regeneration in peripheral nerve injury repair', *Proceedings of the National Academy of Sciences of the United States of America*, 116(44), pp. 22347–22352. doi: 10.1073/pnas.1910292116.

Liu, H. M., Yang, L. H. and Yang, Y. J. (1995) 'Schwann cell properties: 3. C-fos expression, bFGF production, phagocytosis and proliferation during Wallerian degeneration.', *Journal of neuropathology and experimental neurology*, 54(4), pp. 487–96. Available at: http://www.ncbi.nlm.nih.gov/pubmed/7602323 (Accessed: 23 March 2020).

Liu, X., Won, Y. and Ma, P. X. (2006) 'Porogen-induced surface modification of nano-fibrous poly(l-lactic acid) scaffolds for tissue engineering', *Biomaterials*, 27(21), pp. 3980–3987. doi: 10.1016/j.biomaterials.2006.03.008.

Loshaek, S. (1955) 'Crosslinked Polymers. 11. Glass Temperatures of Copolymers of Methyl Methacrylate and Glycol Dimethacrylates"', *JOURNAL OF POLYMER SCIENCE*, XV, pp. 391–404.

Lowe, A. B. (2014) 'Thiol-ene 'click'/coupling chemistry and recent applications in polymer and materials synthesis and modification', *Polymer*, 55(22), pp. 5517–5549. doi: 10.1016/j.polymer.2014.08.015.

Lu, H., Stansbury, J. W. and Bowman, C. N. (2005) 'Impact of Curing Protocol on Conversion and Shrinkage Stress', *Journal of Dental Research*, 84(9), pp. 822–826. doi: 10.1177/154405910508400908.

Mackle, J. N. *et al.* (2011) 'In vitro characterization of an electroactive carbon-nanotube-based nanofiber scaffold for tissue engineering', *Macromolecular bioscience*, 11(9), pp. 1272–1282. doi: 10.1002/mabi.201100029.

Madura, T., Tomita, K. and Terenghi, G. (2011) 'Ibuprofen improves functional outcome after axotomy and immediate repair in the peripheral nervous system', *Journal of Plastic, Reconstructive and Aesthetic Surgery*. Elsevier Ltd, 64(12), pp. 1641–1646. doi: 10.1016/j.bjps.2011.07.014.

Magalingam, K. B., Radhakrishnan, A. and Haleagrahara, N. (2016) 'Protective effects of quercetin glycosides, rutin, and isoquercetrin against 6-hydroxydopamine (6-OHDA)-induced neurotoxicity in rat pheochromocytoma (PC-12) cells', *International Journal of Immunopathology and Pharmacology*, 29(1), pp. 30–39. doi: 10.1177/0394632015613039.

Malcolm, R. K. *et al.* (2005) 'Long-term, controlled release of the HIV microbicide TMC120 from silicone elastomer vaginal rings', *Journal of Antimicrobial Chemotherapy*. Narnia, 56(5), pp. 954–956. doi: 10.1093/jac/dki326.

Manoukian, S., O. *et al.* (2019) 'Aligned Microchannel Polymer-Nanotube Composites for Peripheral Nerve Regeneration: Small Molecule Drug Delivery', *J Control Release*, 296, pp. 54–67. doi: 10.1016/j.jconrel.2019.01.013.Aligned.

Manzo, M. and Ioppolo, T. (2015) 'Untethered photonic sensor for wall pressure measurement.', *Optics letters*, 40(10), pp. 2257–60. doi: 10.1364/OL.40.002257.

Marcelo, G. *et al.* (2016) 'Lignin inspired PEG hydrogels for drug delivery', *Materials Today Communications*, 7, pp. 73–80. doi: 10.1016/j.mtcomm.2016.04.004.

Marques, M. R. C., Loebenberg, R. and Almukainzi, M. (2011) 'Simulated biological fluids with possible application in dissolution testing', *Dissolution Technologies*, 18(3), pp. 15–28. doi: 10.1002/jps.23029.

Martin, E. L. (1959) 'Photopolymerisable compositions and elements and process of making reliefs therefrom'. United States: United States Patent Office.

Martinez, P. R. *et al.* (2017) 'Fabrication of drug-loaded hydrogels with stereolithographic 3D printing', *International Journal of Pharmaceutics*. Elsevier B.V., 532(1), pp. 313–317. doi: 10.1016/j.ijpharm.2017.09.003.

Maruo, S. and Ikuta, K. (2002) 'Submicron stereolithography for the production of freely movable mechanisms by using single-photon polymerization', *Sensors and Actuators, A: Physical*, 100(1), pp. 70–76. doi: 10.1016/S0924-4247(02)00043-2.

Mauricio, D., Alonso, N. and Gratacòs, M. (2020) 'Chronic Diabetes Complications: The Need to Move beyond Classical Concepts', *Trends in Endocrinology & Metabolism*. Elsevier Current Trends, 31(4), pp. 287–295. doi: 10.1016/J.TEM.2020.01.007.

Mehta, Rashi and Mehta, Rupal (2019) 'Hydrophilic Polymer Embolism: Implications for Manufacturing, Regulation, and Postmarket Surveillance of Coated Intravascular Medical Devices', *Journal of Patient Safety*, p. 1. doi: 10.1097/PTS.0000000000000473.

Mellott, M. B., Searcy, K. and Pishko, M. V. (2001) 'Release of protein from highly cross-linked hydrogels of poly(ethylene glycol) diacrylate fabricated by UV polymerization', *Biomaterials*, 22(9), pp. 929–941.

Menczel, J. D. and Prime, R. B. (2009) *Thermal analysis of Polymers*. First, *John Wiley & Sons Inc.* First. Edited by J. D. Menczel and R. B. Prime. New Jersey: John Wiley & Sons, Inc.

Meth, J. L. and Schoenfeld, A. R. (2019) 'Higher percentage of horse serum in culture media blocks attachment of PC12 cells', *Biotechniques*. doi: 10.1080/13518040701205365.

Miguez-Pacheco, V., Hench, L. L. and Boccaccini, A. R. (2015) 'Bioactive glasses beyond bone and teeth: Emerging applications in contact with soft tissues', *Acta Biomaterialia*. Acta Materialia Inc., 13, pp. 1–15. doi: 10.1016/j.actbio.2014.11.004.

Miller, F. A. and Wlkins, C. H. (1952) 'Infrared Spectra and Characteristic Frequencies of Inorganic Ions', *Analytical Chemistry*, 24(8), pp. 1253–1294. doi: 10.1016/j.nimb.2010.12.005.

Moai - Affordable Laser SLA Printer – Peopoly (no date). Available at: https://peopoly.net/products/moai (Accessed: 5 August 2018).

Mobasseri, A. *et al.* (2015) 'Polymer scaffolds with preferential parallel grooves enhance nerve regeneration.', *Tissue engineering. Part A*, 21(5–6), pp. 1152–62. doi: 10.1089/ten.TEA.2014.0266.

Moffat, A. C. *et al.* (2011) *Clarke's Analysis of Drugs and Poison*, *Clarke's Analysis and Poisons- 4th edition*. doi: 10.1300/J123v27n02_07.

Monterroza, D. and León, L. P. De (no date) *Development of a USP Apparatus 3 Dissolution Method for Progesterone Soft Gelatin Capsules . Development of a USP Apparatus 3 Dissolution Method for Progesterone Soft Gelatin Capsules .*

Morgan, C. R., Magnotta, F. and Ketley, A. D. (1977) 'Thiol/Ene Photocurable Polymers.', *J Polym Sci Polym Chem Ed*, 15(3), pp. 627–645. doi: 10.1002/pol.1977.170150311.

Moroder, P. *et al.* (2011) 'Material properties and electrical stimulation regimens through polycaprolactone fumarate-polypyrrole scaffolds as potential conductive nerve conduits', *Acta biomaterialia*, 14(4), pp. 384–399. doi: 10.1080/10810730902873927.Testing.

Mueller, J. and Shea, K. (2015) 'The effect of build orientation on the mechanical properties in inkjet 3D printing', in *Proceedings - 26th Annual International Solid Freeform Fabrication Symposium - An Additive Manufacturing Conference, SFF 2015*, pp. 983–992.

Nair, L. S. and Laurencin, C. T. (2007) 'Biodegradable polymers as biomaterials', *Progress in Polymer Science*, 32(8), pp. 762–798. doi: 10.1016/j.progpolymsci.2007.05.017.

Narendra, N. *et al.* (2012) 'SIMULTANEOUS ESTIMATION OF FAMOTIDINE AND IBUPROFEN IN PURE AND PHARMACEUTICAL DOSAGE FORM BY UV-VIS SPECTROSCOPY', *IRJP*, (4). Available at: www.irjponline.com (Accessed: 30 March 2020).

Nawrotek, K. *et al.* (2016) 'Chitosan-based hydrogel implants enriched with calcium ions intended for peripheral nervous tissue regeneration', *Carbohydrate Polymers*, 136, pp. 764–771. doi: 10.1016/j.carbpol.2015.09.105.

Nectow, A. R., Marra, K. G. and Kaplan, D. L. (2012) 'Biomaterials for the development of peripheral nerve guidance conduits', *Tissue engineering. Part B, Reviews*, 18(1), pp. 40–50. doi: 10.1089/ten.TEB.2011.0240.

Nguyen, K. T. and West, J. L. (2002) 'Photopolymerizable hydrogels for tissue engineering

applications', *Biomaterials*, 23(October 2001), pp. 4307–4314. doi: 10.1016/S0142-9612(02)00175-8.

Nguyen, Q. T., Sanes, J. R. and Lichtman, J. W. (2002) 'Pre-existing pathways promote precise projection patterns.', *Nature neuroscience*, 5(9), pp. 861–867. doi: 10.1038/nn905.

O'Brien, A. K. and Bowman, C. N. (2006) 'Impact of oxygen on photopolymerization kinetics and polyme structure', *Macromolecules*, 39(7), pp. 2501–2506. doi: 10.1021/ma051863l.

O'Brien, J. *et al.* (2000) 'Investigation of the Alamar Blue (resazurin) fluorescent dye for the assessment of mammalian cell cytotoxicity', *European Journal of Biochemistry*, 267(17), pp. 5421–5426. doi: 10.1046/j.1432-1327.2000.01606.x.

Omidian, H. *et al.* (1994) 'Swelling and crosslink density measurements for hydrogels', *Iranian journal of polymer science & technology*, 3(2), pp. 115–119.

Önger, M. E. *et al.* (2017) 'The role of growth factors in nerve regeneration', *Drug discoveries & therapeutics*, 10(6), pp. 285–291. doi: 10.5582/ddt.2016.01058.

Otitoju, T. A., Ahmad, A. L. and Ooi, B. S. (2018) 'Recent advances in hydrophilic modification and performance of polyethersulfone (PES) membrane *via* additive blending', *RSC Advances*. The Royal Society of Chemistry, 8(40), pp. 22710–22728. doi: 10.1039/C8RA03296C.

Pacios, I. E. *et al.* (2007) 'Correlation of swelling and crosslinking density with the composition of the reacting mixture employed in radical crosslinking copolymerization', *Journal of Applied Polymer Science*, 103(1), pp. 263–269. doi: 10.1002/app.25269.

Palispis, W. A. and Gupta, R. (2017) 'Surgical repair in humans after traumatic nerve injury provides limited functional neural regeneration in adults', *Experimental Neurology*. Elsevier Inc., 290, pp. 106–114. doi: 10.1016/j.expneurol.2017.01.009.

Park, H. *et al.* (2009) 'Effect of Swelling Ratio of Intectable Hydrogel Composites on Chondrongenix Differentiation of Encapsculated Rabbit Marrow Mesenchymal Stem Cells In Vitro (Author Manuscript)', *Biomacromolecules*, 10(3), pp. 541–546. doi: 10.1021/bm801197m.Effect.

Park, J. *et al.* (2020) 'Electrically Conductive Hydrogel Nerve Guidance Conduits for Peripheral Nerve Regeneration', *Advanced Functional Materials*, 30(39), pp. 1–14. doi: 10.1002/adfm.202003759.

Pateman, C. J. *et al.* (2015) 'Nerve guides manufactured from photocurable polymers to aid peripheral nerve repair', *Biomaterials*. Elsevier, 49, pp. 77–89. doi: 10.1016/J.BIOMATERIALS.2015.01.055.

Pathak, V. M. and Navneet (2017) 'Review on the current status of polymer degradation: a microbial approach', *Bioresources and Bioprocessing*. Springer Berlin Heidelberg, 4(1). doi: 10.1186/s40643-017-0145-9.

Patterson, J. and Hubbell, J. A. (2010) 'Enhanced proteolytic degradation of molecularly engineered PEG hydrogels in response to MMP-1 and MMP-2', *Biomaterials*. Elsevier Ltd, 31(30), pp. 7836–7845. doi: 10.1016/j.biomaterials.2010.06.061.

Pedro, R. N. *et al.* (2007) 'Wire-Based Ureteral Stents: Impact on Tensile Strength and Compression', *Urology*, 70(6), pp. 1057–1059. doi: 10.1016/j.urology.2007.08.007.

Pellegrino, R. G. *et al.* (1986) 'Events in degenerating cat peripheral nerve: induction of Schwann cell S phase and its relation to nerve fibre degeneration.', *Journal of neurocytology*, 15(1), pp. 17–28. doi: 10.1007/bf02057901.

Peng, Y. *et al.* (2018) 'Beagle sciatic nerve regeneration across a 30 mm defect bridged by chitosan/PGA artificial nerve grafts', *Injury*. Elsevier Ltd, 49(8), pp. 1477–1484. doi: 10.1016/j.injury.2018.03.023.

Peppas, N. a. *et al.* (2006) 'Hydrogels in biology and medicine: From molecular principles to bionanotechnology', *Advanced Materials*, 18, pp. 1345–1360. doi: 10.1002/adma.200501612.

Peyton, S. R. *et al.* (2006) 'The use of poly(ethylene glycol) hydrogels to investigate the impact of ECM chemistry and mechanics on smooth muscle cells', *Biomaterials*, 27(28), pp. 4881–4893.

Pfister, B. J. *et al.* (2011) 'Biomedical engineering strategies for peripheral nerve repair: surgical applications, state of the art, and future challenges', *Crit Rev Biomed Eng*, 39(2), pp. 81–124. doi: 2809b9b432c80c2c,0fb500fc3eef5342 [pii].

Phenomenex Inc (1395) 'Advanced USP methods', pp. 1–88.

PICO2 HD - Products - Asiga (no date). Available at: https://www.asiga.com/products/printers/pico2_series/pico2hd/ (Accessed: 5 August 2018).

Pollyea, D. A. *et al.* (2018) 'Venetoclax with azacitidine disrupts energy metabolism and targets leukemia stem cells in patients with acute myeloid leukemia', *Nature Medicine*. Nature Publishing Group, 24(12), pp. 1859–1866. doi: 10.1038/s41591-018-0233-1.

Porcher, C. *et al.* (2011) 'Positive Feedback Regulation between gamma -Aminobutyric Acid Type A (GABA A) Receptor Signaling and Brain-derived Neurotrophic Factor (BDNF) Release in Developing Neurons *', *The Journal of Biological Chemistry*, 286(24), pp. 21667–21677. doi: 10.1074/jbc.M110.201582.

Pradeep, N. and Sreekumar, A. (2012) 'An in vitro investigation into the cytotoxicity of methyl methacrylate monomer', *The journal of contemporary dental practice*. J Contemp Dent Pract, 13(6), pp. 838–841. doi: 10.5005/JP-JOURNALS-10024-1239.

Quan, Z. and Cotton, C. (2017) 'Printing direction dependence of mechanical behavior of additively manufactured 3D preforms and composites', *Composite Structures*, 184(October), pp. 917–923. doi: 10.1016/j.compstruct.2017.10.055.

Ray, W. Z. and Mackinnon, S. E. (2010) 'Management of nerve gaps: Autografts, allografts, nerve transfers, and end-to-side neurorrhaphy', *Experimental Neurology*, 223(1), pp. 77–85. doi: 10.1016/j.expneurol.2009.03.031.

Reid, A. J. *et al.* (2009) 'N-Acetylcysteine alters apoptotic gene expression in axotomised primary sensory afferent subpopulations', *Neuroscience Research*, 65(2), pp. 148–155. doi: 10.1016/j.neures.2009.06.008.

Reynolds, M. L. and Woolf, C. J. (1993) 'Reciprocal Schwann cell-axon interactions', *Current Opinion in Neurobiology*. Elsevier Current Trends, 3(5), pp. 683–693. doi: 10.1016/0959-4388(93)90139-P.

Routley, C. E. and Ashcroft, G. S. (2009) 'Effect of estrogen and progesterone on macrophage activation during wound healing', *Wound Repair and Regeneration*, 17(1), pp. 42–50. doi: 10.1111/j.1524-475X.2008.00440.x.

de Ruiter, G. C. W. *et al.* (2009) 'Designing ideal conduits for peripheral nerve repair', *Neurosurgical focus*, 26(26), p. E5. doi: 10.1126/scisignal.2001449.Engineering.

Runge, M. B. *et al.* (2010) 'The development of electrically conductive polycaprolactone fumarate-polypyrrole composite materials for nerve regeneration', *Biomaterials*, 31(23), pp. 5916–5926. doi: 10.1016/j.biomaterials.2010.04.012.

Rydevik, B. L. *et al.* (1990) 'An in vitro mechanical and histological study of acute stretching on rabbit tibial nerve', *Journal of Orthopaedic Research*, 8(5), pp. 694–701. doi: 10.1002/jor.1100080511.

Rydholm, A. E., Bowman, C. N. and Anseth, K. S. (2005) 'Degradable thiol-acrylate photopolymers : polymerization and degradation behavior of an in situ forming biomaterial', *Biomaterials*, 26, pp. 4495–4506. doi: 10.1016/j.biomaterials.2004.11.046.

Ryu, J., Beimesch, C. F. and Lalli, T. J. (2011) '(iii) Peripheral nerve repair', *Orthopaedics and Trauma*. Elsevier Ltd, 25(3), pp. 174–180. doi: 10.1016/j.mporth.2011.03.003.

Sagare-patil, V. *et al.* (2013) 'Progesterone utilizes the PI3K-AKT pathway in human spermatozoa to regulate motility and hyperactivation but not acrosome reaction', *Molecular and Cellular Endocrinology*. Elsevier Ireland Ltd, 374(1–2), pp. 82–91. doi: 10.1016/j.mce.2013.04.005.

Salgado, A. J. *et al.* (2013) *Tissue Engineering and Regenerative Medicine*. doi: 10.1016/B978-0-12-410499-0.00001-0.

Sana, S. *et al.* (2012) 'The Netherlands Development and Validation of RP-HPLC Method for the Estimation of N- Acetylcysteine in Wet Cough Syrup', *International Journal of Drug Development and Research*, 4(2), pp. 284–293.

Sawhney, A. S. *et al.* (1994) 'Optimization of photopolymerized bioerodible hydrogel properties for adhesion prevention', *Journal of Biomedical Materials Research*, 28(7), pp. 831–838. doi: 10.1002/jbm.820280710.

Sawhney, A. S., Pathak, C. P. and Hubbell, J. A. (1993) 'Bioerodible hydrogels based on photopolymerized poly(ethylene glycol)-co-poly(.alpha.-hydroxy acid) diacrylate macromers', *Macromolecules*, 26(4), pp. 581–587. doi: 10.1021/ma00056a005.

Schlosshauer, B. *et al.* (2006) 'Synthetic nerve guide implants in humans: a comprehensive survey', *Neurosurgery*, 59(4), pp. 740–747; discussion 747-748. doi: 10.1227/01.NEU.0000235197.36789.42.

Schmidt, C. E. and Leach, J. B. (2003) 'Neural tissue engineering: strategies for repair and regeneration.', *Annual review of biomedical engineering*, 5, pp. 293–347. doi: 10.1146/annurev.bioeng.5.011303.120731.

Schulz, H. and Baranska, M. (2007) 'Identification and quantification of valuable plant substances by IR and Raman spectroscopy', *Vibrational Spectroscopy*, 43(1), pp. 13–25. doi: 10.1016/j.vibspec.2006.06.001.

Scott, R. A. and Peppas, N. A. (1999) 'Highly crosslinked, PEG-containing copolymers for sustained solute delivery', *Biomaterials*, 20(15), pp. 1371–1380.

Seddon, H. J. (1943) 'Three types of nerve injury', *Brain*, 66, pp. 238–283.

Seidlits, S. K. *et al.* (2010) 'The effects of hyaluronic acid hydrogels with tunable mechanical properties on neural progenitor cell differentiation', *Biomaterials*, 31(14), pp. 3930–3940. doi: 10.1016/j.biomaterials.2010.01.125.

Seladi-Schulman, J. and Kay, C. (2020) *Progesterone Function: Chart of Levels, Effects of High, Low Levels*. Available at: https://www.healthline.com/health/progesterone-function#high-progesterone (Accessed: 26 September 2021).

Sensenbrenner, M., Lucas, M. and Deloulme, J. C. (1997) 'Expression of two neuronal markers, growth-associated protein 43 and neuron-specific enolase, in rat glial cells', *Journal of Molecular Medicine*. Springer, pp. 653–663. doi: 10.1007/s001090050149.

Shabir, G. A. (2003) 'Validation of high-performance liquid chromatography methods for pharmaceutical analysis', *Journal of Chromatography A*, 987(1–2), pp. 57–66. doi: 10.1016/s0021-9673(02)01536-4.

Shabir, G. A. (2004) 'A Practical Approach to Validation of HPLC Methods Under Current Good Manufacturing Practices', *J. Validation Technol.*, 10(3), pp. 210–218. Available at: https://pdfs.semanticscholar.org/ccc9/0da2d890281550d6ea6ef5d3e7b37dfc4a4b.pdf.

Sharebot Antares - Sharebot (no date). Available at: https://www.sharebot.it/index.php/sharebot-antares/?lang=en (Accessed: 5 August 2018).

Sharebot Antares review - professional SLA 3D printer (stereolithography) (no date). Available at: https://www.aniwaa.com/product/3d-printers/sharebot-antares/ (Accessed: 5 August 2018).

Shih, H. and Lin, C. (2012) 'Crosslinking and degradation of step-growth hydrogels formed by thiol-ene photo-click chemistry', *Biomacromolecules*, 13(7), pp. 1–28. doi: 10.1038/jid.2014.371.

Shin, Y. K. *et al.* (2013) 'The Neuregulin-Rac-MKK7 pathway regulates antagonistic c-jun/Krox20 expression in Schwann cell dedifferentiation', *Glia*. John Wiley & Sons, Ltd, 61(6), pp. 892–904. doi: 10.1002/glia.22482.

Shoichet, M. S. *et al.* (2008) 'Strategies for regeneration and repair in the injured central nervous system', in Reichart, W. F. (ed.) *Indwelling Neural Implants: Strategies for Contending with the In Vivo Environment*. Boca Raton (Florida): CRC Press, pp. 221–235.

Silverstein, R. M. and Webster (1998) *Spectrometric Identification of Organic Compounds*. Sixth. New York: John Wiley & Sons, Inc.

Skoog, S. A., Goering, P. L. and Narayan, R. J. (2014) 'Stereolithography in tissue engineering', *Journal of Materials Science: Materials in Medicine*, 25(3), pp. 845–856. doi: 10.1007/s10856-013-5107-y.

Stejny, J. (1996) 'The effect of crosslinking on the glass transition temperature and the density of diethylene glycol bis(allylcarbonate) polymer networks', *Polymer Bulletin*, 36, pp. 617–621.

Stoddard, S. D. *et al.* (1945) 'Process of Photopolymerisation'. United States of America: United States Patent Office.

Stoddard, S. D. *et al.* (1962) 'Treatment of Diazo-sensitised lithographic plates'. United States of America: United States Patent Office.

Stoddard, S. D. *et al.* (1969) 'Solvent Development of photopolymerised layers'. United states: United States Patent Office.

Stoll, G., Jander, S. and Myers, R. R. (2002) 'Degeneration and regeneration of the peripheral nervous system: From Augustus Waller's observations to neuroinflammation', *Journal of the Peripheral Nervous System*, 7(1), pp. 13–27. doi: 10.1046/j.1529-8027.2002.02002.x.

Stoll, G. and Muller, H. W. (1999) 'Nerve Injury, Axonal Degeneration and Neural Regeneration: Basic Insights', *Brian Pathology*, 325, pp. 313–325.

Suh, K. Y. and Jon, S. (2005) 'Control over wettability of polyethylene glycol surfaces using capillary lithography', *Langmuir*, 21(15), pp. 6836–6841. doi: 10.1021/la050878+.

Sulaiman, W. and Gordon, T. (2013) 'Neurobiology of peripheral nerve injury, regeneration, and functional recovery: From bench top research to bedside application', *Ochsner Journal*, 13(1), pp. 100–108.

Sulkowski, P. L. *et al.* (2017) '2-Hydroxyglutarate produced by neomorphic IDH mutations suppresses homologous recombination and induces PARP inhibitor sensitivity', *Science Translational Medicine*, 9(375). doi: 10.1126/scitranslmed.aal2463.

Sunderland, S. (1951) 'A classification of peripheral nerve injuries producing loss of function', *Oxford Journals*, (3), pp. 491–516.

Suri, S. *et al.* (2011) 'Solid freeform fabrication of designer scaffolds of hyaluronic acid for nerve tissue engineering', *Biomedical microdevices*, 13(6), pp. 983–993. doi: 10.1007/s10544-011-9568-9.

Suzuki, K., Kadowaki, A. and Tamaoki, B. (1980) 'A rapid measurement of AΔ5-3β-hydroxysteroid dehydrogenase activity coupled with Δ4–Δ5 isomerase by a high pressure liquid chromatography', *Journal of Endocrinological Investigation: Official Journal of the Italian Society of Endocrinology*, 3(4), pp. 441–444. doi: 10.1007/BF03349387.

TA Instruments (1997) 'Measurement of the Glass Transition Temperature Using Dynamic Mechanical Analysis', p. 1.

Tan, B. *et al.* (2016) 'A versatile fluorescent biosensor based on target-responsive graphene oxide hydrogel for antibiotic detection', *Biosensors and Bioelectronics*, 83, pp. 267–273. doi: 10.1016/j.bios.2016.04.065.

Taylor, C. A. *et al.* (2008) 'The incidence of peripheral nerve injury in extremity trauma', *American Journal of Physical Medicine and Rehabilitation*, 87(5), pp. 381–385. doi: 10.1097/PHM.0b013e31815e6370.

The United States Pharmacopeia (2015) 'USP general chapter <621> Chromatography', in *Usp40-Nf35*, pp. 424–434.

Toh, W. S. and Loh, X. J. (2014) 'Advances in hydrogel delivery systems for tissue regeneration', *Materials Science & Engineering. C, Materials for Biological Applications*, 45,

pp. 690–697. doi: 10.1016/j.msec.2014.04.026.

Van Tomme, S. R., Storm, G. and Hennink, W. E. (2008) 'In situ gelling hydrogels for pharmaceutical and biomedical applications', *International Journal of Pharmaceutics*, 355(1–2), pp. 1–18. doi: 10.1016/j.ijpharm.2008.01.057.

Topp, K. S. and Boyd, B. S. (2006) 'Structure and biomechanics of peripheral nerves: nerve responses to physical stresses and implications for physical therapist practice.', *Physical therapy*, 86(1), pp. 92–109.

U.S. Pharmacopoeial Convention (2011) '(905) Uniformity of Dosage Units. Stage 6 Harmonization.', 3, pp. 4–6. doi: 10.1128/AEM.02374-10.

USP (2008) *USP 31 Official Monographs Ibuprofen 1*.

USP (no date a) *USP Monographs: Acetylcysteine*. Available at: http://www.pharmacopeia.cn/v29240/usp29nf24s0_m750.html (Accessed: 22 July 2018).

USP (no date b) *USP Monographs: Progesterone*, *Pharmacopeia online*. Available at: http://www.uspbpep.com/usp31/v31261/usp31nf26s1_m69870.asp (Accessed: 13 February 2020).

Vernon, B. *et al.* (2003) 'Water-borne, in situ crosslinked biomaterials from phase-segregated precursors.', *Journal of biomedical materials research. Part A*, 64, pp. 447–456. doi: 10.1002/jbm.a.10369.

Vijayavenkataraman, S. (2020) 'Nerve guide conduits for peripheral nerve injury repair: A review on design, materials and fabrication methods', *Acta Biomaterialia*. Elsevier Ltd, 106, pp. 54–69. doi: 10.1016/j.actbio.2020.02.003.

Wang, H. B. *et al.* (2009) 'Creation of highly aligned electrospun poly-L-lactic acid fibers for nerve regeneration applications', *Journal of Neural Engineering*, 6(1). doi: 10.1088/1741-2560/6/1/016001.

Wang, J. *et al.* (2016) 'Stereolithographic (SLA) 3D printing of oral modified-release dosage forms', *International Journal of Pharmaceutics*. Elsevier B.V., 503(1–2), pp. 207–212. doi: 10.1016/j.ijpharm.2016.03.016.

Wang, L. *et al.* (2015) 'Hydrogel-based methods for engineering cellular microenvironment with spatiotemporal gradients', *Critical Reviews in Biotechnology*, pp. 1–13. doi: 10.3109/07388551.2014.993588.

Wang, T. *et al.* (2013) 'N-Acetylcysteine and allopurinol up-regulated the Jak/STAT3 and PI3K/Akt pathways via adiponectin and attenuated myocardial postischemic injury in diabetes', *Free Radical Biology and Medicine*. Elsevier, 63, pp. 291–303. doi: 10.1016/j.freeradbiomed.2013.05.043.

Wang, Z.-H. *et al.* (2018) 'Novel 3D Neuron Regeneration Scaffolds Based on Synthetic Polypeptide Containing Neuron Cue', *Macromolecular Bioscience*, 18(3), p. 1700251. doi: 10.1002/mabi.201700251.

Wei, Z. *et al.* (2003) 'Olanzapine protects PC12 cells from oxidative stress induced by hydrogen peroxide', *Journal of Neuroscience Research*, 73(3), pp. 364–368. doi: 10.1002/jnr.10668.

Welin, D. *et al.* (2009) 'Effects of N-acetyl-cysteine on the survival and regeneration of sural sensory neurons in adult rats', *Brain Research*. Elsevier B.V., 1287, pp. 58–66. doi: 10.1016/j.brainres.2009.06.038.

Wenzel, R. N. (1936) 'Resistance of solid surfaces to wetting by water', *Industrial and Engineering Chemistry*, 28(8), pp. 988–994. doi: 10.1021/ie50320a024.

West, J. L. and Hubbell, J. a (1995) 'Photopolymerized hydrogel materials for drug delivery applications', *Reactive Polymers*, 25, pp. 139–147. doi: 10.1016/0923-1137(94)00096-N.

Van De Wetering, P. *et al.* (2005) 'Poly(ethylene glycol) hydrogels formed by conjugate addition with controllable swelling, degradation, and release of pharmaceutically active proteins', *Journal of Controlled Release*, 102, pp. 619–627. doi: 10.1016/j.jconrel.2004.10.029.

Whitley, D. *et al.* (2017) 'In-office fabrication of dental implant surgical guides using desktop stereolithographic printing and implant treatment planning software: A clinical report', *Journal of Prosthetic Dentistry*. Editorial Council for the Journal of Prosthetic Dentistry, 118(3), pp. 256–263. doi: 10.1016/j.prosdent.2016.10.017.

WHO | Essential Medicines List and WHO Model Formulary (2017) *WHO*. World Health Organization. Available at: https://www.who.int/selection_medicines/list/en/ (Accessed: 28 March 2020).

Willand, M. P. *et al.* (2016) 'Electrical Stimulation to Promote Peripheral Nerve Regeneration', *Neurorehabilitation and Neural Repair*, 30(5), pp. 490–496. doi: 10.1177/1545968315604399.

Willison, H. J., Jacobs, B. C. and van Doorn, P. A. (2016) 'Guillain-Barré syndrome', *The Lancet*. Elsevier, 388(10045), pp. 717–727. doi: 10.1016/S0140-6736(16)00339-1.

Wong, R. S. H., Ashton, M. and Dodou, K. (2015) 'Effect of crosslinking agent concentration on the properties of unmedicated hydrogels', *Pharmaceutics*, 7(3), pp. 305–319. doi: 10.3390/pharmaceutics7030305.

Wu, Y. H. *et al.* (2010) 'Water uptake, transport and structure characterization in poly(ethylene glycol) diacrylate hydrogels', *Journal of Membrane Science*, 347(1–2), pp. 197–208. doi: 10.1016/j.memsci.2009.10.025.

Xie, H. *et al.* (2015) 'A Silk Sericin/Silicone Nerve Guidance Conduit Promotes Regeneration of a Transected Sciatic Nerve', *Advanced Healthcare Materials*, 4(15), pp. 2195–2205. doi: 10.1002/adhm.201500355.

Xu, H., Holzwarth, Jeremy M, *et al.* (2014) 'Conductive PPY/PDLLA conduit for peripheral nerve regeneration', *Biomaterials*, 35(1), pp. 225–235. doi: 10.1016/j.biomaterials.2013.10.002.

Xu, H., Holzwarth, Jeremy M., *et al.* (2014) 'Conductive PPY/PDLLA conduit for peripheral nerve regeneration', *Biomaterials*. Elsevier Ltd, 35(1), pp. 225–235. doi: 10.1016/j.biomaterials.2013.10.002.

Yadav, B. *et al.* (2015) 'Searching for Drug Synergy in Complex Dose-Response Landscapes Using an Interaction Potency Model', *Computational and Structural Biotechnology Journal*. Elsevier B.V., 13, pp. 504–513. doi: 10.1016/j.csbj.2015.09.001.

Yao, L. *et al.* (2010) 'Controlling dispersion of axonal regeneration using a multichannel collagen nerve conduit', *Biomaterials*. Elsevier Ltd, 31(22), pp. 5789–5797. doi: 10.1016/j.biomaterials.2010.03.081.

Ye, W. *et al.* (2020) '3D printing of gelatin methacrylate-based nerve guidance conduits with multiple channels', *Materials and Design*. Elsevier Ltd, 192, p. 108757. doi: 10.1016/j.matdes.2020.108757.

Yeh, C. C. *et al.* (2010) 'Timing of applying electrical stimulation is an important factor deciding the success rate and maturity of regenerating rat sciatic nerves', *Neurorehabilitation and Neural Repair*, 24(8), pp. 730–735. doi: 10.1177/1545968310376758.

Yoshii, F. *et al.* (1999) 'Electron beam crosslinked PEO and PEO/PVA hydrogels for wound dressing', *Radiation Physics and Chemistry*, 55(2), pp. 133–138. doi: 10.1016/S0969-806X(98)00318-1.

Yu, H. jun *et al.* (2010) 'Progesterone attenuates neurological behavioral deficits of experimental autoimmune encephalomyelitis through remyelination with nucleus-sublocalized Olig1 protein', *Neuroscience Letters*. Elsevier Ireland Ltd, 476(1), pp. 42–45. doi: 10.1016/j.neulet.2010.03.079.

Zhang, C. G. *et al.* (2005) 'Motorneuron protection by N-acetyl-cysteine after ventral root avulsion and ventral rhizotomy', *British Journal of Plastic Surgery*, 58(6), pp. 765–773. doi: 10.1016/j.bjps.2005.04.012.

Zhao, J., Yu, P. and Dong, S. (2016) 'The influence of crosslink density on the failure behavior in amorphous polymers by molecular dynamics simulations', *Materials*, 9(4). doi: 10.3390/ma9040234.

Zhong, S.-P. (1997) 'Method of providing a substrate with hydrophilic coating and substrates, particularly medical devices, provided with such coatings'. United States Patent. Available at: https://patents.google.com/patent/US5702754A/en (Accessed: 31 May 2019).

Zhou, J. *et al.* (2013) 'Influence of thiol and ene functionalities on thiol-ene networks: Photopolymerization, physical, mechanical, and optical properties', *Polymer Testing*. Elsevier Ltd, 32(3), pp. 608–616. doi: 10.1016/j.polymertesting.2013.01.013.

Zhou, Y. *et al.* (2003) 'Nonsteroidal Anti-Inflammatory Drugs Can Lower Amyloidogenic A 42 by Inhibiting Rho', *Science*, 302(5648), pp. 1215–1217. doi: 10.1126/science.1090154.

Zhu, C., Ninh, C. and Bettinger, C. J. (2014) 'Photoreconfigurable polymers for biomedical applications: chemistry and macromolecular engineering', *Biomacromolecules*, 15(10), pp. 3474–3494. doi: 10.1021/bm500990z.

Zochodne, D. W. (2012) 'The challenges and beauty of peripheral nerve regrowth', *Journal of the Peripheral Nervous System*, 17(1), pp. 1–18. doi: 10.1111/j.1529-8027.2012.00378.x.

Zustiak, S. P. *et al.* (2013) 'Hydrolytically degradable Poly(ethylene glycol) hydrogel scaffolds as a cell delivery vehicle: characterization of PC12 cell response', *Biotechnology Progress*, 29(5), pp. 1255–1264. doi: 10.1002/btpr.1761.

Appendix
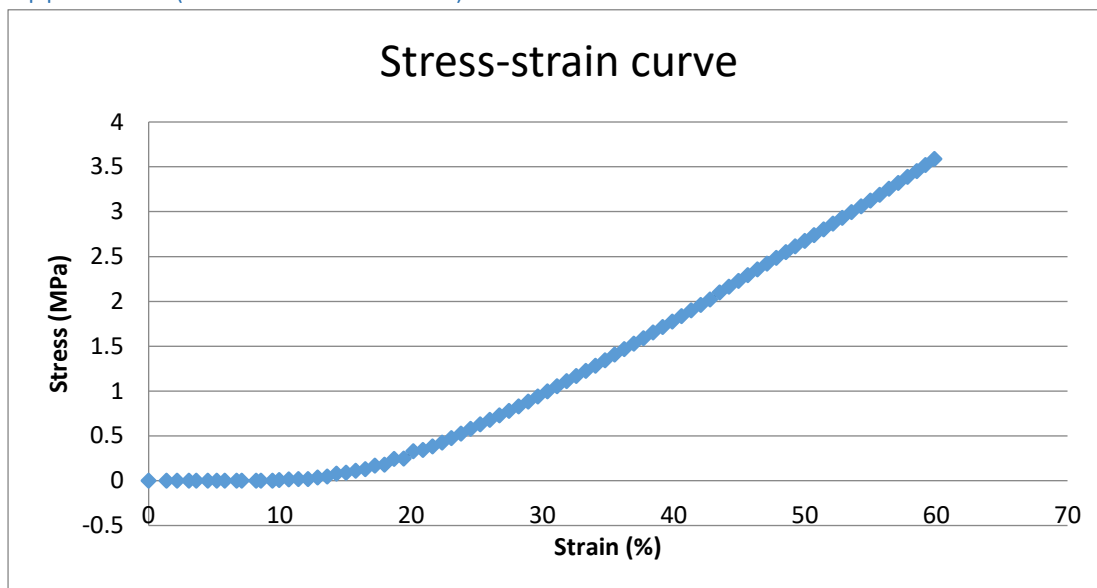
Figure A.1 Sample compressive Stress-strain curve for Unhydrated 100 wt. % PEGDMA, with percentage strain on the x-axis and stress (MPa) on the Y-axis
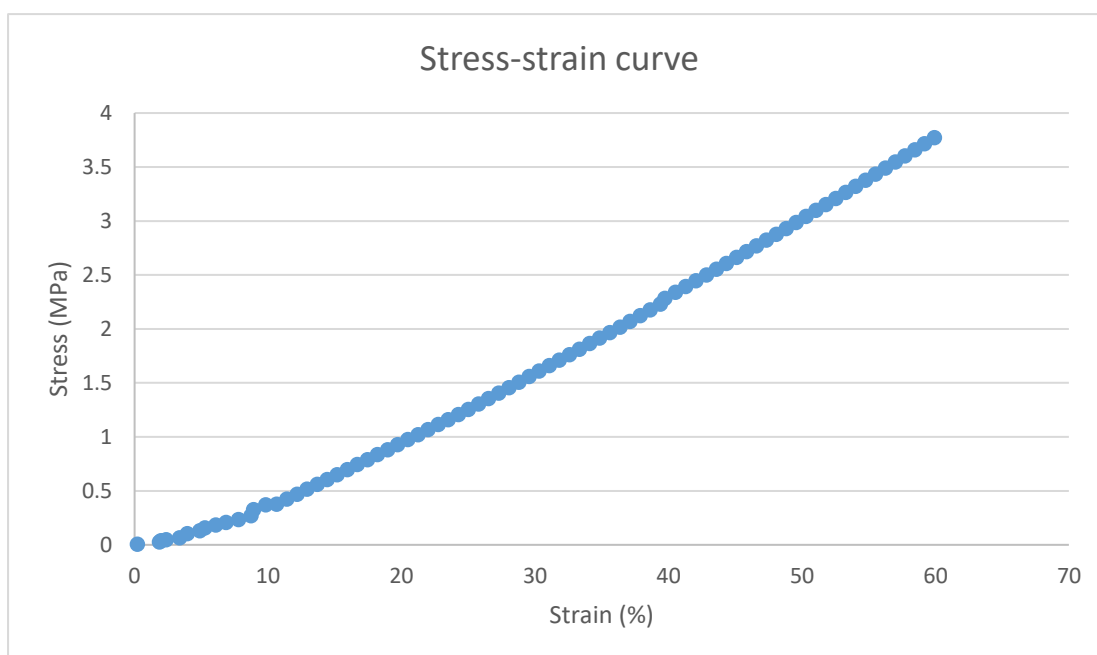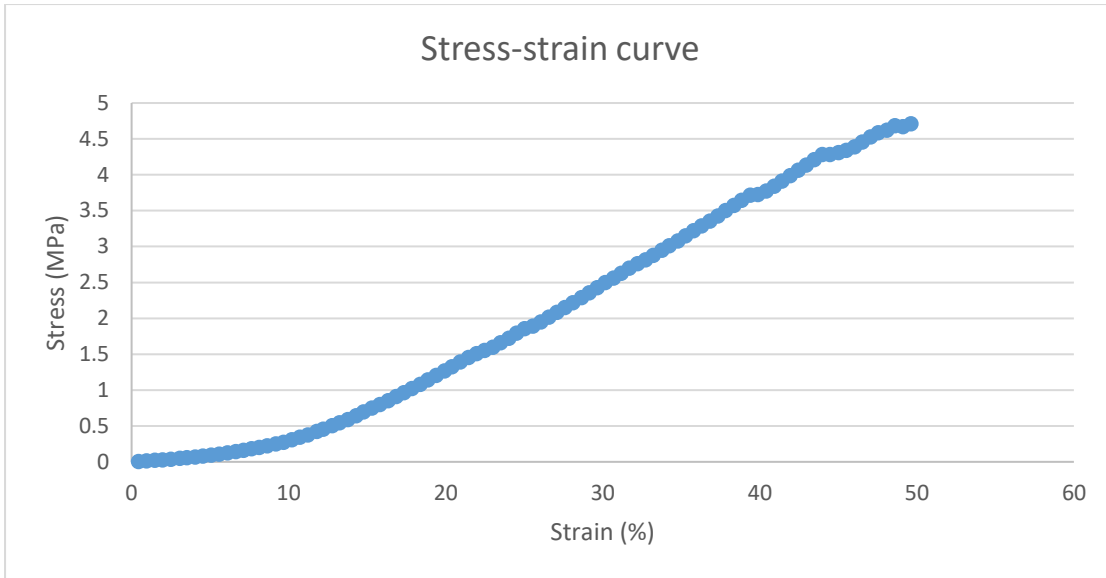

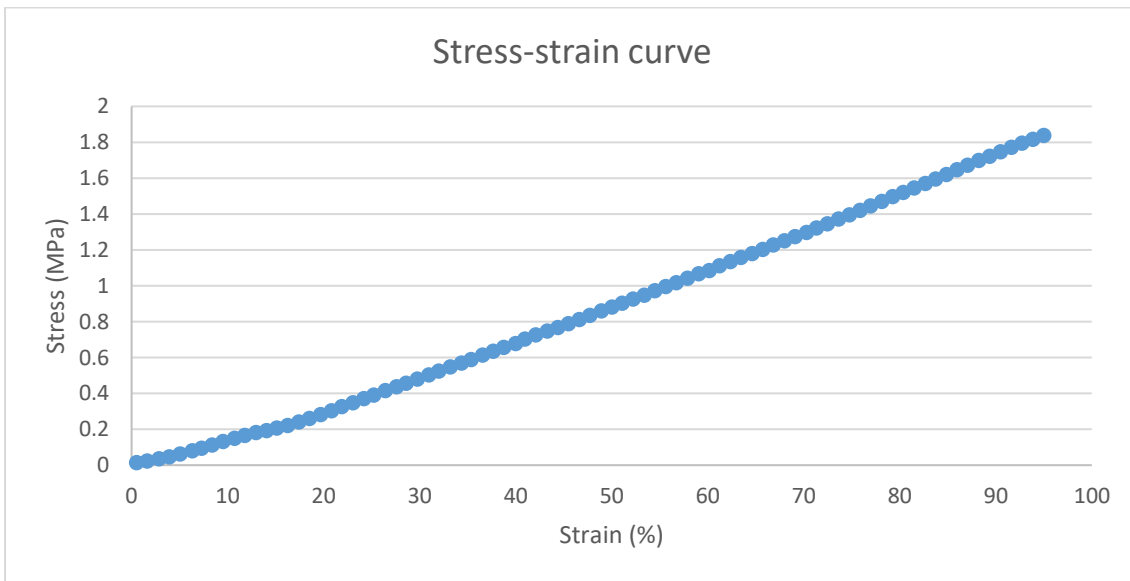Figure A.2 Sample compressive Stress-strain curve for 100 wt. % PEGDMA after 2 days in physiological conditions, with percentage strain on the x-axis and stress (MPa) on the Y-axis
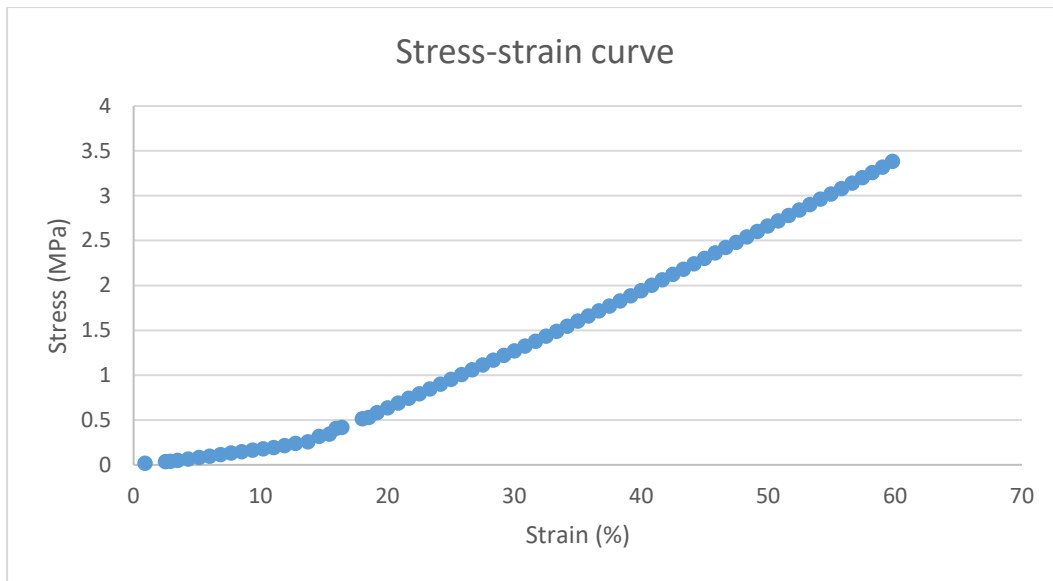
Figure A.3 Sample compressive Stress-strain curve for 100 wt. % PEGDMA after 14 days in physiological conditions, with percentage strain on the x-axis and stress (MPa) on the Y-axis
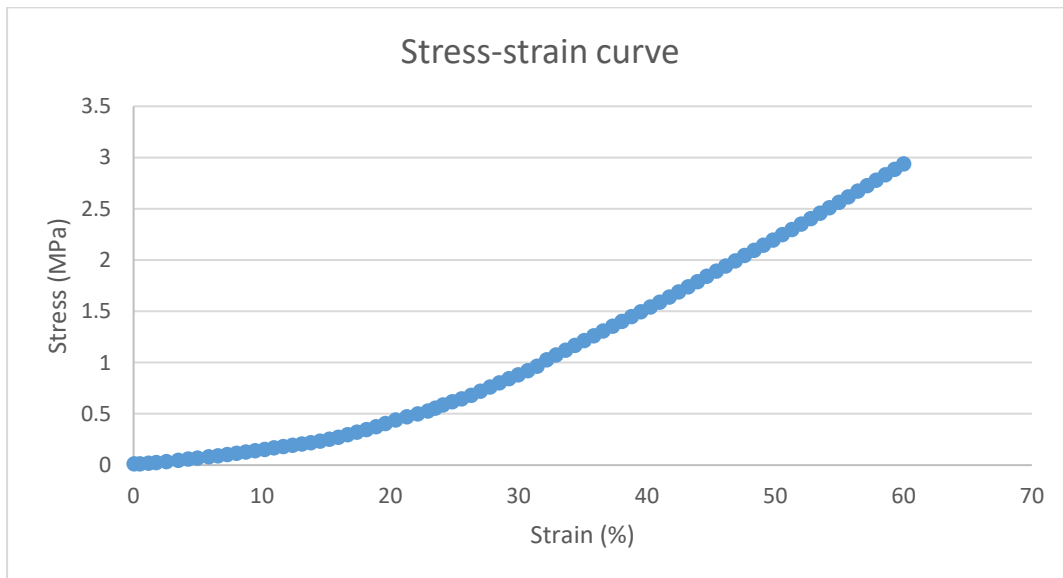
Figure A.4 Sample compressive Stress-strain curve for 100 wt. % PEGDMA after 28 days in physiological conditions, with percentage strain on the x-axis and stress (MPa) on the Y-axis
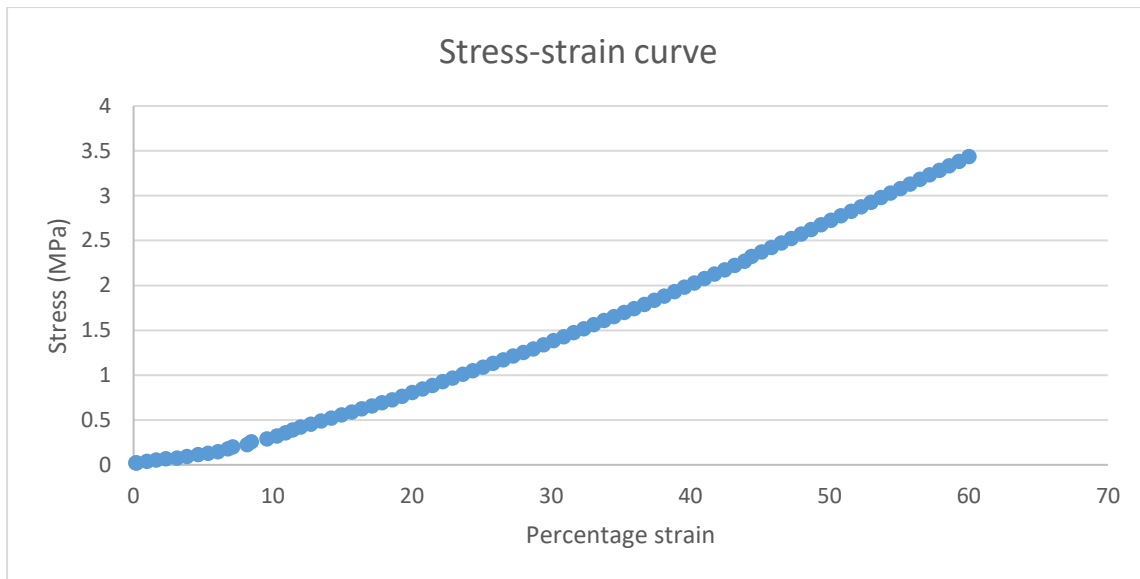
Figure A.5 Sample compressive Stress-strain curve for unhydrated 2.5 wt. % PEGBio samples, with percentage strain on the x-axis and stress (MPa) on the Y-axis
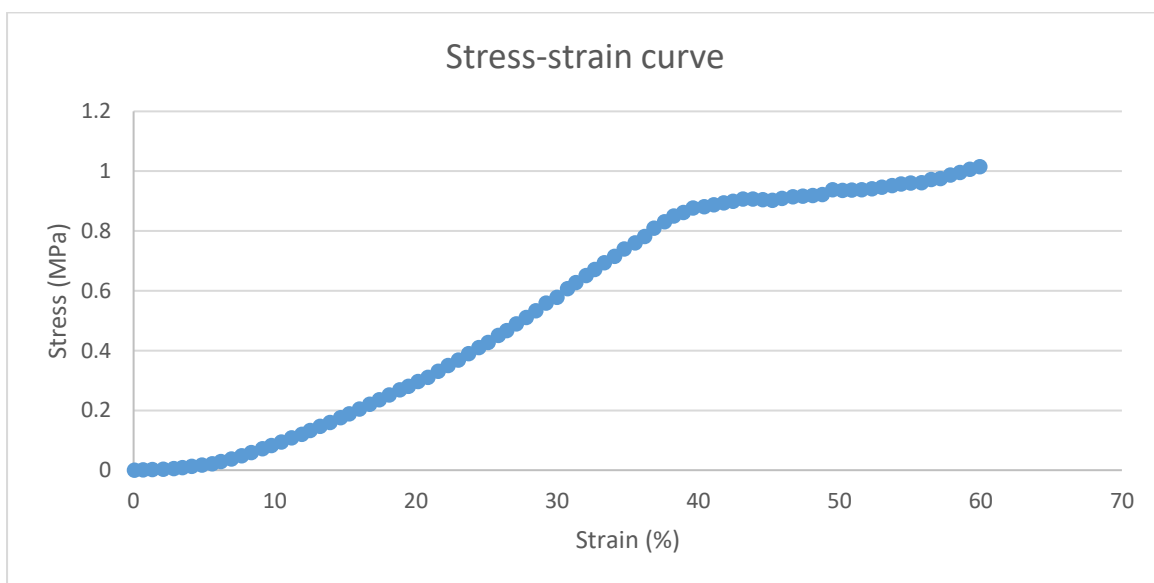
Figure A.6 Sample compressive Stress-strain curve for unhydrated PEGDMA-DiPETMP samples, with percentage strain on the x-axis and stress (MPa) on the Y-axis

Figure A.7 Sample compressive Stress-strain curve for Stereolithography printed unhydrated PEGDMA, with percentage strain on the x-axis and stress (MPa) on the Y-axis

Figure A.8 Sample compressive Stress-strain curve for unhydrated final composition samples containing PEGDMA, DiPETMP, Bioglass, NAC, Ibu and Prog, with percentage strain on the x-axis and stress (MPa) on the Y-axis
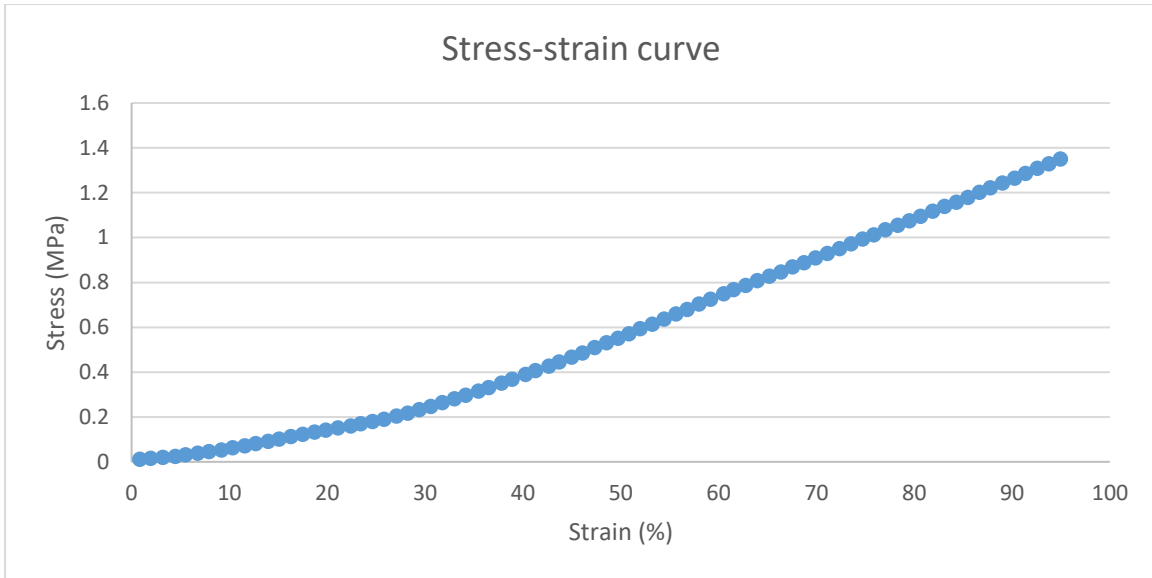
Figure A.9 Sample compressive Stress-strain curve for final composition samples containing PEGDMA, DiPETMP, Bioglass, NAC, Ibu and Prog following 2 days in simulated physiological conditions, with percentage strain on the x-axis and stress (MPa) on the Y-axis
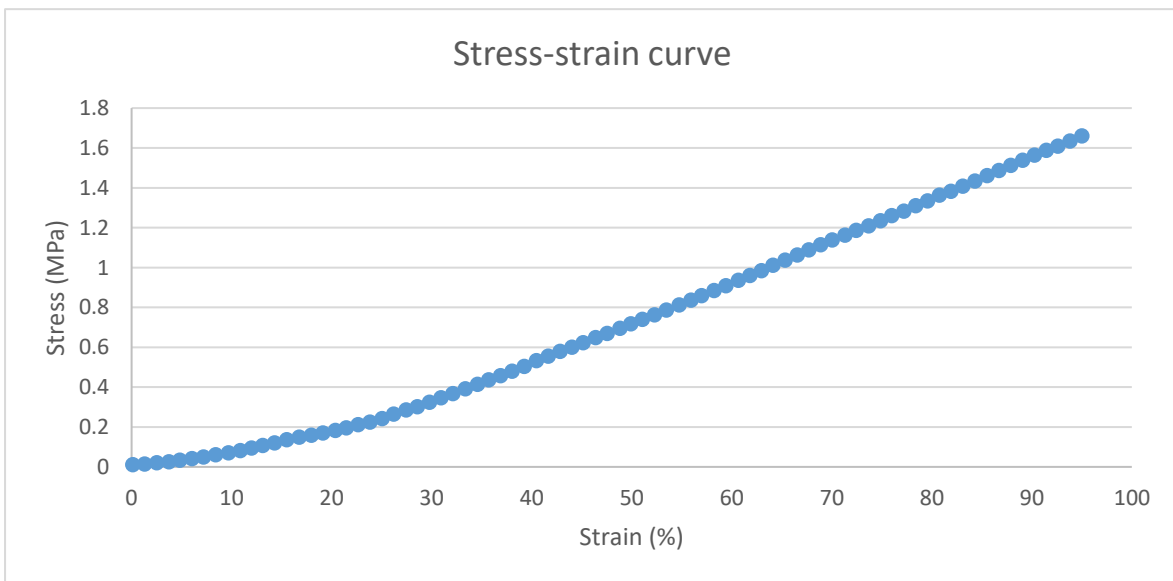
Figure A.10 Sample compressive Stress-strain curve for final composition samples containing PEGDMA, DiPETMP, Bioglass, NAC, Ibu and Prog following 2 days in accelerated degradation conditions, with percentage strain on the x-axis and stress (MPa) on the Y-axis
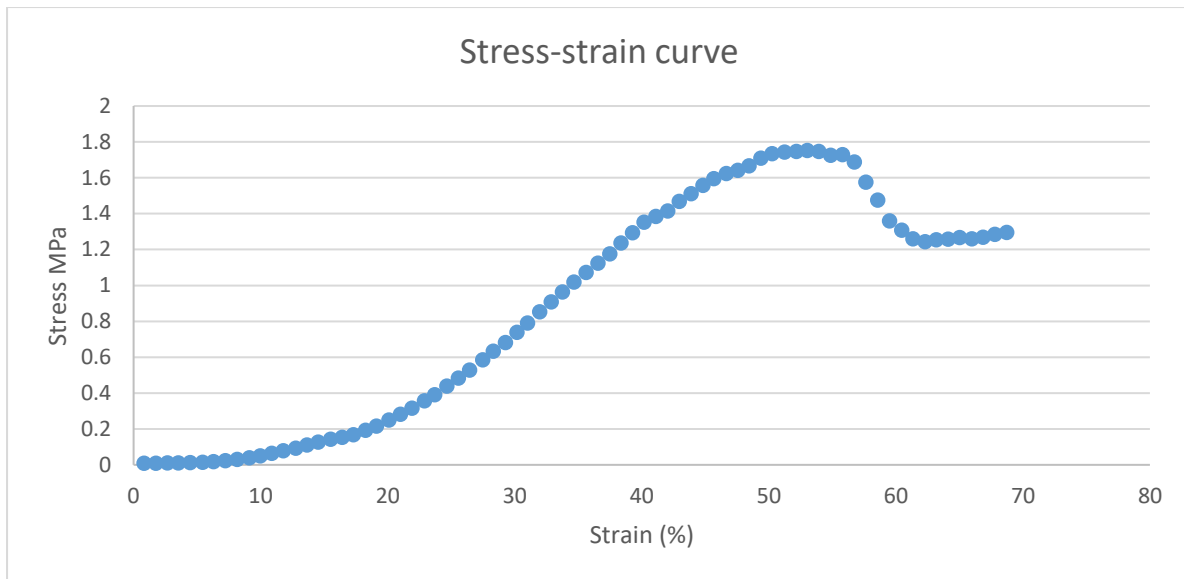
Figure A.11 Sample compressive Stress-strain curve for final composition samples containing PEGDMA, DiPETMP, Bioglass, NAC, Ibu and Prog following 28 days in simulated physiological conditions, with percentage strain on the x-axis and stress (MPa) on the Y-axis
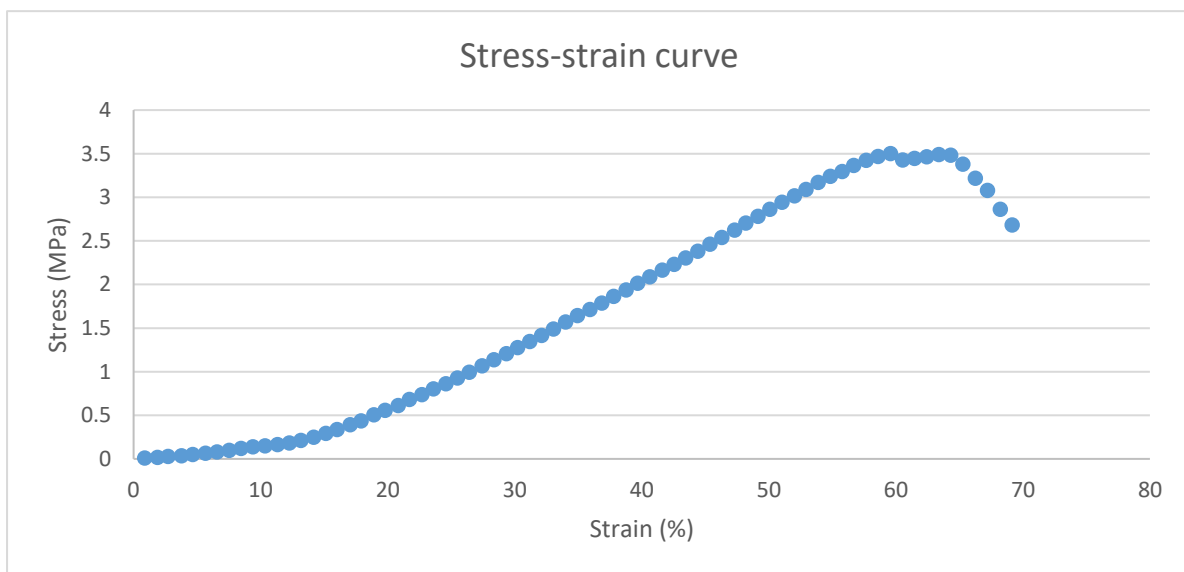
Figure A.12 Sample compressive Stress-strain curve for final composition samples containing PEGDMA, DiPETMP, Bioglass, NAC, Ibu and Prog following 28 days in accelerated degradation conditions, with percentage strain on the x-axis and stress (MPa) on the Y-axis
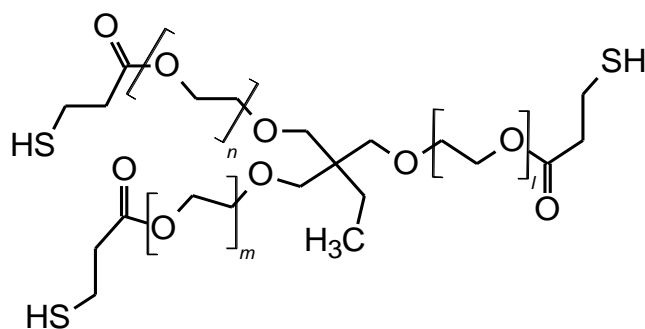
Figure B.1 Chemical structure of ETTMP 700 and 1300 (difference is number of repeating units)
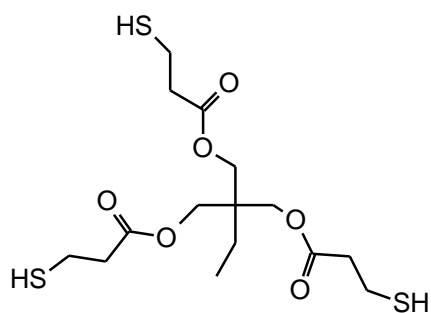
Figure B.2 Chemical structure of TMPMP (Mw 399 Da)
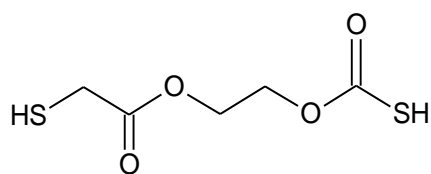
Figure B.3 Chemical structure of GDMA (Mw 210 Da)
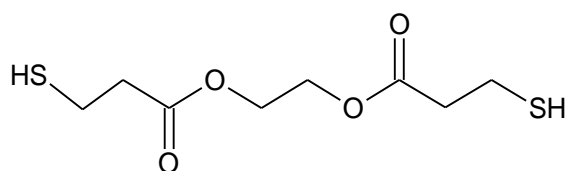
Figure B.4 Chemical structure of GDMP (Mw 238 Da)
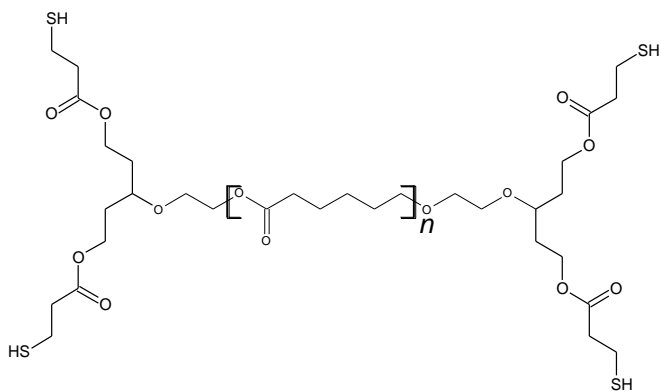
Figure B.5 Chemical structure of PCL4MP (Mw 1350 Da)
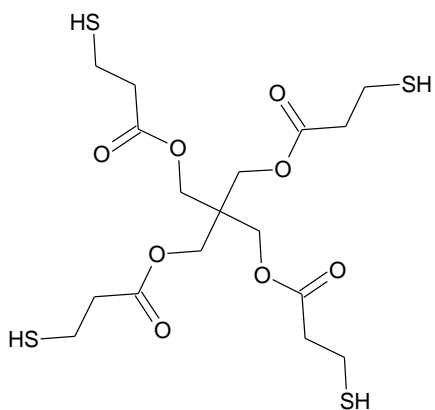
Figure B.6 Chemical structure of PETMP (Mw 489 Da)
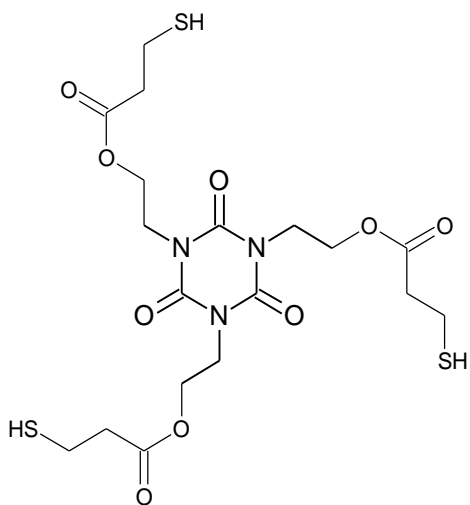
Figure B.7 Chemical structure of TEMPIC (Mw 526 Da)
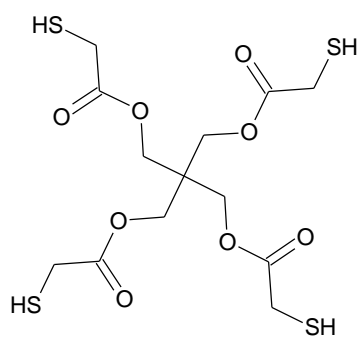
Figure B.8 Chemical structure of PETMA (Mw 433 Da)
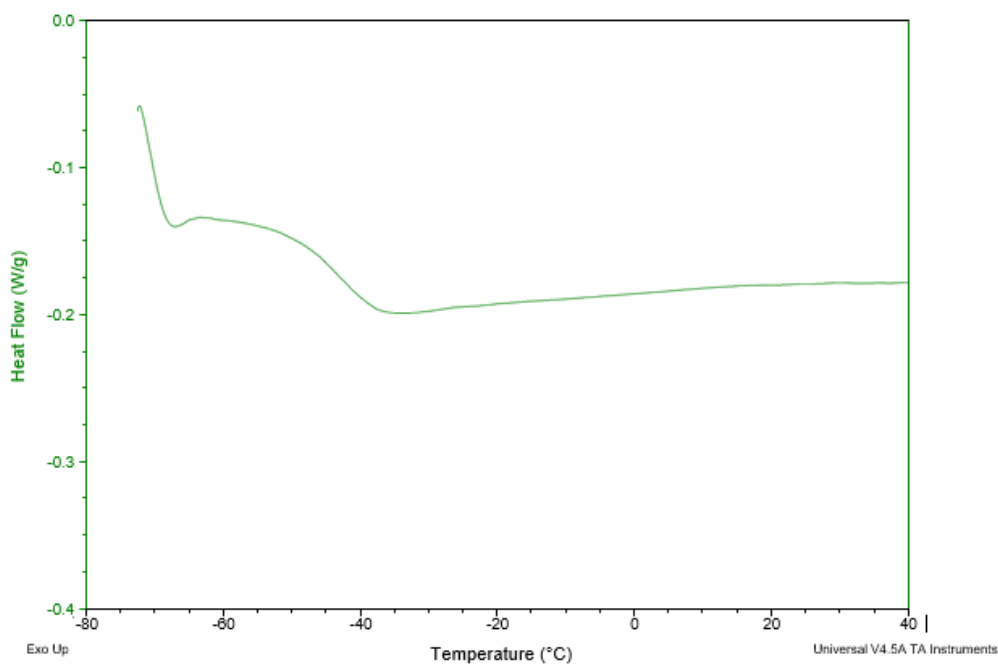
Figure C.1 DSC thermogram for 2.5 wt. % PEGBio samples following 2 days immersion in PBS at 37 degrees Celsius
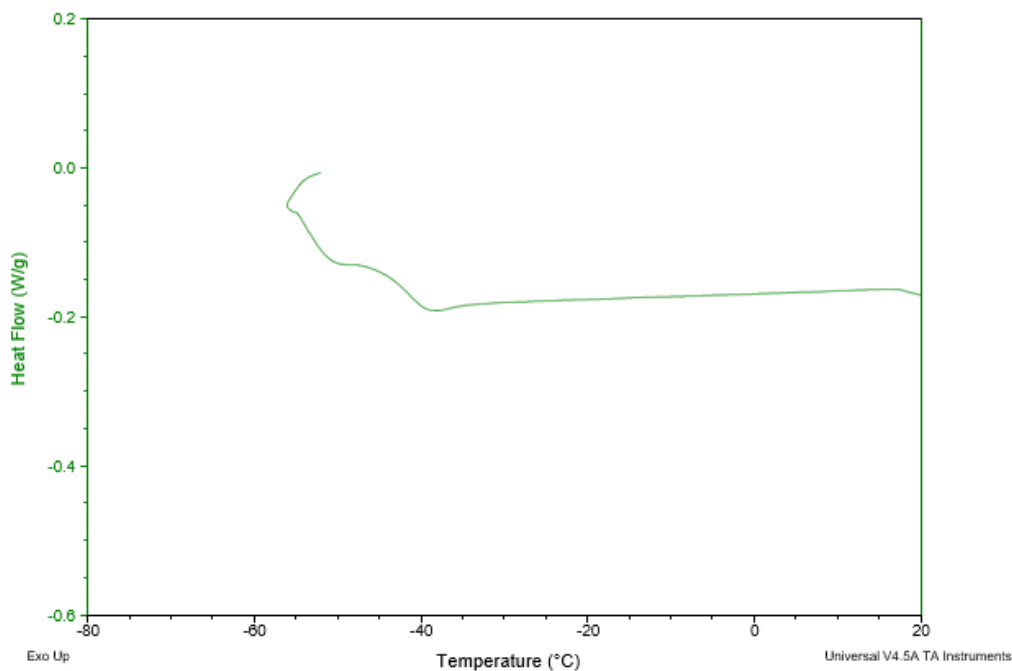
Figure C.2 DSC thermogram for PEGDMA-DiPETMP samples following 2 days immersion in PBS at 37 degrees Celsius
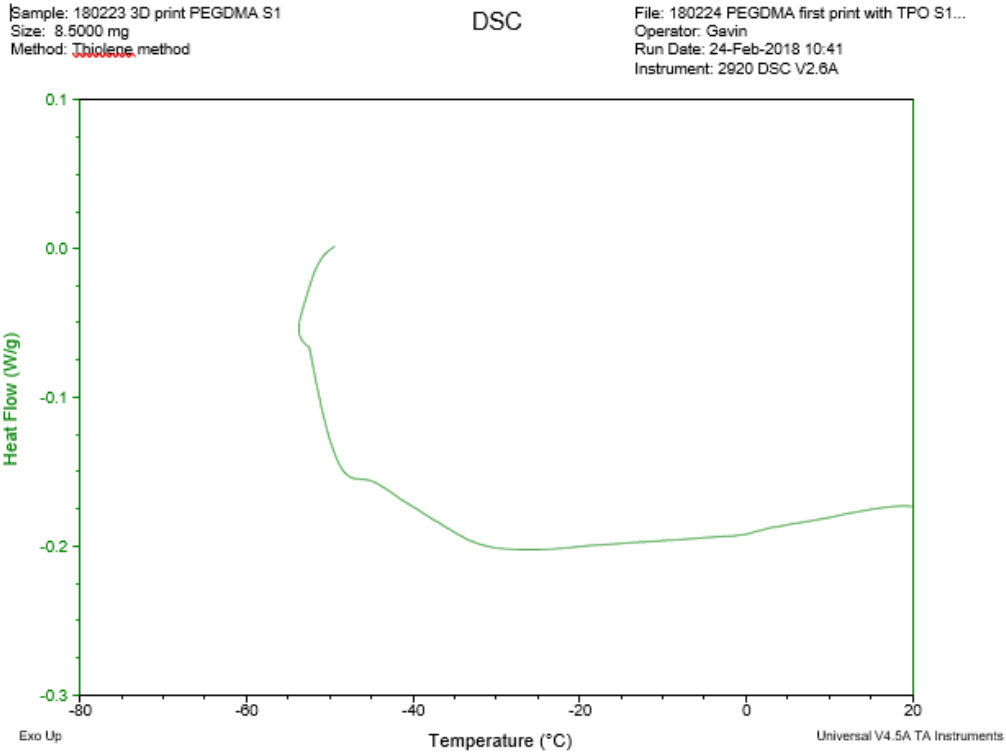
Figure C.3 DSC thermogram for unhydrated stereolithography printed PEGDMA samples
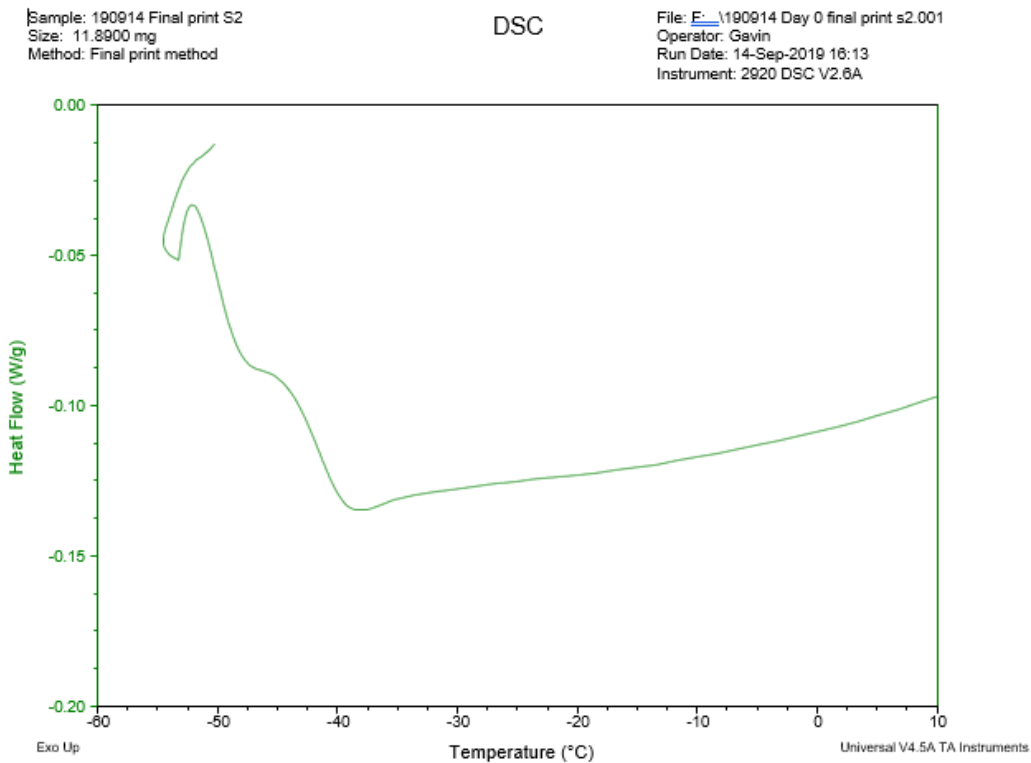
Figure C.4 DSC thermogram for unhydrated final composite containing PEGDMA, DiPETMP, Bioglass, NAC, Ibu and Prog

Appendix D (Bioglass information)

(a)
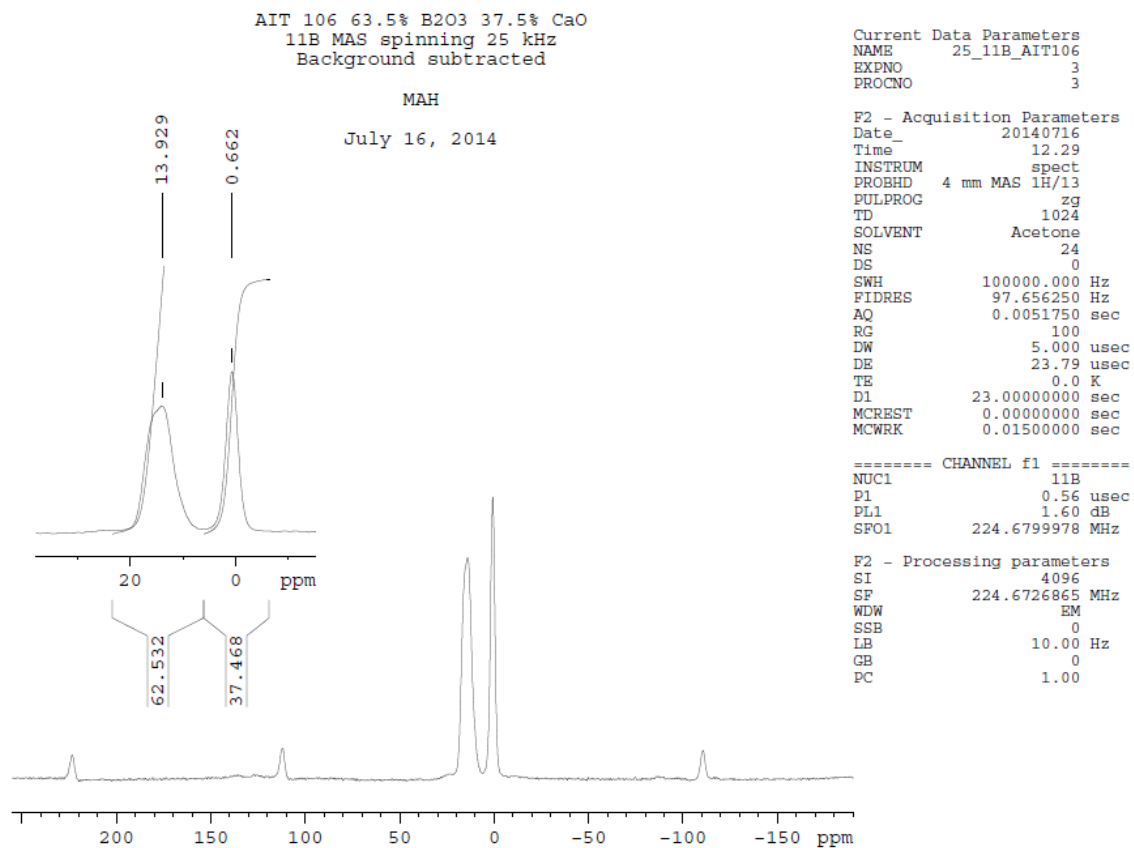
(b)
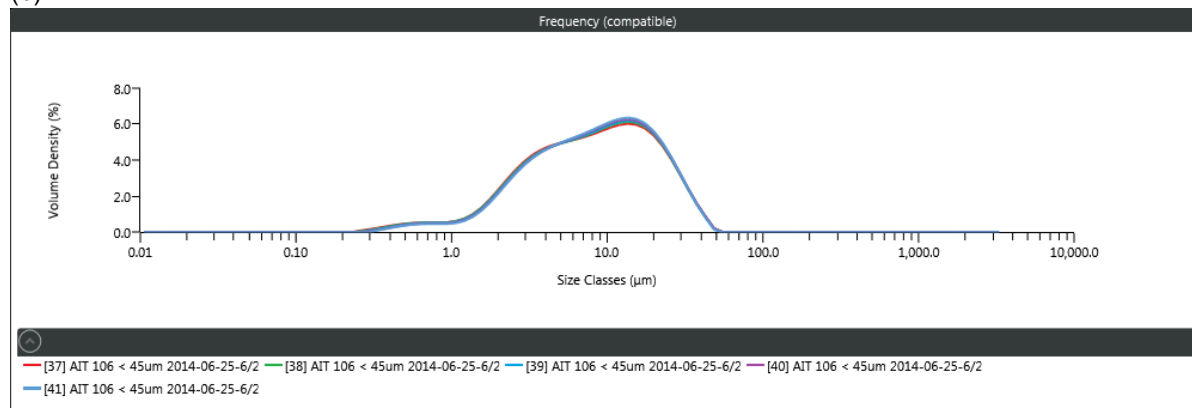
Figure D.1 (a) NMR spectra and (b) particle size analysis of calcium doped borate glasses as provided by producer
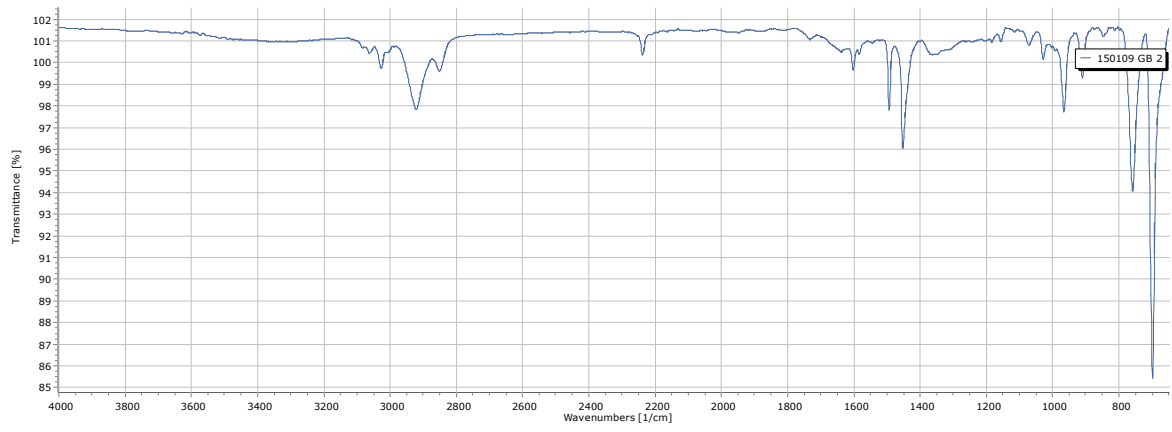
Figure D.2 FTIR spectra of calcium doped borate glasses
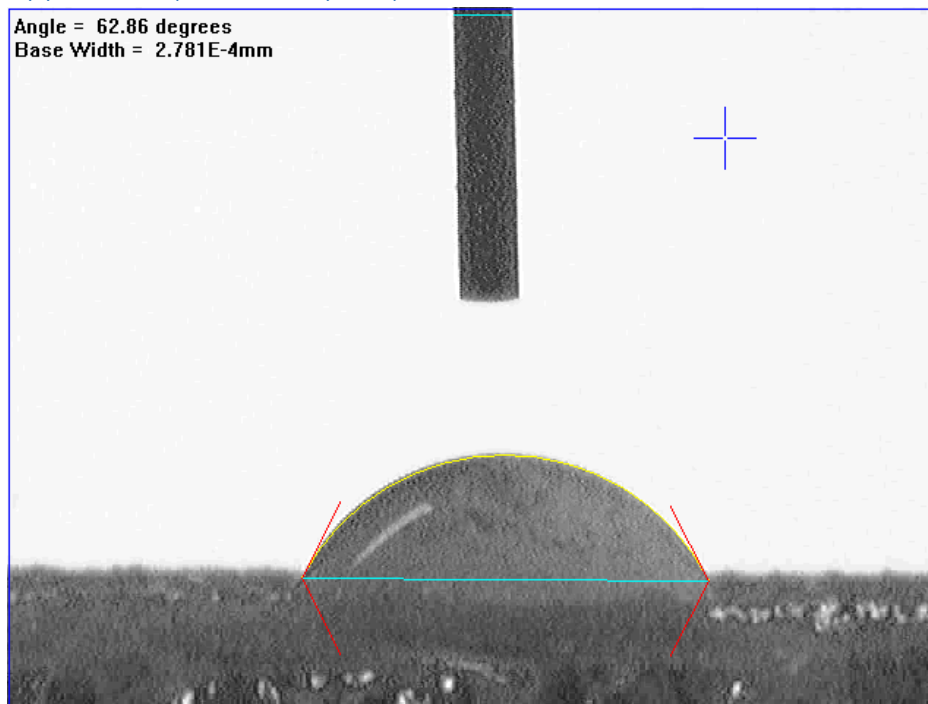
Figure E.1 Sample water droplet from Goniometry measurement, taken for 100 wt. % PEGDMA after 2 days immersion in PBS @ 37°C (image taken at time 0)
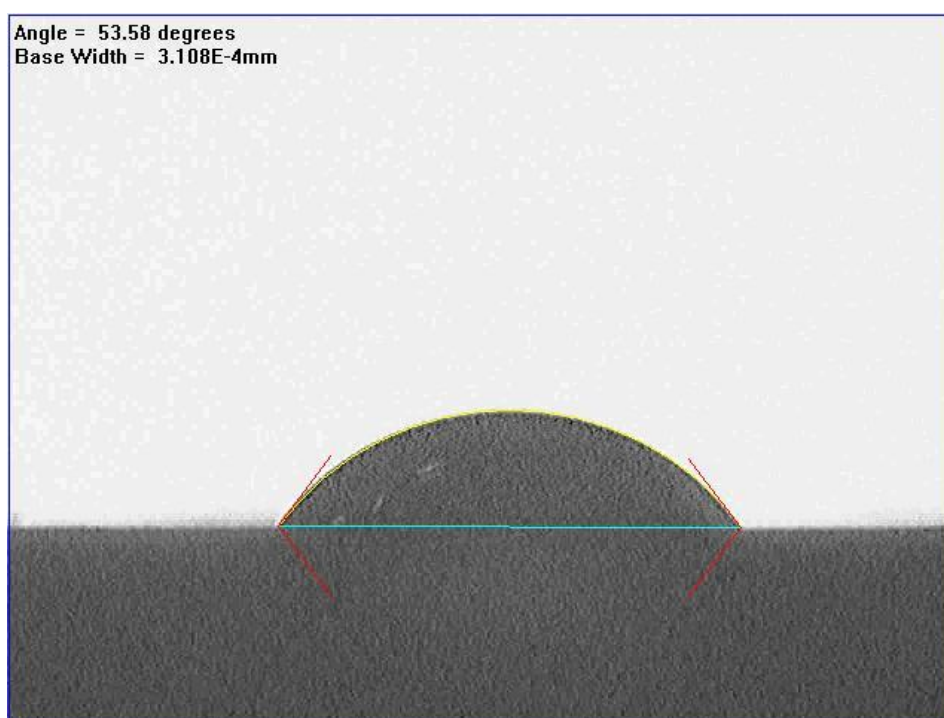

Figure E.2 Sample water droplet from Goniometry measurement, taken for unhydrated 2.5 wt. % PEGBio sample (image taken at time 0)
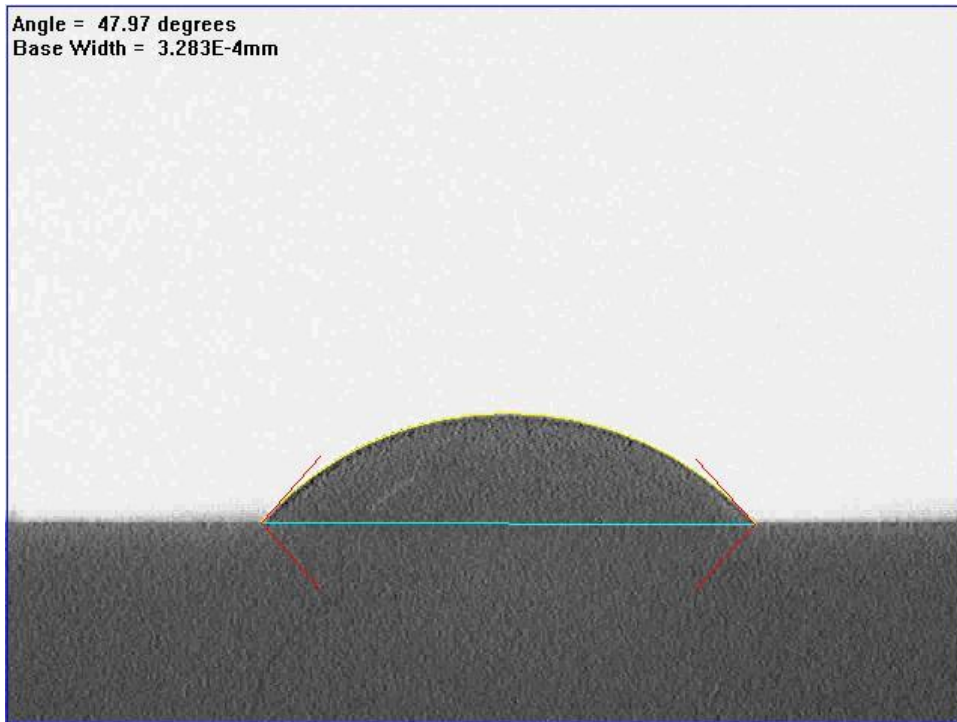
Figure E.3 Sample water droplet from Goniometry measurement, taken for unhydrated 2.5 wt. % PEGBio sample (image taken 26 seconds post drop)

Figure E.4 Sample water droplet from Goniometry measurement, taken for unhydrated PEGDMA-DiPETMP sample (image taken at time 0)

Figure E.5 Sample water droplet from Goniometry measurement, taken for unhydrated Final composition containing PEGDMA, DiPETMP, Bioglass, NAC, Ibu and Prog (image taken at time 0)
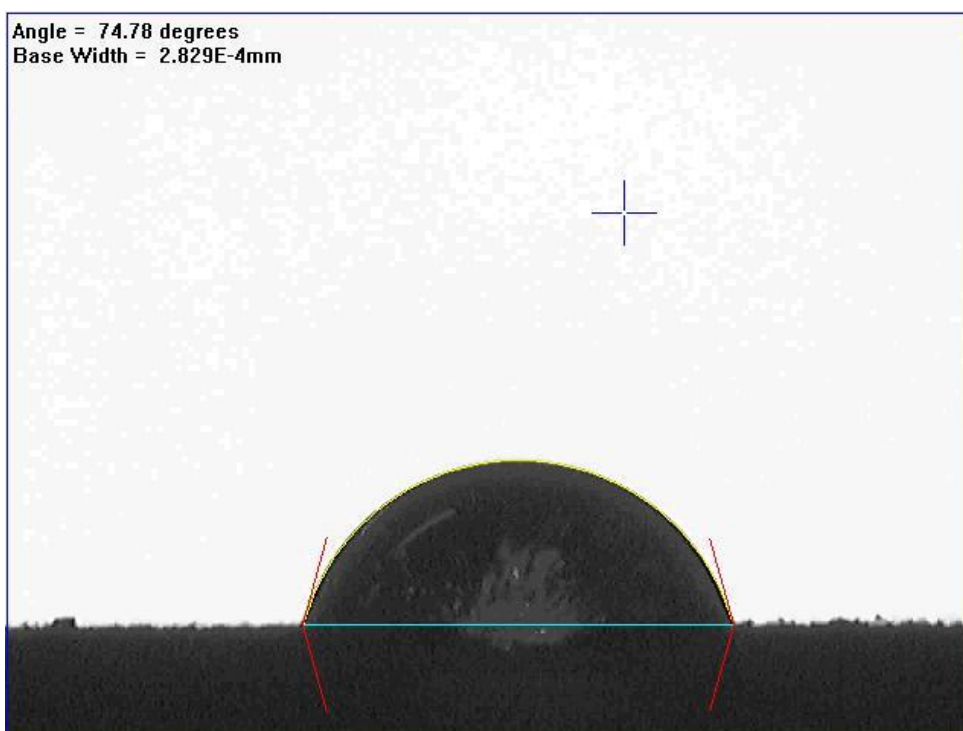

Figure E.6 Sample water droplet from Goniometry measurement, taken for unhydrated Final composition containing PEGDMA, DiPETMP, Bioglass, NAC, Ibu and Prog (image taken 26 seconds after water drop)
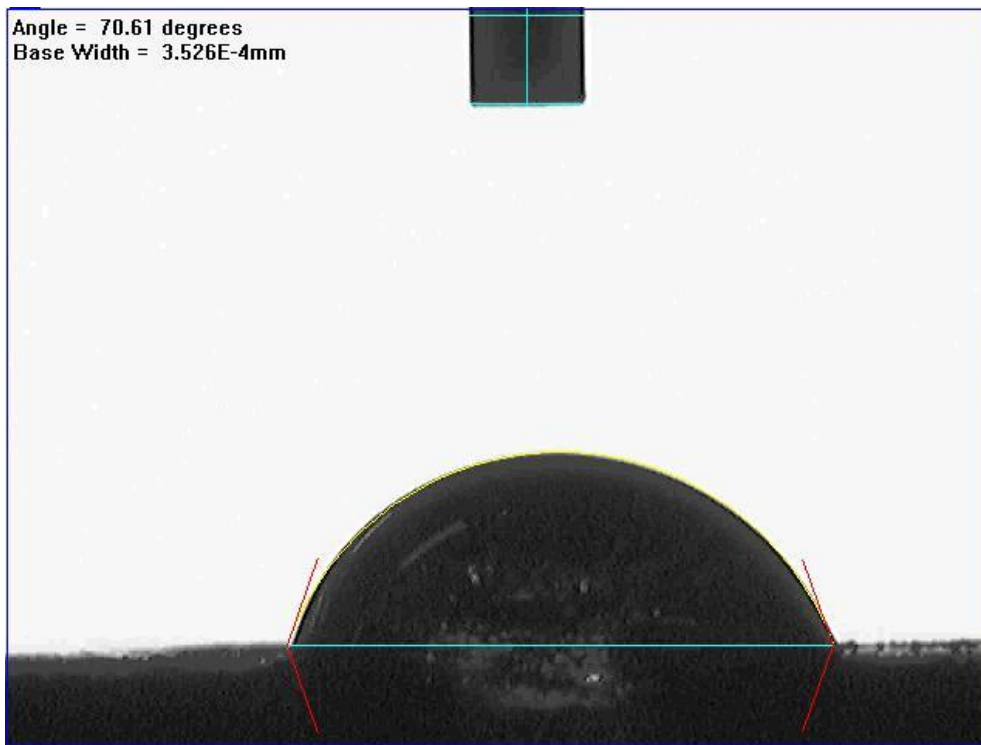
Figure E.7 Sample water droplet from Goniometry measurement, taken for Final composition containing PEGDMA, DiPETMP, Bioglass, NAC, Ibu and Prog after 28 days submersion in NaOH @ 37°C (image taken 26 seconds after water drop)
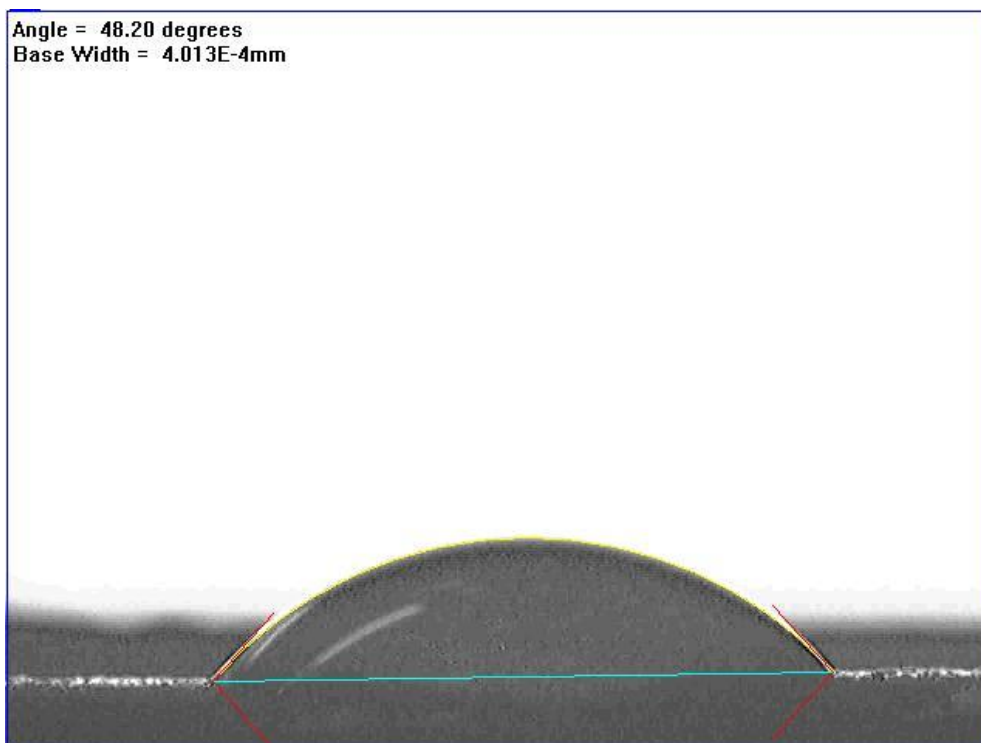

Figure E.8 Sample water droplet from Goniometry measurement, taken for Final composition containing PEGDMA, DiPETMP, Bioglass, NAC, Ibu and Prog after 28 days submersion in PBS @ 37°C (image taken 26 seconds after water drop)

Appendix F (SEM roughness quantification)

Table F.1 Roughness quantification for 25, 50, 75 and 100 wt.% PEGDMA hydrogels after 0, 2, 14 and 28 days in physiological conditions at 250x magnification

weight percentage PEGDMA	Magnification	Day	Ra, Roughness values	N, Roughness
25%	250X	0 day	41.4115	N6
	250X	2 days	11.4694	N4
	250X	14 days	16.7667	N5
	250X	28 days	11.7855	N4
50%	250X	0 day	19.7348	N5
	250X	2 days	9.8460	N4
	250X	14 days	14.4174	N4
	250X	28 days	5.4690	N3
75%	250X	0 day	39.4358	N6
	250X	2 days	10.8701	N4
	250X	14 days	16.2489	N5
	250X	28 days	14.3314	N4
100%	250X	0 day	34.9769	N6
	250X	2 days	26.8748	N5
	250X	14 days	12.5262	N4
	250X	28 days	15.8285	N4

Table F.2 Roughness quantification for 0.5, 1, 1.5 and 2.5 wt.% PEGDMA-bioglass hydrogels after 0, 2, 14 and 28 days in physiological conditions at 250x magnification

PEGBio Bioglass weight percentage	Day	Ra, Roughness values	N, Roughness
0.5%	0 day	21.0219	N5
	2 days	24.4755	N5
	14 days	19.8184	N5
	28 days	18.8657	N5
1%	0 day	17.5241	N5
	2 days	19.0801	N5
	14 days	18.7391	N5
	28 days	15.8576	N5
1.5%	0 day	16.9849	N5
	2 days	16.0457	N5
	14 days	14.7065	N4
	28 days	15.9814	N4
2,5%	0 day	17.9330	N5
	2 days	16.8355	N5
	14 days	18.2695	N5
	28 days	19.3296	N5

Table F.3 Roughness quantification for 0.5 and 1wt.% PEGDMA-bioglass hydrogels after 28 days in physiological conditions at varying magnification

PEGBio Bioglass weight percentage	Magnification	Day	Ra, Roughness values	N, Roughness
1%	1KX	28 days	16.4749	N5
0.5%	140X	28 days	19.4032	N5
1%	140X	28 days	16.5818	N5

Table F.4 Roughness quantification for unhydrated PEGDMA-thiol copolymers at 250x magnification

Surface topography of PEGDMA and PEGDMA-thiol hydrogels	Ra, Roughness values	N, Roughness
PEGDMA	21.5156	N5
PEGDMA-DiPETMP	17.3884	N5
PEGDMA-PETMP	14.2095	N4
PEGDMA-GDMP	17.4784	N5
PEGDMA-ETTMP 1300	14.6269	4N4

Table F.2 Roughness quantification for final PEGDMA compositions after 0, 2, 14 and 28 days in varying degradation conditions (200x magnification)

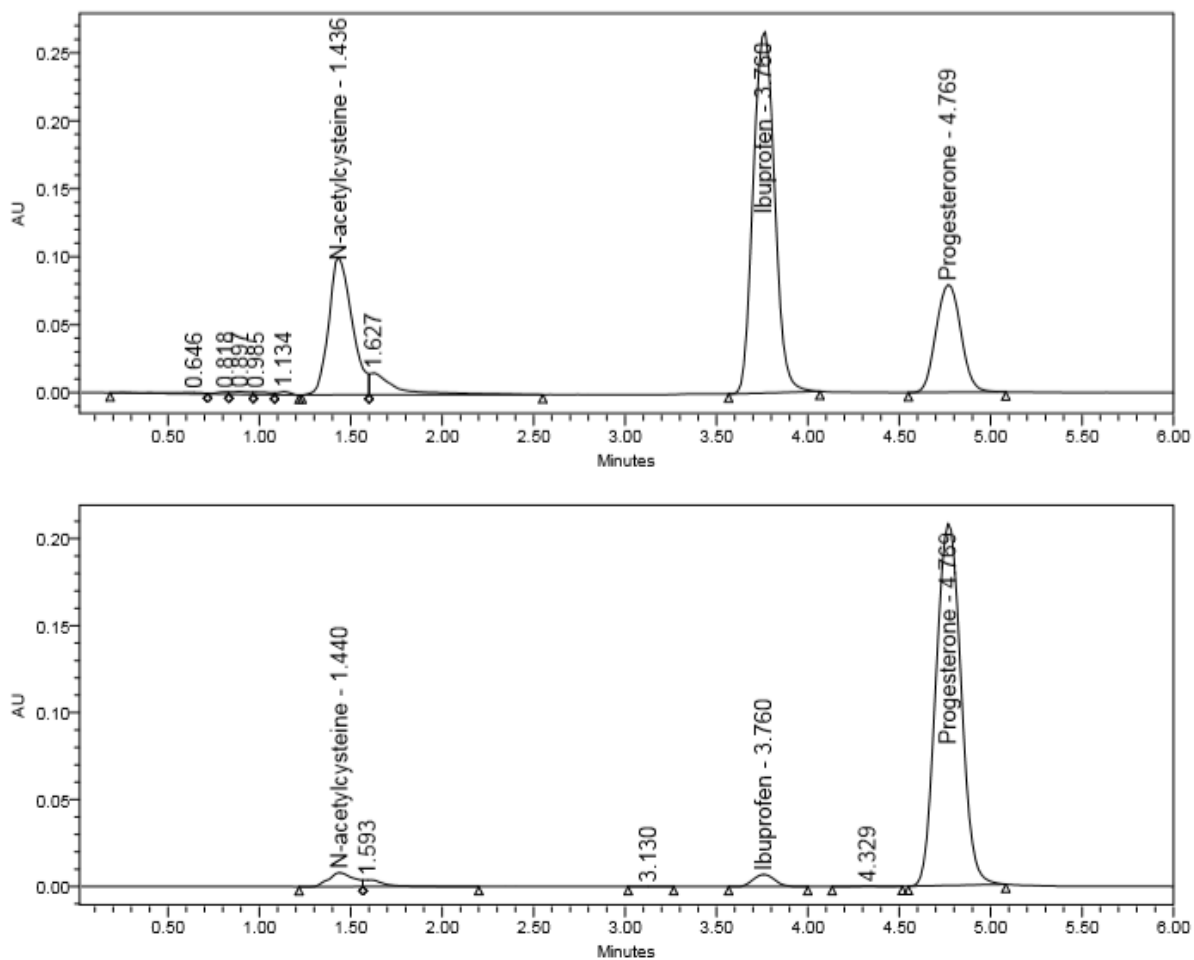| PEGCombo hydrogel	Magnification	Day	Ra, Roughness values	N, Roughness
	200X	0 days	15.9018	N4
In NaOH	200X	2 days	17.5532	N5
In PBS	200X	2 days	20.3833	N5
In NaOH	200X	14 days	9.5602	N4
In PBS	200X	14 days	10.6414	N4
In NaOH	200X	28 days	9.2690	N4
In PBS	200X	28 days	9.2525	N4

Figure G.1 Peaks for N-acetyl cysteine, Ibuprofen and Progesterone prepared in combination at 1mg/ml concentrations. Peaks determined at (A) 214nm and (B) 253nm
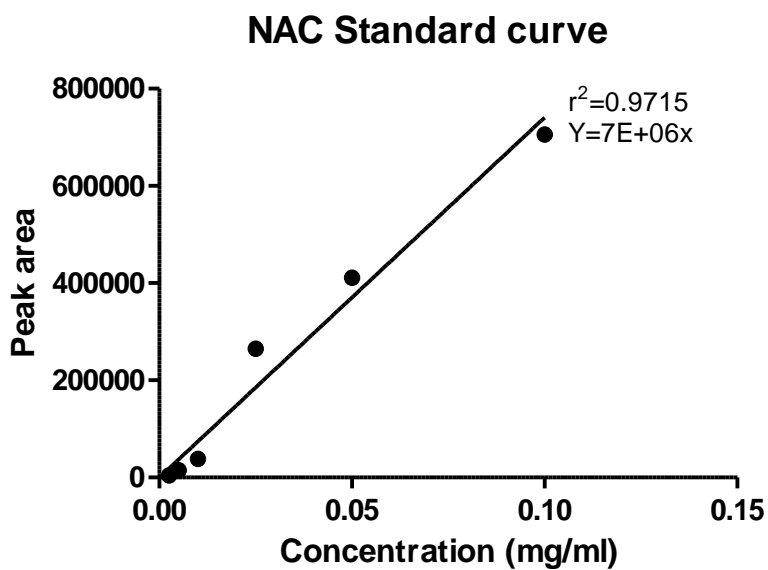
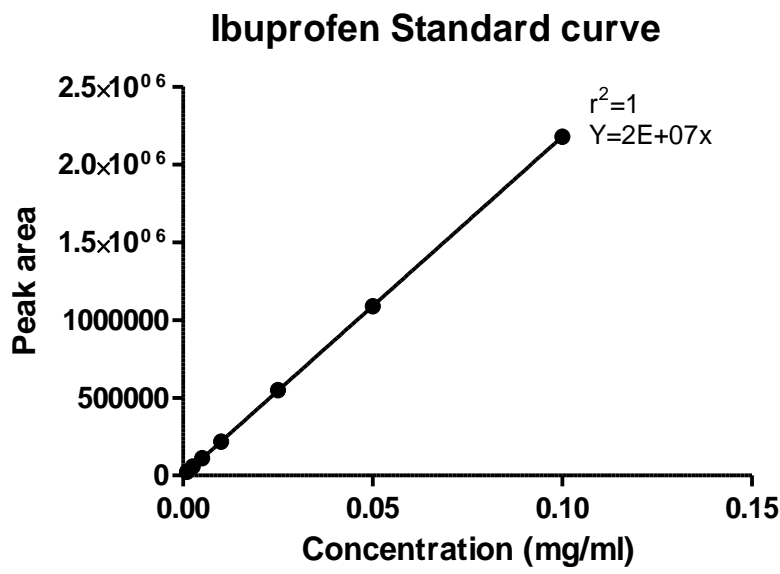Figure G.2 Standard curve of N-acetyl cysteine as a single drug

Ibuprofen Standard curve

$r^2=1$
$Y=2E+07x$

Peak area

Concentration (mg/ml)

Figure G.3 Standard curve of Ibuprofen as a single drug

Progesterone Standard curve

$r^2=0.9988$
$Y=8E+06x$

Peak area

Concentration (mg/ml)
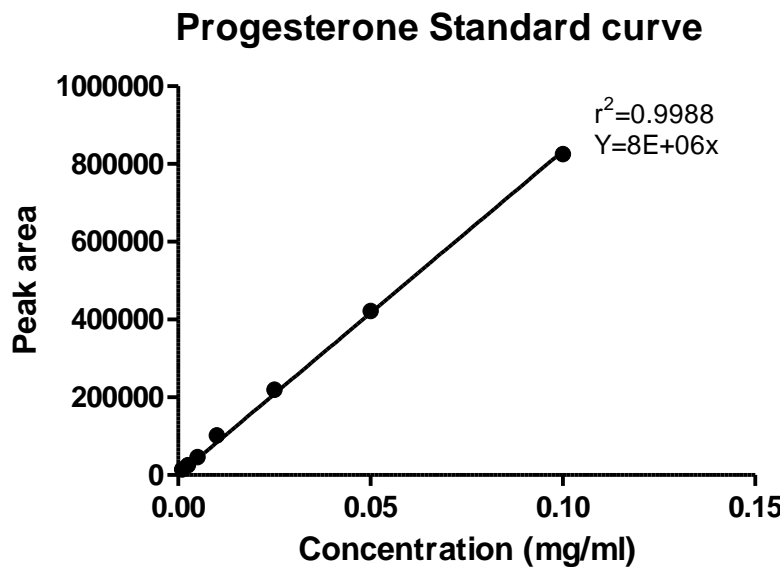
Figure G.4 Standard curve of Progesterone as a single drug

NAClbu Standard curves
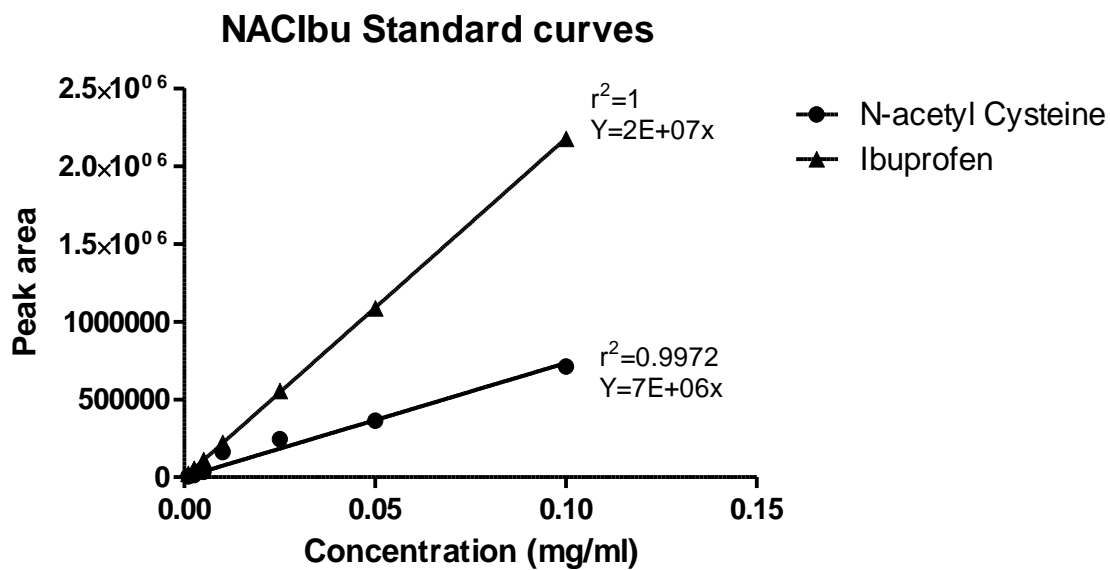
Figure G.5 Standard curves of N-acetyl cysteine and Ibuprofen prepared in combination

NACProg Standard curves
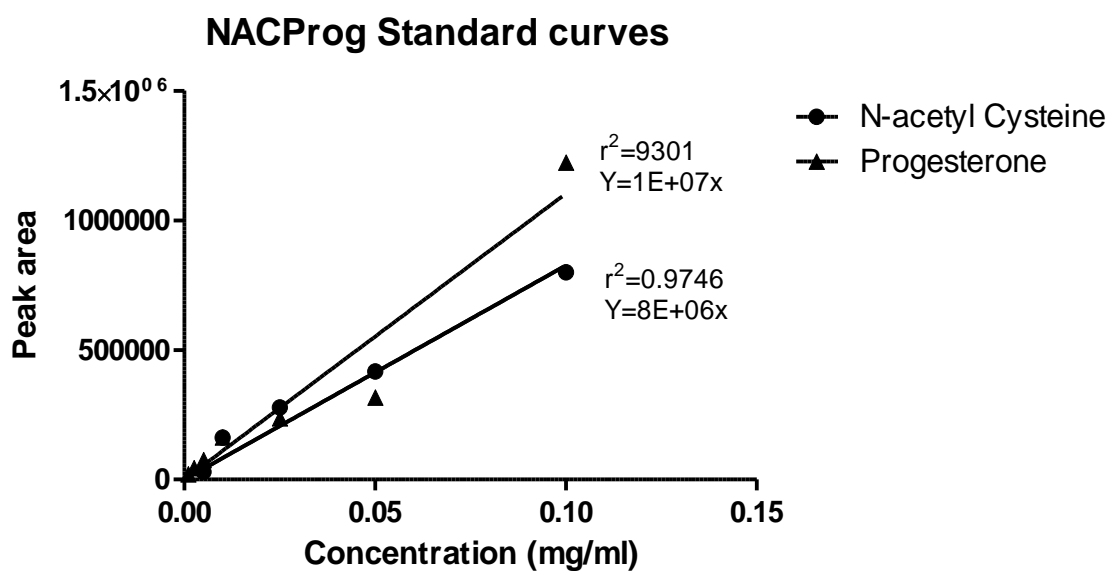
Figure G.6 Standard curves of N-acetyl cysteine and Progesterone prepared in combination

IbuProg Standard curves

$r^2=9995$
Y=2E+07x

$r^2=0.9884$
Y=2E+07x
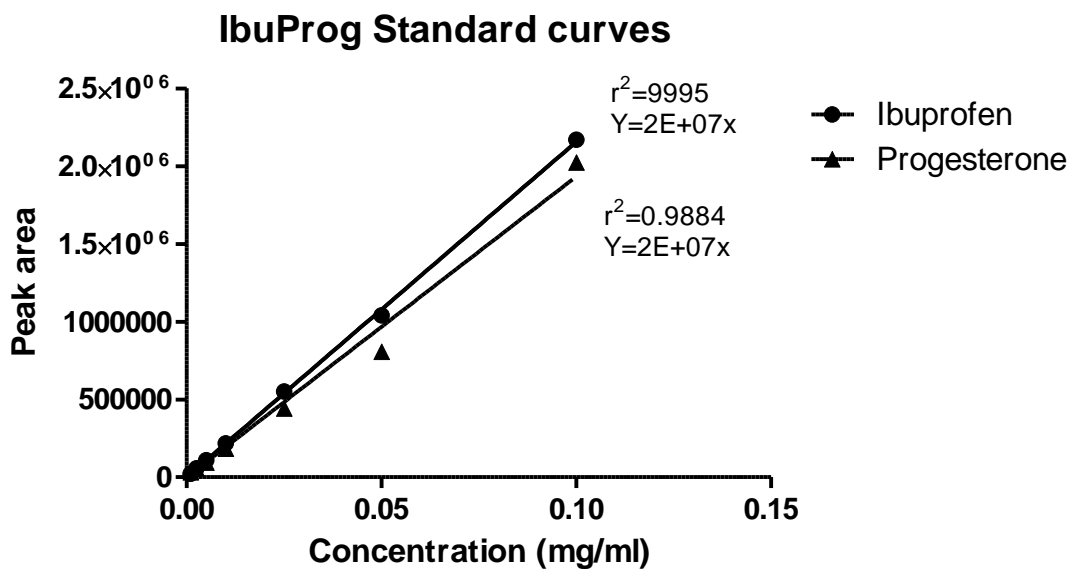
Figure G.7 Standard curves of Ibuprofen and Progesterone prepared in combination

NACIbuProg Standard curves

$r^2=1$
Y=2E+07x

$r^2=0.9999$
Y=2E+07x

$r^2=0.9546$
Y=6E+06x + 23370

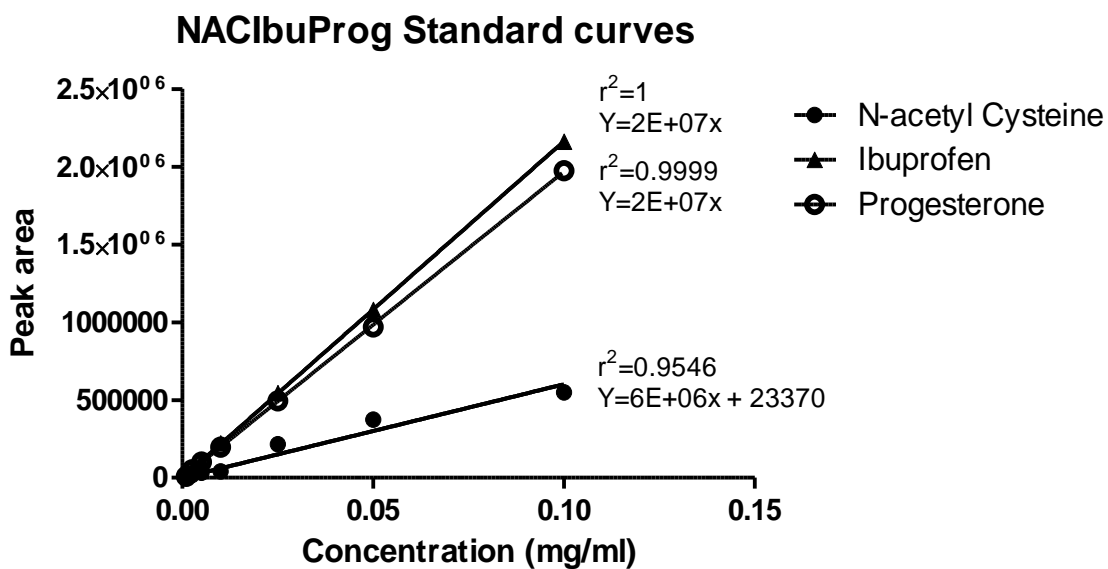Figure G.8 Standard curves of N-acetyl cysteine, Ibuprofen and Progesterone prepared in combination

Figure H.1 Printing outcomes for original PEGDMA samples by Stereolithography